THE UNIVERSITY OF CHICAGO

PIEZOELECTRICALLY-MEDIATED MECHANOCHEMICAL REACTIONS FOR ADAPTIVE POLYMERIC MATERIALS

A DISSERTATION SUBMITTED TO

THE FACULTY OF THE PRITZKER SCHOOL OF MOLECULAR ENGINEERING

IN CANDIDACY FOR THE DEGREE OF

DOCTOR OF PHILOSOPHY

BY

JORGE LUIS AYARZA LEON

CHICAGO, ILLINOIS

JUNE 2022

Publications List

Portions of Chapter 1 have been reprinted with permission from:

Ayarza, J; Wang, Z.; Wang, J; Huang, C. and Esser-Kahn, A. P. 100th Anniversary of Macromolecular Science Viewpoint: Piezoelectrically Mediated Mechanochemical Reactions for Adaptive Materials. *ACS Macro Lett.* **2020**, 9, 1237–1248. Copyright © 2020, American Chemical Society.

Portions of Chapters 2 and 3 have been reprinted with permission from:

Mohapatra, H.; Ayarza, J.; Sanders, E. C.; Scheuermann, A. M.; Griffin, P. J.; Esser-Kahn, A. P., Ultrasound Promoted Step-Growth Polymerization and Polymer Crosslinking Via Copper Catalyzed Azide–Alkyne "Click" Reaction. *Angewandte Chemie International Edition* **2018**, *57*, 11208-11212. Copyright © 2018 Wiley-VCH Verlag GmbH & Co. KGaA, Weinheim.

Wang, Z.; Ayarza, J.; Esser-Kahn, A. P., Mechanically Initiated Bulk-Scale Free-Radical Polymerization. *Angewandte Chemie International Edition* **2019,** *58*, 12023-12026. Copyright © 2019 Wiley-VCH Verlag GmbH & Co. KGaA, Weinheim.

Wang, Z.; Wang, J.; Ayarza, J.; Steeves, T.; Hu, Z.; Manna, S.; Esser-Kahn, A. P. Bio-inspired mechanically adaptive materials through vibration-induced crosslinking. *Nature Materials* **2021**, *20*, 869–874. Copyright © 2021, The Author(s), under exclusive licence to Springer Nature Limited.

Portions of Chapter 3 have been reprinted with permission from:

Ayarza, J.; Wang, Z.; Wang, J.; Esser-Kahn, A. P. Mechanically Promoted Synthesis of Polymer Organogels via Disulfide Bond Cross-Linking. *ACS Macro Letters* **2021**, *10*(7), 799–804. Copyright © 2021, American Chemical Society.

Table of Contents

List of Tables vi
List of Figures vii
Acknowledgements xi
Abstract xii
Chapter 1: Introduction and background 1
1.1 Introduction 1
1.2 Self-strengthening polymers and mechanochemistry 2
1.3 Piezoelectrically-mediated chemical reactions 6
1.4 Piezoelectrochemistry for self-strengthening polymers 14
1.5 References 21
Chapter 2: Piezo-polymerization methodologies 27
2.1 Mechanically-promoted copper ‘click’ polymerization 27
2.1.1 Results and discussion 28
2.1.2 Methods 33
2.2 Mechanically-promoted Fe-mediated free radical polymerization 40
2.2.1 Results and discussion 40
2.2.2 Methods 45
2.3 Mechanically-promoted thiol-ene polymerization 49
2.3.1 Results and discussion 49
2.3.2 Methods 55
2.4 Conclusions 59
2.5 References 60
Chapter 3. Conferring adaptability to polymer organogels via piezo-polymerization 64
3.1 Strengthening of an organogel via mechano-thiol-ene crosslinking 64
3.1.1 Results and discussion 65
3.1.2 Methods 70
3.2 Mechanically-promoted synthesis of reversible organogels through thiol-disulfide crosslinking 71
3.2.1 Results and discussion 72

3.2.2 Methods 80
3.3 Conclusions 87
3.4 References 88
Chapter 4. Mechanically-promoted mineralization of an organogel 90
4.1 Results and discussion 90
4.2 Methods 97
4.3 Conclusions 99
4.4 References 100
Appendix A: Supporting information for Chapter 2.1: Mechanically-promoted copper ‘click’ polymerization 101
Appendix B: Supporting information for Chapter 2.2: Mechanically-promoted Fe-mediated free radical polymerization 114
Appendix C: Supporting information for Chapter 2.3: Mechanically-promoted thiol-ene polymerization 121
Appendix D: Supporting information for Chapter 3.2: Mechanically-promoted synthesis of reversible organogels via thiol-disulfide crosslinking 128
Appendix E: Supporting information for Chapter 4: Mechanically-promoted mineralization of an organogel 146

List of Tables

Table 1. Selected examples of piezoelectrically-mediated chemistries……..18

Table 2. Results for mechano-radical polymerization of various acrylates…….43

Table 3. Gelation study of mercapto-polymers…….……..76

Table B1. Polymerization kinetics for the various model polymerization of BA in DMF…….119

Table B2. Results for mechano-radical polymerization of BA with different initiators……120

Table C1. Summary of reactions between different alkenes and EDT……..…126

Table C2. Zeta potential measurements of different ZnO nanoparticles……...127

Table D1. Molecular weight characterization of mercapto-polymers……...132

Table D2. Physical characterization of mercapto-polymer organogels……141

Table D3. Molecular weight characterization of mercapto-polymers in recycling experiments..143

List of Figures

Figure 1. Examples of mechanophore systems……....4

Figure 2. Scheme showing the self-strengthening of a polymer double-network hydrogel via mechanoradical-induced polymerization…….5

Figure 3. Studies on the influence of ferroelectric materials on chemical reactivity……..….7

Figure 4. Water splitting via piezocatalysis…….….9

Figure 5. Energy diagram schemes……..……10

Figure 6. Dye degradation via piezocatalysis with BZT-BCT microfibers under low frequency vibrations……12

Figure 7. Mechano-ATRP system……..…16

Figure 8. Piezoelectrically-promoted mineralization over the surface of PVDF films under mechanical loading while submerged in a simulated body fluid…….……...19

Figure 9. Ultrasound-mediated ‘click’ polymerization……..29

Figure 10. Ultrasound-mediated polymer crosslinking using mechano-click reaction……..31

Figure 11. Results for mechano-radical polymerization of BA……..…….42

Figure 12. Temperature ramp shear rheology measurements of composites at a constant oscillation frequency of 1 Hz……..….44

Figure 13. Schematic diagram of the experimental setup for electrodynamic shaking system….50

Figure 14. Mechano-thiol-ene polymerization…….……..52

Figure 15. Photos of the thiol-ene crosslinking reaction solution…….…….53

Figure 16. Organogel strengthening via mechano-thiol-ene polymerization……..65

Figure 17. Strengthening of an organogel via mechano-thiol-ene crosslinking…….66

Figure 18. Adaptation of the organogel modulus to different mechanical inputs……69

Figure 19. Mechano-thiol-disulfide crosslinking……...72

Figure 20. Pictures showing dissolution tests of mercapto-PMMA organogels……..74

Figure 21. Recyclability study of mercapto-PMMA organogel……..78

Figure 22. Ultrasound-promoted synthesis of microrods……91

Figure 23. FTIR spectra of microrods, $Zn(McMT)_2$, and McMT……93

Figure 24. Powder XRD spectra microrods, $Zn(McMT)_2$, and ZnO nanoparticles…….93

Figure 25. Shear rheology study of the microrod formation reaction at different timepoints…….95

Figure 26. Synthesis of microrods within an organogel……..96

Figure A1. Photos of mechano-click polymerization……...101

Figure A2. GPC trace depicting the evolution of polymer molecular weight over time……..101

Figure A3. MALDI-TOF spectrum of polytriazole……..102

Figure A4. Temperature ramp shear rheology measurement in the range 50 – 200 ºC of the linear polytriazole……..112

Figure A5. Control experiments for the mechano-crosslinking of azido-polyurethane……113

Figure B1. Photos of the reaction mixture at different reaction times and piezoelectric nanoparticles……117

Figure B2. Optical image of piezoelectric nanoparticles before and after ultrasound agitation in the presence of $FeCl_3 \cdot 6H_2O$/TDA-1 solution…….118

Figure C1. Frequency ranges of commonly encountered environmental vibrations…….121

Figure C2. The output force as a function of input power…….121

Figure C3. GPC traces of thiol-ene polymerization conducted under shaking (2000 Hz, 1.2 N) or stirring (400 rpm) for 4 hours……122

Figure C4. ^{1}H-NMR spectra of polythioether synthesized via mechano-thiol-ene polymerization……122

Figure C5. MALDI-TOF MS spectrum of polythioether……..123

Figure C6. FT-IR spectra of EDT, TEGDE, and polythioether……123

Figure C7. Storage (G') and loss (G") moduli as a function of frequency (Hz) of the mechano-thiol-ene gel……..124

Figure C8. Gelation time as a function of force……124

Figure C9. Plausible reaction mechanism for the mechano-thiol-ene polymerization……..125

Figure C10. GPC traces of mechano-thiol-ene polymerization using different ZnO nanoparticles: positively charged, negatively charged, and silane-coated ZnO…….……..125

Figure D1. FTIR spectra of mercapto-PMMA……..131

Figure D2. FTIR spectra of mercapto-PMA……..…131

Figure D3. FTIR spectra of mercapto-PS……132

Figure D4. Mechanistic analysis of ultrasound-promoted disulfide bond formation……...133

Figure D5. UV-vis study of I_2 formation via piezoelectrochemistry under ultrasound……137

Figure D6. Possible mechanisms for piezo-oxidation of thiol to disulfide……137

Figure D7. Stress-strain curves in the linear region of samples **a**-**e** (mercapto-PMMA)……...138

Figure D8. Stress strain curve in the linear region of sample **f**……..138

Figure D9. Rheological characterization of sample **g**……...……139

Figure D10. Stress strain curves in the linear region of samples **h** and **i** (mercapto-PS)……139

Figure D11. NMR spectrum of recycled mercapto-PMMA……..142

Figure D12. GPC trace curves of mercapto-PMMA gels (samples **a** and **e**) recycling experiments…….....143

Figure D13. Pictures showing dissolution of samples **f** (mercapto-PMA gel) and **h** (mercapto-PS gel) from Table 3……..144

Figure D14. GPC trace curves of mercapto-PMA gel (sample **f**) recycling experiment……..145

Figure D15. GPC trace curves of mercapto-PS gel recycling experiment (sample **h**)……145

Figure E1. XPS spectrum of ZnO nanoparticles……...146

Figure E2. XPS spectrum of microrods……146

Figure E3. SEM image of particles at t = 0 h. Scale bar: 200 nm……...147

Figure E4. SEM image of particles at t = 1 h. Scale bar: 1 μm……...147

Figure E5. SEM image of particles at t = 2 h. Scale bar: 1 μm……...148

Figure E6. SEM image of particles at t = 4 h. Scale bar: 1 μm……148

Figure E7. SEM image of particles at t = 6 h. Scale bar: 1 μm……...149

Figure E8. Shear rheology plots for experiments varying the concentration of ZnO nanoparticles with constant concentration of McMT (66 mg, 0.5 mmol)……149

Figure E9. Shear rheology plots for the experiments varying the concentration of McMT with constant concentration of ZnO (20 mg, 0.25 mmol)……150

Figure E10. Comparison of FTIR spectra of the microrods prepared in solution vs microrods formed within the methyl cellulose organogel……..150

Figure E11. Comparison of FTIR spectra of the McMT disulfide and the microrods……...151

Figure E12. Modulated DSC curve of microrods……..151

Figure E13. Modulated DSC curve of $Zn(McMT)_2$……..152

Figure E14. Modulated DSC curve of McMT……..152

Figure E15. Modulated DSC curve of the McMT disulfide dimer……153

Acknowledgements

I am very grateful to have been part of the Esser-Kahn group during my graduate studies both at the University of California, Irvine and the University of Chicago. To my PhD advisor, Prof. Aaron Esser-Kahn for the opportunity to join your group, and for your exceptional support and guidance all these years. Thank you for teaching me how to become a better scientist and professional.

To the candidacy and thesis committee members, Prof. Stuart Rowan and Prof. Sihong Wang, for their support and helpful discussions about my research.

To Dr. Hemakesh Mohaptra, for being a great mentor during my early days as a PhD student.

To Dr. Zhao Wang and Dr. Jun Wang, for their friendship and research collaborations, thank you for allowing me to be part of such amazing work.

To my friends from graduate school Britteny, Jainu, and Nihesh, for walking with me through this challenging path, and for all the support and fun times we have shared together.

To the rest of the Esser-Kahn group, past and present members that I have had the pleasure of knowing all these years. I enjoyed spending time with you and learning from you.

To Dr. Philip Griffin, Director of the Soft Matter Laboratory at PME, for his patience and support in providing instrument training, and for his helpful advice regarding experimental challenges.

To the funding agencies, especially the National Science Foundation (NSF), the Air Force Office of Scientist Research (AFOSR), and the Army Research Office (ARO), for their generous financial support for all these research projects.

And last but not least, to my parents, my brother, my family, and friends from Peru, for their unconditional love, friendship, and support. I would not have made it this far without you.

Abstract

Biological materials display great adaptability to their environment, as is the case of bones, muscles, and skin which can adapt in response to mechanical stimuli by changing their composition and structure through a process called mechanotransduction. These systems efficiently convert mechanical stimuli into chemical signals that can drive reactions leading to structural changes, deposition, and removal of material. These adaptive properties give them great advantage in terms of efficiency and durability. Currently, synthetic polymeric materials mostly lack similar adaptability, resulting in mismatches in their physical properties, and the need to replace them repeatedly.

Self-strengthening polymeric materials would be useful for reinforcement in fiber composites, improving the lifetime of deployed structural materials, and creating polymers that tailor and fit themselves to individual users, such as prosthetics and robotics. Significant effort has been devoted in designing stimuli-responsive chemistries which impart synthetic polymers with self-reporting and self-healing properties. Several reports have shown the use of heat, light, electricity, pH, and pressure changes to mediate the identification of a failure in polymeric material, deposition of new material, or the formation of new chemical bonds. However, much more work remains to be done to develop mechanoresponsive systems that target adaptation of the material. Conversion of mechanical stimuli into chemical reactivity is an attractive target since mechanical stress is the most common form of energy experienced by materials. Recently, we and others have started investigating methods to use mechanical energy, in the form of ultrasound, mechanical vibrations, and cyclic loading, to conduct controlled polymerization and crosslinking reactions.

Piezoelectricity offers a unique approach to convert mechanical stimuli into chemical energy by creating redox micro-environments within a polymer matrix through the piezoelectrochemical effect. Previously, our group demonstrated that ultrasonic agitation of piezoelectric $BaTiO_3$ nanoparticles could promote atom transfer radical polymerization (ATRP) of acrylate monomers by reducing a Cu(II) complex to Cu(I) polymerization promoters. Subsequently, others showed that ATRP is compatible with other monomers and other ceramic piezoelectric nanoparticles. This thesis describes (1) the current advances in the application of piezoelectric nanoparticles to initiate or promote polymerization and crosslinking reactions via mechanical activation (i.e., piezo-polymerization), (2) the use of piezo-polymerization as a method to fabricate and reinforce composite polymeric gels, and (3) a current study about mechanically-promoted mineralization of polymeric composites.

Chapter 1: Introduction and background

1.1 Introduction

Synthetic polymers are ubiquitous in almost every aspect of contemporary society. Ever since their discovery in the early 1920s by German chemist Hermann Staudinger, a vast repertoire of polymeric materials and plastics have been developed, with diverse applications in academic research, industry, household goods, transport, health, and electronics. Despite all these advances, this science still faces many challenges both at the fundamental research level as well as in engineering and technological applications.

A particularly relevant challenge with synthetic polymers relates to their life-cycle performance and sustainability. Currently available plastics, which consist mainly of synthetic polymers mixed with organic or inorganic additives, are often disposable, have limited lifespans, need to be replaced with relative frequency, and are not readily recyclable. One of the main contributors to the degradation of polymeric materials is mechanical stress. When a material is subjected to continuous mechanical vibration or deformation, the dissipation of energy usually leads to the breakage of chemical bonds. Over time, the structural defects accumulate, and the material no longer maintains an optimal performance, hence it is disposed and replaced.

In polymeric materials, such as the frame of an airplane in flight or a prosthetic limb, mechanical energy (> 100 J) is continuously transmitted through them, however, it is rarely harnessed for constructive or adaptive purposes.[1-3] In contrast, biological materials display great adaptability to their environment. For example, bones, muscles, and skin can adapt in response to mechanical stimuli by changing their composition and structure through a process called

mechanotransduction. These cellular systems efficiently convert the mechanical stress into chemical signals that can drive reactions leading to structural changes, deposition and removal of material. These adaptive properties give them great advantage in terms of efficiency and durability.[4-9]

Currently, synthetic polymeric materials mostly lack similar adaptability. Significant effort in the literature has been devoted to designing novel chemical systems which impart synthetic polymers with self-reporting and self-healing properties. Several reports have shown the use of heat, light, electricity, pH, and pressure changes to mediate the identification of a failure, deposition of new material, or the formation of new chemical bonds.[10,11] However, there is still much more work to be done to develop mechanoresponsive systems .[12,13] Since mechanical energy is perhaps the most common form of energy experienced by materials, we and others have investigated methods to harness it, in the form of sound, vibration, and cyclic loading, to conduct controlled polymerization and crosslinking reactions. Through these constructive chemistries we aim to provide the material with mechanical adaptability, i.e., self-strengthening.

As a disclaimer, parts of this thesis have been reproduced and adapted from previous peer-reviewed publications and manuscripts in preparation for submission.

1.2 Self-strengthening polymers and mechanochemistry

Self-strengthening polymers, i.e., polymers with the ability to change their physical or chemical structure to adapt to their environment, have potential applications for reinforcement of fiber composites, improvement of the lifetime of structural materials, and prosthetic materials that tailor and fit themselves to individual users or wearers.[14-16] In each of these cases, the common

element is a polymeric material that adjusts its mechanical moduli (elastic, shear, bulk) to fit an applied parameter.

Stimuli-responsive systems, which rely on physical and chemical stimuli, have been extensively studied as a potential solution to the adaptability problem. Several sources of external stimuli such as heat, light, electro-chemical potential, pH, and pressure changes, are commonly applied in the context of autonomic self-healing, microscale patterning, adaptive structural polymers, and on-demand synthesis of functional polymers.[10-12] Because of the chain-like chemical structure of polymers, they are also sensitive to mechanical energy input. The response of polymers to mechanical energy can range from physical effects such as conformational changes, dynamics of polymer chains, and structural rearrangements, to chemical effects such as bond bending, stretching, scission, and formation.[13]

Early studies in the field of polymer mechanochemistry, such as those conducted by Staudinger and others, focused primarily on the chemical effects of continuous mechanical stress.[17-19] Ultrasound and cyclic loading were shown to induce covalent bond scission, which led to the generation of free radicals and thus subsequent degradation reactions. For many decades, mechanical energy was mostly considered degradative in nature.[20-23] In the early 2000s, pioneering work from Scott White, Jeffrey Moore, Nancy Sottos, and others proposed the use of mechanical energy as a constructive stimulus to develop autonomous materials.[24] They developed a polymer composite which incorporated microcapsules containing a healing agent that was released upon crack intrusion. In a separate study, the Moore group showed that mechanically-triggered Bergman cyclization of enediyne macrocycles could generate free-radicals that were subsequently used for polymerization and crosslinking reactions.[25] In the following years, the concept of ‘mechanophores’, polymers with mechano-responsive chemical moieties, was further developed

(Figure 1). This led to a wide variety of systems in which mechanical energy triggered events such as color or pH changes, free-radical generation, acid catalyst generation, ring-opening reactions, metal-catalyst generation, bond rearrangements, etc.[25-36] Although these systems have since shown elegant ways of transducing mechanical energy into chemical energy, they still present significant challenges when intended for widespread use, which includes the incorporation of rather complex synthetic motifs in bulk polymers, low levels of activation in the bulk (< 1 %), and the need for large deformations (ε > 5 %) in order to overcome bond energy and entanglement barriers.

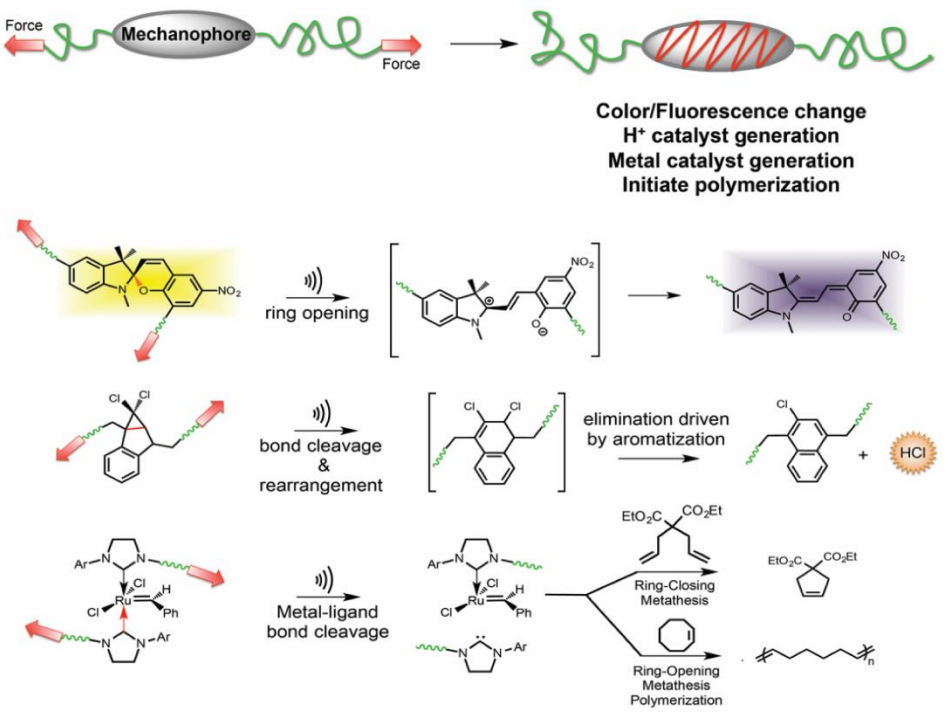

Figure 1. Examples of mechanophore systems used to generate a color change, release of an acid, and activation of a metal-coordination compound for catalysis upon activation with mechanical force. Reprinted with permission from ref. 33 Copyright © 2015, American Chemical Society.

Another approach for conferring adaptability to polymers relies on harnessing the reactivity of mechanoradicals for conducting free-radical mediated chemistries. Mechanoradicals are commonly formed through homolytic scission of polymer chains under the action of mechanical

stress.[34] In a recent example, Matsuda et al. fabricated a double-network acrylamide hydrogel which strengthened under cyclic loading provided by a tensile tester while immersed in a monomer solution (Figure 2).[37] Their system relied on mechanoradical formation from the bond cleavage of a stiff-acrylamide network. These radicals would then react with the monomer and grow new polymer chains. Although a very promising approach, there are still challenges to overcome. As is the case with mechanophores, mechanoradical formation also requires relatively large deformations of the material to induce covalent bond scission. Moreover, the formed radicals are highly reactive species, thus limiting the control over the polymerization kinetics. Finally, most of the reported mechanoradical systems rely on matrices in aqueous environments[37,38], which are not broadly compatible with organic synthetic polymers.

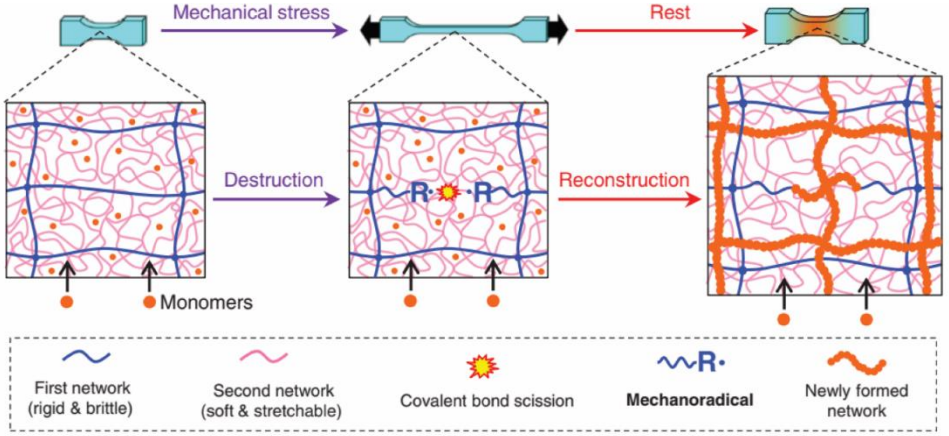

Figure 2. Scheme showing the self-strengthening of a polymer double-network hydrogel via mechanoradical-induced polymerization. Under mechanical stress, the rigid network (blue) breaks while the elastic network (pink) maintains the integrity of the gel. Mechanoradicals generated from the breakage of the rigid network initiate the polymerization of the monomer supply. Reprinted with permission from ref. 37 Copyright © 2019, The American Association for the Advancement of Science.

Within this context, we sought to develop an alternative methodology to overcome these challenges. The main challenge remained harvesting mechanical energy from vibrations

commonly encountered in engineering applications, and then converting it into useful chemical energy for the purpose of polymerization and crosslinking reactions. Piezoelectrically-mediated chemical reactions emerged as viable option.[39]

1.3 Piezoelectrically-mediated chemical reactions

Piezoelectric materials, including inorganic particles, ceramics, organic polymers, and biological materials, have been vastly studied for fabricating sensing and energy harvesting devices.[40,41] Early reports of chemical reactivity mediated with ferroelectric materials studied the effects of charge polarization in the deposition and etching of substances at their surface. Yun and Altman studied the effects of ferroelectric poling on the absorption/desorption kinetics of two polar molecules (acetic acid, 2-propanol) and one non-polar molecule (dodecane) on $LiNbO_3$(0001) surfaces.[42] They showed that the adsorption of acetic acid and 2-propanol (polar compounds) was significantly stronger on the positive surface than on the negative surface, meanwhile, the adsorption of dodecane (non-polar compound) was indifferent of the poling direction (Figure 3a). Calculations of desorption rates showed that there was a difference of 11 orders of magnitude when compared with typical values for small molecules. This was substantial evidence that the adsorption of polar molecules on ferroelectric surfaces was dominated by electrostatic interactions.

Although Yun and Altman had seen differences in adsorption energy and kinetics, there was no evidence of a chemical reaction occurring at these surfaces. Further developments from Giocondi and Rohrer demonstrated that Ag^+ and Pb^{2+} cations in aqueous solutions could be photochemically reduced to Ag^0 and PbO_2, respectively, over $BaTiO_3$ and $Sr_2Nb_2O_7$ microcrystals.[43] They showed that the deposition over the surface of the microcrystals was spatially selective (Figure 3b). They theorized that the generation of photocarriers was affected by

the dipolar fields within the ferroelectric domain structure. Subsequent work by Burbure et al. confirmed such hypothesis.[44-46] Titania films (TiO_2), grown over unpoled, polycrystalline $BaTiO_3$ substrates, were used to photochemically reduce Ag^+/Ag^0 and oxidize Pb^{2+}/Pb^{4+} under UV illumination. Surface characterization showed the deposition of Ag^0 and Pb^{4+} in patterns consistent with the domain structure of the $BaTiO_3$ substrate (Figure 3c). The authors concluded that the dipolar fields from the ferroelectric domains of $BaTiO_3$ generated carriers (electrons and holes) that traveled through the film and caused the reactions at the surface (Figure 3d).

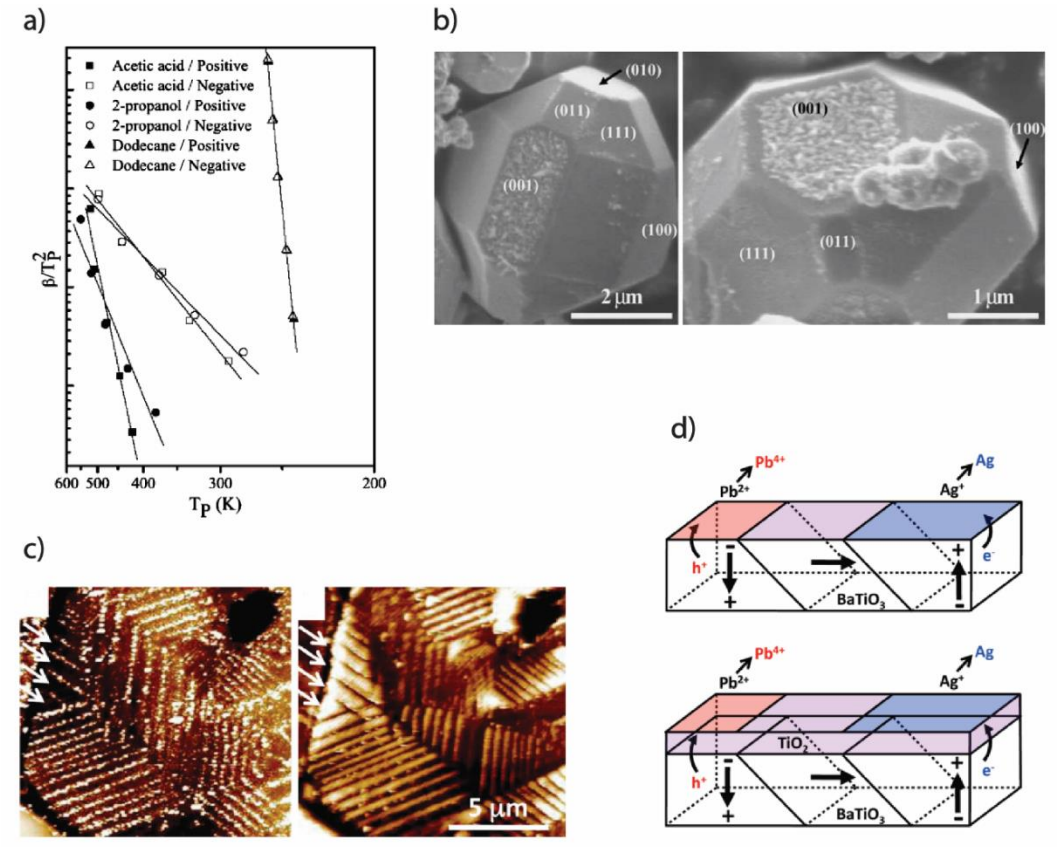

Figure 3. Studies on the influence of ferroelectric materials on chemical reactivity: (a) desorption plots of acetic acid, 2-propanol, and dodecane from positively and negatively poled $LiNbO_3$(0001) surfaces; (b) scanning electron microscopy (SEM) images of Ag^0 deposits on faceted $BaTiO_3$ nanoparticles; (c) atomic force microscopy (AFM) images of a 15 nm thick TiO_2 film surface after reaction with $AgNO_3$ (left) and $Pb(CH_3COO)_2$ (right) aqueous solutions showing Ag^0 and PbO_2 stripes; and (d) schematic illustration of the effect of ferroelectric domains on reactivity in bare

Figure 3 (continued). (top) and film (bottom) surfaces. (a) is reprinted with permission from ref. 42 Copyright © 2007, American Chemical Society. (b) is reprinted with permission from ref. 43 Copyright © 2008, Springer Nature. (c) and (d) are reprinted with permission from ref. 44 Copyright © 2010, American Chemical Society.

The previous studies demonstrated the influence of ferroelectric surfaces on chemical reactivity when using heat or light. In this context, it was also plausible that, in piezoelectric materials, mechanical energy could be harvested and directed to conduct surface mediated reactions in an analogous manner. Hong et al. conducted pioneering experiments in which piezoelectric microfibers under ultrasonication could perform water electrolysis, such process was called the piezoelectrochemical (PzE) effect (Figure 4a).[47] They placed either $BaTiO_3$ or ZnO microdendrites in deionized water (DI water) and subjected the mixture to ultrasound (40 kHz) with a conventional ultrasonic cleaner bath. A linear increase in gas evolution (hydrogen and oxygen) was detected during the sonication. When sonication was stopped, gas evolution was negligible. The study of dendrites with variable size and surface area revealed higher H_2 evolution was achieved with longer dendrites, which was attributed to increased deformability under mechanical vibration and thus higher accumulation of surface charges (Figure 4b).

Further insight into the mechanism of the PzE effect, also referred to as "piezocatalysis", came from Starr et al.[48-50] They developed a system consisting of a single crystalline, poled piezoelectric cantilever made from $Pb(Mg_{1/3}Nb_{2/3})O_3$-$32PbTiO_3$, coated with a gold electrode, embedded in a sealed chamber with DI water, and connected to an actuator with variable frequency and amplitude (Figure 4c). Results showed that H_2 evolution was dependent upon the oscillation frequency and the amplitude (Figure 4d). Additionally, they showed a negative correlation between the concentration of an electrolyte ($NaNO_3$) in water and H_2 evolution. It was theorized

that the electrolyte's spectator ions accumulate at the surface of the piezoelectric material, thus decreasing the capacitive current.

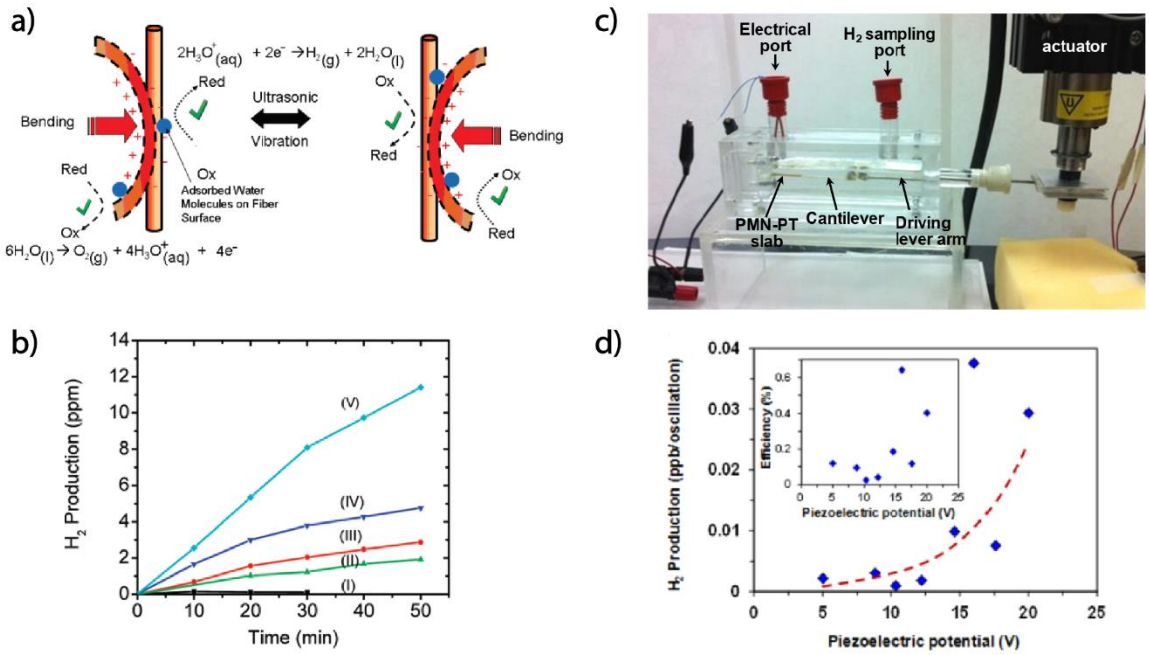

Figure 4. Water splitting via piezocatalysis: (a) scheme showing redox reactions occurring at the surface of strained piezoelectric ZnO microdendrites under ultrasonic vibration; (b) H_2 evolution as a function of ultrasonication time and dendrite length: (I) control or no dendrite, (II) 5.7 μm, (III) 6.3 μm, (IV) 7.3 μm, and (V) 7.8 μm; (c) PMN-PT slab setup for studying water splitting via piezocatalysis; and (d) correlation between H_2 production per oscillation and piezoelectric potential. (a) and (b) are reprinted with permission from ref. 47 Copyright © 2010, American Chemical Society. (c) and (d) are reprinted with permission from ref. 48 Copyright © 2012, WILEY-VCH Verlag GmbH & Co. KGaA, Weinheim.

A model of piezocatalysis on the surface of strained piezoelectric materials was developed by Starr and Wang (Figure 5).[50] The distortion of the particle crystal lattice under mechanical vibration generates a polarization potential at the surface. Such polarization can then alter the energy levels of the conduction (CB) and valence bands (VB) of the material. Assuming the band

gap energy does not change, the mechanical deformation would simultaneously lift and lower the CB and VB energies. Therefore, electrons from the highest occupied molecular orbital (HOMO) of the solution could flow into the CB of the piezoelectric, and electrons from the VB of the piezoelectric could flow into the lowest unoccupied molecular orbital (LUMO) of the solution. Under polarization of the opposite direction, the inverse process would occur. Under such conditions, strained piezoelectric materials could perform reduction and oxidation reactions. From this model, it is evident that the efficiency of the PzE effect is dependent upon the relative energies of the electrode and the HOMO and LUMO of the species in solution. In addition, these energy levels depend on the magnitude of the piezoelectric coefficient and the applied strain.

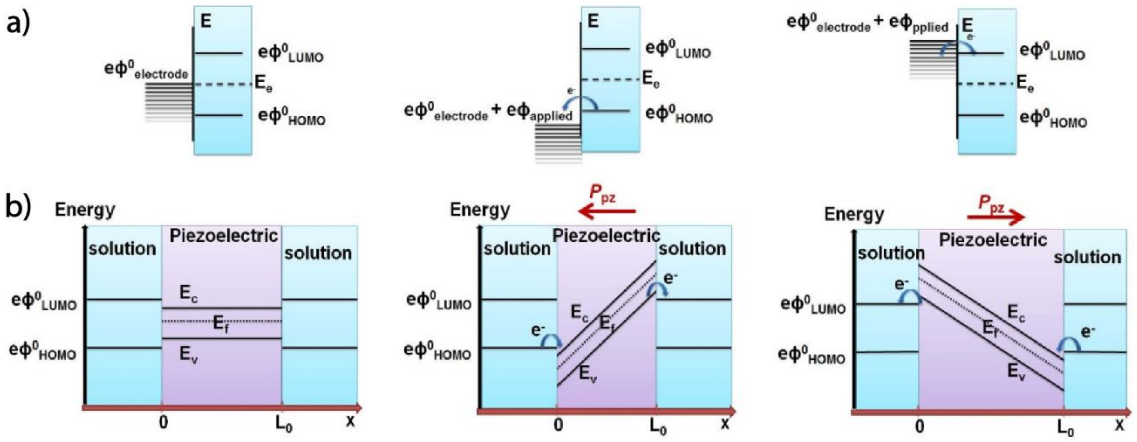

Figure 5. Energy diagram schemes describing (a) a conventional electrochemical process and (b) piezocatalysis. Reprinted with permission from ref. 50 Copyright © 2013, Springer Nature.

In a subsequent study from Hong et al., the application of the PzE effect was expanded to dye degradation in aqueous solution under ultrasonication.[51] Solutions of azo dyes were mixed with $BaTiO_3$ microdendrites and subjected to ultrasonication (40 kHz). Moderate to high degradation efficiencies (60 - 80 %) were achieved for dyes in the μM concentration range. The proposed mechanism involved the generation of $H^{\cdot}$ and $OH^{\cdot}$ radicals resulting from the

accumulation of charge carriers (electrons and holes) at the surface of the microdendrites, which would subsequently react with the dye and lead to degradation products. The formation of radical species in water due to piezocatalysis was confirmed by Zhu et al.[52] In this study, piezoelectric microfibers of $0.5Ba(Zr_{0.2}Ti_{0.8})O_3$-$0.5(Ba_{0.7}Ca_{0.3})TiO_3$ were used to degrade rhodamine B dye in aqueous solutions. Magnetic stirring was shown to also drive the PzE effect. The formation of hydroxy radicals was detected via their reaction with terephthalic acid to form the highly fluorescent product 2-hydroxyterephthalic acid. Additionally, the formation of superoxide anion radicals $\cdot O_2^-$ was detected via their reaction with benzoquinone. This work showed that low frequency mechanical energy could also be harnessed for the purpose of piezocatalysis, although much longer times were required for high conversion (Figure 6).

Piezoelectric microdendrites were preferably used for piezocatalysis based on the assumption that their anisotropy and deformability would generate higher polarization under mechanical vibration. Similarly, Yu et al. demonstrated that 2D $KNbO_3$ nanosheets exhibited higher piezo-photocatalytic activity compared to that of the nanocubes.[53] The computer simulation suggested the easier deformation of nanosheets under stress as the cause. In another example, single-layer MoS_2 nanoflowers showed ultrahigh degradation activity under ultrasonication.[54] However, in principle, spherical particles could also be subjected to shear forces and generate a sufficient potential to promote chemical reactivity. Feng et al. showed that spherical lead zirconate titanate (PZT) microparticles doped with Bi and Fe degraded rhodamine B in aqueous solutions under stirring, achieving moderate conversions (10-40 %).[55] Interestingly, undoped particles showed negligible conversions (0-5 %). The lack of reactivity was attributed to the absence of defects and free charges. They argued that the piezoelectric potential generated solely from

polarized charges within particles of similar surface area and composition was insufficient to generate redox active species at their surface.

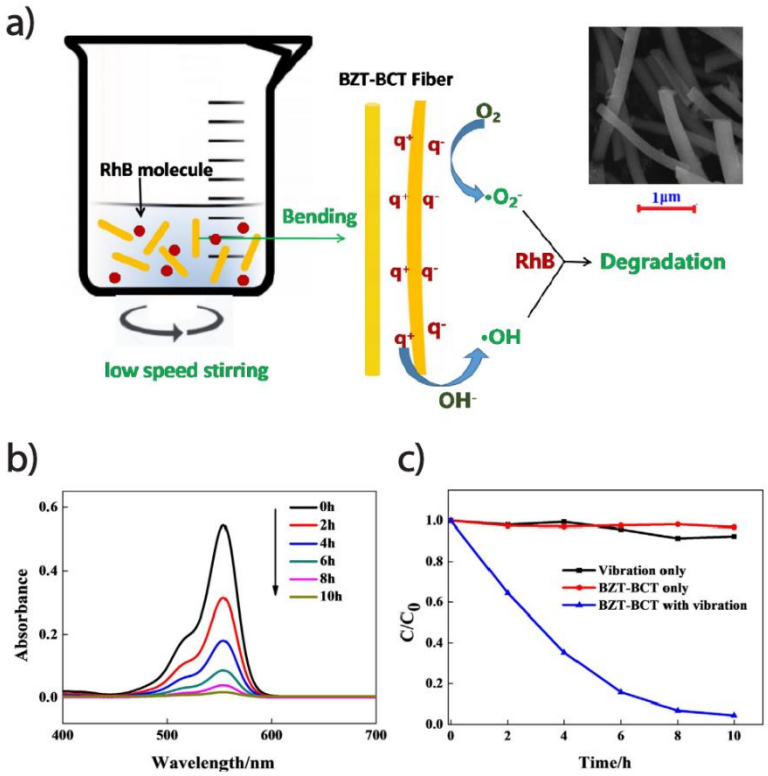

Figure 6. Dye degradation via piezocatalysis with BZT-BCT microfibers under low frequency vibrations: (a) scheme showing the formation of piezo-generated radicals in water which subsequently degrade rhodamine B dye; (b) UV-vis spectra showing the decrease in peak intensity as a function of agitation time; and (c) control reactions showing the degradation of rhodamine B only occurs with the combination of piezoelectric microfibers and mechanical agitation. Reprinted with permission from ref. 51 Copyright © 2018 Elsevier B.V.

A recent study by Kubota et al. showed an example of a mechano-redox system with small organic molecules.[56] Using a ball-mill and $BaTiO_3$ nanoparticles, they conducted several coupling reactions between aryl diazonium salts and either heteroarenes or borolanes. They explored the

effects of the choice of nanoparticles, milling frequency, solvent, and atmosphere conditions with regards to reaction yield. Their optimized method was easily scaled-up to gram scale synthesis with high yields (60-85 %) and applicable to a wide variety of aryl diazonium compounds. Moreover, they demonstrated that the mechanism proceeded via piezocatalytic reduction of the aryl diazonium salt by using 2,2,6,6-tetramethylpiperidinoxyl (TEMPO) to trap intermediate radical species. Kubota's study showed that organic molecules could be directly affected via piezoelectrochemistry and proposed a methodology to do an easy screening of potential reactions.

In summary, piezoelectric particles were shown to transduce mechanical energy into chemical energy via surface-mediated electron transfer processes. This is an advantageous method to harness environmental vibrations with a wide range of frequencies and redirect them for useful chemical processes. Although the PzE effect was large enough to be measured consistently, the conversion efficiencies were on the low end in practical terms considering the concentrations of the reactants. Also, most of the reports focused on aqueous systems, which are not always compatible with organic or polymerization reactions. The choice of an appropriate solvent is critical since there is most likely a trade-off between the PzE effect and chemical thermodynamics and kinetics. Moreover, the exact mechanism by which PzE operates remains open for investigation. The effects of several factors related to the piezoelectric particles need be thoroughly assessed, such as particle composition, morphology, surface area, crystal structure, band gap, and doping. Finally, the correlation between the source of mechanical energy (frequency and amplitude) and the PzE effect still requires a systematic investigation. The calculation of the mechanical stress experienced by the particles under various conditions could be a proxy for the intensity of the PzE effect.

1.4 Piezoelectrochemistry for self-strengthening polymers

The PzE effect emerged as a method to directly convert mechanical energy into chemical energy. Several examples in the literature showed it could be used to modify adsorption/desorption properties of organic molecules[42], perform redox reactions on metal ions[43-46,48-50], conduct water electrolysis[47,57-62], degrade organic molecules in aqueous solutions[51-55,63-66], and perform organic synthesis of small molecules[56]. Our group sought to take advantage of this effect and redirect it to mediate polymerization reactions. The goal was to develop a methodology by which environmental vibrations, which are often detrimental for materials in the long term, could be harnessed to mediate constructive chemistries, and thus provide a polymeric material with adaptive capabilities. Unlike previously studied mechanophores, the PzE effect offered various advantages from a materials science perspective. Piezoelectric particles are able to harness a wider range of vibrations ($1 – 10^6$ Hz) than conventional mechanophores and can also be used for accurate sensing purposes.[40] Moreover, they are low-cost materials that can be readily incorporated into polymeric matrices to form composites, which in turn allows the modulation of their mechanical properties.[41]

Past examples in the literature reported high conversions but only at μM or mM concentrations, thus attempting bulk-scale organic reactions was challenging. In a pioneering work, Mohaptra et al. used the PzE effect to generate a catalytic amount of $Cu(I)L_n$ *in situ* which would then promote ATRP of acrylates.[67] Briefly, a Cu(II) salt with tris[2-(dimethylamino)ethyl]amine (Me_6TREN) as ligand was mixed with ethyl α-bromoisobutyrate (EBiB) initiator, butyl acrylate (BA) and $BaTiO_3$ (Φ = 200 nm, tetragonal) nanoparticles in dimethyl formamide (DMF), and the mixture was sonicated with an ultrasound probe (20 kHz) under inert atmosphere (Figure 7a). The nanoparticles were chosen to maximize surface area and thus enhance reaction kinetics. Poly (butyl acrylate) with a number-average molecular weight (M_n)

of 3 kDa and low dispersity (M_w/M_n) Đ = 1.15 was formed in 6 h. The maximum bulk temperature of the reaction mixture after sonication was between 40-50 °C. Kinetics analysis revealed a first-order polymerization, thus confirming a controlled-radical polymerization mechanism (Figure 7b).

The reaction presented two plausible mechanisms. In the first possibility, the piezopotential at the surface of the nanoparticles would promote a single-electron transfer to the Cu(II) complex to form a Cu(I)-based activator. This would in turn react with the alkyl halide initiator and act as a chain transfer agent. The second possibility was that the sonication itself would form radicals via cavitation.[68] Control reactions in the absence of Cu(II) pre-catalyst, particles, sonication, and substitution of $BaTiO_3$ with non-piezoelectric nanoparticles (carbon black) showed little monomer conversion, thus supporting the hypothesis of a PzE effect-mediated reaction. Further experiments with UV-VIS and electron paramagnetic resonance (EPR) spectroscopies showed the consumption of the Cu(II) complex and the presence of radical species after sonication. It was unclear though whether the solvent and/or the ligand acted as sacrificial electron donors.

Studies conducted by Wang et al. optimized the piezoelectrically-mediated ATRP system (mechano-ATRP).[69,70] The ultrasound probe was substituted with an ultrasound bath (40 kHz), which enabled faster and more homogenous screening of reactions. Tris(2-pyridylmethyl)amine (TPMA) proved a better ligand for stabilizing the Cu(I) complex than Me_6TREN. Dimethyl sulfoxide (DMSO) was chosen as solvent to enhance the solubility of $CuBr_2$ and facilitate electron transfer processes. Various loadings of $BaTiO_3$ nanoparticles were tested. Under these optimized conditions, high molecular weight poly(methyl acrylate) (M_n 10-20 kDa) was synthesized. ON-OFF experiments showed temporal control of the polymerization (Figure 7c).[69] It was also shown that ZnO nanoparticles (Φ = 18 nm) could generate Cu(I) activators for polymerization, even at

significantly lower loadings than $BaTiO_3$. This was attributed to enhanced interfacial interactions between ZnO and Cu(II) pre-catalyst complex (Figure 7d).[70]

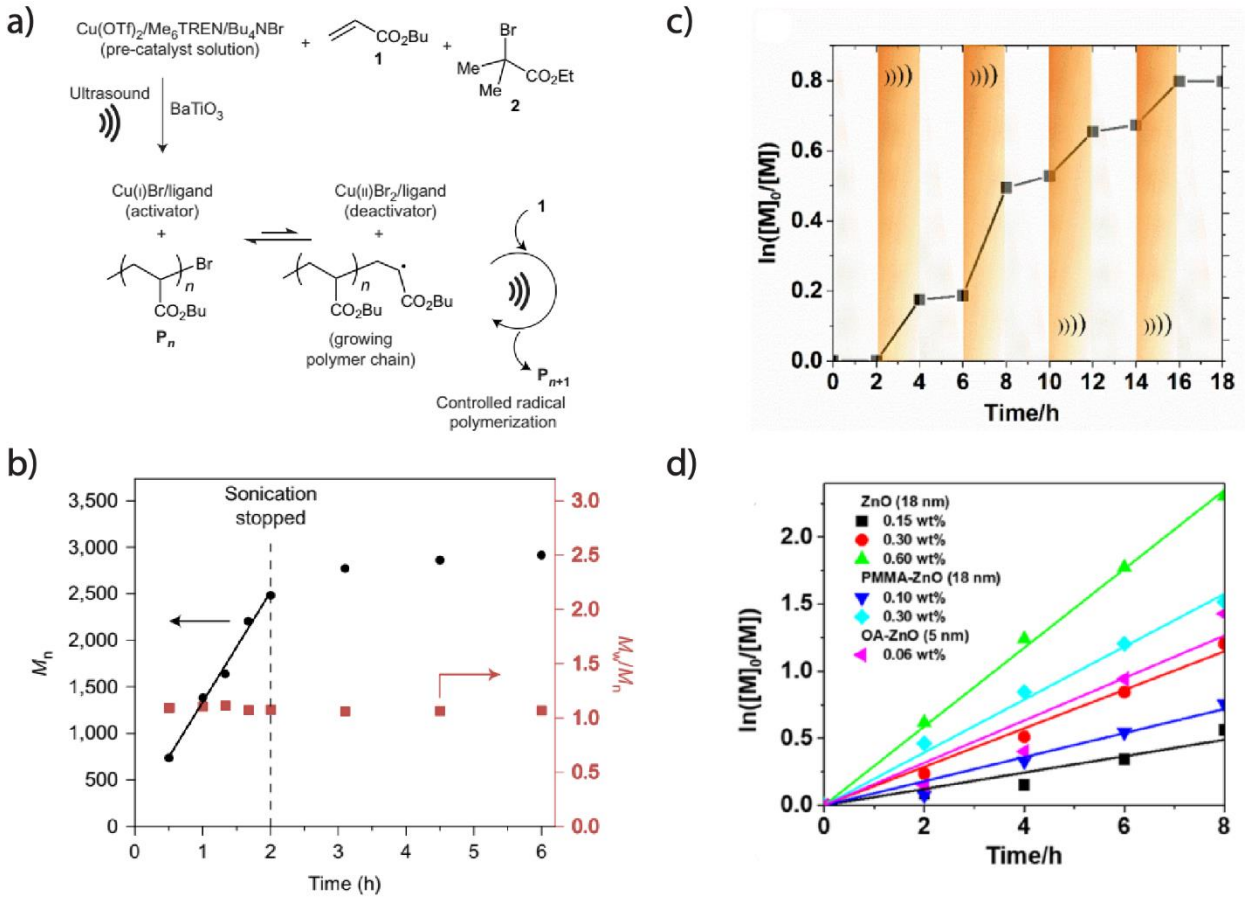

Figure 7. Mechano-ATRP system: (a) ultrasound-induced controlled radical polymerization of butyl acrylate via piezo-reduction of a Cu(II) complex with $BaTiO_3$ NPs in DMF; (b) evolution of M_n and Đ as a function of reaction time in a representative mechano-ATRP polymerization; (c) temporal control in mechano-ATRP under optimized conditions; and (d) reaction kinetics plot of mechano-ATRP of methyl acrylate with ZnO NPs under various nanoparticle loadings. (a) and (b) are reprinted with permission from ref. 67 Copyright © 2016, Springer Nature. (c) is reprinted with permission from ref. 69 Copyright © 2017, American Chemical Society. (d) is reprinted with permission from ref. 70 Copyright © 2017, American Chemical Society.

Further mechanistic insight was provided with cyclic voltammetry (CV) measurements of the reactants and zeta potential ζ measurements of the nanoparticles.[70] CV analysis showed that the oxidation potential of TPMA (+1.04 V vs SCE) was lower than for DMSO (+1.54 V vs SCE). Therefore, it was possible for the ligand to act as sacrificial electron donor. The value of ζ_{ZnO} remained approximately constant during the course of the reaction, indicating charges were properly balanced. A sonication experiment with an alternative Cu(II) salt, $Cu(OTf)_2$ instead of $CuBr_2$, showed higher conversion, meaning that ultrasound induced homolytic cleavage of Cu-Br bromide was not dominating the reaction mechanism. Another experiment involving the sonication of EBiB alone with ZnO nanoparticles showed no degradation products. All in all, these experiments served to corroborate a reaction mechanism dominated by the PzE effect.

Table 1. Selected examples of piezoelectrically-mediated chemistries.[39]

Reaction	Piezoelectric material	Mechanical energy source	Remarks	Ref.
Water splitting	$BaTiO_3$ and ZnO microdendrites	US (40 kHz)	First example of piezocatalysis.	47
	PMN-PT slab	Electrodynamic shaker (10, 20 Hz)	Correlation between piezocatalysis and oscillation frequency and amplitude.	48
Dye degradation (acid orange 7)	$BaTiO_3$ microdendrites (tetragonal)	US (40 kHz)	First example of piezocatalysis for dye degradation.	51
Dye degradation (rhodamine B)	BZT-BCT microfibers	Magnetic stirring (2-12 r/s)	-Piezocatalysis with low frequency vibrations. -Detection of radical species from piezocatalytic redox reactions in water.	52
	$KNbO_3$ nanosheets and nanocubes	US (40 kHz)	2D nanostructures have higher piezocatalytic efficiency.	53
	MoS_2 nanoflowers	US (40 kHz)	High piezocatalytic efficiency with complex nanostructures.	54
	$BiFeO_3$ microsheets	US (40 kHz)	Piezocatalysis with multiferroic nanomaterials.	62
	Doped PZT-Bi,Fe microparticles	Magnetic stirring (200-900 rpm)	Doping ceramic microparticles enhances piezocatalysis.	55
Water splitting and Dye degradation (rhodamine B)	$BaTiO_3$ NPs (spherical, cubes, dendrites)	US (10-60 kHz)	Comparison of piezocatalytic efficiency of various $BaTiO_3$ nanostructures and US frequencies.	57
Pollutant degradation (4-chlorophenol)	$BaTiO_3$ and Ag/$BaTiO_3$ NPs (cubic, tetragonal)	US (40 kHz)	Expanding piezocatalysis for environmental remediation.	65
ATRP (butyl acrylate)	$BaTiO_3$ spherical NPs (tetragonal)	US (20 kHz)	First example of piezo-polymerization: PBA: M_n = 3 kDa, Đ = 1.15	67
ATRP (methyl acrylate)	$BaTiO_3$ spherical NPs (cubic, tetragonal)	US (40 kHz)	-Optimized mechano-ATRP conditions: PMA: M_n = 20 kDa, Đ = 1.06 -Temporal control of polymerization.	69
ATRP (various acrylates)	ZnO spherical NPs	US (40 kHz)	-Various polyacrylates: PMA: M_n = 16 kDa, Đ = 1.06 PBA: M_n = 18 kDa, Đ = 1.08 PEA: M_n = 19 kDa, Đ = 1.06 PMMA: M_n = 12 kDa, Đ = 1.24 - Lower NP loading. -Mechanistic study of piezocatalysis.	70

Mechano-ATRP was the first step in developing a strategy to use piezo-polymerization for conferring adaptability to synthetic polymeric materials. An alternative approach used the PzE effect to change the mechanical properties of a polymer composite. A study by Orrego et al. targeted mineralization at the surface of organic polymeric materials to emulate bone.[71] They immersed a piezoelectric polymer (polyvinylidene difluoride, PVDF $d_{31} \approx 23$ pC N^{-1}) in a simulated body fluid and subjected the material to external mechanical loading. After one-week incubation, they detected mineral deposition (calcite and hydroxyapatite) predominantly in the negatively charged surface of the material (Figure 8). A porous scaffold made of electrospun PVDF fibers ($d_{33} \approx 2$ pC N^{-1}) subjected to the same conditions showed a 30 % increase in modulus (E) and 100 % increase in toughness after 3 days, thus displaying adaptive properties.

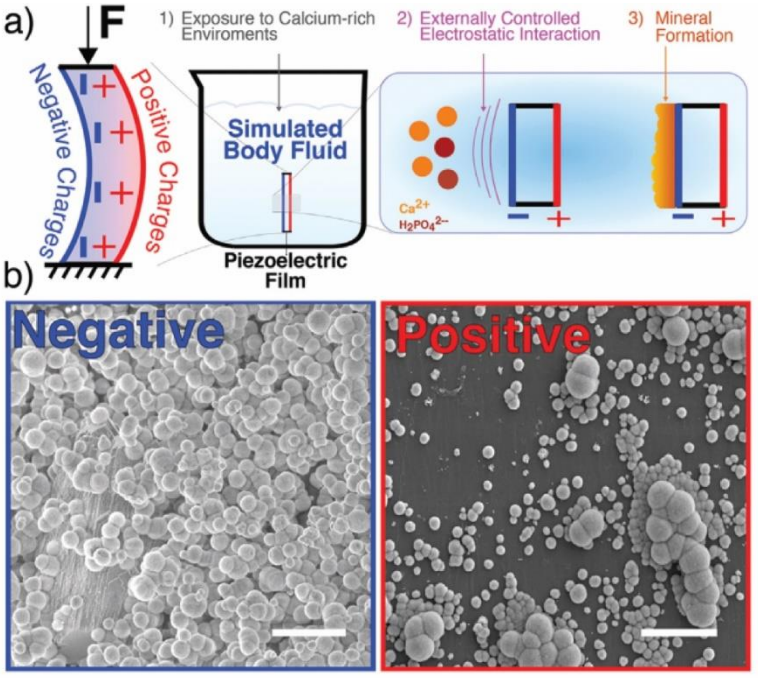

Figure 8. (a) Piezoelectrically-promoted mineralization over the surface of PVDF films under mechanical loading while submerged in a simulated body fluid. (b) SEM images of the negative and positive sides of the film, showing increased mineral deposition on the negative side. Scale bars 10 μm. Reprinted from ref. 71 Copyright © 2020, WILEY-VCH Verlag GmbH & Co. KGaA, Weinheim.

In summary, our group and others have developed pioneering methods to harness the PzE effect in order to conduct constructive chemistries. Piezoelectricity offers a unique approach to convert mechanical energy into chemical energy by creating redox micro-environments within a polymer matrix. This thesis describes (1) the current advances in the application of piezoelectric nanoparticles to initiate or promote polymerization and crosslinking reactions via mechanical activation (i.e., piezo-polymerization), (2) the use of piezo-polymerization as a method to fabricate and reinforce composite polymeric gels, and (3) a current study about mechanically-promoted mineralization of polymeric composites.

1.5 References

1. Wojtecki, R. J.; Meador, M. A.; Rowan, S. J., Using the dynamic bond to access macroscopically responsive structurally dynamic polymers. *Nature Materials* **2011,** *10*, 14-27.

2. Suslick, K. S.; Price, G. J., Applications of Ultrasound to Materials Chemistry. *Annual Review of Materials Science* **1999**, *29*, 295-326.

3. Dultsev, F. N.; Ostanin, V. P.; Klenerman, D., "Hearing" Bond Breakage. Measurement of Bond Rupture Forces Using a Quartz Crystal Microbalance. *Langmuir* **2000**, *16*, 5036-5040.

4. Huang, H.; Kamm, R. D.; Lee, R. T., Cell mechanics and mechanotransduction: pathways, probes, and physiology. *American Journal of Physiology-Cell Physiology* **2004**, *287*, C1-C11.

5. Parfitt, A. M., Trabecular bone architecture in the pathogenesis and prevention of fracture. *The American Journal of Medicine* **1987**, *82*, 68-72.

6. Huiskes, R.; Weinans, H.; Grootenboer, H. J.; Dalstra, M.; Fudala, B.; Slooff, T. J., Adaptive bone-remodeling theory applied to prosthetic-design analysis. *Journal of Biomechanics* **1987**, *20*, 1135-1150.

7. Weinans, H.; Huiskes, R.; Grootenboer, H. J., The behavior of adaptive bone-remodeling simulation models. *Journal of Biomechanics* **1992**, *25*, 1425-1441.

8. Christen, P.; Ito, K.; Ellouz, R.; Boutroy, S.; Sornay-Rendu, E.; Chapurlat, R. D.; van Rietbergen, B., Bone remodelling in humans is load-driven but not lazy. *Nature Communications* **2014**, *5*, 4855.

9. Chen, J.-H.; Liu, C.; You, L.; Simmons, C. A., Boning up on Wolff's Law: Mechanical regulation of the cells that make and maintain bone. *Journal of Biomechanics* **2010**, *43*, 108-118.

10. Roy, D.; Cambre, J. N.; Sumerlin, B. S., Future perspectives and recent advances in stimuli-responsive materials. *Progress in Polymer Science* **2010**, *35*, 278-301.

11. Hager, M. D.; van der Zwaag, S.; Schubert, U. S., *Self-healing Materials*. Springer International Publishing: 2016.

12. Hsu, L.; Weder, C.; Rowan, S. J. Stimuli-responsive, mechanically-adaptive polymer nanocomposites. *J. Mater. Chem.* **2011**, *21*, 2812-2822.

13. Brighenti, R.; Li, Y., Vernerey, F. J. Smart Polymers for Advanced Applications: A Mechanical Perspective Review. *Front. Mater.* **2020**, *7*, 196.

14. Kida, J.; Aoki, D.; Otsuka, H. Self-Strengthening of Cross-Linked Elastomers via the Use of Dynamic Covalent Macrocyclic Mechanophores. *ACS Macro Letters.* **2021**, *10*, 5, 558–563.

15. Ramirez, A.; Kean, Z.; Orlicki, J.; Champhekar, M.; Elskar, S. M.; Krause, W. E.; Craig, S. L. Mechanochemical strengthening of a synthetic polymer in response to typically destructive shear forces. *Nature Chemistry* **2013**, *5*, 757–761.

16. Xu, Z.; Fan, C.; Zhang, Q.; Liu, Y.; Cui, C.; Liu, B.; Wu, T.; Zhang, X.; Liu, W. A Self-Thickening and Self-Strengthening Strategy for 3D Printing High-Strength and Antiswelling Supramolecular Polymer Hydrogels as Meniscus Substitutes. *Advanced Functional Materials* **2021**, *31*, 2100462.

17. Staudinger, H.; Bondy, H., Isoprene and rubber. XIX. The molecular size of rubber and balata. *Rubber Chemistry and Technology* **1930**, *3*, 519-521.

18. Staudinger, H.; Leupold, E., Isoprene and rubber. XVIII. Studies of the viscosity of balata. *Ber. Dtsch. Chem. Ges. B* **1930**, *63*, 730-733.

19. Staudinger, H.; Heuer, W., Highly polymerized compounds. *XCIV. An insoluble polystyrene. Ber. B* **1934**, *67*, 1164-1172.

20. Melville, H. W.; Murray, A. J. R., The ultrasonic degradation of polymers. *Transactions of the Faraday Society* **1950**, *46*, 996-1009.

21. Culter, J. D.; Zakin, J. L.; Patterson, G. K., Mechanical degradation of dilute solutions of high polymers in capillary tube flow. *Journal of Applied Polymer Science* **1975,** *19*, 3235-3240.

22. Basedow, A. M.; Ebert, K. H. In *Ultrasonic degradation of polymers in solution*, Berlin, Heidelberg, Springer Berlin Heidelberg: Berlin, Heidelberg, 1977; pp 83-148.

23. Horn, A. F.; Merrill, E. W., Midpoint scission of macromolecules in dilute solution in turbulent flow. *Nature* **1984**, *312*, 140-141.

24. White, S. R.; Sottos, N. R.; Geubelle, P. H.; Moore, J. S.; Kessler, M. R.; Sriram, S. R.; Brown, E. N.; Viswanathan, S., Autonomic healing of polymer composites. *Nature* **2001**, *409*, 794-797.

25. Rule, J. D.; Wilson, S. R.; Moore, J. S., Radical Polymerization Initiated by Bergman Cyclization. *Journal of the American Chemical Society* **2003**, *125*, 12992-12993.

26. Sohma, J., Mechanochemistry of polymers. *Progress in Polymer Science* **1989**, *14*, 451-596.

27. Hickenboth, C. R.; Moore, J. S.; White, S. R.; Sottos, N. R.; Baudry, J.; Wilson, S. R., Biasing reaction pathways with mechanical force. *Nature* **2007**, *446*, 423-427.

28. Piermattei, A.; Karthikeyan, S.; Sijbesma, R. P., Activating catalysts with mechanical force. *Nature Chemistry* **2009**, *1*, 133-137.

29. Caruso, M. M.; Davis, D. A.; Shen, Q.; Odom, S. A.; Sottos, N. R.; White, S. R.; Moore, J. S., Mechanically-Induced Chemical Changes in Polymeric Materials. *Chemical Reviews* **2009**, *109*, 5755-5798.

30. Black, A. L.; Lenhardt, J. M.; Craig, S. L., From molecular mechanochemistry to stress-responsive materials. *Journal of Materials Chemistry* **2011**, *21*, 1655-1663.

31. Black, A. L.; Orlicki, J. A.; Craig, S. L. Mechanochemically triggered bond formation in solid-state polymers. *Journal of Materials Chem*istry **2011**, *21*, 8460-8465.

32. Larsen, M. B.; Boydston, A. J., "Flex-Activated" Mechanophores: Using Polymer Mechanochemistry To Direct Bond Bending Activation. *Journal of the American Chemical Society* **2013**, *135*, 8189-8192.

33. Li, J.; Nagamani, C.; Moore, J. S., Polymer Mechanochemistry: From Destructive to Productive. *Accounts of Chemical Research* **2015**, *48*, 2181-2190.

34. Chen, Y.; Mellot, G.; van Luijk, D.; Creton, C.; Sijbesma, R. P. Mechanochemical tools for polymer materials. *Chemical Society Reviews* **2021**, *50*, 4100-4140.

35. Wang, J.; Piskun, I.; Craig, S. L. Mechanochemical Strengthening of a Multi-mechanophore Benzocyclobutene Polymer. *ACS Macro Letters* **2015**, *4*, 834-837.

36. Zhang, H.; Gao, F.; Cao, X.; Li, Y.; Xu, Y.; Weng, W.; Boulatov, R. Mechanochromism and Mechanical-Force-Triggered Cross-Linking from a Single Reactive Moiety Incorporated into Polymer Chains. *Angewwandte Chemie International Edition* **2016**, *55*, 3040-3044.

37. Matsuda, T.; Kawakami, R.; Namba, R.; Nakajima, T.; Gong, J. P., Mechanoresponsive self-growing hydrogels inspired by muscle training. *Science* **2019**, *363*, 504-508.

38. Wang, Z. J.; Jiang, J.; Mu, Q.; Maeda, S.; Nakajima, T; Gong, J. P. Azo-Crosslinked Double-Network Hydrogels Enabling Highly Efficient Mechanoradical Generation. *Journal of the American Chemical Society* **2022**, *144* (7), 3154–3161.

39. Ayarza, J; Wang, Z.; Wang, J; Huang, C. and Esser-Kahn, A. P. 100th Anniversary of Macromolecular Science Viewpoint: Piezoelectrically Mediated Mechanochemical Reactions for Adaptive Materials. *ACS Macro Letters* **2020**, *9*, 1237–1248.

40. Tressler, J. F.; Alkoy, S.; Newnham, R. E., Piezoelectric Sensors and Sensor Materials. *Journal of Electroceramics* **1998**, *2*, 257-272.
41. Briscoe, J.; Dunn, S., Piezoelectric nanogenerators – a review of nanostructured piezoelectric energy harvesters. *Nano Energy* **2015**, *14*, 15-29.

42. Yun, Y.; Altman, E. I., Using Ferroelectric Poling to Change Adsorption on Oxide Surfaces. *Journal of the American Chemical Society* **2007**, *129*, 15684-15689.

43. Giocondi, J. L.; Rohrer, G. S., The Influence of the Dipolar Field Effect on the Photochemical Reactivity of $Sr_2Nb_2O_7$ and $BaTiO_3$ Microcrystals. *Topics in Catalysis* **2008**, *49*, 18-23.

44. Burbure, N. V.; Salvador, P. A.; Rohrer, G. S., Photochemical Reactivity of Titania Films on $BaTiO_3$ Substrates: Origin of Spatial Selectivity. *Chemistry of Materials* **2010**, *22*, 5823-5830.

45. Bhardwaj, A.; Burbure, N. V.; Gamalski, A.; Rohrer, G. S., Composition Dependence of the Photochemical reduction of Ag by $Ba_{1-x}Sr_xTiO_3$. *Chemistry of Materials* **2010**, *22*, 3527-3534.

46. Bhardwaj, A.; Burbure, N. V.; Rohrer, G. S., Enhanced Photochemical Reactivity at the Ferroelectric Phase Transition in $Ba_{1-x}Sr_xTiO_3$. *Journal of the American Ceramic Society* **2010**, *93*, 4129-4134.

47. Hong, K.-S.; Xu, H.; Konishi, H.; Li, X., Direct Water Splitting Through Vibrating Piezoelectric Microfibers in Water. *The Journal of Physical Chemistry Letters* **2010**, *1*, 997-1002.

48. Starr, M. B.; Shi, J.; Wang, X., Piezopotential-Driven Redox Reactions at the Surface of Piezoelectric Materials. *Angewandte Chemie International Edition* **2012**, *51*, 5962-5966.

49. Starr, M. B.; Wang, X., Coupling of piezoelectric effect with electrochemical processes. *Nano Energy* **2015**, *14*, 296-311.

50. Starr, M. B.; Wang, X., Fundamental Analysis of Piezocatalysis Process on the Surfaces of Strained Piezoelectric Materials. *Scientific Reports* **2013**, *3*, 2160.

51. Hong, K.-S.; Xu, H.; Konishi, H.; Li, X., Piezoelectrochemical Effect: A New Mechanism for Azo Dye Decolorization in Aqueous Solution through Vibrating Piezoelectric Microfibers. *The Journal of Physical Chemistry C* **2012**, *116*, 13045-13051.

52. Zhu, R.; Xu, Y.; Bai, Q.; Wang, Z.; Guo, X.; Kimura, H., Direct degradation of dyes by piezoelectric fibers through scavenging low frequency vibration. *Chemical Physics Letters* **2018**, *702*, 26-31.

53. Yu, D.; Liu, Z.; Zhang, J.; Li, S.; Zhao, Z.; Zhu, L.; Liu, W.; Lin, Y.; Liu, H.; Zhang, Z., Enhanced catalytic performance by multi-field coupling in $KNbO_3$ nanostructures: Piezo-photocatalytic and ferro-photoelectrochemical effects. *Nano Energy* **2019**, *58*, 695-705.

54. Wu, J. M.; Chang, W. E.; Chang, Y. T.; Chang, C.-K., Piezo-Catalytic Effect on the Enhancement of the Ultra-High Degradation Activity in the Dark by Single- and Few-Layers MoS_2 Nanoflowers. *Advanced Materials* **2016**, *28*, 3718-3725.

55. Feng, Y.; Ling, L.; Wang, Y.; Xu, Z.; Cao, F.; Li, H.; Bian, Z., Engineering spherical lead zirconate titanate to explore the essence of piezo-catalysis. *Nano Energy* **2017**, *40*, 481-486.

56. Kubota, K.; Pang, Y.; Miura, A.; Ito, H., Redox reactions of small organic molecules using ball milling and piezoelectric materials. *Science* **2019**, *366*, 1500-1504.

57. Su, R.; Hsain, H. A.; Wu, M.; Zhang, D.; Hu, X.; Wang, Z.; Wang, X.; Li, F.-t.; Chen, X.; Zhu, L.; Yang, Y.; Yang, Y.; Lou, X.; Pennycook, S. J., Nano-Ferroelectric for High Efficiency Overall Water Splitting under Ultrasonic Vibration. *Angewandte Chemie International Edition* **2019**, *58*, 15076-15081.

58. Wu, J. M.; Sun, Y.-G.; Chang, W.-E.; Lee, J.-T., Piezoelectricity induced water splitting and formation of hydroxyl radical from active edge sites of MoS_2 nanoflowers. *Nano Energy* **2018**, *46*, 372-382.

59. Chen, Y.; Wang, L.; Gao, R.; Zhang, Y.-C.; Pan, L.; Huang, C.; Liu, K.; Chang, X.-Y.; Zhang, X.; Zou, J.-J., Polarization-Enhanced direct Z-scheme ZnO-WO_{3-x} nanorod arrays for efficient piezoelectric-photoelectrochemical water splitting. *Applied Catalysis B: Environmental* **2019**, *259*, 118079.

60. Bai, Y.; Zhao, J.; Lv, Z.; Lu, K., Enhanced piezo-phototronic effect of ZnO nanorod arrays for harvesting low mechanical energy. *Ceramics International* **2019**, *45*, 15065-15072.

61. Tong, W.; Zhang, Y.; Huang, H.; Xiao, K.; Yu, S.; Zhou, Y.; Liu, L.; Li, H.; Liu, L.; Huang, T.; Li, M.; Zhang, Q.; Du, R.; An, Q., A highly sensitive hybridized soft piezophotocatalyst driven by gentle mechanical disturbances in water. *Nano Energy* **2018**, *53*, 513-523.

62. You, H.; Wu, Z.; Zhang, L.; Ying, Y.; Liu, Y.; Fei, L.; Chen, X.; Jia, Y.; Wang, Y.; Wang, F.; Ju, S.; Qiao, J.; Lam, C.-H.; Huang, H., Harvesting the Vibration Energy of $BiFeO_3$ Nanosheets for Hydrogen Evolution. *Angewandte Chemie International Edition* **2019**, *58*, 11779-11784.

63. Sun, Q.; Li, J.; Yan, Z.; Zhang, X.; Le, T., Facile synthesis of zinc oxide crystal and insight into its morphological effect on organic dye photodegradation in water. *Applied Nanoscience* **2019**, *9*, 93-103.

64. Lin, H.; Wu, Z.; Jia, Y.; Li, W.; Zheng, R.-K.; Luo, H., Piezoelectrically induced mechano-catalytic effect for degradation of dye wastewater through vibrating $Pb(Zr_{0.52}Ti_{0.48})O_3$ fibers. *Applied Physics Letters* **2014**, *104*, 162907.

65. Lan, S.; Feng, J.; Xiong, Y.; Tian, S.; Liu, S.; Kong, L., Performance and Mechanism of Piezo-Catalytic Degradation of 4-Chlorophenol: Finding of Effective Piezo-Dechlorination. *Environmental Science & Technology* **2017**, *51*, 6560-6569.

66. Liang, Z.; Yan, C.-F.; Rtimi, S.; Bandara, J., Piezoelectric materials for catalytic/photocatalytic removal of pollutants: Recent advances and outlook. *Applied Catalysis B: Environmental* **2019**, *241*, 256-269.

67. Mohapatra, H.; Kleiman, M.; Esser-Kahn, A. P., Mechanically controlled radical polymerization initiated by ultrasound. *Nature Chemistry* **2017**, *9*, 135-139.

68. Mišík, V.; Riesz, P., EPR study of free radicals induced by ultrasound in organic liquids II. Probing the temperatures of cavitation regions. *Ultrasonics Sonochemistry* **1996**, *3*, 25-37.

69. Wang, Z.; Pan, X.; Yan, J.; Dadashi-Silab, S.; Xie, G.; Zhang, J.; Wang, Z.; Xia, H.; Matyjaszewski, K., Temporal Control in Mechanically Controlled Atom Transfer Radical Polymerization Using Low ppm of Cu Catalyst. *ACS Macro Letters* **2017**, *6*, 546-549.

70. Wang, Z.; Pan, X.; Li, L.; Fantin, M.; Yan, J.; Wang, Z.; Wang, Z.; Xia, H.; Matyjaszewski, K., Enhancing Mechanically Induced ATRP by Promoting Interfacial Electron Transfer from Piezoelectric Nanoparticles to Cu Catalysts. *Macromolecules* **2017**, *50*, 7940-7948.

71. Orrego, S.; Chen, Z.; Krekora, U.; Hou, D.; Jeon, S.-Y.; Pittman, M.; Montoya, C.; Chen, Y.; Kang, S. H., Bioinspired Materials with Self-Adaptable Mechanical Properties. *Advanced Materials* **2020**, *32*, 1906970.

Chapter 2: Piezo-polymerization methodologies

The first challenge in designing adaptive materials through piezo-polymerization was developing the chemical methods to run and control polymerization and crosslinking reactions with mechanical force in the form of sound or vibrations. The original study in mechano-ATRP suggested that single-electron transfer processes were responsible for the chemical reactivity of piezoelectric nanoparticles under mechanical stress.[1] Therefore, we investigated the reactivity of piezoelectric nanoparticles in the context of radical-mediated polymerization and crosslinking reactions. In this chapter, we describe the current progress in the piezo-polymerization strategies developed in our lab.

2.1 Mechanically-promoted copper 'click' polymerization*

Given the ease with which Cu(II) was reduced to Cu(I) via ultrasound under amenable conditions, we looked into other reactions that were promoted by Cu(I). Notably, the copper-catalyzed azide-alkyne cycloaddition (CuAAC), commonly referred to as copper 'click' reaction would lead to the potential control of both step-growth and crosslinking reactions owing to the A+B type coupling reaction.[2] Mechanical force, such as ultrasound and cyclic loading, has been used previously to promote 'click' reaction in the context of small molecules, where ultrasound promotes reaction through enhanced diffusion or depassivation of metallic surfaces.[3-8] Moreover, this reaction shows largely favorable thermodynamics and kinetics. Consequently, we conducted a step-growth linear polymerization via ultrasound-promoted copper 'click' reaction (i.e.,

* This chapter was published in *Angewandte Chemie International Edition* **2018**, *57*, 11208−11212. First authorship of this work corresponds to Dr. Hemakesh Mohaptra. It is included in this thesis due to my significant contributions in the conceptualization of the project and the design and execution of the experiments.

mechano-click reaction) to synthesize a polytriazole. Likewise, we used the same method to synthesize an organogel via copper 'click' crosslinking of a polyurethane with azide side-groups.[9]

2.1.1 Results and discussion

Based on safety concerns[10], previous work[11], and creating compatibility with current commercial resins, we synthesized BPA-diazide in one step from commercial a bisphenol A epoxide.[11] This monomer also had an alcoholic functionality that we used for further urethane polymerization. The BPA-dialkyne was also synthesized by single synthetic step from bisphenol A.[12] For our initial attempts at mechano-click polymerization we used equimolar amounts of BPA-diazide and BPA-dialkyne as the co-monomers. The model reaction mixture contained each monomer (1 M in DMF), $Cu(OTf)_2/Me_6TREN$ (50/55 mM respectively), and $BaTiO_3$ nanoparticles (10 wt%, Φ = 200 nm, tetragonal). The reaction mixture was degassed and sonicated using an ultrasonic bath (Figures 9a and A1a). The preliminary reaction conditions were adapted from the mechano-ATRP polymerization. Our preliminary experiments with a reaction time of 24 h provided high conversions of the azide (> 95%), as determined by proton nuclear magnetic resonance (^{1}H-NMR), and linear polymers of average molecular weights of ~18 kDa, as determined by gel permeation chromatography (GPC).

To further investigate the mechano-click polymerization, we followed the progress of the polymerization. Aliquots of the reaction mixture were analyzed by ^{1}H-NMR and GPC at set intervals (Appendix A: NMR spectra, Figure A2). We observed that the diazide was consumed quickly, about 85% of it was consumed within 4 h. The mechano-click polymerization followed similar kinetics to conventional catalyzed step-growth polymerization, i.e., high values of M_n were only obtained at very high conversion (Figure 9b). There was no significant increase of the polymer

molecular weight beyond 24 h. The dispersity (Đ) of the polymer was around 2.9, which was expected for a step-growth polymerization.

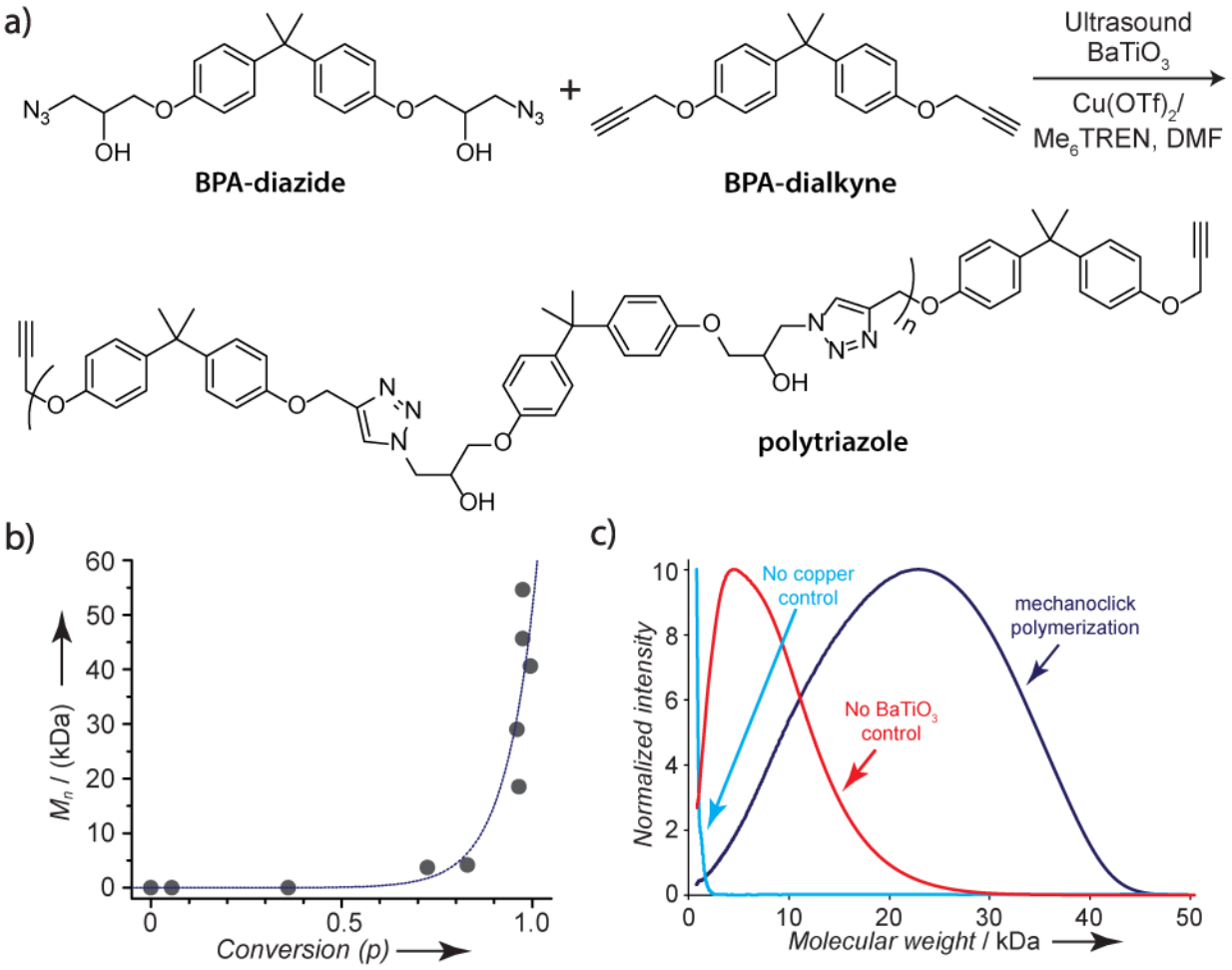

Figure 9. Ultrasound-mediated 'click' polymerization. a) Reaction scheme for the synthesis of a polytriazole from BPA-diazide and BPA-dialkyne; b) Evolution of the number average molecular weight (M_n) over increasing monomer conversion (dashed line showing trend); and c) Analysis of polymers obtained in control experiments. GPC traces of aliquots from mechano-click polymerization where either copper precursor solution or $BaTiO_3$ nanoparticles were absent. GPC trace of a representative mechano-click polymerization is shown for comparison.

In order to demonstrate that the mechano-click polymerization was indeed mediated by piezoelectric reduction of Cu(II) to active Cu(I) catalyst, we conducted control experiments. The polymerizations were repeated in the absence of either Cu(II) salt or $BaTiO_3$ nanoparticles (Figure 9c). As shown in the GPC traces of reaction mixtures obtained after a reaction time of 24 h, no polymerization was observed in the absence of Cu(II) precursor salt. This supports the hypothesis that thermal energy generated during ultrasonic agitation of solution is not sufficient to account for the observed polymerization. However, we observed the formation of short polymers when Cu(II) was present in the reaction mixture, but $BaTiO_3$ was absent. This observation suggests that there is a mode of reduction of Cu(II) that is not mediated by the piezoelectric effect of $BaTiO_3$. A possible source of background reactivity could be the generation of radicals through non-specific homolytic bond cleavage in Me_6TREN or DMF as observed elsewhere. In a control experiment where Me_6TREN was absent in the polymerization mixture, we saw a small amount polymerization consistent with non-specific background polymerization observed previously. This suggests degradation of DMF through ultrasound could be responsible for the background reactivity.[13] Finally, ultrasound is usually considered complicit in the cleavage of polymer chains in solutions.[14] We did not, however, observe any significant degradation or reduction in molecular weight of the polytriazole when we allowed the polymerization to continue for extended periods of time.

The polytriazole was soluble in polar, aprotic solvents including DMF and DMSO. These solvents allowed us to solvent cast the polymer for materials testing. We also conducted mass spectrometric analysis (MALDI-TOF) to confirm the chemical identity of the polymer (Figure A3). We obtained a set of MALDI peaks separated by 734 Da, matching the weight of a single repeat unit. We also obtained a set of MALDI peaks of lower molecular weight fragments

separated by 426 and 304 Da. These peak separations suggested fragments corresponding to the pattern A-B and A-B-A respectively, where A and B refer to the dialkyne and the diazide respectively. Polytriazoles, obtained through 'click' reactions are expected to have rigid polymeric chains leading to high materials strength. During the mechano-click reaction the suspension turned into a highly viscous fluid. However, when the reaction mixture was dried under reduced pressure, we obtained a tough and rigid glassy polymer (Figure A1b). We performed a temperature ramp shear rheology measurement between the temperature range of 50–180 °C at a constant frequency of 1 Hz (Figure A4). At temperatures below 75 °C, the polymer is in the glassy state, exhibiting a storage modulus (G') in the range of 10^9 Pa. In the range of 75–120 °C, the polymer shows a considerably sharp decrease in G' from 10^9 to 10^7 Pa, indicating the formation of a rubbery state. Finally, at temperatures above 150 °C, the loss modulus (G'') overcomes G', indicating the formation of a polymer melt.

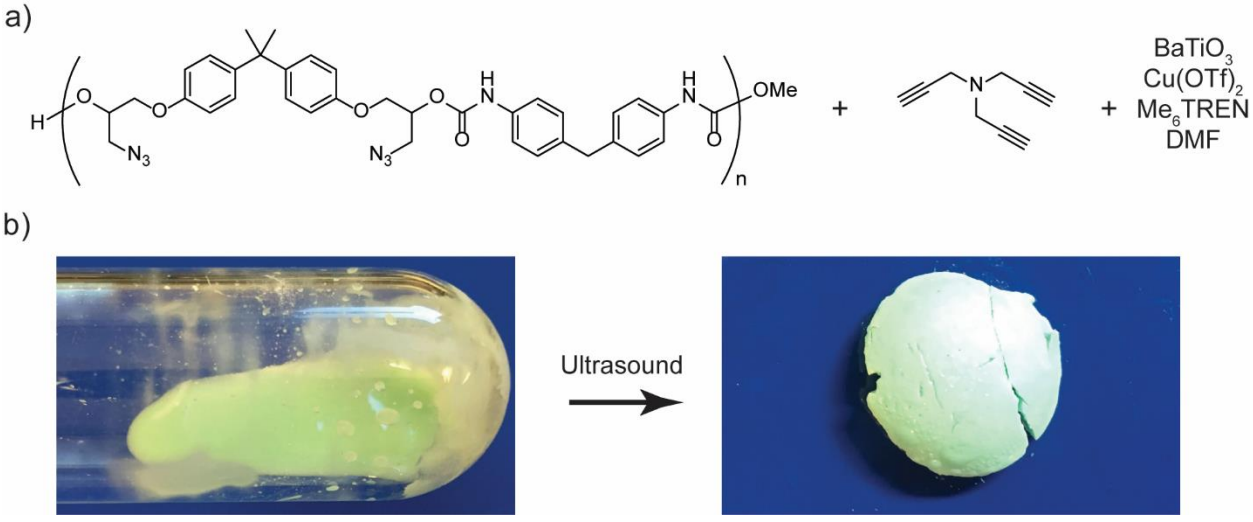

Figure 10. Ultrasound mediated polymer crosslinking using mechano-click reaction (a) Components of pre-crosslinked polyurethane-trialkyne mixture; (b) Photographs depicting the starting reaction mixture (left) and the solid polymer gel obtained after sonication (right).

After demonstrating the synthesis of a linear polymer using mechano-click polymerization, we looked into using this method to crosslink polymers. Crosslinking reactions mediated by mechanical force would provide us with the capability to fabricate polymers of a wider range of materials properties. We synthesized a linear polyurethane (azido polyurethane) containing 2 equivalents of azide per repeating unit providing multiple sites for potential crosslinking reactions. The azido-polyurethane was synthesized using conventional base-catalyzed polycondensation of BPA-diazide and methylene diphenyl diisocyanate (MDI). The resulting polyurethane (M_w = 21.5 kDa) was crosslinked using the mechano-click reaction with tripropargyl amine as the crosslinker. Briefly, a mixture containing azido-polyurethane (c.a. 0.89 mmol N_3), tripropargyl amine (0.89 mmol alkyne), $BaTiO_3$ (10 wt%), $Cu(OTf)_2$/Me_6TREN (5/5.5 mol%) and DMF (0.5 mL) was degassed and then sonicated for 24 h (Figure 10a). At the end of the reaction, we obtained a gel that was resistant to flow. The gel was brittle but hardened to a tough plastic when the solvent was removed under reduced pressure (Figure 10b).

In a control experiment in which we ran an equivalent crosslinking experiment in the absence of added Cu(II) precursor, we observed no crosslinking, supporting our previous hypothesis that Cu(I) is necessary for the mechano-click chemistry to function. When the experiment was repeated with the Cu(II) precursor present, but the $BaTiO_3$ was absent, we observed some crosslinking. The polymeric mixture obtained in this case was, however, a soft gel that disintegrated under compression (Figure A5). This observation suggests that a small amount of crosslinking likely occurs that is not mediated by piezocatalysis either through local increased temperatures or other means. This is consistent with the small amount of background we observed in the linear polymerization.

In conclusion, we demonstrated that we could use mechanical energy in the form of ultrasound to activate the Cu(I) catalyzed 'click' reaction to form a linear polytriazole and a crosslinked organogel. This was the first example of a reaction where ultrasonic agitation mediated copper 'click' polymerization through piezocatalysis. Ultrasonic energy is usually considered destructive in polymer chemistry, however, through the use of piezochemical activation of a copper-based catalyst we can design polymeric systems that can harness ultrasound and mechanical energy in a constructive role.

2.1.2 Methods

Characterization techniques

*NMR spectr*a were recorded on a Bruker AVANCE II+ (^{1}H: 500 MHz, ^{13}C: 125 MHz) spectrometer at 25 °C (unless otherwise stated). Chemical shifts (δ) are reported in parts per million (ppm). ^{1}H NMR spectra are referenced to the peak corresponding to the ^{1}H in Me_4Si (0.00 ppm), while ^{13}C NMR spectra are referenced to either the peak corresponding to Me_4Si (0.00 ppm) or the residual solvent resonance ($CDCl_3$: δ [^{13}C] = 77.16 ppm, $(CD_3)_2SO$: δ [^{13}C] = 39.50 ppm).

FT-IR spectra were recorded in the 4000-400 cm^{-1} region using a Perkin-Elmer Spectrum Two spectrometer equipped with an ATR accessory. Resolution was 4 cm^{-1} and 16 scans.

High resolution mass spectra (HRMS) were recorded on an Agilent 6224 TOF LC/MS instrument using electrospray ionization (ESI) and a time of flight (TOF) detector.

MALDI-TOF spectra were recorded either in a AB SCIEX MALDI TOF-TOF instrument, or in a Bruker Ultraflextreme MALDI-TOF-TOF instrument. Briefly, the sample was prepared by mixing 5 μL of the polymer solution (1 mg mL^{-1} in DMF), 10 μL of the matrix solution (α-cyano

hydroxycinnamic acid, 20 mg mL^{-1} in DMF) and 3 μL of the trifluoracetic acid solution (10 % v/v in THF). 1 μL of the sample was spotted directly onto the MALDI steel plate and left to dry under ambient conditions. The spectra were recorded in the linear positive mode in the range of 2-20 kDa.

Gel permeation chromatography (GPC) data was obtained either with an Agilent 1100 GPC instrument or a Shimadzu Prominence LC instrument. The details for each GPC system used are:

- Agilent 1100 GPC - two Agilent PLGel Mixed-D (5 μm) columns, eluent: stabilized THF (BHT 250 ppm), flow rate: 1 mL min^{-1}, T = 25 °C and a refractive index (RI) detector. The GPC system was calibrated using polystyrene standards.
- Shimadzu Prominence LC – one Agilent PLgel 5 μm MiniMix-D separation column, eluent: stabilized THF (BHT 250 ppm), flow rate: 1 mL min^{-1}, T = 25 °C, a Shimadzu UV-VIS detector, a Wyatt DAWN HELEOS II multi-angle light scattering (MALS) detector (658 nm laser), a Wyatt ViscoStar III detector and a Wyatt OptiLab T-rEX RI detector. The dn/dc of polymer samples was estimated from processing the RI signal with the Wyatt Astra software.
- Shimadzu Prominence LC – one TOSOH TSKgel SuperAW4000 column, eluent: DMF 0.1 M LiBr, flow rate: 0.4 mL min^{-1}, T = 25 °C and a Wyatt OptiLab T-rEX RI detector. The GPC system was calibrated using polystyrene standards.

Rheological characterization was conducted in an ARES G2 Shear Rheometer equipped with 25 mm and 8 mm parallel plates and an environmental test chamber under nitrogen gas. The sample was mounted as a square shaped film (1 cm x 1 cm x 0.5 mm) and heat pressed under 0.1 N of force at 100 ºC within the test chamber to achieve proper contact between the plates.

Temperature ramp measurements were performed in the range of 50-200 ºC with a constant oscillation frequency of 1 Hz.

Synthetic procedures

Representative mechano-click linear polymerization procedure:

In a typical experiment, a 1 M solution of BPA-diazide (0.426 g, 1 mmol) and BPA-dialkyne (0.306 g, 1 mmol) was prepared in a mixture of DMF (1 mL) and Me_6TREN (12.7 mg, 55 µmol), and loaded into a 25 mL Schlenk flask. The mixture was sonicated for 10 min to ensure complete dissolution. $Cu(OTf)_2$ (18.1 mg, 50 µmol) was added as a solid and dissolved. Finally, $BaTiO_3$ nanoparticles (tetragonal, 200 nm, 10 wt%) were added and thoroughly mixed with the solution. The reaction mixture was degassed by freeze-pump-thaw until no gas bubbles were detected (3-6 cycles), and flushed with Ar. The reaction mixture was immersed 1 in into the ultrasound bath and sonicated (40 kHz) for 24 h. Aliquots were collected at intervals and analyzed by ^{1}H-NMR and GPC. Finally, the reaction mixture was diluted with 2 mL of DMF, then 3 mL of THF and centrifuged (3500 g) to remove the $BaTiO_3$ nanoparticles. The supernatant was filtered through a silica gel plug, using THF as an eluent, to remove the residual copper salts. The filtrate was concentrated *in vacuo*, and the polymer was precipitated in about ethyl acetate (5× by volume) and dried under reduced pressure for 24 h.

^{1}H NMR (500 MHz, $(CD_3)_2SO$, TMS): δ_H (ppm) = 8.16 (s, 2H, C=CH-N), 7.10 (d, 8H, $^3J_{H\text{-}H}$ = 6.9 Hz, Ar-$C_{3,5}$-H and Ar'-$C_{3,5}$-H), 6.92 (d, 4H, $^3J_{H\text{-}H}$ = 8.7 Hz, Ar-$C_{2,6}$-H), 6.83 (d, 4H, $^3J_{H\text{-}H}$ = 8.7 Hz, Ar'-$C_{2,6}$-H), 5.54 (d, 2H, $^3J_{H\text{-}H}$ = 5.5 Hz, OH), 5.08 (s, 4H, Ar-C_1-O-$\underline{CH_2}$), 4.73 (s, 2H, O-$C\underline{H_2}$-C≡CH), 4.57 (dd, 2H, $^3J_{H\text{-}H}$ = 14 Hz, N-CH_2), 4.43 (dd, 2H, $^3J_{H\text{-}H}$ = 14 Hz, N-CH_2), 4.2 (m, 2H, C$\underline{H}$-OH), 3.89 (m, 4H, Ar'-C_1-O-$C\underline{H_2}$), 3.53 (s, 1H, C≡CH), 1.57 (s, 12H, CH_3). **^{13}C NMR** (125

MHz, $(CD_3)_2SO$, TMS): δ_C (ppm) = 155.9 (Ar-C_1), 155.7 (Ar'-C_1), 142.7 (Ar-C_4 and Ar'-C_4), 142.4 (C=CH-N), 127.3 (Ar-$C_{3,5}$ and Ar'-$C_{3,5}$), 125.3 (C=CH-N), 113.8 (Ar-$C_{2,6}$ and Ar'-$C_{2,6}$), 77.9 (C≡CH), 69.3 (Ar'-C_1-O-CH_2), 67.7 (CH-OH), 60.9 (Ar-C_1-O-CH_2), 55.2 (O-CH_2-C≡CH), 52.5 (N-CH_2), 41.0 (Ar-C_4-C_{quat} and Ar'-C_4-C_{quat}), 30.6 (CH_3).

Synthesis of Bisphenol A di(3-azido-2 hydroxy propan-1-ol) ether (**BPA-diazide**):

A solution of bisphenol A diglycidyl ether (16.8 g, 49.5 mmol) and $LiClO_4$ (16.6 g, 157 mmol) in acetonitrile (150 mL) was prepared. NaN_3 (10.0 g, 154 mmol) was added in portions and the reaction mixture was heated to 90 ºC under Ar atmosphere with vigorous stirring for 24 h. Afterwards, the reaction was cooled down to room temperature and water (300 mL) was added. The reaction mixture was extracted with ethyl acetate (3 × 150 mL), and the combined organic layer was washed with water (3 × 100 mL) and brine (3 × 100 mL), dried over anhydrous Na_2SO_4 and concentrated *in vacuo* to yield a light yellow viscous oil. The product was further purified by flash column chromatography using an ISCO Teledyne instrument with a 330 g RediSep Rf silica column while eluting with a mixture of hexanes and ethyl acetate (gradient of 0 to 40 % EtOAc). Fractions were combined and concentrated *in vacuo*, yielding a pale viscous oil of bisphenol A di(3-azido-2 hydroxy propan-1-ol) ether (15.8 g, 37.1 mmol, yield 75 %).

^{1}H NMR (500 MHz, $(CD_3)_2SO$): δ_H (ppm) 7.10 (d, 4H, $^3J_{H-H}$ = 8.7 Hz, Ar-$C_{3,5}$-H), 6.83 (d, 4H, $^3J_{H-H}$ = 8.7 Hz, Ar-$C_{2,6}$-H), 5.51 (d, 2H, $^3J_{H-H}$ = 5 Hz, OH), 3.99 (m, 2H, CH), 3.88 (m, 4H, O-CH_2), 3.35 (m, 4H, CH_2-N_3), 1.57 (s, 6H, CH_3). **^{13}C NMR** (125 MHz, $CDCl_3$): δ_C (ppm) 156.0 (Ar-C_1), 143.8 (Ar-C_4), 127.8 (Ar-$C_{3,5}$), 113.9 (Ar-$C_{2,6}$), 69.3 (CH), 69.0 (O-CH_2), 53.3 (CH_2-N_3), 41.7 (C_{quat}), 30.9 (CH_3). **HRMS** ESI-TOF (m/z): $[M+Cl]^-$ calcd. for $C_{21}H_{26}N_6O_4Cl$: 461.1704 found: 461.1685.

Synthesis of Bisphenol A dipropargyl ether (**BPA-dialkyne**):

Bisphenol A (4.00 g, 17.5 mmol) was dissolved in 120 mL of 0.4 M NaOH and heated to 70 ºC until a clear solution was obtained. Tetrabutylammonium bromide (600 mg, 2 mmol) was added as a phase transfer catalyst. To this solution, propargyl bromide (3.10 mL, 36.0 mmol) in 40 mL of toluene was added in portions, and the reaction was heated to 90 ºC overnight under vigorous stirring. After cooling, a solid product was recovered by filtration. The toluene layer was neutralized by repeated washes with 0.1 M aqueous NaOH and finally washed with deionized water (3 × 50 mL) and brine (3 × 50 mL). The organic layer was dried over anhydrous Na_2SO_4, filtered, and concentrated *in vacuo* to yield additional solid material. The two batches of solid products were combined and recrystallized from methylene chloride by slow evaporation. The white crystals were filtered and washed with small portions of cold hexane. The product was further purified by flash column chromatography using an ISCO Teledyne instrument with a 330 g RediSep Rf silica column while eluting with a mixture of hexanes and ethyl acetate (gradient of 0 to 40 % EtOAc). Fractions were combined and concentrated *in vacuo*, yielding white crystals (3.22 g, 10.5 mmol, yield 60 %).

^{1}H NMR (500 MHz, $(CD_3)_2SO$): δ_H (ppm) = 7.12 (d, 4H, $^3J_{H\text{-}H}$ = 8.7 Hz, Ar-$C_{3,5}$-H), 6.87 (d, 4H, $^3J_{H\text{-}H}$ = 8.7 Hz, Ar-$C_{2,6}$-H), 4.74 (d, 4H, O-CH_2), 3.53 (s, 2H, C≡C-H), 1.59 (s, 6H, CH_3). **^{13}C NMR** (125 MHz, $(CD_3)_2SO$): δ_C (ppm) = 155.0 (Ar-C_1), 143.2 (Ar-C_4), 127.4 (Ar-$C_{3,5}$), 114.2 (Ar-$C_{2,6}$), 79.4 (<u>C</u>≡CH), 78.1 (C≡<u>CH</u>), 55.3 (O-CH_2), 41.2 (C_{quat}), 30.6 (CH_3). **HRMS** ESI-TOF (m/z): $[M+H]^+$ calcd. for $C_{21}H_{21}O_2$: 305.1542 found: 305.1607.

Synthesis of azido-polyurethane:

4,4'-methylene diphenyl diisocyanate (MDI) was purified by dissolving it in ethyl acetate, filtering the solution through a nylon membrane (0.2 µm), concentrating the filtrate *in vacuo,* and drying the resulting solid under reduced pressure for 24 h. A solution of BPA-diazide (1.0 g, 2.34 mmol) in 1 mL of dry toluene was prepared. Then, DABCO (26 mg, 0.234 mmol, 10 mol %) was added to the solution and dissolved. Separately, MDI (590 mg, 2.34 mmol) was dissolved in 1 mL of dry toluene, then added to the former solution and thoroughly mixed. The reaction mixture was heated to 90 ºC under inert atmosphere with a reflux condenser for 3 h. To quench the reaction, methanol (0.5 mL) was added. Afterwards, the reaction mixture was allowed to cool down to room temperature and precipitated in hexanes (30 mL). To further purify the polymer, it was dissolved in acetone (5 mL), precipitated in hexanes (30 mL) and dried under reduced pressure for 24 h. Finally, the polymer was dissolved in acetone (5 mL) and cast into a film (diameter = 4 cm), which was subsequently dried under ambient conditions for 2 days and at 50 °C for 24 h *in vacuo*. The final product was a glassy, transparent solid (1.27 g, theoretical yield = 1.59 g, yield 80 %).

^{1}H NMR (500 MHz, $(CD_3)_2SO$, TMS): δ_H (ppm) = 9.82 (s, 2H, CONH), 7.38 (d, 4H, Ar'-$C_{2,6}$-H), 7.09 (d, 8H, Ar'-$C_{3,5}$-H and Ar-$C_{3,5}$-H), 6.84 (d, 4H, Ar-$C_{2,6}$-H), 5.18 (m, 2H, CH), 4.13 (d, 4H, $^{3}J_{H-H}$ = 4 Hz, O-CH_2), 3.79 (s, 2H, CH_2), 3.70 (m, 4H, CH_2-N_3), 1.56 (s, 6H, CH_3). **^{13}C NMR** (125 MHz, $(CD_3)_2SO$, TMS): δ_C (ppm) = 155.8 (Ar-C_1), 152.6 (CONH), 143.1 (Ar-C_4), 136.8 (Ar'-C_4), 135.7 (Ar'-C_1), 128.9 (Ar'-$C_{3,5}$), 127.5 (Ar-$C_{3,5}$), 118.5 (Ar'-$C_{2,6}$), 113.9 (Ar-$C_{2,6}$), 70.6 (CH), 66.7 (O-CH_2), 50.6 (CH_2-N_3), 41.2 (C_{quat}), 39.8 (CH_2), 30.7 (CH_3). **IR** (film): ν_{max} (cm^{-1}) = 3326, 2967, 2101, 1729, 1599, 1506, 1410, 1301, 1205, 1041, 827, 743.

Mechano-crosslinking of azido-polyurethane:

In a typical experiment, the azido-polyurethane (300 mg, 0.443 mmol, 1 equiv azide) was dissolved in 500 μL of dry DMF in a Schlenk flask. Me_6TREN (6.5 μL, 5.5 mol % of azide) and tripropargyl amine (42 μL, 0.296 mmol, 1 equiv alkyne) were added and dissolved. $Cu(OTf)_2$ (8 mg, 5.0 mol % of azide) was added as a solid and dissolved until a clear solution was obtained. Finally, $BaTiO_3$ nanoparticles (83 mg) were added and dispersed in the solution by shaking vigorously. The reaction mixture was degassed under vacuum and purged with Ar. It was then immersed 1 inch in the ultrasound bath (40 kHz) and sonicated for 24 h.

2.2 Mechanically-promoted Fe-mediated free radical polymerization*

We continued our investigation of piezocatalysis beyond the Cu(II)/Cu(I) system and studied a new method for bulk-scale free radical polymerization based on an Fe(III) coordination compound and ZnO nanoparticles as the piezoelectric transducers. Through bulk-scale free radical polymerization we aimed to synthesize high-molecular weight (HMW) polymers as well as mechanically-robust organogels from a variety of acrylates. In this study, we demonstrated the mechano-radical polymerization of acrylate monomers via piezocatalytic cleavage of alkyl halides. To achieve new reactivity and higher radical concentrations, we integrated the established ZnO piezoelectric nanoparticle with an Fe(III) complex ($FeCl_3 \cdot 6H_2O$,tris[2-(2-methoxyethoxy)ethyl]amine (TDA-1)).[15] We hypothesized that the Fe(III) would facilitate the free radical transfer during the ultrasonic agitation.

2.2.1 Results and discussion

Our initial experimental setup consisted of n-butyl acrylate (BA) as the monomer, ethyl α-bromoisobutyrate (EBiB) as the alkyl halide initiator, and ZnO nanoparticles (9 wt%, Φ = 18 nm) as the piezoelectric transducers. The reaction mixture was degassed and sonicated using an ultrasonic bath (40 kHz) for 12 h. Afterwards, aliquots were analyzed with ^{1}H-NMR and GPC to measure the monomer conversion and molecular weight, respectively. We observed that ZnO nanoparticles enabled the polymerization of BA with a monomer conversion of 74 % and M_n of 241 600 Da (Figure 11a and B1). Interestingly, we observed a time-dependent evolution of

* This chapter was published in *Angewandte Chemie International Edition* **2019**, 58, 12023−12026. First authorship of this work corresponds to Dr. Zhao Wang. It is included in this thesis due to my significant contributions in the conceptualization of the project and the design and execution of the experiments.

monomer conversion. HMW poly(BA) was detected at the early stage of polymerization period, indicating a fast chain-growth mechanism in contrast to all previously reported controlled chain-growth methods (Figure 11c). The M_n decreased slightly over time. We presume this decrease is due to the chain terminations and chain scissions caused by ultrasound.[16,17]

In addition, we conducted control reactions with $BaTiO_3$ piezoelectric nanoparticles and without any nanoparticles (Figure 11b and B1). No polymerization was detected in the control reaction without nanoparticles, which indicated that ultrasound-induced cavitation of the solvent was not sufficient to initiate a polymerization at 40 kHz ultrasound frequency.[16,18] Additionally, no polymerization was detected with $BaTiO_3$, presumably due to the weak surface interaction between $BaTiO_3$ and the Fe(III) coordination compound.[19] To validate this hypothesis, we analyzed the $BaTiO_3$ and ZnO nanoparticles before and after sonication by high-angle annular dark field scanning transmission electron microscopy (HAADF-STEM) coupled with energy dispersive X-ray spectroscopy (EDS). Traces of Fe were observed only on the surface of ZnO (Figure B2). Inductively coupled plasma atomic emission spectroscopy (ICP-OES) analysis was used to determine the amount of Fe within the nanoparticle. The results showed a Fe loading of 1.75 wt% (mass Fe/mass ZnO) for ZnO nanoparticles, much higher than the Fe content on $BaTiO_3$ (0.32 wt%). These results suggest that an Fe complex on the ZnO is the active agent that promotes the mechano-radical polymerization.

The concentration of radicals during the polymerization was estimated by running the reaction in the presence of increasing concentrations of a radical quencher, 4-methoxyphenol (MEHQ). A concentration of 0.70 mM of MEHQ fully stopped the polymerization. We observed partial inhibition at lower MEHQ concentrations. The polymerization was almost inhibited with 0.58 mM MEHQ. Therefore, we concluded the working concentration of radicals to be ~0.58 mM.

(a)

Entry	Nanoparticle	Conversion	Mn
1	ZnO	74%	246100
2	$BaTiO_3$	0	N/A
3	None	0	N/A

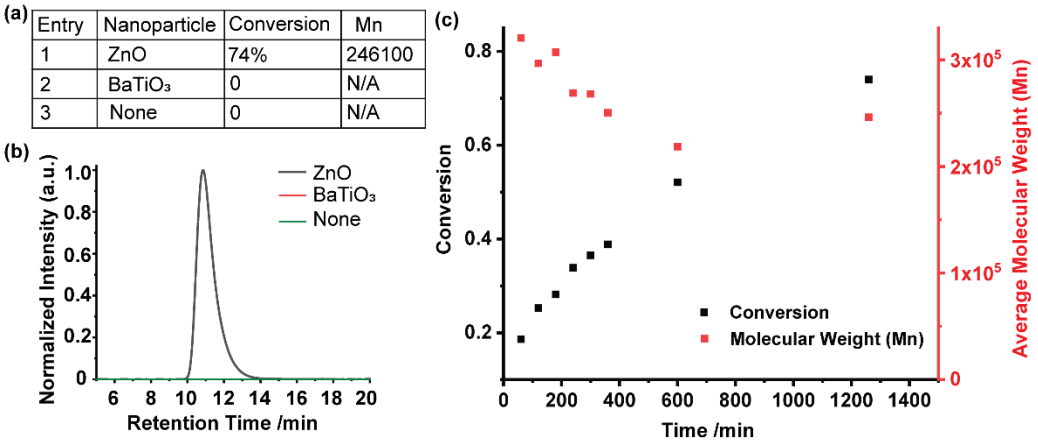

Figure 11. (a) Results for mechano-radical polymerization of BA. Reaction conditions: [monomer]: [EBiB]: [$FeCl_3 \cdot 6H_2O$]: [TDA-1] = 16: 0.16: 0.16: 0.32 mmol in 2 mL DMF; loading 9 wt% ZnO. Ultrasound (40 kHz, 70 W) for 21 hours. (b) GPC traces of the products. (c) Monomer conversion and M_n for ZnO system.

Additional control reactions were conducted by selectively removing $FeCl_3 \cdot 6H_2O$, TDA-1, and EBiB. Low monomer conversion (<20 %) was observed when either the Fe(III) salt, ligand, or the initiator were absent (Table B1). Other radical initiators were tested, including methyl α-bromoisobutyrate (MBiB), methyl 2-bromopropionate (MBP), methyl bromoacetate (MBAc) and poly(ethylene glycol) methyl ether 2-bromoisobutyrate with M_n of 5000 g/mol (mPEG-Br). Overall, these alkyl halides worked considerably well, resulting in monomer conversions ranging from 18-62 % and polymers with M_n around 2 x 10^5 Da (Table B2). A variety of polar solvents were tested, such as dimethyl acetamide (DMAc), N-methyl-2-pyrrolidone (NMP), and dimethyl sulfoxide (DMSO). Polymerizations in DMAc and NMP worked considerably well, with monomer conversions around 50 %; however, in DMSO, the conversion was low (< 10 %).

The method was extended to other acrylates, including tert-butyl acrylate (tBA), methyl acrylate (MA), methyl methacrylate (MMA), ethyl acrylate (EA), 2-ethylhexyl methacrylate (EHMA) and 2-hydroxyethyl methacrylate (HEMA) (Table 2). tBA exhibited the highest

reactivity with a conversion of 80 % and M_n of 341 100 Da, whereas MMA showed the lowest with a conversion of 52 % and M_n of 49 500 Da. Furthermore, we found that the polymerization of HEMA resulted in the formation of a persistent gel without a crosslinking agent. A possible mechanism could be the initiation by hydroxyl radicals derived from HEMA units.

Table 2. Results for mechano-radical polymerization of various acrylates.

Entry[a]	**Monomer**	**Conversion (%)[b]**	**M_n[c]**	**Đ**
1	BA	74	246 100	1.22
2	tBA	80	341 100	1.27
3	MA[d]	71	61 800	1.18
4	MMA[d]	52	49 500	1.30
5	EA	55	212 100	1.27
6	EHMA	60	144 700	1.22

[a] Reaction conditions: [monomer]: [EBiB]: [$FeCl_3 \cdot 6H_2O$]: [TDA-1] = 16: 0.16: 0.16: 0.32 mmol in 2 mL DMF; loading 9 wt% ZnO. Ultrasound (40 kHz, 70 W) for 21 hours. [b] Conversion was determined by ^{1}H-NMR. [c] M_n was determined by GPC-Multi Angle Light Scattering (MALS) in THF. [d] Reaction conditions: [monomer]: [EBiB]: [$FeCl_3 \cdot 6H_2O$]: [TDA-1] = 8: 0.16: 0.16: 0.32 mmol in 2 mL DMF; loading 9 wt% ZnO. Ultrasound (40 kHz, 70 W) for 21 hours.

Polymer crosslinking mediated by mechanical force allowed us to fabricate materials of a wider range of mechanical properties. Therefore, we investigated the use of mechano-radical crosslinking polymerization to fabricate organogels. As mentioned before, the use of HEMA as a monomer generated a poly(HEMA) gel without the need for a crosslinker. Subsequently, we used an analogous approach to fabricate an organogel using MA as the monomer and ethylene glycol dimethylacrylate (EDGMA) as the crosslinker. The poly(MA) and poly(HEMA) crosslinked gels formed stable solid polymeric composites after removing the excess solvent. TGA analysis of both samples showed approximately 3 % weight loss due to the elimination of residual solvent and moisture.

To examine the mechanical properties of the crosslinked solid polymeric composites, we measured the mechanical properties at various temperatures by temperature ramp shear rheology measurement in the range from -20 ºC to 100 ºC (Figure 12). In each case, the storage modulus (G′) remained higher than the loss modulus (G″), indicating that the sample remains in the solid state. At temperatures below 4 ºC, both composites were in the glassy state, exhibiting G′ in the range of 10^7 Pa and 10^8 Pa for poly(MA) and poly(HEMA), respectively. For poly(MA), G′ started to decrease from 10^7 to 10^5 Pa, suggesting the transition of sample from glass state to rubbery state. Similarly, the poly(HEMA) shows a decrease in G′ from 10^8 to 10^6 Pa in the range of 4–75°C, indicating the formation of a rubbery state. The glass transition temperature (T_g) of the poly(MA) composite was determined to be 54 ºC which was higher than the reported value[20], probably due to the confinement effect from well dispersed ZnO inside the polymer matrix[21]. In contrast, the poly(HEMA) composite had a T_g of 63 ºC, lower than the value in literature.[22] We reasoned that the residual solvent (plasticizer) was the dominant factor since ZnO was not homogenously dispersed within the matrix.

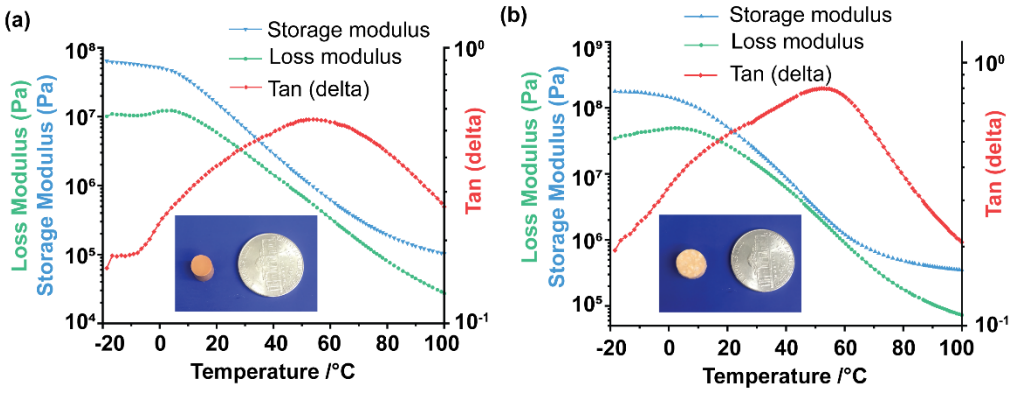

Figure 12. Temperature ramp shear rheology measurements of composites at a constant oscillation frequency of 1 Hz. The G′ (blue), G″ (green), and the viscoelastic loss factor, tan δ (red), are plotted as a function of temperature. The glass transition temperature is determined from the maximum value of tan δ. (a) Poly(MA) and (b) poly(HEMA) solid polymeric composite.

In conclusion, we developed a new piezoelectrically-mediated mechano-radical polymerization method for acrylate monomers. We showed the successful polymerization of various HMW polyacrylates, as well as crosslinked polymer organogels. Finally, we presented evidence that this polymerization method relies on the piezocatalytic cleavage of alkyl halides promoted by Fe species generated at the surface of ZnO nanoparticles under sonication.

2.2.2 Methods

Characterization techniques

NMR spectra were recorded on a Bruker AVANCE II+ (500 MHz) spectrometer at 25 °C. Chemical shifts (δ) are reported in parts per million (ppm). ^{1}H-NMR spectra are referenced to the peak corresponding to the ^{1}H in Me_4Si (0.00 ppm).

Gel permeation chromatography (GPC) data was obtained either with an Agilent 1100 GPC instrument or a Shimadzu Prominence LC instrument. The details for each system used are:

Agilent 1100 GPC - two Agilent PLGel Mixed-D (5 μm) columns, eluent: stabilized THF (BHT 250 ppm), flow rate: 1 mL min^{-1}, T = 25 °C and a refractive index (RI) detector. The GPC system was calibrated using polystyrene standards. Shimadzu Prominence LC – one Agilent PLgel 5 μm MiniMix-D separation column, eluent: stabilized THF (BHT 250 ppm), flow rate: 1 mL min^{-1}, T = 25 °C, a Shimadzu UV-VIS detector, a Wyatt DAWN HELEOS II multi-angle light scattering detector (658 nm laser), a Wyatt ViscoStar III detector and a Wyatt OptiLab T-rEX RI detector. The dn/dc of polymer samples was estimated from processing the RI signal with the Wyatt Astra software.

The Fe concentration was quantified by inductively coupled plasma-optical emission spectrometry (ICP-OES) using a Thermo iCAP 7600 ICP-OES. The sample was stirred in concentrated HNO_3 for 12 h before analysis.

STEM-EDS characterization, both imaging and spectroscopy, was done using a Hitachi HD2300A microscope operating at 200 kV (beam current: 49 µA, extraction voltage: 2.4 kV), which is equipped with dual Thermo Fischer Scientific (Waltham, MA) EDS detectors (total X-ray collection angle ~0.7 steradian). Dark field STEM images were acquired using Gatan Digital Micrograph software (Roper Technologies, Sarasota, FL). Bright field STEM images and EDS data were acquired using Thermo Fischer Scientific NSS software. Analysis and visualization of EDS data was done using Thermo Fischer Scientific NSS software. All nanoparticle samples for STEM EDS characterization were prepared by micropipette drop-casting 4 µL of solution onto lacey carbon TEM grids, allowing the droplet to sit on grid ~20 s in ambient conditions, and then using filter paper to wick away the solution and dry the grids. For M_n particles, a Cu mesh TEM grid was used. For Ni and Co particles, Au mesh TEM grids were used.

Rheological characterization was conducted in an ARES G2 Shear Rheometer equipped with 25 mm and 8 mm parallel plates and an environmental test chamber under nitrogen gas. The sample was mounted as a square shaped film (1 cm x 1 cm x 0.5 mm) and heat pressed under 0.1 N of force at 100 ºC within the test chamber to achieve proper contact between the plates. Temperature ramp measurements were performed in the range of -20-100 ºC with a constant oscillation frequency of 1 Hz. Preliminary tests were performed to ensure the applied oscillatory strain and the corresponding stress remained in the linear viscoelastic region over the whole temperature range. Insert images show the cylindric samples for shear rheology measurement

Synthetic procedures

Experimental procedure for mechano-radical polymerization:

In a typical experiment, 0.16 mmol of $FeCl_3 \cdot 6H_2O$ and 0.32 mmol of tris[2-(2-methoxyethoxy)ethyl]amine were mixed in 2 mL solvent and loaded into a 25 mL Schlenk flask. Then, 16 mmol of the monomer (8 mmol for methyl acrylate and methyl methacrylate) and 0.16 mmol of ethyl α-bromoisobutyrate were added into the reaction mixture. Finally, ZnO nanoparticles (9 wt%) were added and thoroughly mixed with the solution. The reaction mixture was degassed by freeze-pump-thaw (5X) until no gas bubbles were detected and flushed with Ar. The reaction mixture was immersed in the ultrasound bath (20–30 °C, 40 kHz, 70 W) and sonicated for 21 h. Aliquots were collected at intervals and analyzed using ^{1}H-NMR and GPC for calculating the conversion and molecular weight.

Experimental procedure for mechano-radical crosslinking polymerization:

Poly(MA) gel: 0.32 mmol of $FeCl_3 \cdot 6H_2O$ and 0.64 mmol of tris[2-(2-methoxyethoxy)ethyl]amine were mixed in 4 mL DMF and loaded into a 25 mL Schlenk flask. Then, 16 mmol of MA, 0.32 mmol of ethyl α-bromoisobutyrate, and 1.8 mmol of ethylene glycol dimethylacrylate were added into the reaction mixture. Finally, ZnO nanoparticles (4.5 wt%) were added and thoroughly mixed with the solution. A 2 mL glass vial was added and immersed into the solution as the mold. The reaction mixture was degassed by freeze-pump-thaw (5X) until no gas bubbles were detected and flushed with Ar. The reaction mixture was immersed in the ultrasound bath and sonicated (40 kHz) for 21 h. The mold was taken from the flask and dried under vacuum to remove excess solvent.

Poly(HEMA) gel: 0.32 mmol of $FeCl_3 \cdot 6H_2O$ and 0.64 mmol of tris[2-(2-methoxyethoxy)ethyl]amine were mixed in 4 mL DMF and loaded into a 25 mL Schlenk flask. Then, 32 mmol of 2-hydroxyethyl methacrylate and 0.32 mmol of ethyl α-bromoisobutyrate were added into the reaction mixture. Finally, ZnO nanoparticles (9 wt%) were added and thoroughly mixed with the solution. A 2 mL glass vial was added and immersed into the solution as a mold. The reaction mixture was degassed by freeze-pump-thaw (5X) until no gas bubbles were detected and flushed with Ar. The reaction mixture was immersed in the ultrasound bath and sonicated (40 kHz) for 21 h. The mold was taken from the flask and dried under vacuum to remove the excess of solvent.

2.3 Mechanically-promoted thiol-ene polymerization*

Our previous efforts to develop piezoelectrically-mediated polymerization methods relied on redox reactions of metal ions in solution to generate active catalysts or promoters *in situ*. Although consistent results were obtained for these systems, they required inert atmosphere conditions and prolonged exposure to ultrasound to achieve good conversions and high molecular weights. Such conditions limited their applicability to reinforce existing materials, since these materials are often exposed to environmental conditions. Moreover, our original goal was to develop systems that could harness a wider range of mechanical vibration frequencies, such as the ones commonly encountered in piezoelectric devices (mid-range frequency 10-5000 Hz)[23,24], and not just the ones of conventional ultrasound baths (20 or 40 kHz). To overcome these challenges, we developed a new approach using thiol-ene chemistry and ZnO nanoparticles as piezoelectric transducers.[25]

2.3.1 Results and discussion

In our previous work, we showed that piezoelectric nanoparticles under mechanical agitation promoted single-electron transfer processes with metal species in solution. Therefore, free radical-based chemistry involving thiols emerged as a viable alternative to metal catalysis. Thiols were an attractive target for piezoreactivity since they have standard redox potentials in the range of -200 to -400 mV [26], similar to Cu(II)/Cu(I) (E° = 0.16 V) and Fe(III)/Fe(II) (E° = 0.77

* This chapter was published in *Nature Materials* **2021**, 20, 869–874. First authorship of this work corresponds to Dr. Zhao Wang and Dr. Jun Wang. It is included in this thesis due to my significant contributions in the conceptualization of the project and the design and execution of the experiments.

V). Moreover, they can be used for a variety of polymerization reactions, such as thiol-ene, thiol-yne, and thiol-disulfide reactions.[27]

As mentioned before, we sought to harness a wider range of mechanical vibration frequencies (Figure C1)[28-36], thus, we developed an electrodynamic shaker system based on existing vibration testing instruments (Figure 13). This system enabled us to load a sample containing the reaction mixture on top of a vibrating platform. The frequency and amplitude of the vibration were controlled electronically, thus allowing the sample to be probed at frequency ranges from 10 - 5000 Hz. These lower frequencies reduced the vibrational load previously demonstrated for piezoreactivity as well as providing minimal strain to the material.

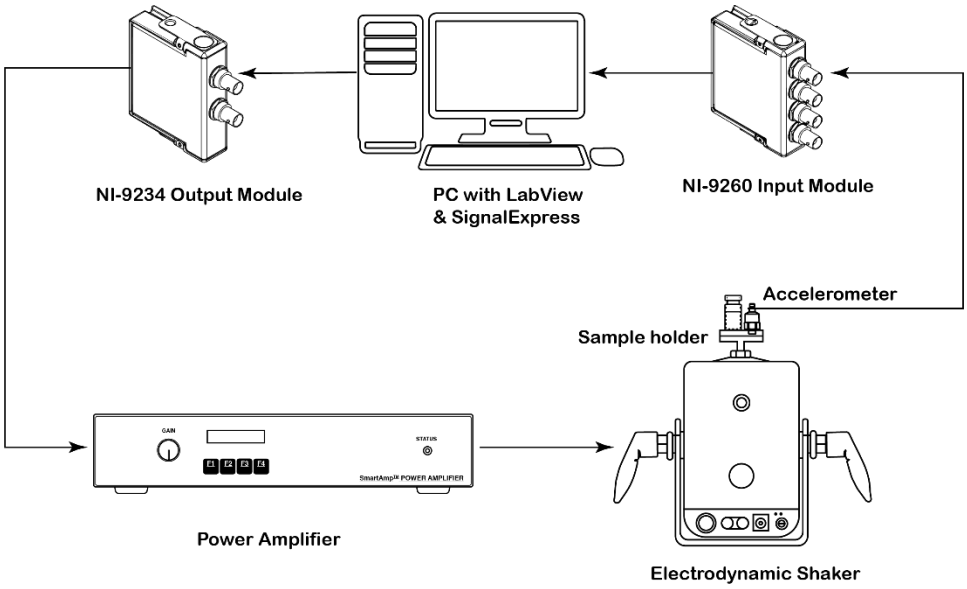

Figure 13. Schematic diagram of the experimental setup for electrodynamic shaking system.

With the electrodynamic shaker setup, we tested the piezoreactivity of ZnO nanoparticles towards thiol-ene polymerization. This chemistry seemed suitable for developing adaptive polymeric materials given its wide monomer and solvent compatibility, as well as oxygen tolerance. However, it had not been tested with mid-range frequency vibrations or using

piezoelectric nanoparticles as the promoters of mechano-radicals. To begin with, we conducted a linear, step-growth polymerization containing equimolar amounts of tri(ethylene glycol) divinyl ether (TEGDE) and 2,2′-(ethylenedioxy) diethanethiol (EDT)[37] in DMF and ZnO nanoparticles (Φ = 18 nm). The reaction mixture was vibrated at 2000 Hz for 5 h in the dark to prevent light-induced reactivity (Figure 14A). Based on calculations, the sample experienced a mechanical force of approximately 1.2 N from the acceleration of the vibrating platform (Figure C2). The resulting solution was characterized by ^{1}H-NMR and GPC at 1 h intervals (Figure 14B and C). Only in the presence of ZnO nanoparticles, monomer, and vibration, was a polymer (M_n = 3800 Da) obtained with very high monomer conversion (95%), suggesting a similar kinetics to step-growth polymerization.[38] In contrast, no polymerization was observed without the ZnO nanoparticles or in the presence of non-piezoelectric TiO_2 nanoparticles. We also observed a background polymerization in the presence of ZnO by mechanical stirring (400 rpm). However, the mechanical activation from stirring was insufficient to achieve the same reactivity from mechanical vibration (Figure C3). The resulting polythioether was purified and further characterized by spectroscopy. The ^{1}H-NMR spectrum of the polymer confirmed the formation of the desired polythioether (Figure C4). MALDI-TOF MS showed that the experimental values of m/z matched with the theoretical ones. The peaks were observed with a repeating unit of 384 Da intervals, which corresponded to the molar mass of the repeating unit (Figure C5). FT-IR data also showed the disappearance of -SH stretching peak at 2556 cm^{-1} and C=C stretching peak at 1615 cm^{-1} after polymerization (Figure C6).

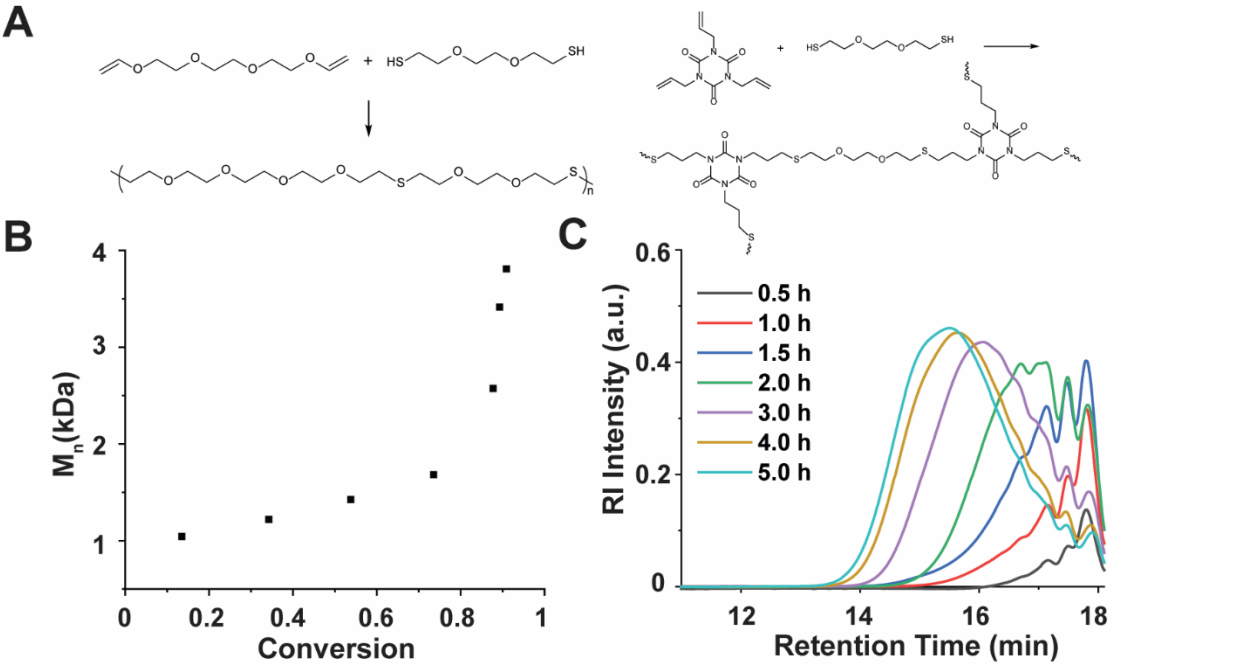

Figure 14. Mechano-thiol-ene polymerization: (A) The linear polymerization between TEGDE and EDT, as well as the crosslinking reaction between EDT and TTT. (B) Evolution of the number average molecular weight (M_n) over increasing monomer conversion of polymer via mechano-thiol-ene polymerization. (C) GPC trace depicting the evolution of polymer molecular weight over time. The polymerization mixture contained 1 mmol of each monomer in 0.5 mL DMF and 70 mg ZnO nanoparticles. The mixture was vibrated at 2000 Hz using the electrodynamic shaker system. Aliquots from the reaction were analyzed by ^{1}H-NMR, and GPC with polystyrene standards.

Having established a protocol for a linear polymerization, we tested the same method for the synthesis of crosslinked organogel. To do so we replaced the TEGDE with the trifunctional alkene 1,3,5-triallyl-1,3,5-triazine-2,4,6(1H,3H,5H)-trione (TTT) (Figures 14A and 15). The resulting gel showed a rubber-like behavior with a storage modulus of 89 kPa at 1 Hz (Figure C7). To confirm whether this crosslinking reaction would be suitable for dynamically modifying the modulus of an existing material, we controlled the acceleration and frequency of the vibrating platform and confirmed that higher force and mechanical energy resulted in a higher gelation rate (Figure C8).

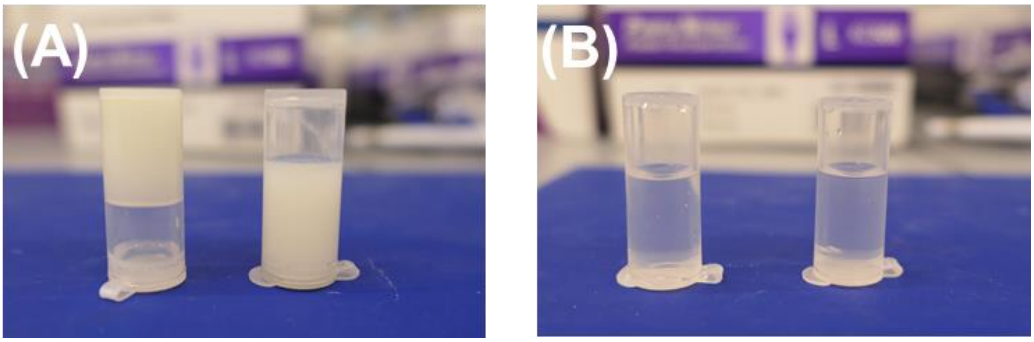

Figure 15. Photos of the thiol-ene crosslinking reaction solution. (A) Solution containing ZnO. left vial: under sonication (2000 Hz, 0.8 N) for 4 hours; right vial: without vibration. (B) Solution without ZnO. Left vial: under vibration (2000 Hz, 0.8 N) for 4 hours; right vial: without vibration.

To assess the mechanism of this mechanically-mediated thiol-ene reaction (mechano-thiol-ene) we conducted additional experiments. We theorized that, under mechanical vibration, piezoelectric ZnO nanoparticles generate a piezoelectric potential at their surface which then induces the formation of thiyl radicals (R-S·). These radicals subsequently promote the propagation step with an alkene functional group via an anti-Markovnikov addition to form a carbon-centered radical. A chain-transfer step removes a hydrogen radical from a thiol, which can then participate in multiple propagation steps (Figure C9).[38] We observed that the mechano-thiol-ene reaction was inhibited by the addition of MEHQ, a radical quencher, confirming that the reaction proceeded by a radical transfer process.[39]

The compatibility of this chemistry was further investigated with different alkenes and EDT. The order of alkene reactivity (propyl vinyl ether> 1-octene ~ vinyl propionate >allyl butyl ether) agrees with UV initiated thiol-ene reaction (Table C1).[38] The control experiments showed much less reactivity than the reactions under shaking. We also tried the polymerization of TEGDE and EDT as well as the reaction of propyl vinyl ether and EDT using $BaTiO_3$. However, little

reactivity was observed for $BaTiO_3$ compared with ZnO. We hypothesized that the interaction between the surface of the ZnO nanoparticles and the monomer was important for the reaction.[40] To further investigate this, we determined that a strong negative charge of the ZnO particles, (measured as zeta potential) was necessary to achieve higher reactivity (Figure C10). This finding was also supported by theoretical calculations.[41] We also concluded the reaction occurs at or near the surface, since ZnO coated with silane (1 wt%, ~ 0.2 nm) with a similar zeta potential did not result in polymerization despite generating a potential upon vibration (Table C2). Altogether, these results implied that both negative charges and direct interaction of ZnO with thiol species are responsible for the generation of thiyl radicals that undergo a standard thiol-ene polymerization.

These experiments confirmed that ZnO nanoparticles could act as mechano-chemical transducers to promote organic radical-based reactions by harnessing mechanical vibrations in the mid-range frequency. In the next chapter, we show how we used this method to fabricate an adaptive material with an elastic modulus that was a function of the frequency and force of the mechanical vibration.

2.3.2 Methods

Characterization techniques

NMR spectra were recorded on a Bruker AVANCE II+ (500 MHz) spectrometer at 25 °C and processed them in MestReNova 11.0.4.

Gel permeation chromatography (GPC) data was obtained with a Shimadzu Prominence LC instrument. The details for GPC analysis are as follows: Shimadzu Prominence LC-one Agilent PLgel 5 μm MiniMix-D separation column, eluent: stabilized THF (BHT 250 ppm), flow rate: 1 mL/min, T = 25 °C, a Shimadzu UV-VIS detector, a Wyatt DAWN HELEOS II multi-angle light scattering detector (658 nm laser), a Wyatt ViscoStar III detector, and a Wyatt OptiLab T-rEX RI detector. The GPC system was calibrated using polystyrene standards.

FT-IR measurement was conducted via PerkinElmer Spectrum Two FT-IR Spectrometer in attenuated total reflectance (ATR)mode.

Matrix-assisted laser desorption/ionization time-of-flight (MALDI-TOF MS) spectra were acquired with a Bruker Ultraflextreme mass spectrometer operated in the positive linear mode. The solution for MALDI-TOF MS analysis was obtained by mixing 2,5-dihydroxybenzoic acid matrix (10 mg mL^{-1}), and polymer solution in a 1/1 volumetric ratio. Then, 1 μL portion of the mixture was analyzed on MALDI-TOF MS in the positive ion mode.

Zeta potential measurement was conducted via a Mobius® Zeta Potential Analyzer at the sample concentration of 0.2 mg/mL in DMF.

Plasma treatment was conducted via a 200 W Plasma etcher & cleaning system (Plasma Etch PE-100LF) for 10 mins.

Rheological characterization was conducted in an ARES G2 Shear Rheometer equipped with 25 mm and 8 mm parallel plates. The sample was mounted as a cylinder (2.5 mm thick) and compressed up to 0.5 N of force to achieve proper contact between the plates. Preliminary tests were performed to ensure the applied oscillatory strain and the corresponding stress remained in the linear viscoelastic region over the whole temperature range. The frequency sweep experiments were performed at the frequency range from 0.1 Hz to 10 Hz. The compression experiments were conducted at a constant rate of 0.01 mm/s.

Synthetic procedures

Electro-Dynamic Shaker Experimental Setup:

The electrodynamic shaking system was set up as shown in Figure 13. Mechanical vibration was generated via an electrodynamic shaker (Modal Shop, Model 2025E). The signal inputs for operating the electrodynamic shaker were created using National Instrument data acquisition (DAQ) system (Module NI 9234) from a virtual function generator in LabView 2018 environment (National Instrument Inc.). To produce the cyclic force of required magnitude and frequency, a power amplifier (SmartAmp^{TM}, Model 2100E21-400) was connected to shaker and signal sources. Ceramic shear ICP$^{®}$ accelerometer (PCB, Model 352A60) were employed to measure the vibration acceleration (10 mV/g) and the output signals were acquired and monitored through a DAQ Module (NI 9218) using NI SignalExpress 2015 software (National Instrument Inc.). Upon completion, the system was capable of delivery sine wave oscillation to a platform (2.54 cm by 2.54 cm) for mass up to 1 kg. The system could perform vibration in frequencies ranging from 10 to 5000 Hz and with total power of up to 140 watts. Using the accelerometer, we

converted these power and frequency to N of force experienced by the sample during each experiment.

Experimental procedure for linear mechano-thiol-ene polymerization:

In a typical experiment, 70 mg of ZnO was dispersed in 0.5 mL DMF by ultrasound for 20 seconds. Two monomers TEGDE (1 mmol, 202 mg, 0.204 mL) and EDT (1 mmol, 182 mg, 0.163 mL) were mixed in a glass vial. The vial was directly attached to the adhesive mount by finger pressing (one side had an acrylic adhesive that sticked to the vial surface) and mounted on the electrodynamic shaker. The shaker was typically operated at 2000 Hz (1.2 N) for the vibration experiments unless otherwise noted. Aliquots were collected at intervals and analyzed using ^{1}H-NMR and GPC for calculating the conversion and molecular weight. After the reaction, the final product was purified by precipitation in cold methanol. The sample was dried in vacuum overnight.

Experimental procedure for screening of various alkenes:

In a typical experiment, ZnO (70 mg, 0.86 mmol) or $BaTiO_3$ (201 mg, 0.86 mmol) was dispersed in 0.5 mL DMF by ultrasound for 20 seconds. Different alkenes (2 mmol) and EDT(1 mmol, 182 mg, 0.163 mL) were mixed in a glass vial. The vial was directly attached to the adhesive mount by finger pressing and mounted on the electrodynamic shaker. The shaker was typically operated at 2000 Hz (1.2 N) for the vibration experiments unless otherwise noted. Aliquots were collected at intervals and analyzed using ^{1}H-NMR for calculating the conversion.

Experimental procedure for mechano-thiol-ene crosslinking:

In a typical experiment, 40 mg of ZnO was dispersed in 2 mL DMF by ultrasound for 20 second. Two monomers TTT (2.67 mmol, 666 mg, 0.574 mL) and EDT (4 mmol, 728 mg, 0.652 mL) were mixed in a polypropylene vial. The vial was directly attached to the adhesive mount by finger pressing and mounted on the electrodynamic shaker (2000 Hz, 0.8 N) for the vibration experiments.

Experimental procedure for generation of charged ZnO nanoparticles:

The highly negative charged ZnO nanoparticles were obtained by placing commercially available nanoparticles (~ 2 g) in a drying oven for 48 h followed by a charging treatment at 6000 V for 2 hours. The charging treatment consisted of placing the dried nanoparticles squeezed between two charged plates. The control, positively charged ZnO nanoparticles, were obtained via treatment with a 200 W Plasma etcher for 10 mins. Positively charged, negatively charged, and silane coated ZnO were analyzed by DLS to determine their zeta potential (6.9 mV, -24.0 mV, and -22.6 mV, respectively).

2.4 Conclusions

In this chapter, we showed that piezoelectric nanoparticles, such as $BaTiO_3$ and ZnO, can facilitate single-electron transfer processes between redox active species. This method allowed us to directly transduce mechanical energy into chemical energy, and then conduct polymerization and crosslinking reactions, such as Cu(I)-mediated atom transfer radical polymerization (ATRP), Cu(I) azide-alkyne cycloaddition (CuAAC) step-growth polymerization, Fe-mediated free-radical polymerization, and step-growth thiol-ene polymerization. These methods add to the repertoire of mechanically-promoted chemistries available for designing adaptive polymeric materials.

2.5 References

1. Mohapatra, H.; Kleiman, M.; Esser-Kahn, A. P., Mechanically controlled radical polymerization initiated by ultrasound. *Nature Chemistry* **2017**, *9*, 135-139.

2. Binder, W. H.; Sachsenhofer, R., 'Click' Chemistry in Polymer and Material Science: An Update. *Macromolecular Rapid Communications* **2008**, *29*, 952-981.

3. Cintas, P.; Barge, A.; Tagliapietra, S.; Boffa, L.; Cravotto, G. Alkyne–azide click reaction catalyzed by metallic copper under ultrasound. *Nature Protocols* **2010**, *5*, 607–616.

4. Tu, N.P.; Hochlowski, J.E.; Djuric, S.W. Ultrasound-assisted click chemistry in continuous flow. *Molecular Diversity* **2012**, *16*, 53–58.

5. Rinaldi, L.; Martina, K.; Baricco, F.; Rotolo, L.; Cravotto, G. Solvent-Free Copper-Catalyzed Azide-Alkyne Cycloaddition under Mechanochemical Activation. *Molecules* **2015**, *20*, 2837-2849.

6. Cella, R.; Stefani, H. A. Ultrasound in heterocycles chemistry. *Tetrahedron* **2009**, *65*, 2619-2641.

7. Stefani, H. A.; Silva, N. C. S.; Manarin, F.; Lüdtke, D. S.; Zukerman-Schpector, J.; Madureira, L. S.; Tiekik, E. R. T. Synthesis of 1,2,3-triazolylpyranosides through click chemistry reaction. *Tetrahedron Letters* **2012**, *53*, 1742–1747.

8. Michael, P.; Binder, W. H. A Mechanochemically Triggered "Click" Catalyst. *Angewandte Chemie International Edition* **2015**, *54*, 13918–13922.

9. Mohapatra, H.; Ayarza, J.; Sanders, E. C.; Scheuermann, A. M.; Griffin, P. J.; Esser-Kahn, A. P., Ultrasound Promoted Step-Growth Polymerization and Polymer Crosslinking Via Copper Catalyzed Azide–Alkyne "Click" Reaction. *Angewandte Chemie International Edition* **2018**, *57*, 11208-11212.

10. Keicher, T.; Löbbecke, S. Part 1: Synthesis and safety. In *Organic Azides: Syntheses and Applications*, 1st ed.; Wiley-Blackwell, 2010; pp 1–27.

11. Liu, Y.; Díaz, D. D.; Accurso, A. A.; Sharpless, K. B.; Fokin, V. V.; Finn, M. G. Click chemistry in materials synthesis. III. Metal-adhesive polymers from Cu(I)-catalyzed azide–alkyne cycloaddition. *Journal of Polymer Science, Part A: Polymer Chemistry* **2007**, *45*, 5182–5189.

12. Sheng, X.; Mauldin, T.C.; Kessler, M.R. Kinetics of bulk azide/alkyne "click" polymerization. *Journal of Polymer Science, Part A: Polymer* Chemistry **2010**, *48*, 4093-4102.

13. Mišík, V.; Riesz, P., EPR study of free radicals induced by ultrasound in organic liquids II. Probing the temperatures of cavitation regions. *Ultrasonics Sonochemistry* **1996,** *3*, 25-37.

14. Basedow, A. M.; Ebert, K. H. In *Ultrasonic degradation of polymers in solution*, Berlin, Heidelberg, Springer Berlin Heidelberg: Berlin, Heidelberg, 1977; pp 83-148.

15. Wang, Z.; Ayarza, J.; Esser-Kahn, A. P., Mechanically Initiated Bulk-Scale Free-Radical Polymerization. *Angewandte Chemie International Edition* **2019,** *58*, 12023-12026.

16. Collins, J.; McKenzie, T. G.; Nothling, M. D.; Allison-Logan, S.; Ashokkumar, M.; Qiao, G. G. Sonochemically Initiated RAFT Polymerization in Organic Solvents. *Macromolecules* **2019**, *52*, 185-195.

17. Rudin, A.; Choi, P. Chapter 8 - Free Radical Polymerization. In *The Elements of Polymer Science & Engineering*, 3rd ed.; Academic Press, Boston, 2013; pp. 341-389.

18. Wang, Z.; Wang, Z.; Pan, X.; Fu, L.; Lathwal, S.; Olszewski, M.; Yan, J.; Enciso, A. E.; Wang, Z.; Xia, H.; Matyjaszewski, K. Ultrasonication-Induced Aqueous Atom Transfer Radical Polymerization *ACS Macro Letters* **2018**, *7*, 275-280.

19. Wang, Z.; Pan, X.; Li, L.; Fantin, M.; Yan, J.; Wang, Z.; Wang, Z.; Xia, H.; Matyjaszewski, K., Enhancing Mechanically Induced ATRP by Promoting Interfacial Electron Transfer from Piezoelectric Nanoparticles to Cu Catalysts. *Macromolecules* **2017**, *50*, 7940-7948.

20. Meseguer Dueñas, J.; Gomez Ribelles, J. L. DSC study of the miscibility of poly(methyl acrylate)-polystyrene sequential interpenetrating polymer networks **2003,** *72*, 695-705.

21. Wong, M.; Tsuji, R.; Nutt, S.; Sue, H. J. Glass transition temperature changes of melt-blended polymer nanocomposites containing finely dispersed ZnO quantum dots. *Soft Matter* **2010**, *6*, 4482-4490.

22. Caykara, T.; Özyürek, C.; Kantoğlu, O. Investigation of thermal behavior of Poly (2-hydroxyethyl methacrylate-co-itaconic acid) networks. *Journal of Applied Polymer Science* **2007**, *103*, 1602-1607.

23. Tressler, J. F.; Alkoy, S.; Newnham, R. E., Piezoelectric Sensors and Sensor Materials. *Journal of Electroceramics* **1998**, *2*, 257-272.

24. Briscoe, J.; Dunn, S., Piezoelectric nanogenerators – a review of nanostructured piezoelectric energy harvesters. *Nano Energy* **2015**, *14*, 15-29.

25. Wang, Z.; Wang, J.; Ayarza, J.; Steeves, T.; Hu, Z.; Manna, S.; Esser-Kahn, A. P. Bio-inspired mechanically adaptive materials through vibration-induced crosslinking. *Nature Materials* **2021**, *20*, 869–874.

26. Mirzahosseini, A.; Noszál, B., Species-Specific Standard Redox Potential of Thiol-Disulfide Systems: A Key Parameter to Develop Agents against Oxidative Stress. *Scientific Reports* **2016,** *6*, 37596.

27. Hoyle, C. E.; Lowe, A. B.; Bowman, C. N., Thiol-click chemistry: a multifaceted toolbox for small molecule and polymer synthesis. *Chemical Society Reviews* **2010**, *39*, 1355-1387.

28. Le, M. Q.; Capsal, J. F.; Lallart, M.; Hebrard, Y.; Van Der Ham, A.; Reffe, N.; Geynet, L.; Cottinet, P. J. Review on energy harvesting for structural health monitoring in aeronautical applications. *Progress in Aerospace Sciences* **2015**, *79*, 147-157.

29. Corda, S.; Franz, R. J.; Blanton, J. N.; Vachon, M. J.; DeBoer, J. B. *In-flight vibration environment of the NASA F-15B flight test fixture*. NASA Dryden Flight Research Center, 2002. https://www.nasa.gov/centers/dryden/pdf/88734main_H-2468.pdf (accessed 2022-03-04).

30. Scharton, T. D. *Force limited vibration testing*. NASA, 1997. https://mechanical-engineering.gsfc.nasa.gov/NASA-RP1403_Vibration_Monograph.pdf (accessed 2022-03-04).

31. Xu, H.; Yuan, S.; Zong, L. Analysis of the time-frequency characteristics of internal combustion engine vibration signal based on Hilbert-Huang transform. In *Image and Signal Processing (CISP), 2010 3rd International Congress on Image and Signal Processing*, Vol. 7; IEEE, 2010; pp. 3400-3404.

32. Yu, Y.; Naganathan, N. G.; Dukkipati, R. V. A literature review of automotive vehicle engine mounting systems. *Mechanism and machine theory* **2001**, *36*, 123-142.

33. Yang, T.; Wang, T.; Li, G.; Shi, J.; Sun, X. Vibration Characteristics of Compression Ignition Engines Fueled with Blended Petro-Diesel and Fischer-Tropsch Diesel Fuel from Coal Fuels. *Energies* **2018**, *11*, 2043.

34. Shalaby, M.; Saitou, K. Design of Heat Reversible Snap Joints for Space Frame Bodies. In *Proceedings of IDETC/CIE 2005 ASME 2005 International Design Engineering Technical Conferences & Computers and Information in Engineering Conference September 24-28, 2005, Long Beach, California USA*, ASME, 2005.

35. Malaji, P.; Ali, S. Analysis of energy harvesting from multiple pendulums with and without mechanical coupling. *The European Physical Journal Special Topics* **2015**, *224*, 2823-2838.

36. S. L. Kok, M. F. A. Rahman, D. F. W. Yap and Y. H. Ho. Bandwidth widening strategies for piezoelectric based energy harvesting from ambient vibration sources. In *2011 IEEE International Conference on Computer Applications and Industrial Electronics*; ICCAIE, 2011; pp. 492-496.

37. Lowe, A. B. Thiol–ene “click” reactions and recent applications in polymer and materials synthesis: a first update. *Polymer Chemistry* **2014**, *5*, 4820-4870.

38. Xu, J.; Boyer, C. Visible Light Photocatalytic Thiol–Ene Reaction: An Elegant Approach for Fast Polymer Postfunctionalization and Step-Growth Polymerization. *Macromolecules* **2015**, *48*, 520-529.

39. Cole, M. A.; Jankousky, K. C.; Bowman, C. N. Redox initiation of bulk thiol–ene polymerizations. *Polymer Chemistry* **2013**, *4*, 1167-1175.

40. Mohinuddin, P. M. K.; Gangi Reddy, N. C. Zinc Oxide Catalyzed Solvent-Free Mechanochemical Route for C–S Bond Construction: A Sustainable Process. *European Journal of Organic Chemistry* **2017**, 8, 1207-1214.

41. Kim, S. M.; Kim, H.; Nam, Y.; Kim, S. Effects of external surface charges on the enhanced piezoelectric potential of ZnO and AlN nanowires and nanotubes. *AIP Advances* **2012**, *2*, 042174.

Chapter 3. Conferring adaptability to polymer organogels via piezo-polymerization

In the previous chapter, we described several methodologies to conduct mechanically-promoted polymerization and crosslinking reactions through the PzE effect. Our goal is to integrate those chemistries with existing materials to give them adaptive properties. In this chapter, we describe two systems where piezoelectrically-mediated chemistries were used to synthesize and strengthen organogels in response to mechanical vibrations. Gels were selected as model matrices because of their high solvent content and relatively low elastic moduli. The high solvent content facilitated the molecular diffusion of the reactants and the piezoelectric activation of particles, thus allowing the efficient transport of polymerization promoters generated at the surface of the piezoelectric nanoparticles. The initial low elastic modulus allowed us to accurately measure the change in the mechanical properties of the gel with dynamic mechanical analysis (DMA) techniques.

3.1 Strengthening of an organogel via mechano-thiol-ene crosslinking[*]

We had previously shown that thiol-ene polymerization and crosslinking reactions could be controlled with mechanical vibration at a frequency of 2000 Hz. Consequently, we used this method to fabricate a double network composite which could sense and adapt to the vibration frequency and energy.[1] To achieve this, we required the ZnO nanoparticles to be homogenously dispersed within the matrix. Therefore, we loaded a methyl cellulose (MC) organogel in DMF with

[*] This chapter was published in *Nature Materials* **2021**, 20, 869–874. First authorship of this work corresponds to Dr. Zhao Wang and Dr. Jun Wang. It is included in this thesis due to my significant contributions in the conceptualization of the project and the design and execution of the experiments.

the thiol-ene monomers and ZnO nanoparticles. The gel composition included TTT (15 wt %), EDT (16 wt %), ZnO (0.9 wt %, Φ = 18 nm), and MC (2 wt %). Because the components remained fixed within the primary organogel, this composite would then form a crosslinked double network upon mechanical vibration (Figure 16).

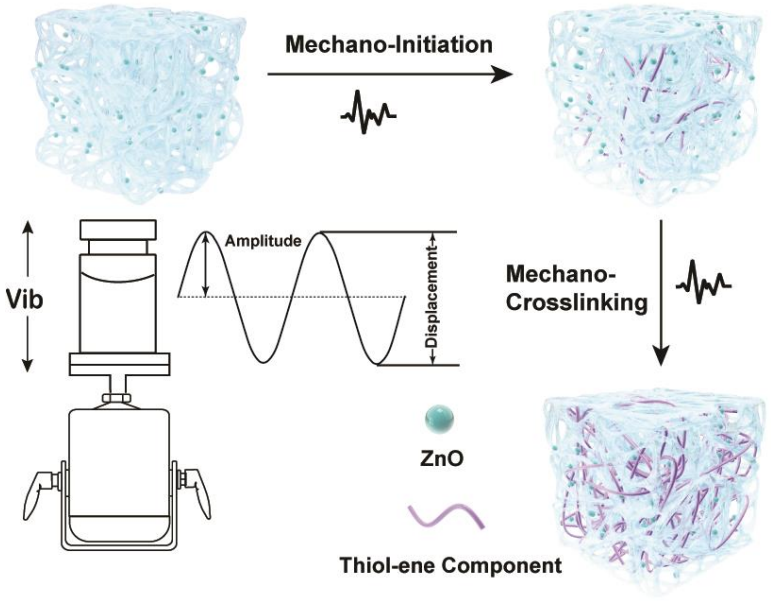

Figure 16. Organogel strengthening via mechano-thiol-ene polymerization – mechanical activation of piezoelectric ZnO results in selective polymerization reinforcing segments within the organogel matrix. The sample was mounted on an electrodynamic shaker and vibrated with an up-and-down motion.

3.1.1 Results and discussion

In the initial experiments, we observed that only gels that contained ZnO and were vibrated increased their modulus during the 16 h stimulation (2000 Hz, 1.2 N). The material increased its strength over controls which contain all the same components but were not vibrated. The strengthened gel (2000 Hz, 1.2 N, 16 h) via mechano-thiol-ene crosslinking was tested with a DMA compression test, exhibiting much less deformation and full recovery after release of the axial force. In a compression test under constant strain rate (0.01mm/s), the strengthened sample

retained its shape and showed a compression stress at 30 % strain of 18 kPa. In contrast, the control sample which was not vibrated showed an irreversible deformation to the applied axial force (Figure 17). The difference between the two samples indicates a 36 X increase in stress response with vibration. This change suggests that the strengthening was the result of higher crosslinking density via the formation of the secondary thiol-ene network.

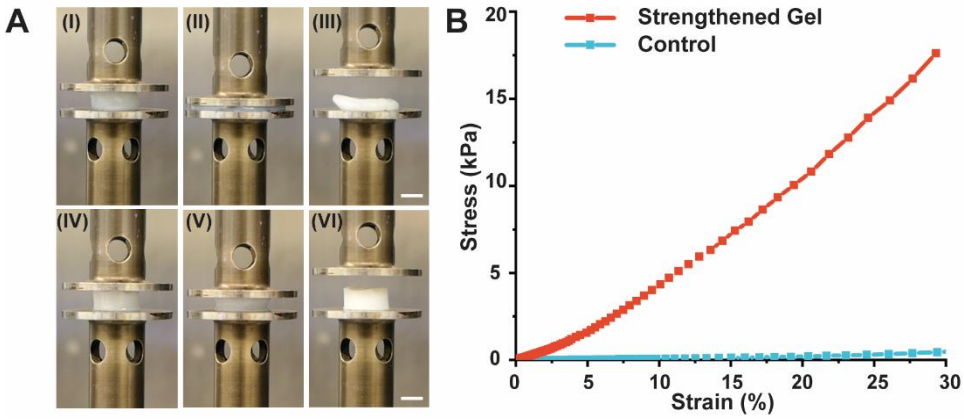

Figure 17. Strengthening of an organogel via mechano-thiol-ene crosslinking. (A) Snapshots of the compression test on a DMA instrument. Images of the control gel (without vibration) captured before (I), during (II) and after (III) applying a 10 N axial force. Images of the strengthened gel captured before (IV), during(V) and after (VI) applying a 10 N axial force. Only the strengthened gel retained its shape after compression. Scale bar: 5 mm. (B) Stress–strain curves for the same both gels.

To confirm that the strengthening was mediated by both vibration and the PzE effect, we performed several control experiments to eliminate other potential mechanisms. We relied on DMA compression testing and the measurement of the storage moduli of the control samples to compare them. Samples were vibrated at 2000 Hz (0.8 N) for 8 h. The organogel without the ZnO remained weak after vibration. When ZnO was included, the resulting gel showed an increase in G'. To determine if the presence of 0.9 wt % nanoparticles could alter the organogel on its own, we conducted an experiment with similarly sized non-piezoelectric particles, TiO_2. Gels that

contained TiO_2 instead of ZnO showed a negligible increase in G' (Figure 18A). These results indicate that ZnO acts as a transducer of mechanical energy into chemical energy, presumably operating via the same mechanism as the solution-based thiol-ene crosslinking.

After confirming that the MC-ZnO organogel self-strengthening was mediated by ZnO, we sought to test if the material could adapt its strength to the input energy, including parameters such as applied force, frequency, and time. To minimize differences in experimental conditions, we used the storage modulus change (ΔG') to describe the strengthening contribution from the mechanical vibration, calculated by the following equation (1):

$$\Delta G' = G'_{vibration} - G'_{control} \quad \ldots (1)$$

, where $G'_{vibration}$ is the storage modulus of a sample after vibrational strengthening, $G'_{control}$ is the storage modulus of an identical sample and conditions without application of vibration.

First, we sought to determine if the material would change its modulus based on the input force the material experienced for a fixed time. Fixing the vibration frequency at 2000 Hz, we altered the force of each vibration by changing the power applied to the oscillator via an in-line power amplifier. Force here refers to the root mean square (rms) force unless otherwise specified. The results showed that identical starting gels increased their ΔG' from 1 to 10 kPa as a function of increased applied force from 0.4 N to 1.2 N (Figure 18B).

Second, we wanted to determine how frequency would affect the modulus. We varied the frequency of the vibration from 500 - 5000 Hz and vibrated each sample for 8 h. The results showed that the modulus of identical samples changed as a function of input frequency achieving a peak ΔG' at the frequency of 2000 Hz, with higher and lower frequencies providing proportional changes in modulus (Figure 18C). A caveat to this experiment, in an electrodynamic shaking

experiment, the frequency cannot be fully separated from force.[2] However, in examining the force corresponding to each frequency, we observed that ΔG' changed for nearly equivalent forces with different frequencies. We conclude from this experiment that both frequency and force are inputs that the materials use to adapt its modulus.

Finally, we examined if our material could adapt its G' as a function of vibration time. Before vibration, the gel showed a G' of 1 kPa. The samples were vibrated at 2000 Hz (1.2 N) for 16 h taking sample data every 2 or 3 h. The resulting materials showed a continuous increase in ΔG' under mechanical vibration overtime. After 6 h, the ΔG' increased quickly and reached a plateau of 66.6 kPa at the 16 h timepoint (Figure 18D). This result is consistent with our observations in solution regarding the formation of a higher molecular weight polythioether via a step-growth polymerization. It is possible that the sharp increase in ΔG' corresponds to when the crosslinking achieves percolation, but we do not have direct evidence yet to confirm this conjecture.

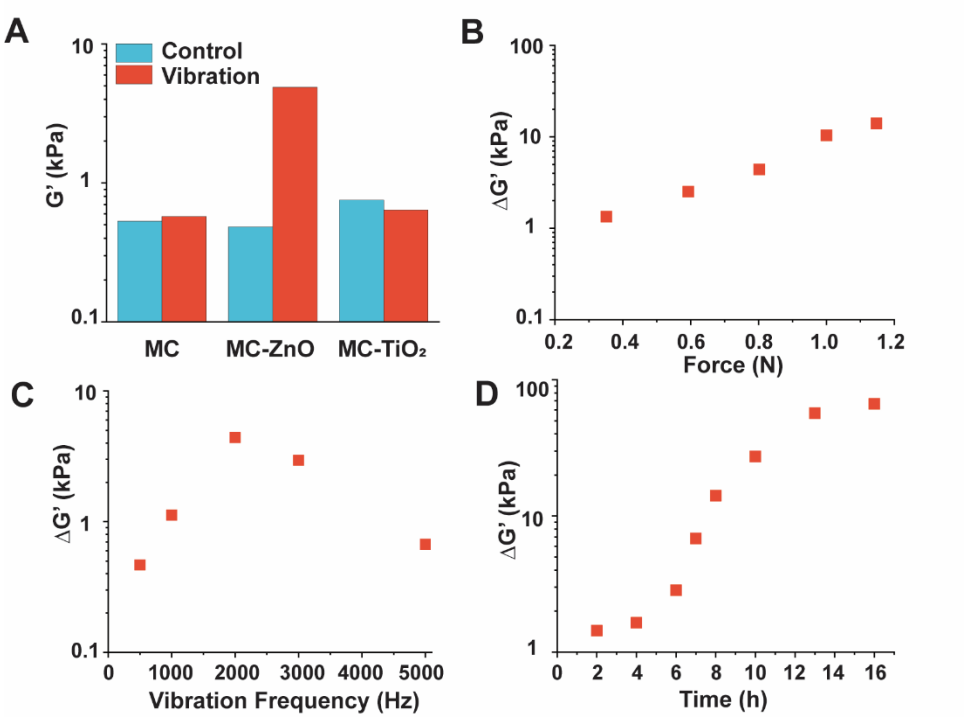

Figure 18. Adaptation of the organogel modulus to different mechanical inputs. (A) Control experiments indicating the necessity for ZnO in self-strengthening. The storage modulus (G') of different gels with and without vibration strengthening (2000 Hz, 0.8 N, 8 h). (B) Storage modulus change (ΔG') of the gels after vibration-induced strengthening as a function of force (2000 Hz, 8 h). (C) ΔG' of the gels after vibration-induced strengthening as a function of vibration frequency (8 h). (D) ΔG' of the gels after vibration-induced strengthening as a function of reaction time (2000 Hz, 1.2 N). Note: force refers to the root mean square (rms) force unless otherwise specified.

In summary, we showed the first example of a material that adapts itself via piezoelectrically-mediated polymerization, and responds to force, frequency, and time of vibration. Each of these parameters alters the modulus of the material with a different relationship – indicating that the material adapts its response to different input parameters. Altogether, we conclude that the material provides an important mechanism in self-strengthening and an example of using a mechanochemical feedback loop to create an adaptive modulus response.

3.1.2 Methods

Characterization techniques

Dynamic mechanical analysis (DMA) was conducted in a TA instruments RSA-G2 Solid Analyzer equipped with 25 mm and 8 mm parallel plates. The sample was mounted as a cylinder (2.5 mm thick) and compressed up to 0.5 N of force to achieve proper contact between the plates. Preliminary tests were performed to ensure the applied oscillatory strain and the corresponding stress remained in the linear viscoelastic region over the whole temperature range. The frequency sweep experiments were performed at the frequency range from 0.1 Hz to 100 Hz. The compression experiments were conducted at a constant rate of 0.01 mm/s.

Synthetic procedures

Mechano-thiol-ene crosslinking for gel strengthening:

Methyl cellulose (MC) gel was prepared by adding MC (490 mg) in 15 mL of DMF and heating to 90 °C. After complete dissolution, ZnO nanoparticles (200mg) were then added to the solution at 90 ºC and sonicated for 20 seconds to fully disperse them. Afterwards, the mixture was stirred at 90 ˚C for another 20 mins, and then the monomers TTT (13.3 mmol, 3.32 g, 2.86 mL) and EDT (20 mmol, 3.64 g, 3.26 mL) were added under vigorous stirring. After further mixing for 2 min, the mixture was poured into a cylindrical polypropylene vial and cooled down to room temperature to obtain the physical organogel with a radius of 0.5 cm and a height of 1.3 cm. The vial was then attached to the adhesive mount by finger pressing and mounted on the electrodynamic shaker for the vibration experiment. After vibration, a 2.5 mm thick cylinder was cut from the top of the sample and analyzed by DMA.

3.2 Mechanically-promoted synthesis of reversible organogels through thiol-disulfide crosslinking*

We have previously shown that we can use the PzE effect to synthesize organogels from multifunctional monomers or polymers with reactive functionalities. However, the reactions we have relied on thus far have all led to irreversible covalent bonds between polymer chains. To develop adaptive materials, many systems have employed dynamic linkages that can be selectively formed and broken. The thiol-disulfide reaction is a prime example of a reversible reaction which has been extensively used to develop stimuli-responsive and self-healing materials.[3-5] However, most of the literature has focused on using heat or light for the oxidation of thiols to disulfides or the metathesis of disulfide bonds within a polymer matrix.[6,7] Other reports have shown that mechanical stress (ultrasound or cyclic loading) can cleave polymer-embedded disulfide bonds.[8] Another report showed that under ultrasonication, small-molecule thiols could be oxidized in the presence of air and a stoichiometric amount of a non-nucleophilic base.[9]

In this context, we theorized that the thiol-disulfide redox pair (RSH/RSSR) would be a suitable target for nanoparticle-mediated piezoelectrochemistry because of its relatively low standard redox potential. Although $E°_{RSH/RSSR}$ is dependent on the substituent on the thiol, reported values for glutathione and cysteine are in the range of -250 to -200 mV.[10] In this chapter, we demonstrate a mechanically-promoted synthesis of organogels via the formation of disulfide linkages between polymers with thiol functionalities.[11] Furthermore, we show that these organogels can be dissolved with a reducing agent, and the recovered polymer can be reused to form another organogel.

* This chapter was published in *ACS Macro Letters* **2021**, *10*, 799–804.

3.2.1 Results and discussion

To test the crosslinking of a polymeric material via disulfide bond, we started by synthesizing three linear polymers with thiol side-groups: a polymethacrylate variant (mercapto-PMMA), a polyacrylate variant (mercapto-PMA), and a polystyrene variant (mercapto-PS) (Figure 19a). Mercapto-PMMA and mercapto-PMA were synthesized via reversible addition-fragmentation chain transfer polymerization (RAFT) from a modified literature procedure, and mercapto-PS was synthesized via free-radical polymerization with a thermal initiator.[12] All mercapto-polymers were fully characterized (Appendix D: NMR spectra, Figures D1-3, Table D1).

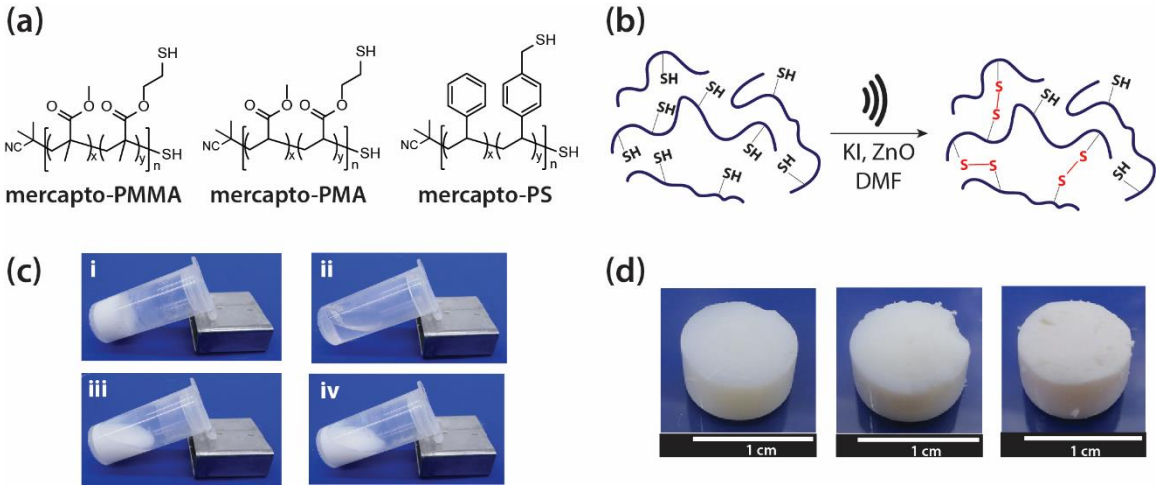

Figure 19. Mechano-thiol-disulfide crosslinking: (a) Chemical structures of mercapto-polymers. (b) Reaction scheme for mechanically-promoted crosslinking of mercapto-polymers via disulfide bond formation. (c) Pictures of control reactions for the ultrasound-promoted gelation of mercapto-PMMA: (i) all reaction components, (ii) no ZnO, (iii) no ultrasonication (stirring at 100 rpm) and (iv) no KI. (d) Pictures of organogels for mercapto-PMMA, mercapto-PMA and mercapto-PS (from left to right, respectively).

Our first goal was to test if these polymers could form organogels via mechanically-promoted disulfide bond formation. We dissolved mercapto-PMMA (150 mg, 1 eq thiol) in DMF (400 μL) and added KI (11 mg, 0.5 eq) and ZnO nanoparticles (30 mg, 5 w%, Φ = 18 nm). After homogenizing, the sample was sonicated in an ultrasound bath (40 kHz) for 6 h at room temperature (Figure 19b). Based on previous literature, we theorized KI would act as an intermediary reagent. In a conventional synthesis of disulfides, KI is oxidized in situ with H_2O_2 to form I_2, which subsequently converts thiols to disulfides.[13] We hypothesized that piezoelectric nanoparticles under mechanical agitation could similarly oxidize iodide anions, thus promoting the oxidation of thiols to disulfides and the crosslinking of the polymers. The gelation of mercapto-PMMA was confirmed by the inversion test. The gel was allowed to set for 12 h before removing it from the vial. Control experiments were run by selectively removing ZnO and KI. When we removed either of these substances, no gel was formed. From these results, we made preliminary observations that gelation was mechanically-promoted and required not just ZnO but also KI to accelerate the formation of presumably a disulfide bond. Using an analogous procedure, organogels were synthesized from mercapto-PMA and mercapto-PS (Figures 19c-d).

After finding increasing evidence that disulfide bonds were the reason behind the crosslinking of the polymers, we studied the reversibility of the gelation. The mercapto-PMMA gel dissolved in a solution of tris(2-carboxyethyl)phosphine hydrochloride (TCEP) in DMF (0.16 M) after mild heating at 50 °C for 12 h (Figure 20). As TCEP is a commonly used reducing agent which converts disulfides into thiols, we hypothesized it would readily solubilize the gels. Nevertheless, there was also the possibility that the ZnO was acting as a binder via coordination with the thiol side-groups of the polymer and that the formed disulfides were incidental. Therefore, we tested the gel by treating it with a strong acid solution which would dissolve the ZnO but not

break the disulfide bonds. As shown in Figure 20, a trifluoroacetic acid (TFA) solution in DMF (0.1 M) did not dissolve the gel, even though the ZnO was solubilized. To serve as a reference, we synthesized a mercapto-PMMA gel via conventional thermal curing. We replaced the ZnO with H_2O_2 (30 v%, 2 µL) as the oxidizing agent and heated the sample at 60 °C for 1 h. We tested this gel with both the TCEP and TFA solutions, and only TCEP dissolved it.

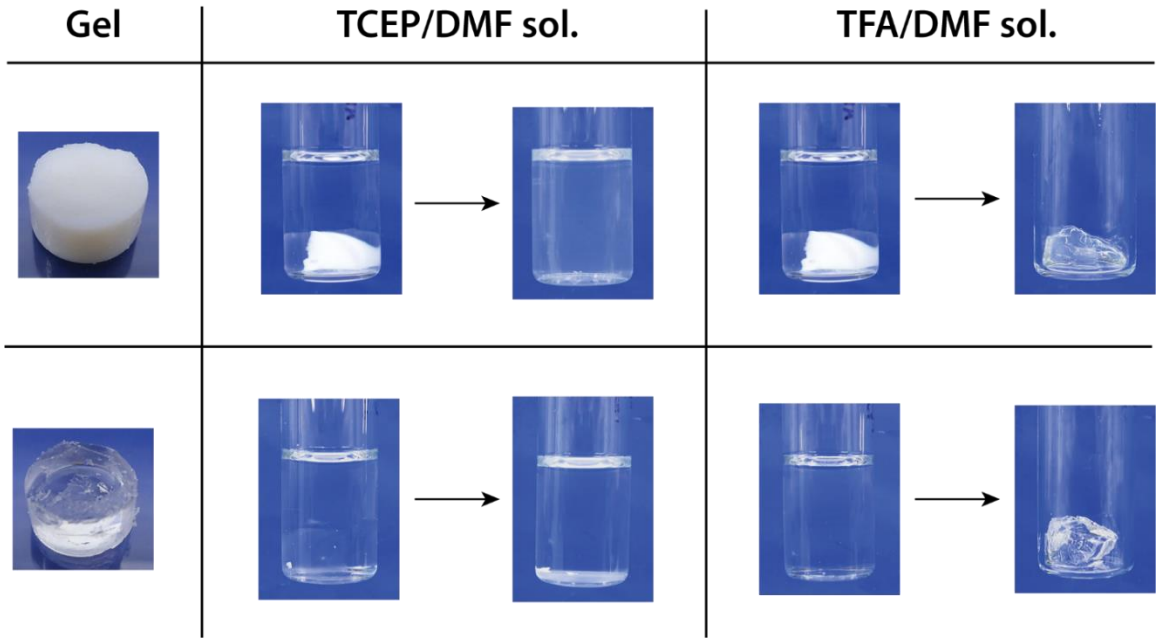

Figure 20. Pictures showing dissolution tests of mercapto-PMMA organogels: mechano-gel (top) and control gel (bottom). For the dissolution experiments, the samples were stirred in 2 mL of either TCEP hydrochloride (40 mg/mL, 016 M) or TFA (0.1 M) solutions in DMF for 12 h at 50 ºC. Both gels dissolve with TCEP (reducing agent). The TFA solution dissolves ZnO nanoparticles but the gel retains its shape.

To probe the mechanism behind the gelation, we used a small molecule thiol (benzyl mercaptan) in place of the mercapto-polymers and measured the conversion of thiol to disulfide via quantitative ^{1}H-NMR (Figure D4). The results showed a relatively low conversion (18 %) of the benzyl mercaptan to dibenzyl disulfide. Control reactions in the absence of ZnO, KI, or

ultrasound resulted in considerably lower yields of disulfide. Although the observed conversions were low, it would still be sufficient for crosslinking to occur in the mercapto-polymer system. In addition to the NMR study, the formation of I_2 was confirmed with UV-vis spectroscopy in a similar experiment (Figure D5). We postulate that one plausible mechanism is that the ZnO nanoparticles serve both to activate the thiol via surface interactions and to promote its oxidation to a disulfide.[14-16] As for the KI, one interpretation of the results is a mechanism in which the iodide anions facilitate the oxidation by reacting with the surface of the nanoparticles to form iodine, which can then easily oxidize the thiol to disulfide (Figure D6). However, as the 'No KI' control indicated, ZnO by itself can weakly oxidize thiols.

After concluding that the chemical product was indeed disulfides, we sought to study different gelation conditions. Mechanical characterization of the organogels was conducted via DMA under compression mode (Figures D7-10). First, using mercapto-PMMA as a representative polymer, the concentration of ZnO was varied between 5.0, 2.5, and 1.0 w% (Table 3a-c). In all of these cases, gelation occurred after ultrasonication (40 kHz) for 6 h, however, the elastic moduli of the resulting gels decreased along with the concentration of ZnO. In the previous chapter, we showed that an electrodynamic shaker could also promote piezo-polymerization. As shown in Table 3d, a mercapto-PMMA gel was also formed by mechanical shaking (2 kHz). Although the frequency of the vibrations was significantly less than in ultrasound, the resulting gel had a comparable elastic modulus to the one synthesized with ultrasound. In addition to these experiments, we also tested the reference gel described before (Table 3e). Its elastic modulus (42 kPa) was comparable to the gel obtained using 1 w% ZnO concentration (178 kPa).

For the mercapto-PMA and mercapto-PS polymer systems, organogels were synthesized using both the ultrasound and the shaker (Table 3f-i). The mercapto-PMA gel synthesized with

ultrasound (40 kHz) had an elastic modulus almost an order of magnitude lower in comparison to the analogous gel with mercapto-PMMA, though it was still solid. However, the gel synthesized via shaking at 2 kHz showed weak consistency after being removed from the vial. Oscillatory strain and frequency measurements confirmed that the sample was crosslinked, but its elastic modulus was comparatively low at 2 kPa. In the case of mercapto-PS, both 40 kHz ultrasound and 2 kHz shaker yielded consistent gels. However, for the shaker case, the elastic modulus was lower by about half. In general, these results indicate that the lower energy output of the shaker in comparison to the ultrasound leads to lower reactivity and thus lower modulus.

Table 3. Gelation study of mercapto-polymers.

Sample	Polymer	ZnO (w %)	Energy source*	E (kPa)‡
a	mercapto-PMMA	5.0	ultrasound	776
b		2.5	ultrasound	658
c		1.0	ultrasound	178
d		5.0	shaker	760
e†		-	heat	42
f	mercapto-PMA	5.0	ultrasound	90
g		5.0	shaker	2
h	mercapto-PS	5.0	ultrasound	570
i		5.0	shaker	202

* Conditions: ultrasound bath (40 kHz, 110 W, 6 h), electrodynamic shaker (2 kHz, 130 W, 8 h), and heat (60 °C, 1 h). Gels were allowed to set for 12 h after sonication (or heating).

† Control reaction: H_2O_2 30 v% (2 μL). Shear modulus (G, kPa) measured with rheometer.

‡ Young's modulus determined from slope of stress-strain curve.

To further examine the physical properties of the organogels, we selected representative samples **a**, **f** and **h**, corresponding to the mechano-crosslinking of mercapto-PMMA, mercapto-PMA and mercapto-PS with ZnO (5 w%) and ultrasound (40 kHz), respectively. The gel fractions were determined by extraction of the soluble polymer with DMF. The mercapto-PMMA gel showed the highest gel fraction at 93 %, meanwhile, the mercapto-PMA and mercapto-PS gels showed similar values at 80 % and 83 %, respectively. Additionally, swelling experiments in DMF showed a nearly a 5X increase in mass of the mercapto-PMA sample due to solvent absorption, in comparison to the 1.8X and 1.5X increments for mercapto-PMMA and mercapto-PS, respectively (Table D2).

In previous experiments, we examined the potential gel dissolution to prove the formation of disulfide linkages. However, we were also intrigued that disulfide cleavage could be used as a mechanism for polymer recyclability. To test this idea, we subjected the mechanically-crosslinked mercapto-PMMA gel to TCEP reduction. We obtained mercapto-PMMA back from the solution, with a recovery yield of 70 w% (Figure 21). However, the recycled polymer showed lesser solubility in organic solvents, including DMF, than the virgin polymer. NMR analysis showed no significant chemical differences between them (Figure D11); however, GPC analysis revealed the recycled polymer contained higher molecular weight species (Table D3, Figure D12). We considered two explanations for this phenomenon. One possibility is that Zn^{2+} cations from solubilized ZnO act as ionic cross-linkers, therefore some polymer chains contain additional crosslinks. The other possibility is that some irreversible covalent bonds might have formed, such as thioether bonds from the desulfurization of disulfides.[17] Nevertheless, the recycled mercapto-PMMA could still be used to synthesize a new gel via mechano-gelation, albeit half of the total polymer was replaced with virgin mercapto-PMMA to account for the lesser solubility of the

recycled polymer. This new gel showed similar mechanical properties as the original one and could also be dissolved with a TCEP solution. In addition, we conducted analogous experiments with the mercapto-PMA and mercapto-PS gels (Figure D13). The dissolution method with TCEP resulted in the parent) polymers as characterized by GPC (Table D3, Figures D14-15). Unlike the case of mercapto-PMMA, the dissolution process of mercapto-PMA and mercapto-PS gels yielded polymers of nearly the same molecular weight as the original ones. Mercapto-PMA and mercapto-PS were recovered with yields of 83 % and 90 %, respectively, and reused to form new gels via mechano-crosslinking.

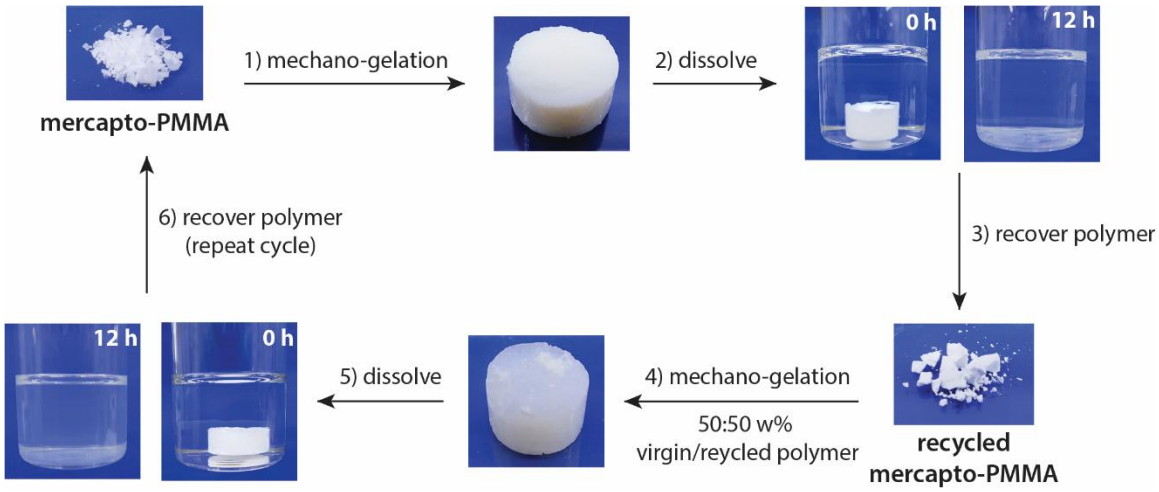

Figure 21. Recyclability study of mercapto-PMMA organogel. (1) Mercapto-PMMA (150 mg) and KI (11 mg) were dissolved in DMF (400 μL) and mixed with ZnO nanoparticles (30 mg, 5 w%). The mixture was ultrasonicated (40 kHz) for 6 h and the gel was left to set for 12 h. (2) The gel was placed in a solution of TCEP·HCl in DMF (8 mL, 0.16 M) and stirred at 50 °C for 12 h. (3) The solution was centrifuged at 10k rpm to remove the ZnO nanoparticles, concentrated under vacuum, and the polymer was precipitated in methanol (30 mL), washed and dried at 60 °C for 24 h. (4) Virgin mercapto-PMMA (75 mg), recycled mercapto-PMMA (75 mg) and KI (11 mg) were dissolved in DMF (400 μL) and mixed with ZnO nanoparticles (30 mg, 5 w%). The mixture was ultrasonicated (40 kHz) for 6 h and the gel was left to set for 12 h. (5) and (6) Same dissolution and recovery procedure as described above.

In summary, we have demonstrated a new method that relies on mechanical force coupled with piezoelectrochemistry to fabricate reversible organogels via disulfide bond formation. Gels within a range of elastic moduli were obtained from three different polymers with thiol side-groups. Mechanical activation and subsequent gelation of the mercapto-polymers was achieved with both high (40 kHz ultrasound) and low (2 kHz shaking) frequency sources of vibration. A reversibility experiment showed that the gelation could be dissolved by treatment with a reducing agent, and that the mercapto-polymers could be recycled for another round of mechano-crosslinking.

3.2.2 Methods

Characterization techniques

NMR spectroscopy: ^{1}H and ^{13}C nuclear magnetic resonance (NMR) spectra were recorded either on a Bruker Avance II+ 500 MHz spectrometer equipped with a Bruker QNP probe (^{1}H: 500 MHz, ^{13}C: 125 MHz) or a Bruker Ascend 9.4 T 400 MHz spectrometer equipped with an Avance III HD console and a BBFO "smart" probe (^{1}H: 400 MHz, ^{13}C: 100 Hz) at 25 °C. Chemical shifts (δ) are reported in parts per million (ppm). ^{1}H NMR spectra are referenced to TMS (0.00 ppm), while ^{13}C NMR spectra are referenced to either TMS (0.00 ppm) or the residual solvent ($CDCl_3$: δ [^{13}C] = 77.23 ppm).

FTIR spectroscopy: Fourier transform infrared (FT-IR) spectra were recorded on a Perkin Elmer Spectrum Two FT-IR spectrometer in the MIR range (4000-400 cm^{-1}) using the ATR mode.

Quantification of thiol-disulfide conversion of benzyl mercaptan via quantitative ^{1}H-NMR: Benzyl mercaptan (59 μL, 0.50 mmol) and KI (42 mg, 0.25 mmol) were dissolved in DMF (400 μL). ZnO nanoparticles (15 mg, 2.5 wt %) were added. The mixture was homogenized and sonicated for 12 h in an ultrasound bath (40 kHz). Control experiments: (i) no ZnO, (ii) no ultrasonication (stirred at 100 rpm), and (iii) no KI. After the ultrasonication (or stirring), the samples were homogenized, and the nanoparticles precipitated by centrifugation (10k rpm for 2 min). Aliquots (25 μL) were taken and dissolved in $CDCl_3$ (700 μL). A solution of ethylene carbonate NMR standard in $CDCl_3$ (0.38 M approx., 50 μL) was added for each sample. Solids were removed by centrifugation (10 000 rpm for 2 min). ^{1}H-NMR spectra (400 MHz) were recorded with a 90º pulse, D1 = 50 s and NS = 16. The methylene proton (CH_2) signals from the

thiol and disulfide were used for quantification. Chemical shifts were referenced to TMS (0.00 ppm).

The thiol-disulfide conversion was calculated via quantitative ^{1}H-NMR with the following equations:

$$M_{std} = P_{std} \cdot \frac{w_{std}}{MW_{std}} \cdot \frac{V_{std}}{V_{std,stock}}$$

$$M_{disulfide} = \frac{I_{disulfide}}{I_{std}} \cdot \frac{N_{std}}{N_{disulfide}} \cdot M_{std}$$

$$\%\ conversion = \frac{2 \cdot M_{disulfide}}{M_{thiol,0}}$$

where **std** denotes the standard, **M** is mmol, **P** is purity, **w** is mass (mg), **MW** is molecular weight (g/mol), **V** is volume (mL), **I** is peak integral, and **N** is number of protons.

Detection of I_2 formation via UV-vis spectroscopy: In a polypropylene vial (0.126 oz.), KI (11.0 mg) was dissolved in DMF (400 μL) and ZnO nanoparticles (30.0 mg) were added. The mixture was sonicated (40 kHz) for 6 h. Two control reactions were run simultaneously: i) no ZnO, and ii) no ultrasonication (stirred at 100 rpm). The samples were centrifuged at 10 000 rpm for 2 min to separate the nanoparticles. Aliquots (2 μL) were taken and analyzed by UV-vis spectroscopy (Thermo Scientific NanoDrop 2000c spectrophotometer) in the range 220-750 nm using pure DMF as a blank. Solutions of KI and I_2 in DMF were also measured as references.

Mechanical characterization. The gels were synthesized as described in the manuscript, removed from the vials, their exterior was dried with tissue paper, and a short slice of their top was removed with a razor blade to ensure a flat surface. Their diameter was approximately 1 cm. Oscillatory amplitude and frequency sweep measurements were conducted in either a DMA instrument (uniaxial compression mode) or a rheometer (shear mode). A parallel disc geometry (Φ = 15 mm) was used. The oscillatory frequency sweeps were conducted at strains within the linear region, usually between 0.5 - 1.0 % strain. Parallel storage and loss moduli confirmed that the gels were crosslinked. Stress-strain curves under uniaxial compression mode were obtained in a DMA instrument using the same geometry as before. The Young's moduli (E, kPa) of the gels were determined by the slope of the stress-strain curve in the linear region.

Synthetic procedures

Synthesis of poly(methyl methacrylate-co-2-mercaptoethyl methacrylate) (**mercapto-PMMA**):

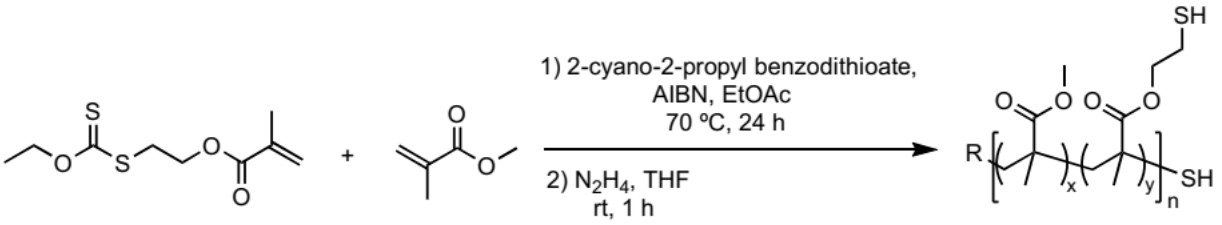

Methyl methacrylate (3.20 g, 32.0 mmol) and 2-(ethyl xanthate)ethyl methacrylate (0.80 g, 3.4 mmol) were dissolved in ethyl acetate (6 mL). A solution of 2-cyano-2-propyl benzodithioate (26.0 mg, 0.12 mmol) and azobisisobutyronitrile (AIBN) (6.4 mg, 0.060 mmol) in ethyl acetate (2 mL) was added. The solution was degassed via three cycles of freeze-pump-thaw, flushed with Ar and stirred at 70 ºC for 24 h. The reaction mixture was cooled down to room

temperature and diluted with ethyl acetate (4 mL). The polymer was precipitated in cold n-hexane (50 mL), washed with n-hexane (25 mL) for 1 h under mechanical agitation and dried under vacuum at 60 ºC for 24 h. Red, glassy solid (3.1 g, 78 %).

^{1}H-NMR ($CDCl_3$ with 0.05% v/v TMS, 400 MHz): δ_H 4.68 (br, q, CH_2), 4.20 (br, t, CH_2), 3.60 (s, CH_3), 3.42 (br, t, CH_2), 2.10-1.70 (br, CH_2), 1.46 (t, CH_3), 1.15-0.75 (br, CH_3).

The copolymer was deprotected via aminolysis. Briefly, poly(methyl methacrylate-*co*-2-(ethyl xanthate) ethyl methacrylate) (3.0 g, 2.6 mmol thiol monomer, 1.0 eq) was dissolved in THF (40 mL) and flushed with Ar for 10 min in a sealed flask. A solution of anhydrous hydrazine (161 μL, 5.1 mmol, 2.0 eq) in THF (5 mL) was added under Ar. The mixture was stirred at room temperature for 1 h, and then concentrated under vacuum. The polymer was purified by filtration through silica column with DCM as eluent, and then it was precipitated in cold n-hexane (50 mL) and dried under vacuum at 60 ºC for 24 h. White, glassy solid (2.1 g, 70 %).

^{1}H-NMR ($CDCl_3$ with 0.05% v/v TMS, 400 MHz): δ_H 4.09 (br, t, CH_2), 3.60 (s, CH_3), 2.78 (br, t, CH_2), 2.10-1.70 (br, CH_2), 1.15-0.75 (br, CH_3).

Synthesis of poly(methyl acrylate-co-2-mercaptoethyl acrylate) (**mercapto-PMA**):

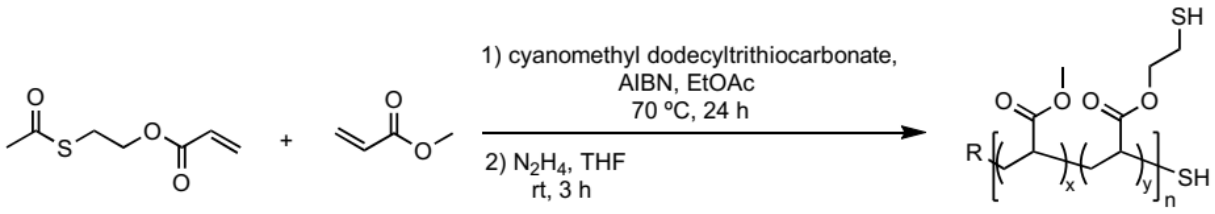

Methyl acrylate (2.58 g, 30.0 mmol) and 2-(acetylthio)ethyl acrylate (0.52 g, 3.0 mmol) were dissolved in ethyl acetate (6 mL). A solution of cyanomethyl dodecyl trithiocarbonate (38.0 mg, 0.12 mmol) and AIBN (6.4 mg, 0.060 mmol) in ethyl acetate (2 mL) was added. The solution was degassed via three cycles of freeze-pump-thaw, flushed with Ar and stirred at 70 ºC for 24 h. The reaction mixture was cooled down to room temperature and diluted with ethyl acetate (4 mL). The polymer was precipitated in cold n-hexane (50 mL), washed with n-hexane (25 mL) for 1 h under mechanical agitation and dried under vacuum at 60 ºC for 24 h. Yellow, soft solid (3.0 g, 97 %).

^{1}H-NMR ($CDCl_3$ with 0.05% v/v TMS, 400 MHz): δ_H 4.17 (br, t, CH_2), 3.66 (s, CH_3), 3.13 (br, t, CH_2), 2.37 (s, CH_3), 2.31 (br, CH), 1.94 (br, CH_2), 1.80-1.40 (br, CH_2).

The copolymer was deprotected via aminolysis. Briefly, poly(methyl acrylate-*co*-2-(acetylthio)ethyl acrylate) (3.0 g, 2.9 mmol thiol monomer, 1.0 eq) was dissolved in THF (40 mL) and flushed with Ar for 10 min in a sealed flask. A solution of anhydrous hydrazine (182 µL, 5.8 mmol, 2.0 eq) in THF (5 mL) was added under Ar. The mixture was stirred at room temperature for 3 h, and then concentrated under vacuum. The polymer was precipitated in cold n-hexane (50 mL), washed with methanol (25 mL) for 1 h under mechanical agitation and dried under vacuum at 60 ºC for 24 h. Colorless, soft solid (2.6 g, 87 %).

^{1}H-NMR ($CDCl_3$ with 0.05% v/v TMS, 400 MHz): δ_H 4.20 (br, t, CH_2), 3.66 (s, CH_3), 2.75 (br, CH_2), 2.31 (br, CH), 1.94 (br, CH_2), 1.80-1.40 (br, CH_2).

Synthesis of poly(styrene-co-4-vinylbenzyl thiol) (**mercapto-PS**):

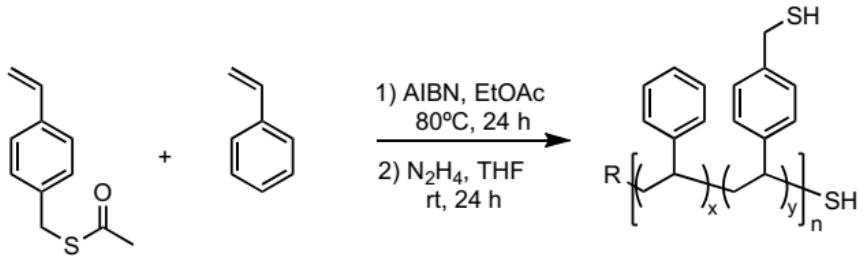

Styrene (3.12 g, 30.0 mmol) and 4-vinylbenzyl thioacetate (0.58 g, 3.0 mmol) were mixed with ethyl acetate (2 mL). A solution of AIBN (27.0 mg, 0.17 mmol) in ethyl acetate (1 mL) was added to the monomer solution. The solution was degassed via three cycles of freeze-pump-thaw, flushed with Ar and stirred at 80 ºC for 24 h. The reaction mixture was cooled down to room temperature, and the polymer was precipitated in cold methanol (25 mL), washed with methanol (25 mL) for 1 h and dried under vacuum at 60 ºC for 24 h. White, glassy solid (2.8 g, 76 %).

^{1}H-NMR ($CDCl_3$ with 0.05% v/v TMS, 400 MHz): δ_H 7.20-6.80 (br, m, Ar-H), 6.80-6.20 (br, m, Ar-H), 4.05 (br, s, CH_2), 2.32 (br, s, CH_3), 2.20-1.60 (br, CH), 1.60-1.20 (br, CH_2).

The copolymer was deprotected via aminolysis. Briefly, poly(styrene-*co*-4-vinylbenzyl thioacetate) (1.5 g, 1.3 mmol thiol monomer, 1.0 eq) was dissolved in THF (20 mL) and flushed with Ar for 10 min in a sealed flask. A solution of anhydrous hydrazine (78 µL, 2.5 mmol, 2.0 eq) in THF (5 mL) was added under Ar. The mixture was stirred at room temperature for 24 h, and

then concentrated under vacuum. The polymer was purified by filtration through silica column with DCM as eluent, and then it was precipitated in cold methanol (25 mL) and dried under vacuum at 60 ºC for 24 h. White, glassy solid (1.2 g, 80 %).

^{1}H-NMR ($CDCl_3$ with 0.05% v/v TMS, 400 MHz): δ_H 7.20-6.80 (br, m, Ar-H), 6.80-6.20 (br, m, Ar-H), 3.64 (br, s, CH_2), 2.20-1.60 (br, CH), 1.60-1.20 (br, CH_2).

Representative procedure for mechano-crosslinking of mercapto-polymer:

Mercapto-PMMA (150 mg, 1 eq thiol) was dissolved in DMF (400 μL) in a cylindrical polypropylene vial (dimensions: 0.68" x 1.09"). KI (11 mg, 0.5 eq) and ZnO nanoparticles (30 mg, 5 w%) were added. After homogenizing, the sample was sonicated in an ultrasound bath (40 kHz) for 6 h at room temperature. The gel was left to set for 12 h at room temperature.

Notes.- In the case of mercapto-PMA, the amounts of polymer and KI were adjusted to 200 mg and 16 mg, respectively; while in the case of mercapto-PS, they were set at 150 mg and 11 mg, respectively.

When using the electrodynamic shaker, the sample was vibrated at 2000 Hz for 8 h.

Procedure for synthesis of control mercapto-polymer gel:

Mercapto-PMMA (150 mg, 1 eq thiol) was dissolved in DMF (400 μL) in a cylindrical polypropylene vial (dimensions: 0.68" x 1.09"). KI (11 mg, 0.5 eq) and H_2O_2 30 vol. % (2 μL) were added. The sample was heated at 60 ºC for 1 h followed by setting at ambient conditions for 12 h.

3.3 Conclusions

In this chapter, we showed two methods to fabricate mechanically-adaptive polymeric materials by harnessing mechanical vibrations through piezoelectrochemistry. In the first example, we relied on the piezoreactivity of ZnO nanoparticles to promote a thiol-ene crosslinking reaction within a physical organogel, thus improving its mechanical properties. Moreover, we showed that the gel adapted in response to different mechanical input such as force, frequency, and time of vibration. In the second example, we used a similar approach with ZnO nanoparticles to synthesize a reversible organogel via disulfide bond formation. Additionally, we showed that the gel could be dissolved with a simple chemical treatment, and the polymer was recycled for further use.

3.4 References

1. Wang, Z.; Wang, J.; Ayarza, J.; Steeves, T.; Hu, Z.; Manna, S.; Esser-Kahn, A. P. Bio-inspired mechanically adaptive materials through vibration-induced crosslinking. *Nature Materials* **2021**, *20*, 869–874.

2. Lang, G. F.; Snyder, D. Understanding the physics of electrodynamic shaker performance. *Sound & Vibration* **2001**, *35*, 24-33.

3. Wojtecki, R. J.; Meador, M. A.; Rowan, S. J., Using the dynamic bond to access macroscopically responsive structurally dynamic polymers. *Nature Materials* **2011,** *10*, 14-27.

4. Roy, D., Cambre, J. N.; Sumerlin, B. S. Future Perspectives and Recent Advances in Stimuli-Responsive Materials. *Progress in Polymer Science* **2010**, *35*, 278–301.

5. Martin, H. D.; van der Zwaag, S.; Schubert, U. S. Self-Healing Materials. *Advances in Polymer Science* **2016**, 273.

6. Yoon, J. A.; Kamada, J.; Koynov, K.; Mohin, J.; Nicola, R.; Zhang, Y.; Balazs, A. C.; Kowalewski, T.; Matyjaszewski, K. Self-Healing Polymer Films Based on Thiol-Disulfide Exchange Reactions and Self-Healing Kinetics Measured Using Atomic Force Microscopy. *Macromolecules* **2012**, *45*, 142–149.

7. Fritze, U. F.; Craig, S. L.; von Delius, M. Disulfide-Centered Poly(Methyl Acrylates): Four Different Stimuli to Cleave a Polymer. *Journal of Polymer Science, Part A: Polymer Chemistry* **2018**, *56*, 1404–1411.

8. Fritze, U. F.; von Delius, M. Dynamic disulfide metathesis induced by ultrasound. *Chemical Communications* **2016**, *52*, 6363-6366.

9. García Ruano, J. L.; Parra, A.; Alemán, J. Efficient synthesis of disulfides by air oxidation of thiols under sonication. *Green Chemistry* **2008**, *10*, 706–711.

10. Mirzahosseini, A; Noszál, B. Species-Specific Standard Redox Potential of Thiol-Disulfide Systems: A Key Parameter to Develop Agents against Oxidative Stress. *Scientific Reports* **2016**, *6*, 37596.

11. Ayarza, J.; Wang, Z.; Wang, J.; Esser-Kahn, A. P. Mechanically Promoted Synthesis of Polymer Organogels via Disulfide Bond Cross-Linking. *ACS Macro Letters* **2021**, *10*(7), 799–804.

12. Kröger, A. P. P.; Boonen, R. J. A. E.; Paulusse, J. M. J. Well-defined single-chain polymer nanoparticles via thiol-Michael Addition. *Polymer* **2017**, *120*, 119-128.

13. Kirihara, A.; Asai, Y.; Ogawa, S.; Noguchi, T.; Hatano, A.; Hirai, Y. A Mild and Environmentally Benign Oxidation of Thiols to Disulfides. *Synthesis* **2007**, *21*, 3286–3289.

14. Sandmann, A.; Kompch, A.; Mackert, V.; Liebscher, C. H.; Winterer, M. Interaction of L-Cysteine with ZnO: Structure, Surface Chemistry, and Optical Properties. *Langmuir* **2015**, *31*, 5701−5711.

15. Sadik, P. W.; Pearton, S. J.; Norton, D. P.; Lambers, E.; Ren, F. Functionalizing Zn- and O-terminated ZnO with thiols. *Journal of Applied Physics* **2007**, 101, 104514.

16. Guglieri, C.; Aquilanti, G.; Díaz-Moreno, S.; Chaboy, J. Determination of the S–ZnO structural interaction in thiol-capped ZnO nanoparticles: a sulfur K-edge XAS study. *Nanotechnology* **2017**, *28*, 055704.

17. Dvorak, J.; Jirsak, T.; Rodriguez, J. A. Fundamental studies of desulfurization process: reaction of methanethiol on ZnO and Cs/ZnO. *Surface Science* **2001**, *479*, 155-168.

Chapter 4. Mechanically-promoted mineralization of an organogel

In our previous work, we explored the piezoreactivity of ZnO nanoparticles for polymerization and crosslinking reactions involving thiols, i.e., thiol ene and thiol-disulfide chemistries. As part of our attempts to have a better understanding of the underlying chemistry[1-5], we screened different types of small molecule thiols in solution towards reactivity with ZnO under ultrasound and vibration (using the electrodynamic shaker). Incidentally, we came across a particularly interesting phenomenon involving one of those molecules, 2-mercapto-5-methyl-1,3,4-thiadiazole (McMT). We observed the formation of a thick slurry after sonication for several hours.[6,7] Further analysis with SEM revealed that the slurry consisted of a suspension of rod-shaped microparticles. We envisioned such reaction could find a potential application for providing mechanical adaptability to synthetic materials via mineralization, similar to how hydroxyapatite mineralization occurs in bone.

4.1 Results and discussion

In our initial experiments, we made a solution of McMT in DMF (0.5 M) and added ZnO nanoparticles (5 wt%). The nanoparticles were homogenously dispersed, and the mixture was sonicated in an ultrasound bath (40 kHz) for 12 h, in the dark (Figure 22a-b(i)). The product was diluted with methanol, and the precipitate recovered by centrifugation. The precipitate was washed 3 times with methanol to remove any starting material and soluble by-products, and then dried under vacuum at 50 ºC overnight. SEM imaging of the precipitate revealed micron-sized rod-shaped particles (microrods) (Figure 22c).[7] The microrods were insoluble in water and most organic solvents, except for DMSO (although it required heating to 70 ºC for full dissolution).[8] Interestingly the microrods easily dissolved in a TCEP solution in DMF. In addition, we conducted

control reactions by removing either the ZnO nanoparticles or the ultrasound (instead mechanical stirring at 100 rpm). No precipitate formed when ZnO was absent from the reaction mixture (Figure 22b(ii)). When ultrasound was removed, we observed some microrod formation but at a much lower yield (Figure 22b(iii)). These results indicated that both components were necessary for the efficient formation of the microrods. Moreover, we ran two other control reactions, one where we substituted ZnO with soluble $ZnBr_2$ salt (Figure 22b(iv)), and another one where we substituted McMT with its corresponding disulfide dimer (Figure 22b(v)).[9] In neither case we observed the formation of the microrods.

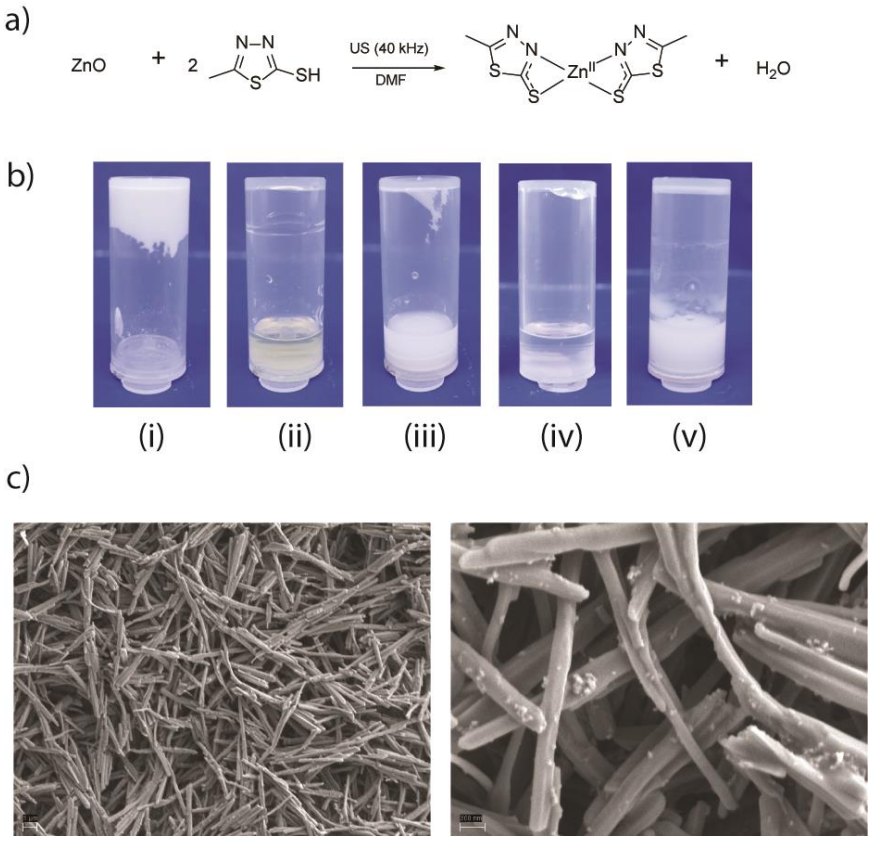

Figure 22. Ultrasound-promoted synthesis of microrods. a) Plausible reaction for the formation of microrods from McMT and ZnO nanoparticles under ultrasound. b) Synthesis of microrods: McMT (66 mg, 0.50 mmol), ZnO (30 mg, 5 wt%), DMF (400 μL). Ultrasound (40 kHz) for 12 h. Photos of control reactions: (i) all components, (ii) no ZnO, (iii) no ultrasound (stirring 100 rpm), (iv) with $ZnBr_2$ (5 wt%), and (v) with disulfide (66 mg, 0.25 mmol). The slurry only forms when

Figure 22 (continued). all components are present. c) SEM images of microrods, average dimension 0.3 x 5.2 μm. Scale bars: left image (1 μm) and right image (200 nm).

To determine the chemical composition of the microrods, we used FTIR, X-ray photoelectron (XPS), and powder X-ray diffraction (XRD) spectroscopies. We hypothesized that the microrods were an insoluble, crystalline compound formed via coordination of McMT with Zn^{2+} ions.[6-8,10-12] To test this hypothesis, we used conventional chemical synthesis to form a coordination compound, presumably $Zn(McMT)_2$, by mixing $Zn(NO_3)_2 \cdot 6H_2O$ with McMT in basic aqueous solution.[6,7] The resulting product, an insoluble precipitate, was compared with the one obtained via the sonication experiment. The XPS spectrum of the microrods showed the characteristic peaks of Zn (2p/3), O (1s/4), N (1s/5), C (1s/6), and S (2s/7), thus confirming the presence of McMT as part of their chemical composition (Figures E1-2). The FTIR spectrum of the microrods matched the spectrum of $Zn(McMT)_2$ (Figure 23). The XRD spectrum of the microrods also matched the spectrum of $Zn(McMT)_2$, although it also contained phases of the ZnO in considerably smaller proportion (Figure 24). All these results indicate that the microrods consist predominantly of the coordination compound $Zn(McMT)_2$. A plausible mechanism would be that the thiol interacts with the surface of the ZnO nanoparticles, and under the effect of ultrasound it sequesters Zn^{2+} ions to form $Zn(McMT)_2$, which then crystallizes *in situ* forming the microrods. Further confirmation of the chemical structure of the microrods will be assessed with single crystal XRD.

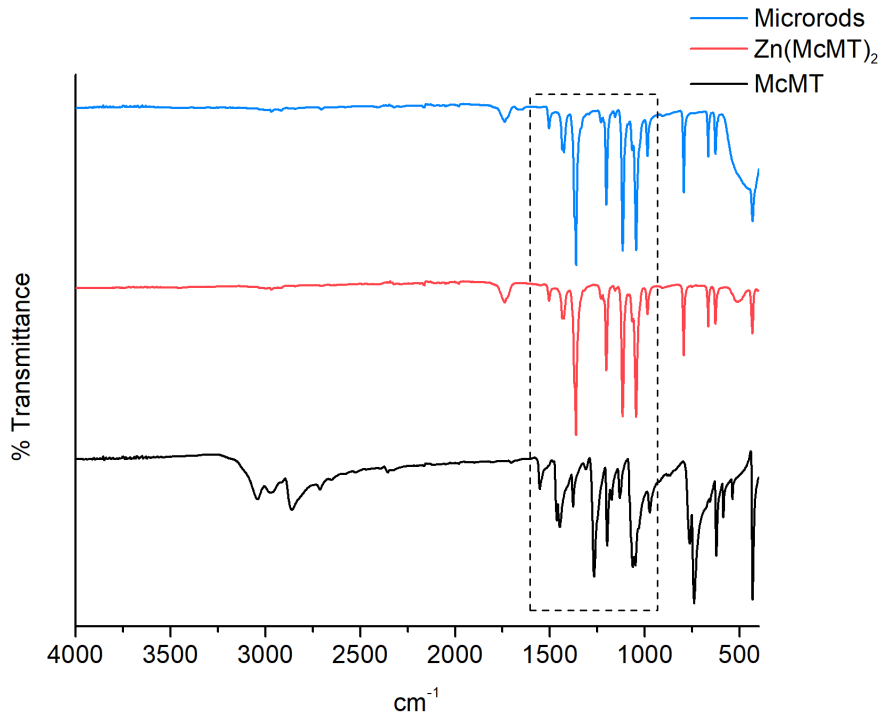

Figure 23. FTIR spectra of microrods, $Zn(McMT)_2$, and McMT.

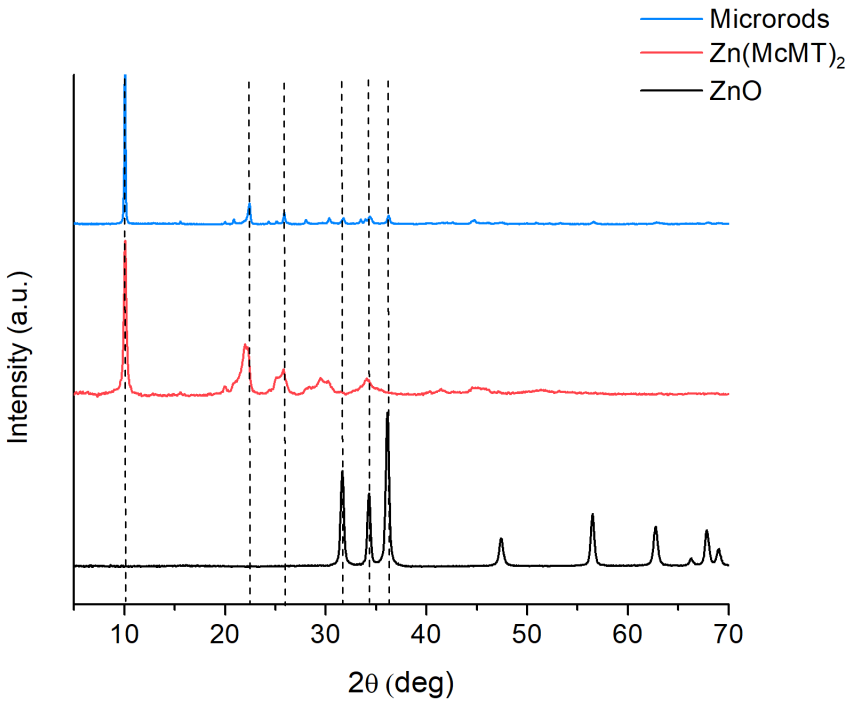

Figure 24. Powder XRD spectra microrods, $Zn(McMT)_2$, and ZnO nanoparticles.

With a reasonable idea of the composition of the microrods, we sought to examine the rheological properties of the slurry formed under sonication. We assumed the microrods consisted of $Zn(McMT)_2$ and varied the reaction conditions accordingly. To begin with, we examined the reaction kinetics by measuring the shear viscosity (Pa.s) of the slurry at different timepoints during the sonication. Additionally, we isolated the precipitate at each timepoint and took SEM images (Figures E3-7). As shown in Figure 25, the slurry always exhibited shear thinning behavior. The viscosity varied from the order of 1 Pa.s at 0 h to 1000 Pa.s at 6 h, reaching a maximum between 4 - 6 h of sonication time. From the SEM images, we observed that at 0 h the precipitate consists of the round-shaped ZnO nanoparticles. At the 1 and 2 h timepoints, the images show a mixture of round- and rod-shaped particles. Based on the mechanism discussed before, we hypothesize that the ZnO nanoparticles act as nucleation sites for the growth of the microrods. Finally, at the 4 and 6 h timepoints, we primarily see the microrod structures.

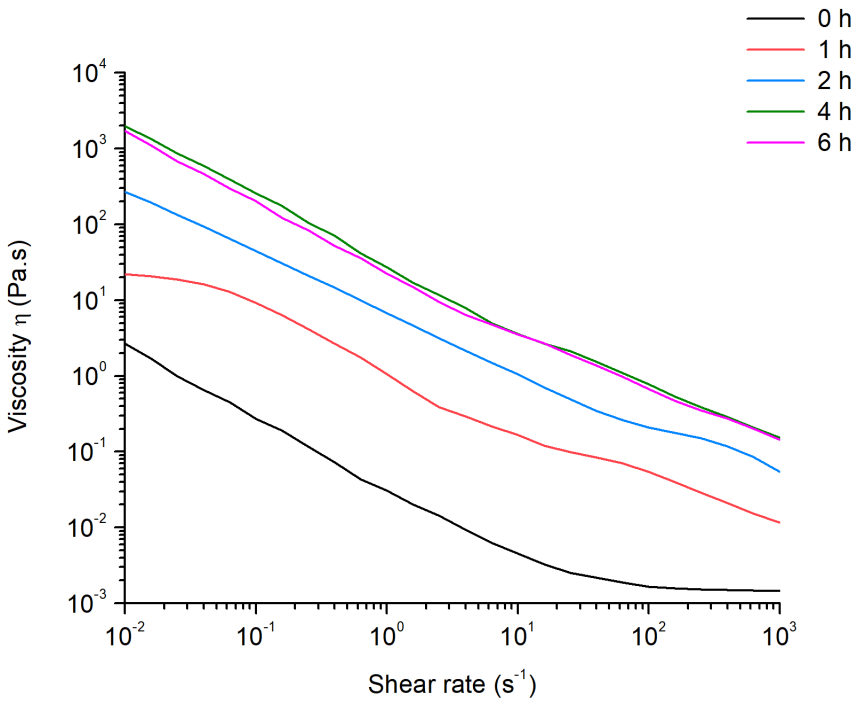

Figure 25. Shear rheology study of the microrod formation reaction at different timepoints. McMT (66 mg, 0.50 mmol), ZnO (20 mg, 0.25 mmol), DMF(400 μL). Ultrasound (40 kHz) for 6 h.

Next, we similarly studied the effect of varying the concentration of ZnO nanoparticles while maintaining the concentration of McMT constant. We assumed the optimal reaction stoichiometry would be 1 eq of ZnO per 2 eq of McMT. The highest viscosity was obtained when the [ZnO], in terms of equivalents of Zn^{2+}, was equal or greater than half the equivalents of McMT (Figure E8). In an analogous experiment, we maintained the [ZnO] constant and varied the [McMT]. In this case, we saw that the maximum viscosity was only obtained when the equivalents of McMT to Zn^{2+} were stoichiometrically balanced, as described above (Figure E9).

Finally, to show the potential use of this mechanically-promoted crystal growth method to reinforce polymeric materials, we sought to synthesize the microrods within a methyl cellulose organogel, similar to the one described in Chapter 3.1. Briefly, we dissolved methyl cellulose in

DMF at 90 ºC, then added McMT (2 eq), and stirred the solution until it was fully dissolved. We then added ZnO nanoparticles (1 eq) and dispersed them by sonicating the mixture for 20 s, followed by 5 min of vigorous stirring. We poured the mixture in a polypropylene vial and allowed it to cool to room temperature for 10 min. The vial was sonicated in an ultrasound bath (40 kHz) for 6 h (Figure 26). To confirm that the microrods had grown within the gel, we sliced a piece of it and dissolved in abundant DMF at 90 ºC for 15 min. We then isolated the precipitate by centrifugation and dried it at 50 ºC under vacuum overnight (Figure 26). The FTIR spectrum and SEM image of the precipitate confirmed that the microrods had formed within the MC organogel (Figure E10).

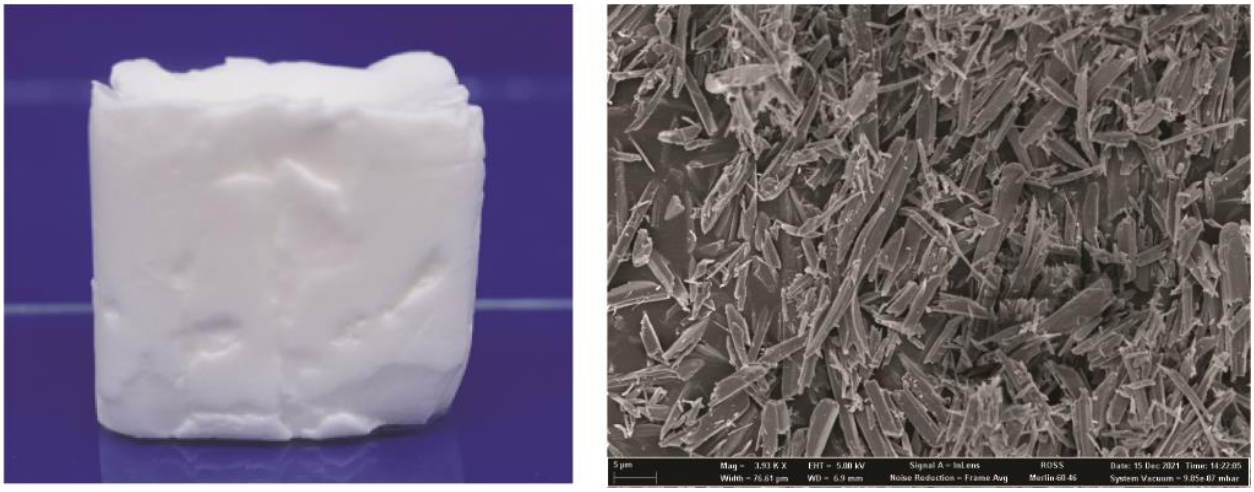

Figure 26. Synthesis of microrods within an organogel. *Left*: photo of MC organogel (1 x 1 x 1 cm) with McMT and ZnO nanoparticles after sonication (40 kHz). *Right*: SEM image of microrods formed within the organogel. Average dimensions: 1.3 x 3.3 μm. Scale bar: 5 μm.

4.2 Methods

Characterization techniques

SEM imaging: Scanning electron microscopy (SEM) was conducted in a Carl Zeiss Merlin high-resolution Field Emission Scanning Electron Microscope (FE-SEM). Samples were previously coated with a Pt film (10 nm thickness) using a Cressington 208 HR sputter coater with Pd/Pt target.

FTIR spectroscopy: Fourier transform infrared (FT-IR) spectra were recorded on a Perkin Elmer Spectrum Two FT-IR spectrometer in the MIR range (4000-400 cm^{-1}) using the ATR mode.

X-ray spectroscopy: Samples were analyzed in a KRATOS AXIS NOVA X-ray Photoelectron Spectrometer and in a Bruker D8 Powder X-ray Diffractometer.

Rheology measurements: Samples were analyzed with a rotational rheometer (TA Instruments, ARES G2) with a peltier element and a parallel plate fixture (25 mm). A volume of 100 μL of sample was used for each measurement, with a measuring gap of 200 μm, and the temperature set at 25 ºC.

DSC measurements: Samples were analyzed with a DSC 2500 instrument (TA Instruments) using a modulated DSC program in the range -90 to 250 ºC.

Synthetic procedures

Representative procedure for the synthesis of microrods:

In a polypropylene vial, McMT (66 mg, 0.50 mmol) was dissolved in DMF (400 μL). ZnO nanoparticles (20 mg, 0.25 mmol) were added to the solution, and homogenously dispersed via sonication for 20 s. The mixture was sonicated (40 kHz) in the dark for 4 h. The product was

diluted with methanol (5 mL) and separated by centrifugation (4000 rpm) for 10 min). The precipitate was washed twice with methanol (10 mL) and again separated by centrifugation. The product was dried at 50 ºC under vacuum overnight. Yield: 71 mg.

Synthesis of $Zn(McMT)_2$:

A solution of $Zn(NO_3)_2 \cdot 6H_2O$ (149 mg, 0.50 mmol) in water (1 mL) was prepared. In a separate vial, McMT (132 mg, 1.00 mmol) was dissolved in a $NaOH_{(aq)}$ 1 M solution (1 mL). The zinc nitrate solution was added dropwise to the McMT solution under vigorous stirring. A white precipitate formed, and the mixture was stirred for 30 min. The solid was recovered by filtration and washed thoroughly with water. The product was dried at 50 ºC under vacuum overnight. Yield: 128 mg.

Synthesis of microrods within MC organogel:

Methyl cellulose (200 mg) was dissolved in DMF (5 mL) at 90 ºC under vigorous stirring for 30 min. McMT (660 mg, 5.0 mmol) was added to the MC solution and dissolved for 10 min. Then, ZnO nanoparticles (204 mg, 2.5 mmol) were added, and homogenously dispersed by ultrasonication (40 kHz) for 30 s. The mixture was stirred at 90 ºC for 5 min, poured into a polypropylene vial, and let to cool down to room temperature for 10 min. Finally, it was sonicated (40 kHz) for 6 h.

4.3 Conclusions

In summary, we showed a novel approach to form organometallic microparticles (microrods) from the reaction of a small molecule thiol (McMT) with ZnO nanoparticles under ultrasonication. Additionally, we demonstrated that the microrods can form within a physical organogel matrix. We envision that this method can be used to reinforce polymeric materials under the influence of mechanical vibration, through a process that emulates the mineralization of bone. The next steps include finding a polymeric composite system to test our hypothesis and proving the strengthening of the material via mechanical testing.

4.4 References

1. Sadik, P. W.; Pearton, S. J.; Norton, D. P.; Lambers, E.; Ren, F. Functionalizing Zn- and O-terminated ZnO with thiols. *Journal of Applied Physics* **2007**, 101, 104514.

2. Pandurang, B. B.; Eknath, M. P.; Tribhuvannathji, K. V.; Suresh, S. S. Convenient and Efficient Synthesis of Thiol Esters using Zinc Oxide as a Heterogeneous and Eco-Friendly Catalyst. *Australian Journal of Chemistry* **2008**, 61, 1006-1010.

3. Sandmann, A.; Kompch, A.; Mackert, V.; Liebscher, C. H.; Winterer, M. Interaction of L-Cysteine with ZnO: Structure, Surface Chemistry, and Optical Properties. *Langmuir* **2015**, *31*, 5701−5711.

4. Guglieri, C.; Aquilanti, G.; Díaz-Moreno, S.; Chaboy, J. Determination of the S–ZnO structural interaction in thiol-capped ZnO nanoparticles: a sulfur K-edge XAS study. *Nanotechnology* **2017**, *28*, 055704.

5. Mohinuddin, P. M. K.; Gangi Reddy, N. C. Zinc Oxide Catalyzed Solvent-Free Mechanochemical Route for C–S Bond Construction: A Sustainable Process. *European Journal of Organic Chemistry* **2017**, 1207-1214.

6. Yuting, L.; Baojun, S.; Ying, Z.; Dawei, Y. Synthesis of Thiadiazole Zineb. *Procedia Engineering* **2011**, 24, 519–522.

7. Fabretti, A. C.; Franchini, G. C.; Peyronel, G.; Bellei, M. Zinc (II), cadmium (II) and mercury (II) complexes of 2-methyl-5-mercapto-1,3,4-thiadiazole. *Spectrochimica Acta Part A: Molecular Spectroscopy* **1981**, *37*(8), 587-590.

8. Chen, X.; Zhou, L.; Laborda, P.; Zhao, Y.; Li, K.; Liu, F. First method for dissolving zinc thiazole and re-evaluation of its antibacterial properties against rice bacterial blight disease. *Phytopathology Research* **2019**, *1*, 30.

9. Tian, H.; Jiang, X.; Yu, Z.; Kloo, L.; Hagfeldt, A.; Sun, L. Efficient Organic-Dye-Sensitized Solar Cells Based on an Iodine-Free Electrolyte. *Angewandte Chemie International Edition* **2010**, *49*, 7328-7331.

10. Hipler, F.; Winter, M.; Fischer, R. A. N–H···S hydrogen bonding in 2-mercapto-5-methyl-1,3,4-thiadiazole. Synthesis and crystal structures of mercapto functionalised 1,3,4-thiadiazoles. *Journal of Molecular Structure* **2003**, *658*(3), 179-191.

11. Hu, Y.; Li, C. Y.; Wang, X. M.; Yang, Y. H.; Zhu, H. L. 1,3,4-Thiadiazole: Synthesis, Reactions, and Applications in Medicinal, Agricultural, and Materials Chemistry *Chemical Reviews* **2014**, *114*(10), 5572–5610.

12. Pal, S.; Singh, V.; Kumar, R.; Gogoi, R. Design and development of 1,3,4-thiadiazole based potent new nano-fungicides. *Journal of Molecular Structure* **2020**, *1219*, 128507.

Appendix A: Supporting information for Chapter 2.1: Mechanically-promoted copper ‘click’ polymerization

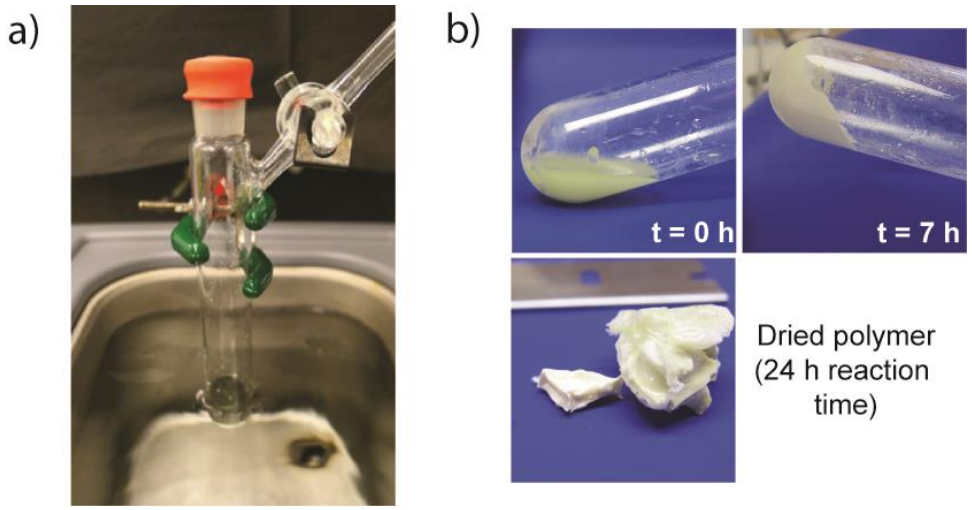

Figure A1. Photos of mechano-click polymerization. a) Photo of representative setup of a mechano-click polymerization reaction. The volume of the Schlenk tube is 25 mL and is approximately 6.12 in height; and b) Photos of mechano-click polymerization reaction mixture before and after sonication, and dried polytriazole after 24 h reaction time.

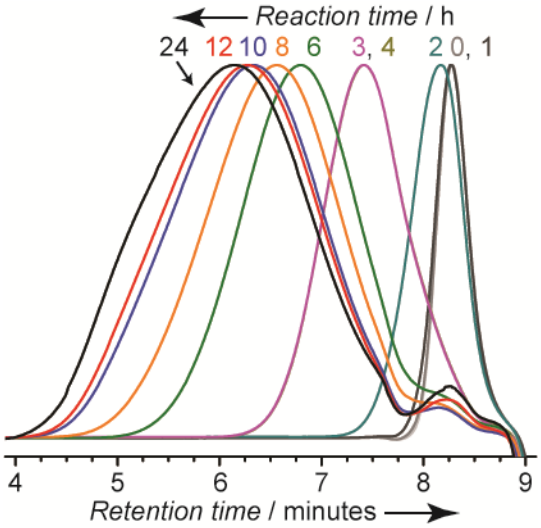

Figure A2. GPC trace depicting the evolution of polymer molecular weight over time.

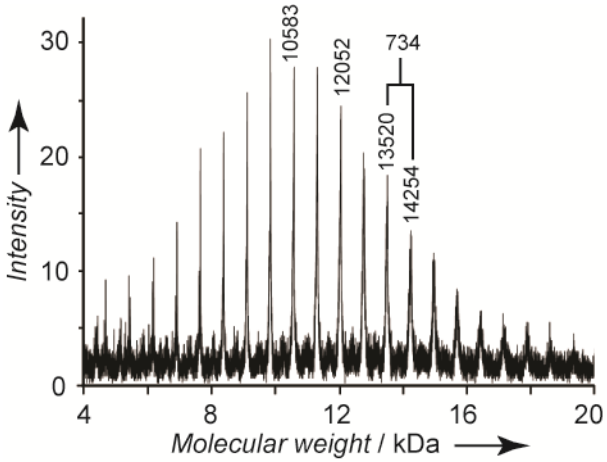

Figure A3. MALDI-TOF spectrum of polytriazole.

NMR spectra

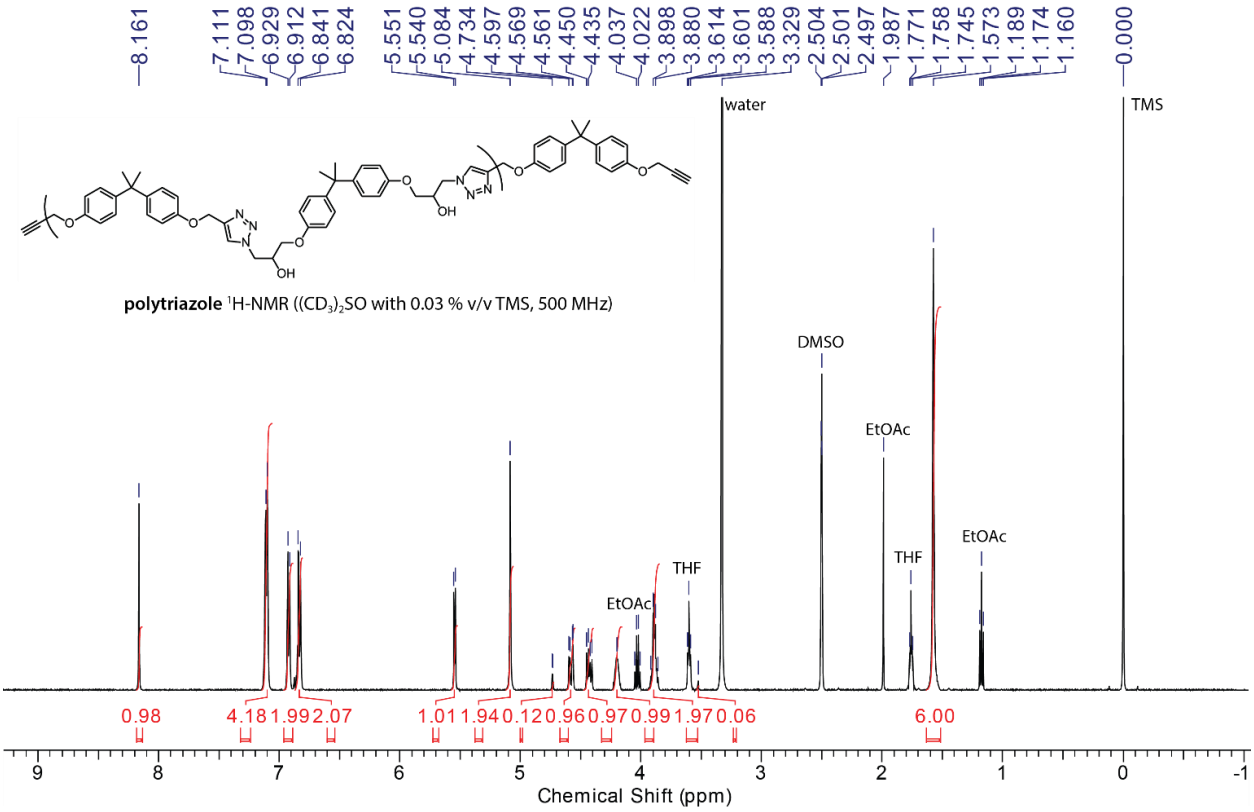

polytriazole ^{1}H-NMR ((CD$_3$)$_2$SO with 0.03 % v/v TMS, 500 MHz)

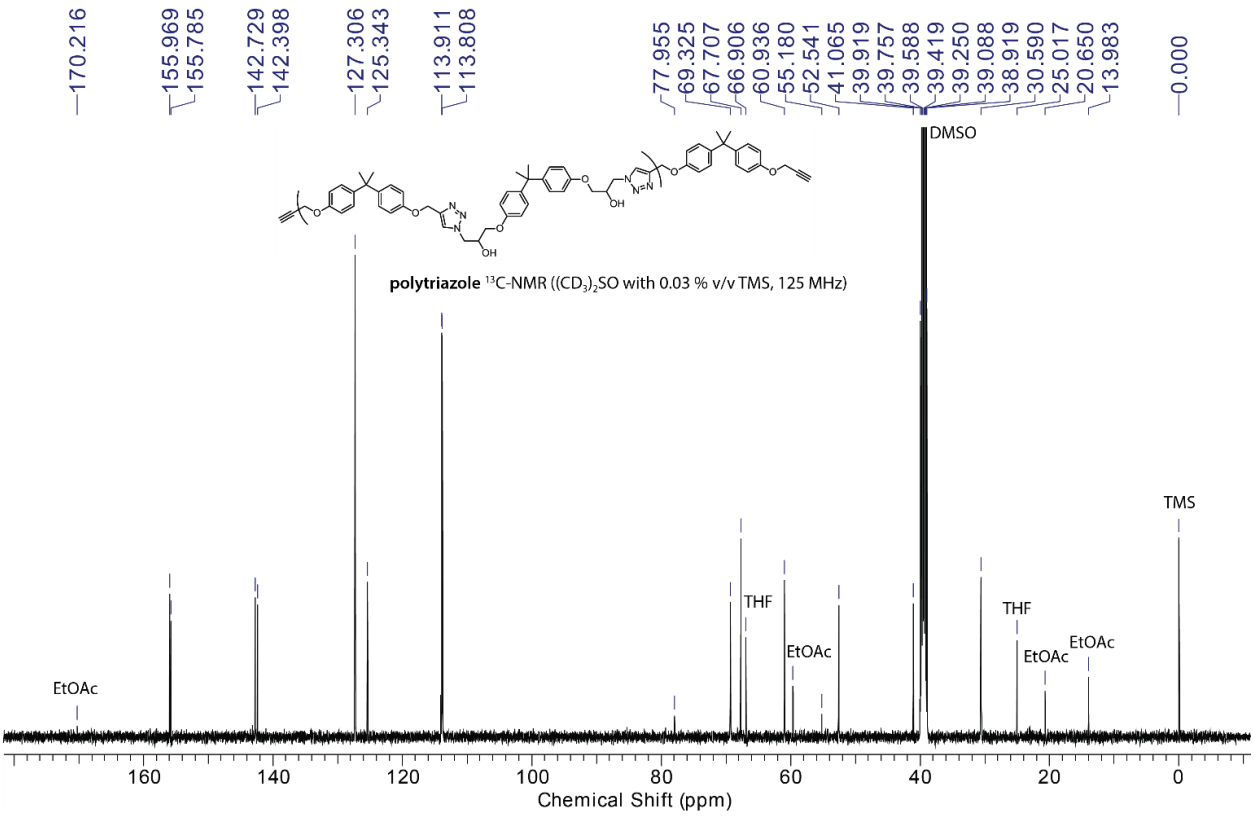

polytriazole ^{13}C-NMR ((CD$_3$)$_2$SO with 0.03 % v/v TMS, 125 MHz)

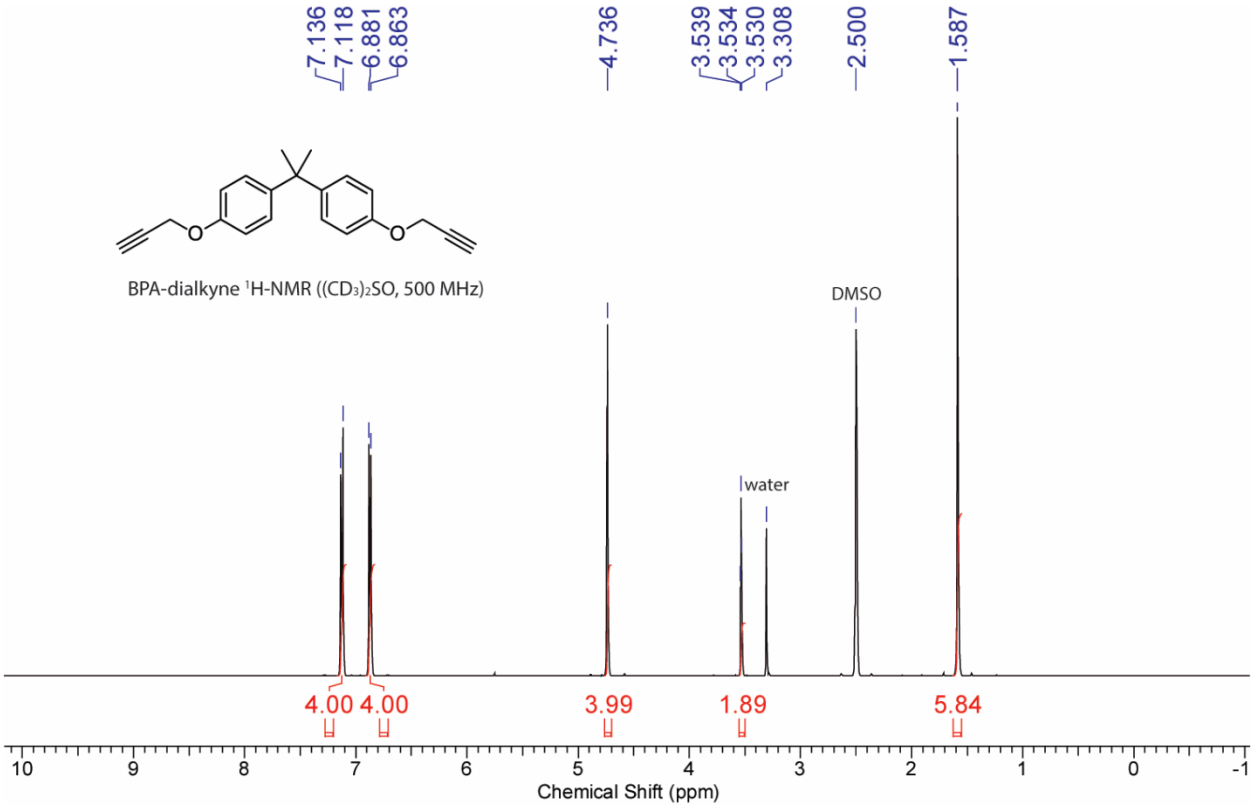
7.136
7.118
6.881
6.863
4.736
3.539
3.534
3.530
3.308
2.500
1.587
BPA-dialkyne ¹H-NMR ((CD₃)₂SO, 500 MHz)
DMSO
water
4.00
4.00
3.99
1.89
5.84
Chemical Shift (ppm)

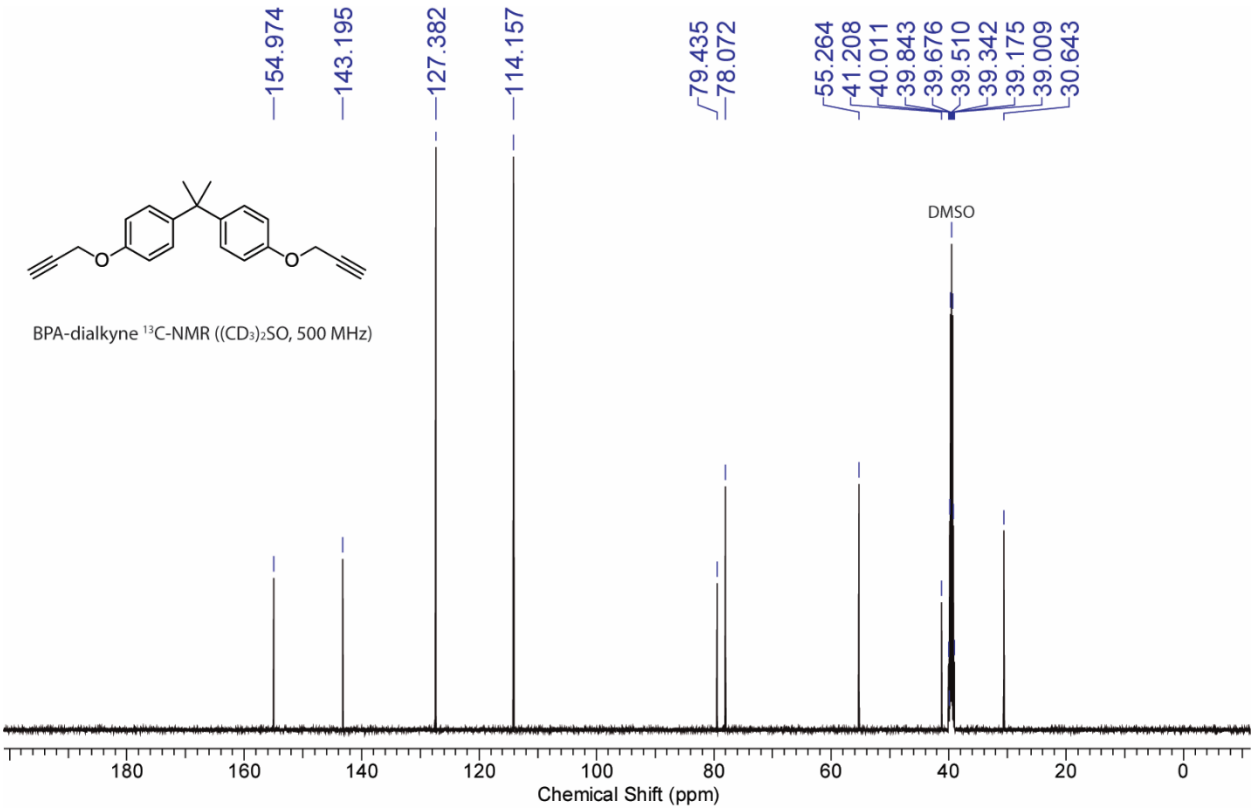
154.974
143.195
127.382
114.157
79.435
78.072
55.264
41.208
40.011
39.843
39.676
39.510
39.342
39.175
39.009
30.643
BPA-dialkyne ¹³C-NMR ((CD₃)₂SO, 500 MHz)
DMSO
Chemical Shift (ppm)

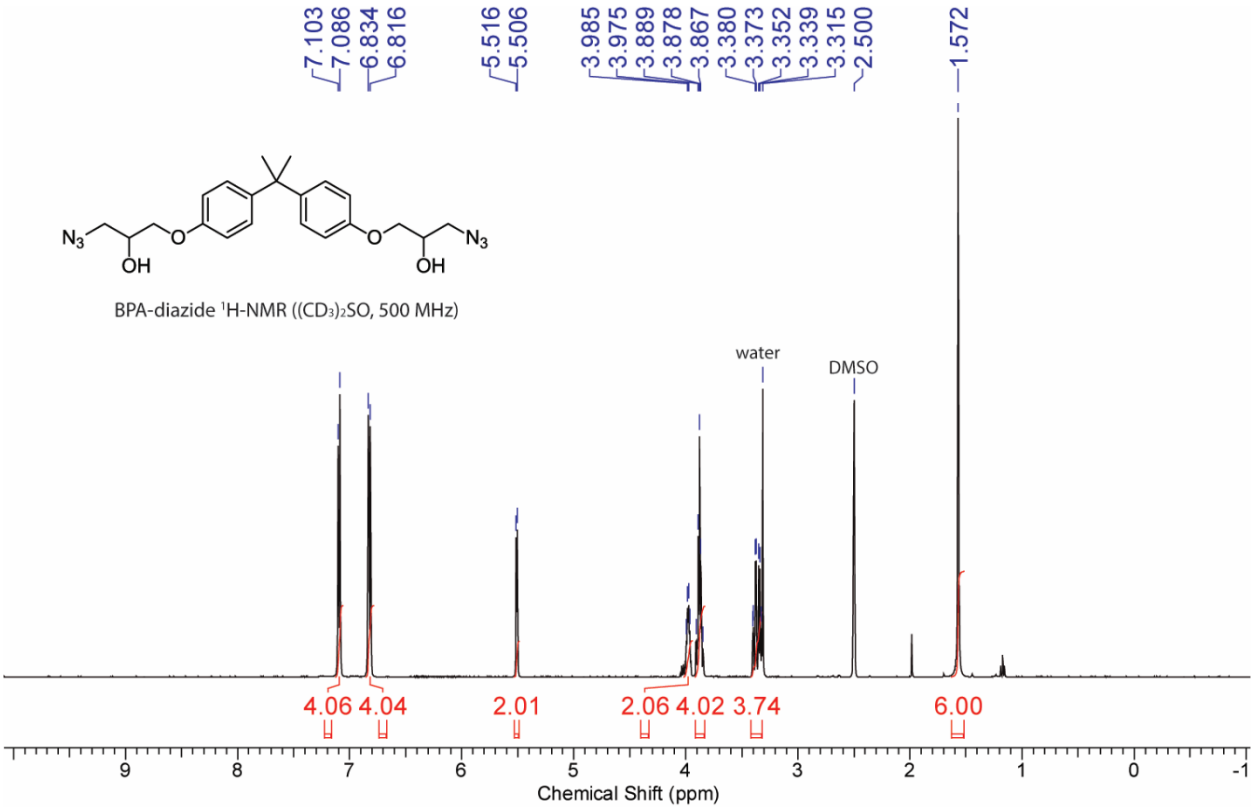

BPA-diazide ^{1}H-NMR ((CD$_3$)$_2$SO, 500 MHz)

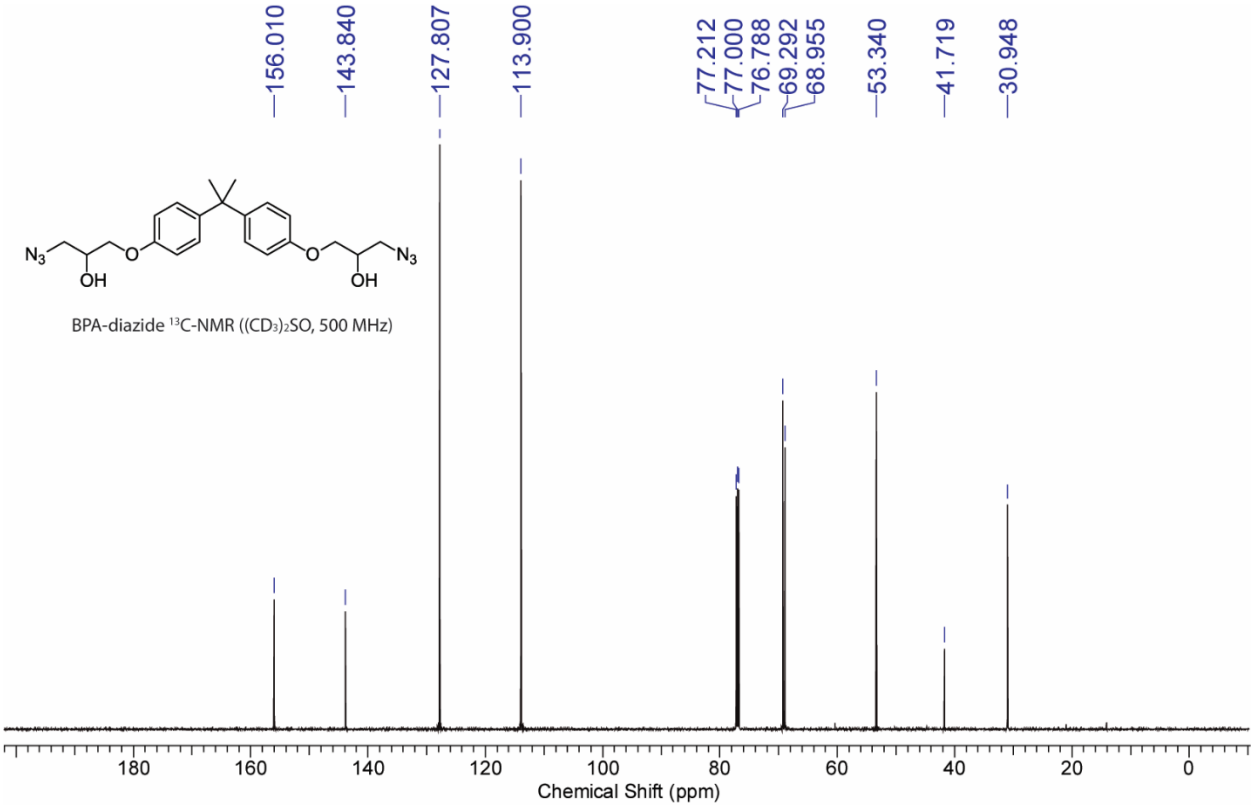

BPA-diazide ^{13}C-NMR ((CD$_3$)$_2$SO, 500 MHz)

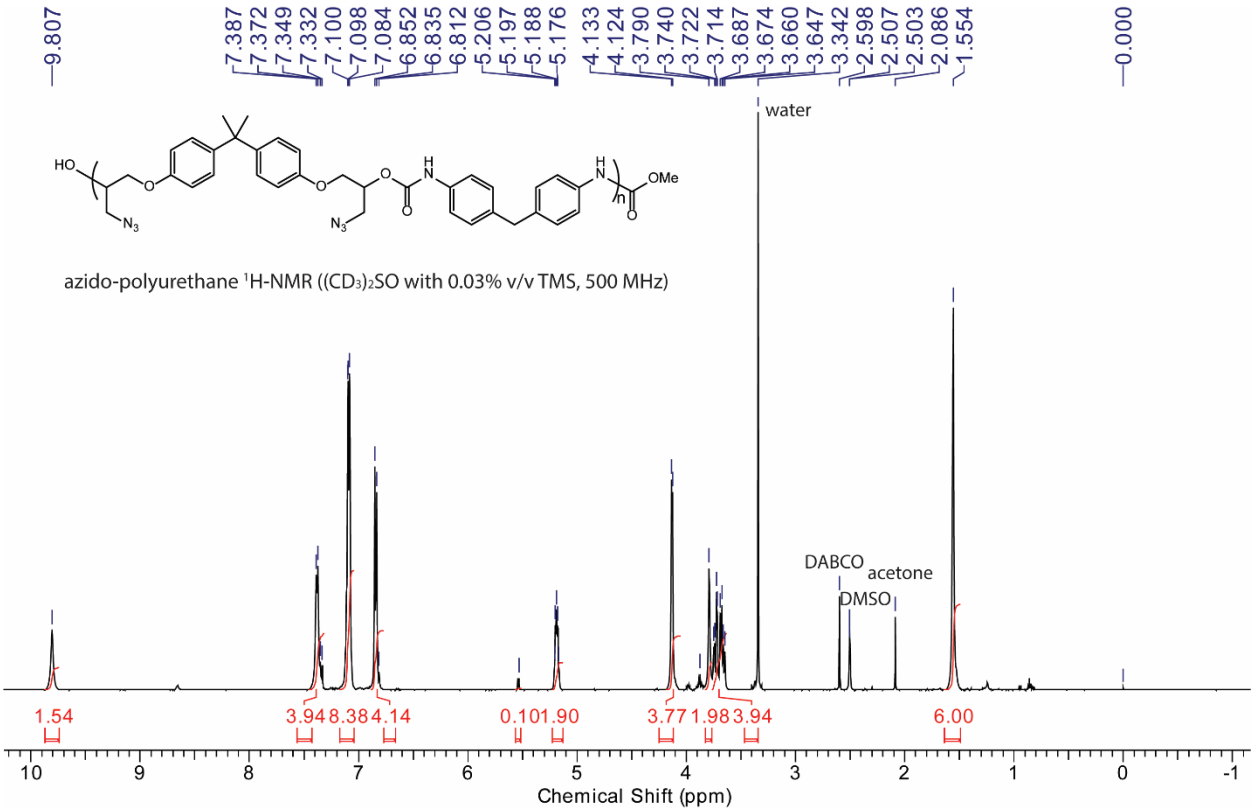

azido-polyurethane ^{1}H-NMR ($(CD_3)_2SO$ with 0.03% v/v TMS, 500 MHz)

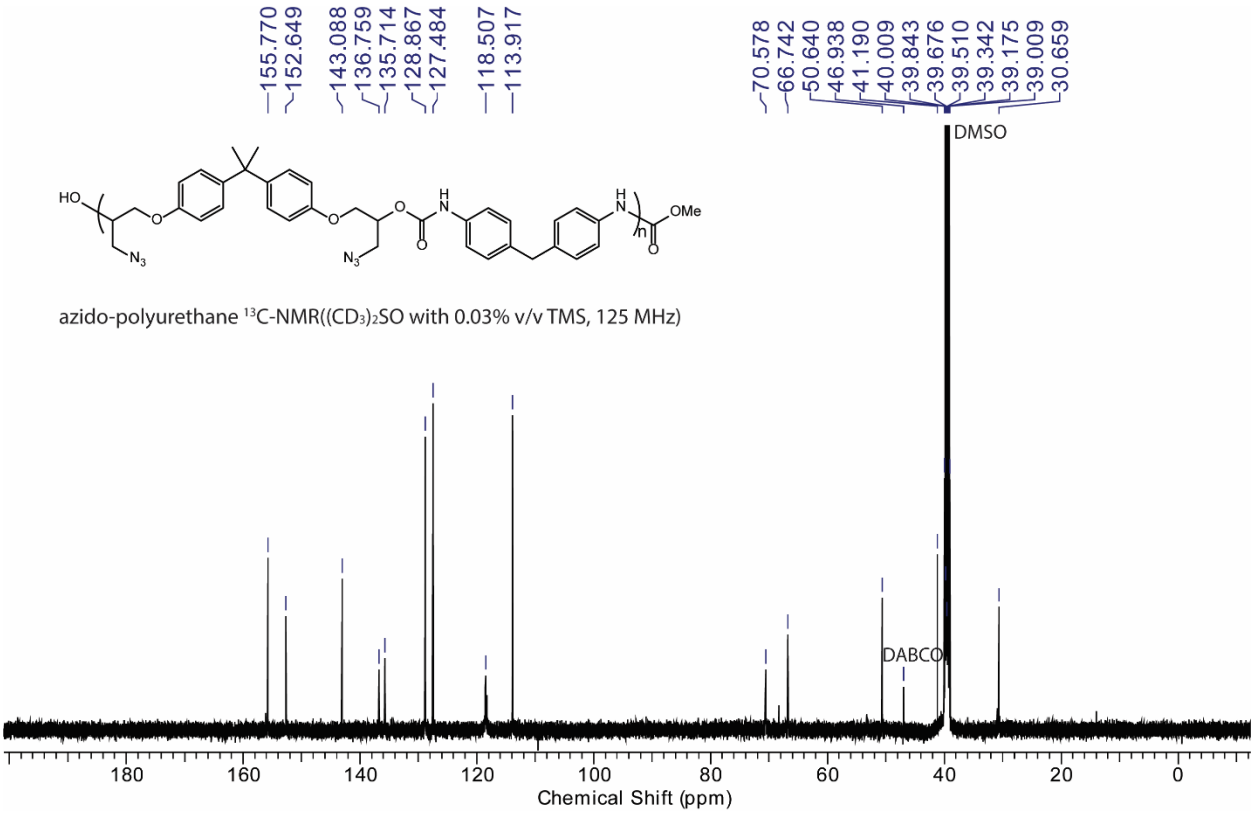

azido-polyurethane ^{13}C-NMR($(CD_3)_2SO$ with 0.03% v/v TMS, 125 MHz)

^{1}H-NMR spectra corresponding to kinetics experiment of mechano-click polymerization

t = 0 h

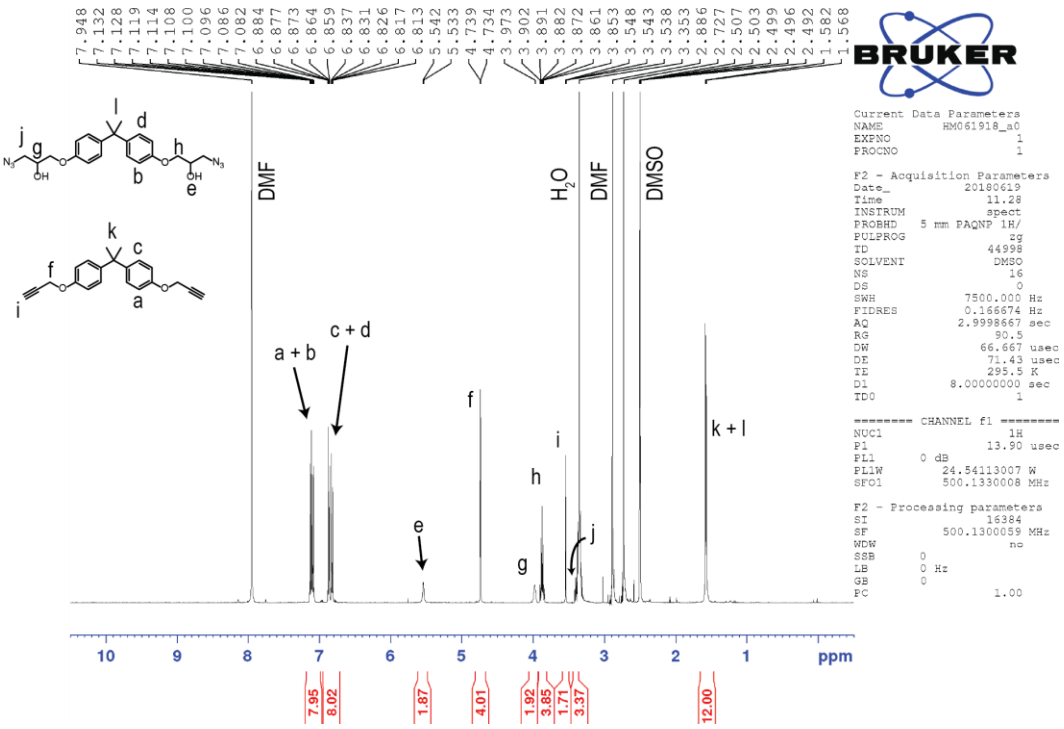

t = 1 h

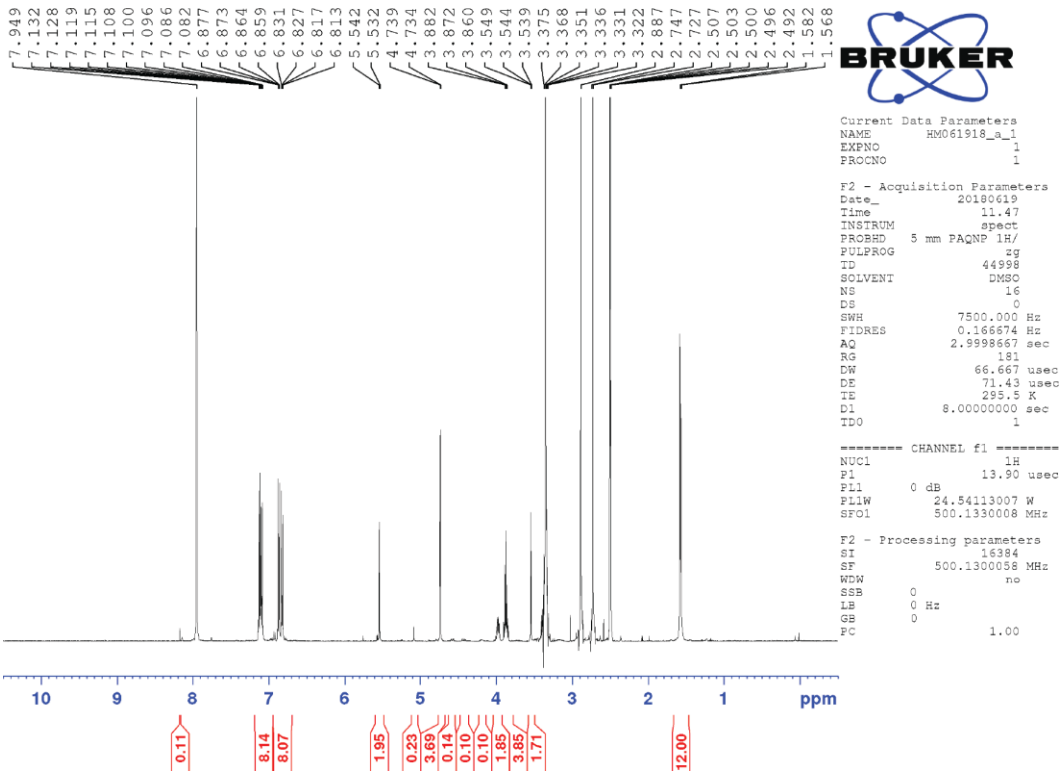

t = 2 h

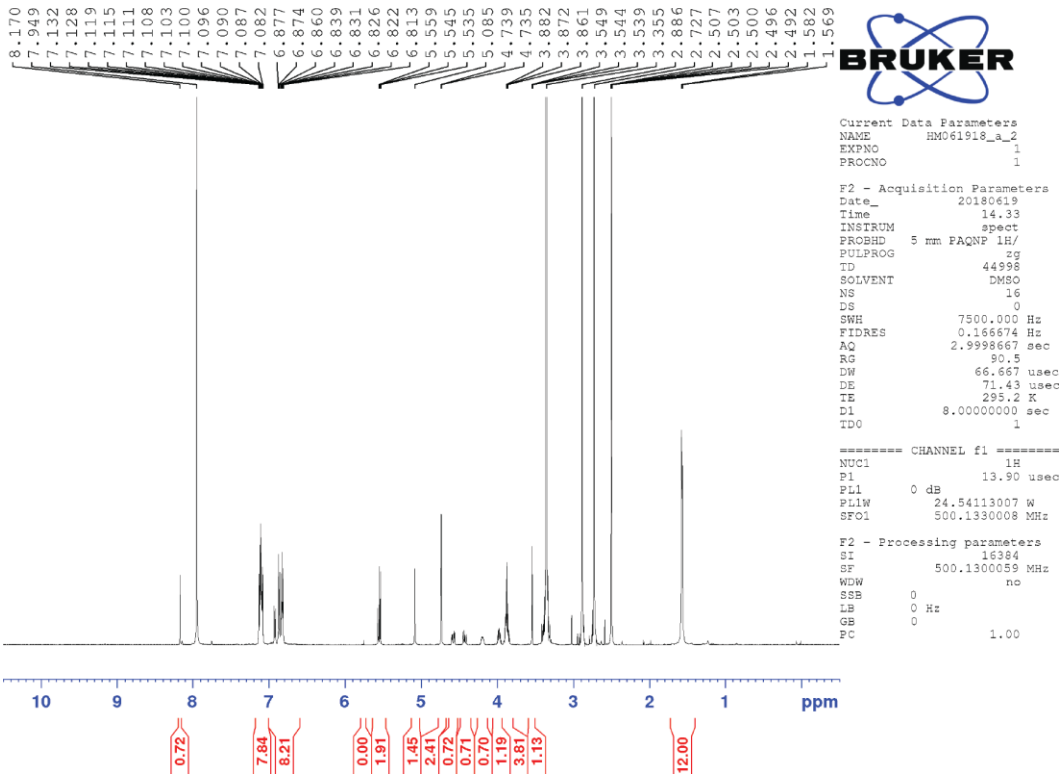
8.170
7.949
7.132
7.128
7.119
7.115
7.111
7.108
7.103
7.100
7.096
7.090
7.087
7.082
6.877
6.874
6.860
6.839
6.831
6.826
6.822
6.813
5.559
5.545
5.535
5.085
4.739
4.735
3.882
3.872
3.861
3.549
3.544
3.539
3.355
2.886
2.727
2.507
2.503
2.500
2.496
2.492
1.582
1.569
BRUKER
Current Data Parameters
NAME HM061918_a_2
EXPNO 1
PROCNO 1
F2 - Acquisition Parameters
Date_ 20180619
Time 14.33
INSTRUM spect
PROBHD 5 mm PAQNP 1H/
PULPROG zg
TD 44998
SOLVENT DMSO
NS 16
DS 0
SWH 7500.000 Hz
FIDRES 0.166674 Hz
AQ 2.9998667 sec
RG 90.5
DW 66.667 usec
DE 71.43 usec
TE 295.2 K
D1 8.00000000 sec
TD0 1
======== CHANNEL f1 ========
NUC1 1H
P1 13.90 usec
PL1 0 dB
PL1W 24.54113007 W
SFO1 500.1330008 MHz
F2 - Processing parameters
SI 16384
SF 500.1300059 MHz
WDW no
SSB 0
LB 0 Hz
GB 0
PC 1.00
10 9 8 7 6 5 4 3 2 1 ppm
0.72 7.84 8.21 0.00 1.91 1.45 2.41 0.72 0.71 0.70 1.19 3.81 1.13 12.00

t = 3 h

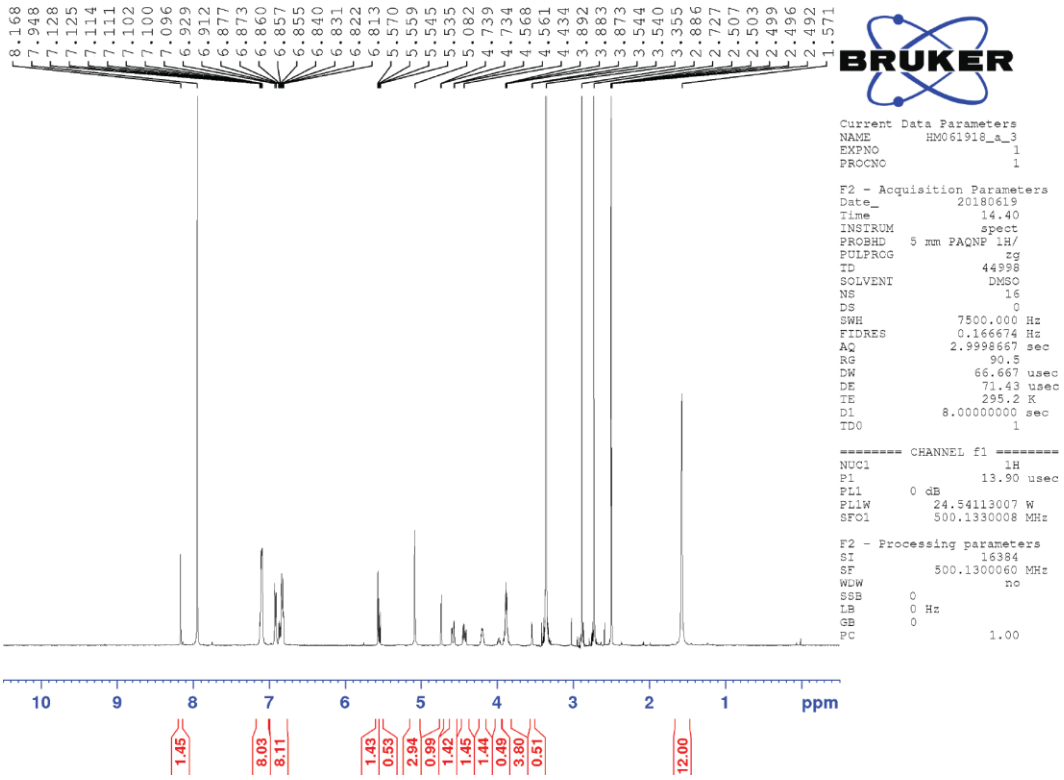
8.168
7.948
7.128
7.125
7.114
7.111
7.102
7.100
7.096
6.929
6.912
6.877
6.873
6.860
6.857
6.855
6.840
6.831
6.822
6.813
5.570
5.559
5.545
5.535
5.082
4.739
4.734
4.568
4.561
4.434
3.892
3.883
3.873
3.544
3.540
3.355
2.886
2.727
2.507
2.503
2.499
2.496
2.492
1.571
BRUKER
Current Data Parameters
NAME HM061918_a_3
EXPNO 1
PROCNO 1
F2 - Acquisition Parameters
Date_ 20180619
Time 14.40
INSTRUM spect
PROBHD 5 mm PAQNP 1H/
PULPROG zg
TD 44998
SOLVENT DMSO
NS 16
DS 0
SWH 7500.000 Hz
FIDRES 0.166674 Hz
AQ 2.9998667 sec
RG 90.5
DW 66.667 usec
DE 71.43 usec
TE 295.2 K
D1 8.00000000 sec
TD0 1
======== CHANNEL f1 ========
NUC1 1H
P1 13.90 usec
PL1 0 dB
PL1W 24.54113007 W
SFO1 500.1330008 MHz
F2 - Processing parameters
SI 16384
SF 500.1300060 MHz
WDW no
SSB 0
LB 0 Hz
GB 0
PC 1.00
10 9 8 7 6 5 4 3 2 1 ppm
1.45 8.03 8.11 1.43 0.53 2.94 0.99 1.42 1.45 1.44 0.49 3.80 0.51 12.00

t = 4 h

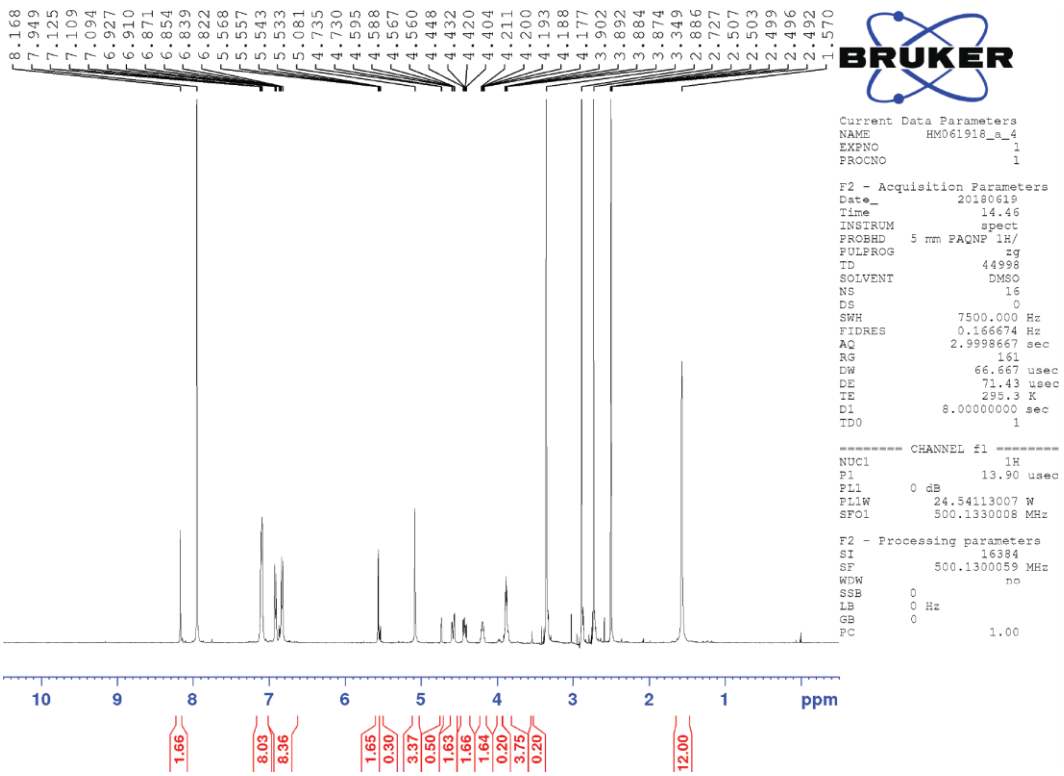
8.168
7.949
7.125
7.109
7.094
6.927
6.910
6.871
6.854
6.839
6.822
5.568
5.557
5.543
5.533
5.081
4.735
4.730
4.595
4.588
4.567
4.560
4.448
4.432
4.420
4.404
4.211
4.200
4.193
4.188
4.177
3.902
3.892
3.884
3.874
3.349
2.886
2.727
2.507
2.503
2.499
2.496
2.492
1.570
BRUKER
Current Data Parameters
NAME HM061918_a_4
EXPNO 1
PROCNO 1
F2 - Acquisition Parameters
Date_ 20180619
Time 14.46
INSTRUM spect
PROBHD 5 mm PAQNP 1H/
PULPROG zg
TD 44998
SOLVENT DMSO
NS 16
DS 0
SWH 7500.000 Hz
FIDRES 0.166674 Hz
AQ 2.9998667 sec
RG 161
DW 66.667 usec
DE 71.43 usec
TE 295.3 K
D1 8.00000000 sec
TD0 1
======== CHANNEL f1 ========
NUC1 1H
P1 13.90 usec
PL1 0 dB
PL1W 24.54113007 W
SFO1 500.1330008 MHz
F2 - Processing parameters
SI 16384
SF 500.1300059 MHz
WDW no
SSB 0
LB 0 Hz
GB 0
PC 1.00
10 9 8 7 6 5 4 3 2 1 ppm
1.66
8.03
8.36
1.65
0.30
3.37
0.50
1.63
1.66
1.64
0.20
3.75
0.20
12.00

t = 6 h

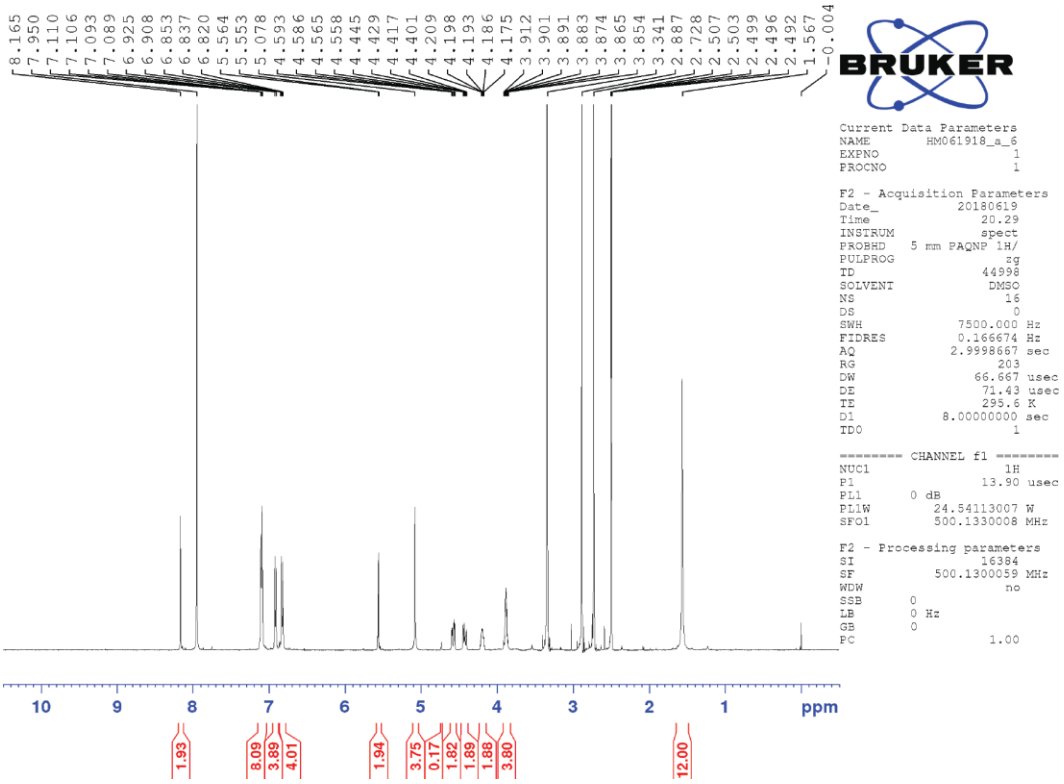
8.165
7.950
7.110
7.106
7.093
7.089
6.925
6.908
6.853
6.837
6.820
5.564
5.553
5.078
4.593
4.586
4.565
4.558
4.445
4.429
4.417
4.401
4.209
4.198
4.193
4.186
4.175
3.912
3.901
3.891
3.883
3.874
3.865
3.854
3.341
2.887
2.728
2.507
2.503
2.499
2.496
2.492
1.567
-0.004
BRUKER
Current Data Parameters
NAME HM061918_a_6
EXPNO 1
PROCNO 1
F2 - Acquisition Parameters
Date_ 20180619
Time 20.29
INSTRUM spect
PROBHD 5 mm PAQNP 1H/
PULPROG zg
TD 44998
SOLVENT DMSO
NS 16
DS 0
SWH 7500.000 Hz
FIDRES 0.166674 Hz
AQ 2.9998667 sec
RG 203
DW 66.667 usec
DE 71.43 usec
TE 295.6 K
D1 8.00000000 sec
TD0 1
======== CHANNEL f1 ========
NUC1 1H
P1 13.90 usec
PL1 0 dB
PL1W 24.54113007 W
SFO1 500.1330008 MHz
F2 - Processing parameters
SI 16384
SF 500.1300059 MHz
WDW no
SSB 0
LB 0 Hz
GB 0
PC 1.00
10 9 8 7 6 5 4 3 2 1 ppm
1.93
8.09
3.89
4.01
1.94
3.75
0.17
1.82
1.89
1.88
3.80
12.00

t = 8 h

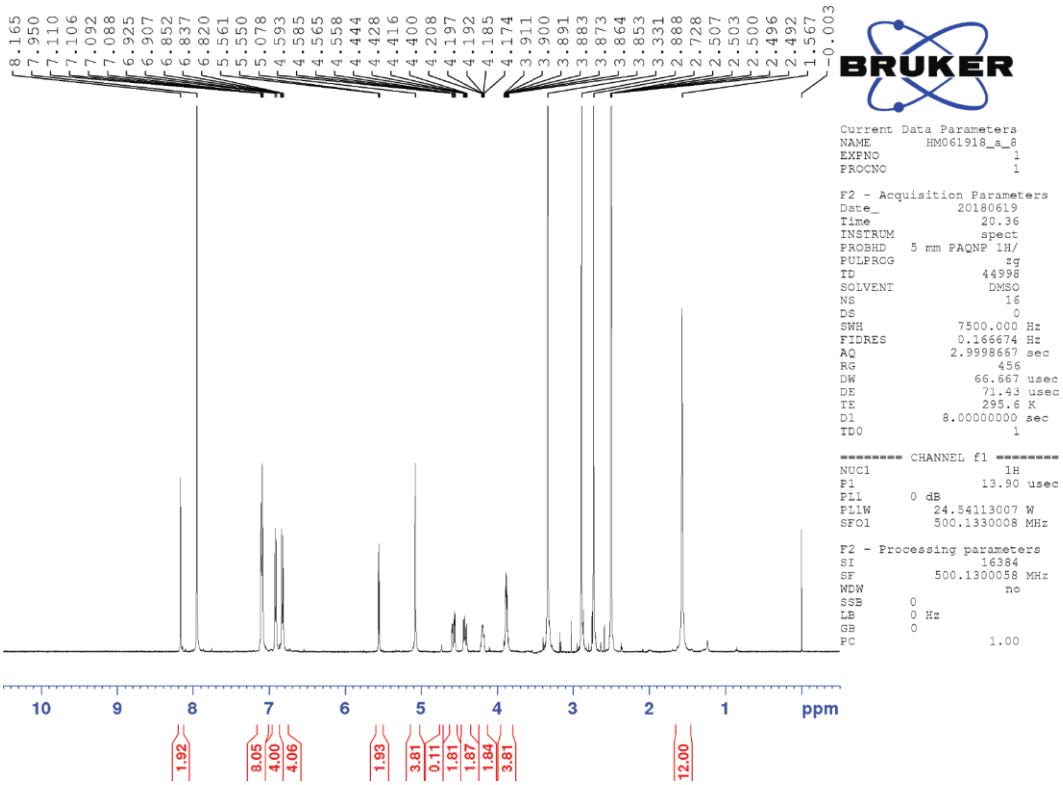
8.165
7.950
7.110
7.106
7.092
7.088
6.925
6.907
6.852
6.837
6.820
5.561
5.550
5.078
4.593
4.585
4.565
4.558
4.444
4.428
4.416
4.400
4.208
4.197
4.192
4.185
4.174
3.911
3.900
3.891
3.883
3.873
3.864
3.853
3.331
2.888
2.728
2.507
2.503
2.500
2.496
2.492
1.567
-0.003
BRUKER
Current Data Parameters
NAME HM061918_a_8
EXPNO 1
PROCNO 1
F2 - Acquisition Parameters
Date_ 20180619
Time 20.36
INSTRUM spect
PROBHD 5 mm PAQNP 1H/
PULPROG zg
TD 44998
SOLVENT DMSO
NS 16
DS 0
SWH 7500.000 Hz
FIDRES 0.166674 Hz
AQ 2.9998667 sec
RG 456
DW 66.667 usec
DE 71.43 usec
TE 295.6 K
D1 8.00000000 sec
TD0 1
======== CHANNEL f1 ========
NUC1 1H
P1 13.90 usec
PL1 0 dB
PL1W 24.54113007 W
SFO1 500.1330008 MHz
F2 - Processing parameters
SI 16384
SF 500.1300058 MHz
WDW no
SSB 0
LB 0 Hz
GB 0
PC 1.00
10
9
8
7
6
5
4
3
2
1
ppm
1.92
8.05
4.00
4.06
1.93
3.81
0.11
1.81
1.87
1.84
3.81
12.00

t = 10 h

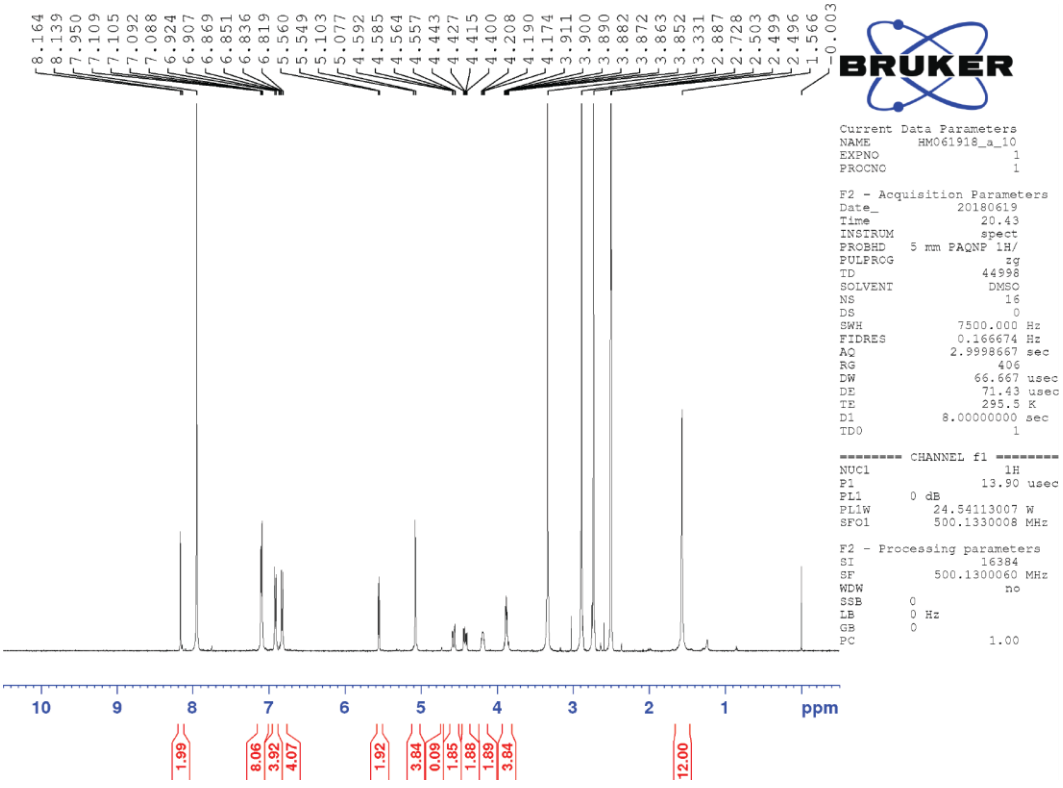
8.164
8.139
7.950
7.109
7.105
7.092
7.088
6.924
6.907
6.869
6.851
6.836
6.819
5.560
5.549
5.103
5.077
4.592
4.585
4.564
4.557
4.443
4.427
4.415
4.400
4.208
4.190
4.174
3.911
3.900
3.890
3.882
3.872
3.863
3.852
3.331
2.887
2.728
2.503
2.499
2.496
1.566
-0.003
BRUKER
Current Data Parameters
NAME HM061918_a_10
EXPNO 1
PROCNO 1
F2 - Acquisition Parameters
Date_ 20180619
Time 20.43
INSTRUM spect
PROBHD 5 mm PAQNP 1H/
PULPROG zg
TD 44998
SOLVENT DMSO
NS 16
DS 0
SWH 7500.000 Hz
FIDRES 0.166674 Hz
AQ 2.9998667 sec
RG 406
DW 66.667 usec
DE 71.43 usec
TE 295.5 K
D1 8.00000000 sec
TD0 1
======== CHANNEL f1 ========
NUC1 1H
P1 13.90 usec
PL1 0 dB
PL1W 24.54113007 W
SFO1 500.1330008 MHz
F2 - Processing parameters
SI 16384
SF 500.1300060 MHz
WDW no
SSB 0
LB 0 Hz
GB 0
PC 1.00
10
9
8
7
6
5
4
3
2
1
ppm
1.99
8.06
3.92
4.07
1.92
3.84
0.09
1.85
1.88
1.89
3.84
12.00

t = 12 h

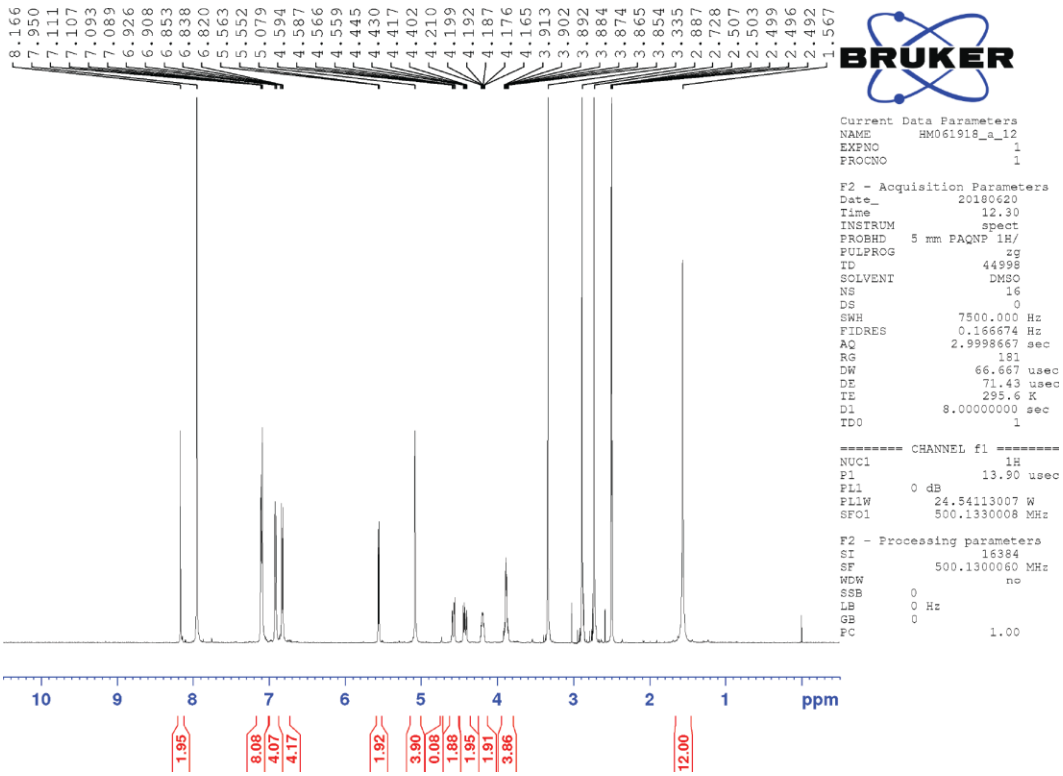
8.166 7.950 7.111 7.107 7.093 7.089 6.926 6.908 6.853 6.838 6.820 5.563 5.552 5.079 4.594 4.587 4.566 4.559 4.445 4.430 4.417 4.402 4.210 4.199 4.192 4.187 4.176 4.165 3.913 3.902 3.892 3.884 3.874 3.865 3.854 3.335 2.887 2.728 2.507 2.503 2.499 2.496 2.492 1.567
BRUKER
Current Data Parameters
NAME HM061918_a_12
EXPNO 1
PROCNO 1
F2 - Acquisition Parameters
Date_ 20180620
Time 12.30
INSTRUM spect
PROBHD 5 mm PAQNP 1H/
PULPROG zg
TD 44998
SOLVENT DMSO
NS 16
DS 0
SWH 7500.000 Hz
FIDRES 0.166674 Hz
AQ 2.9998667 sec
RG 181
DW 66.667 usec
DE 71.43 usec
TE 295.6 K
D1 8.00000000 sec
TD0 1
======== CHANNEL f1 ========
NUC1 1H
P1 13.90 usec
PL1 0 dB
PL1W 24.54113007 W
SFO1 500.1330008 MHz
F2 - Processing parameters
SI 16384
SF 500.1300060 MHz
WDW no
SSB 0
LB 0 Hz
GB 0
PC 1.00
10 9 8 7 6 5 4 3 2 1 ppm
1.95 8.08 4.07 4.17 1.92 3.90 0.08 1.88 1.95 1.91 3.86 12.00

t = 24 h

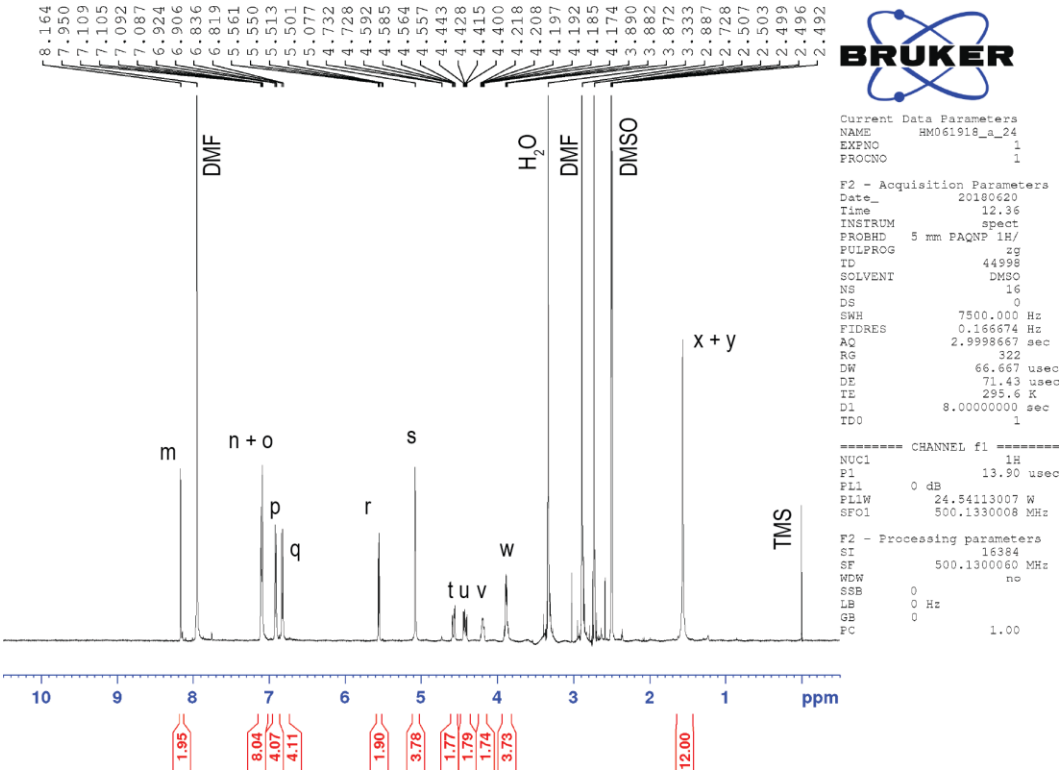
8.164 7.950 7.109 7.105 7.092 7.087 6.924 6.906 6.836 6.819 5.561 5.550 5.513 5.501 5.077 4.732 4.728 4.592 4.585 4.564 4.557 4.443 4.428 4.415 4.400 4.218 4.208 4.197 4.192 4.185 4.174 3.890 3.882 3.872 3.333 2.887 2.728 2.507 2.503 2.499 2.496 2.492
DMF
H2O
DMF
DMSO
x + y
m
n + o
p
q
r
s
t u v
w
TMS
BRUKER
Current Data Parameters
NAME HM061918_a_24
EXPNO 1
PROCNO 1
F2 - Acquisition Parameters
Date_ 20180620
Time 12.36
INSTRUM spect
PROBHD 5 mm PAQNP 1H/
PULPROG zg
TD 44998
SOLVENT DMSO
NS 16
DS 0
SWH 7500.000 Hz
FIDRES 0.166674 Hz
AQ 2.9998667 sec
RG 322
DW 66.667 usec
DE 71.43 usec
TE 295.6 K
D1 8.00000000 sec
TD0 1
======== CHANNEL f1 ========
NUC1 1H
P1 13.90 usec
PL1 0 dB
PL1W 24.54113007 W
SFO1 500.1330008 MHz
F2 - Processing parameters
SI 16384
SF 500.1300060 MHz
WDW no
SSB 0
LB 0 Hz
GB 0
PC 1.00
10 9 8 7 6 5 4 3 2 1 ppm
1.95 8.04 4.07 4.11 1.90 3.78 1.77 1.79 1.74 3.73 12.00

Peak assignment for linear polytriazole:

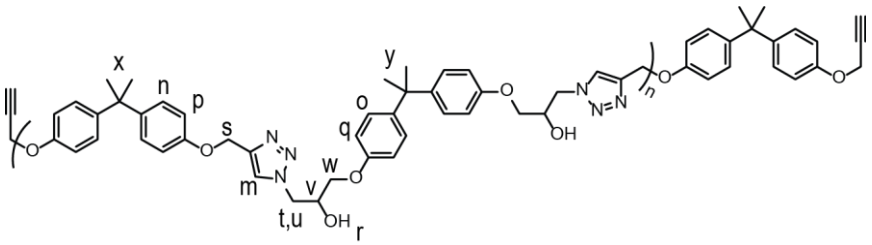

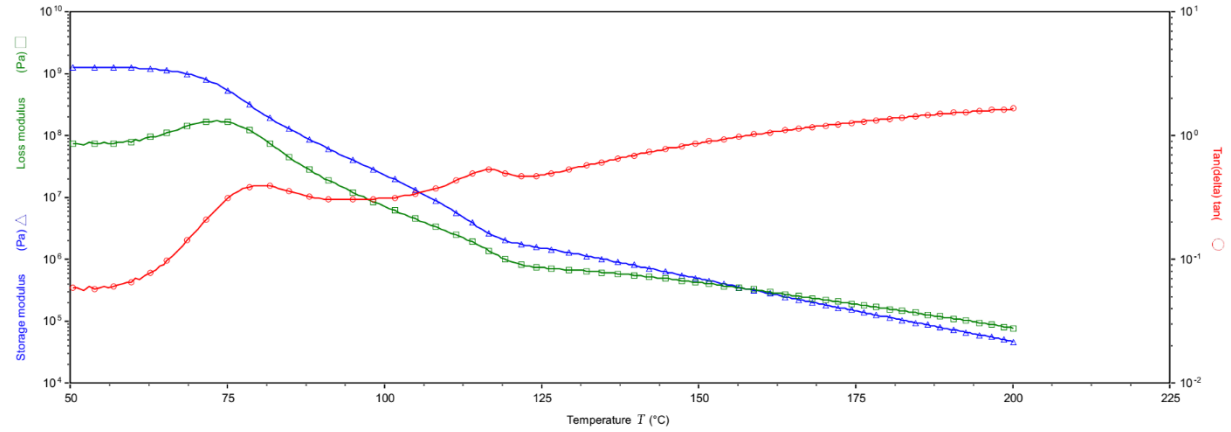

Figure A4. Temperature ramp shear rheology measurement in the range 50 – 200 ºC of the linear polytriazole using 8 and 25 mm parallel plates and a constant oscillation frequency of 1 Hz. Preliminary tests were performed to ensure the applied oscillatory strain and the corresponding stress remained in the linear viscoelastic region over the whole temperature range.

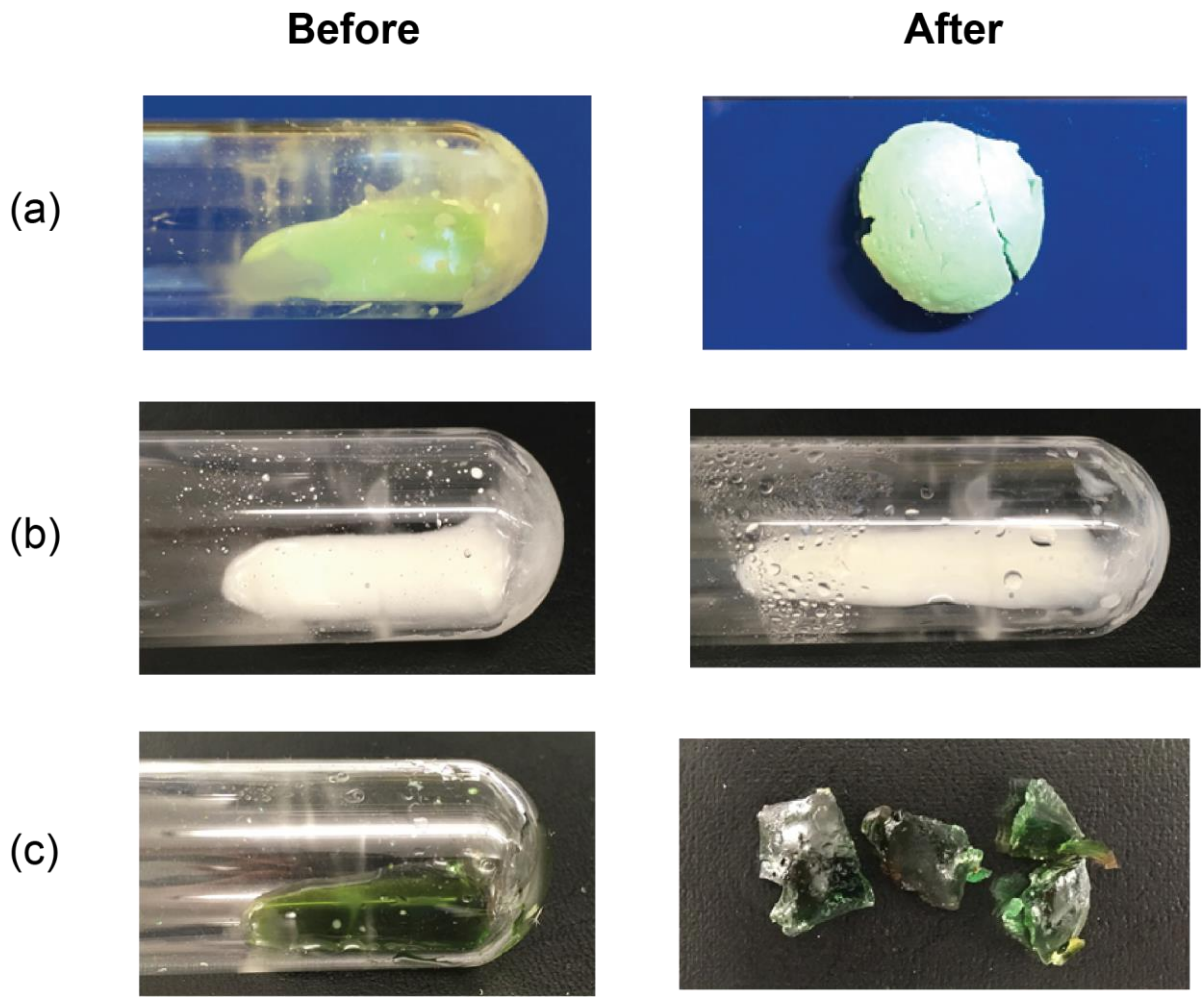

Figure A5. Control experiments for the mechano-crosslinking of azido-polyurethane before and after sonication (40 kHz) for 24 h. (a) Standard mechano-crosslinking reaction, (b) *No copper control*: standard mechano-crosslinking reaction but without $Cu(OTf)_2$. (c) *No nanoparticles control*: standard mechano-crosslinking reaction but without $BaTiO_3$ nanoparticles.

Appendix B: Supporting information for Chapter 2.2: Mechanically-promoted Fe-mediated free radical polymerization

NMR spectra for reaction mixtures using BA at (a) t = 0 h and (b) t = 21 h

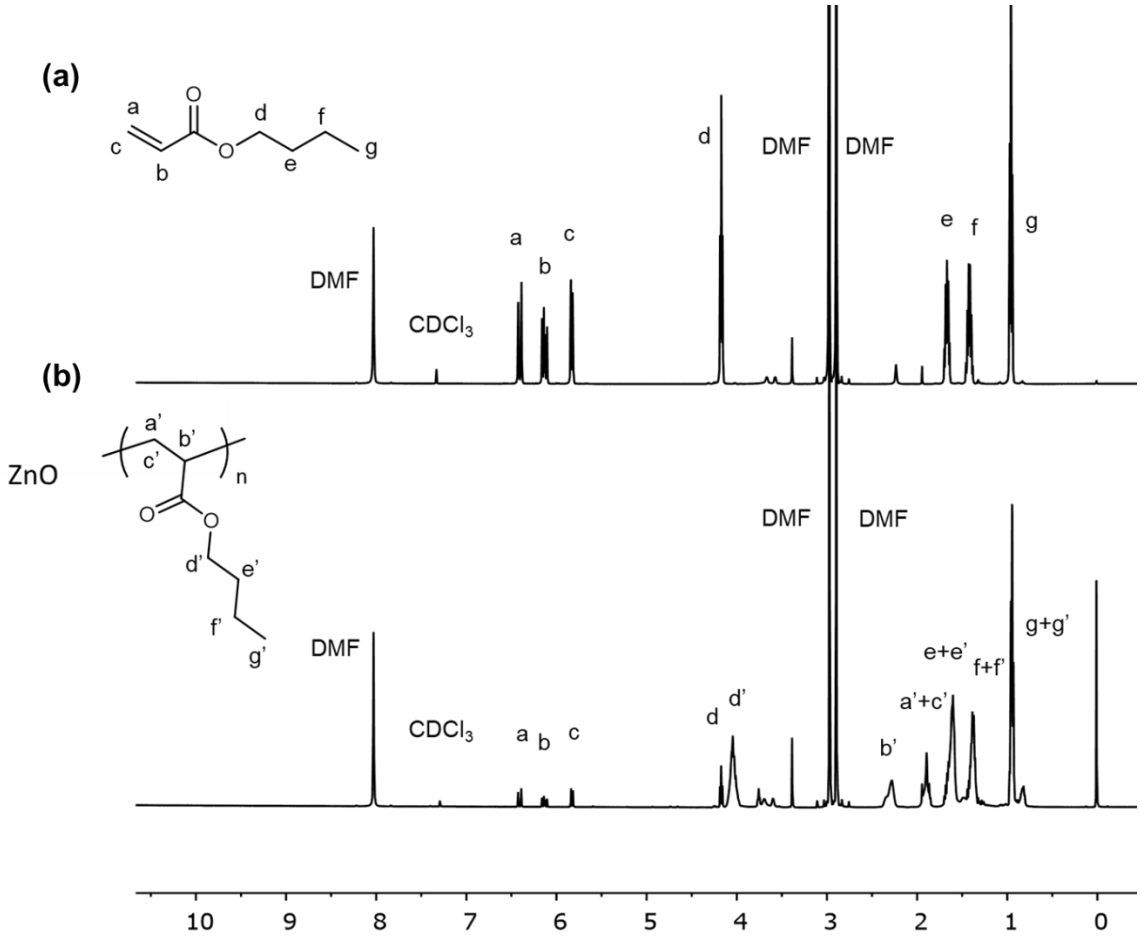

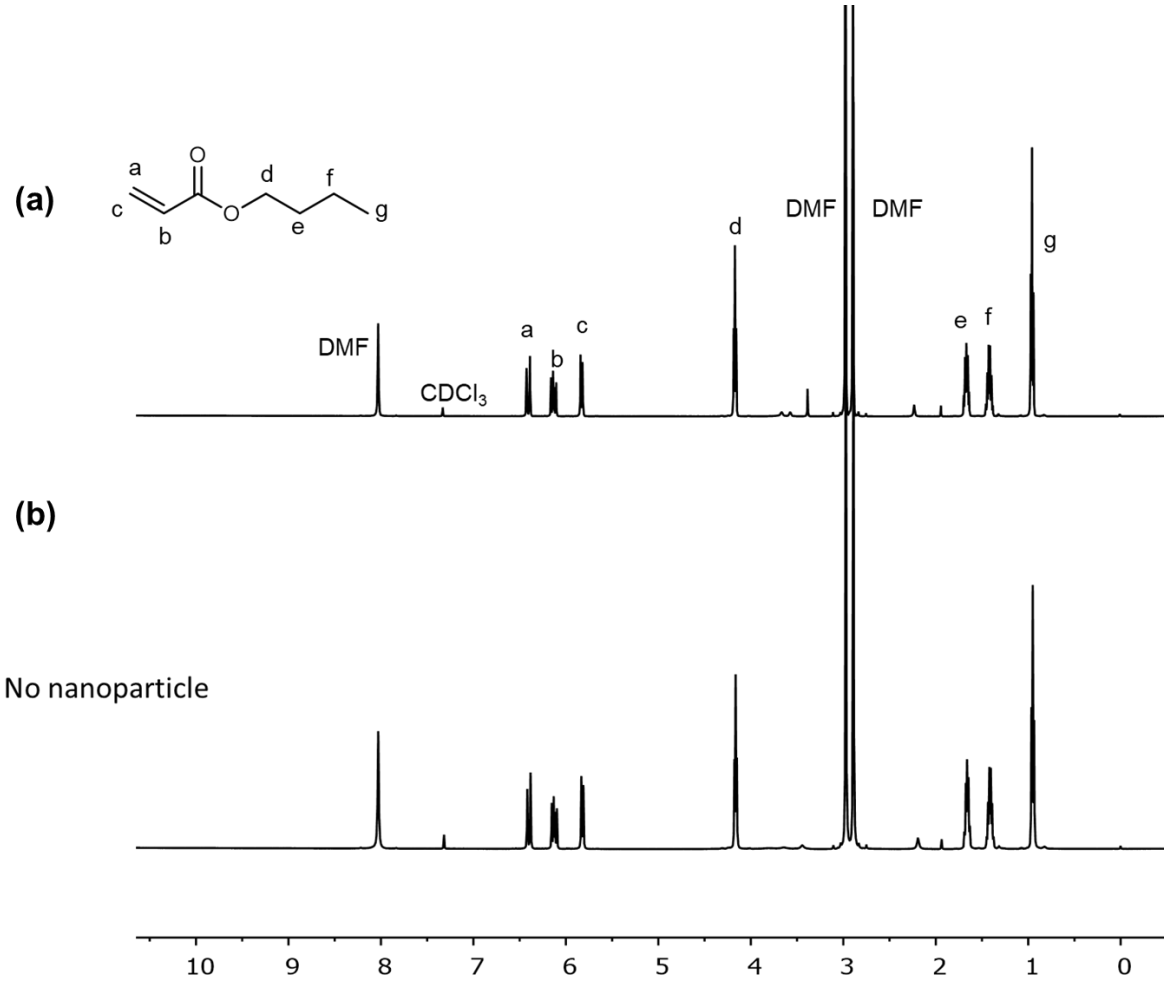
(a)
a
c
b
O
O
d
e
f
g
DMF
CDCl3
a
b
c
d
DMF
DMF
e
f
g
(b)
No nanoparticle
10
9
8
7
6
5
4
3
2
1
0

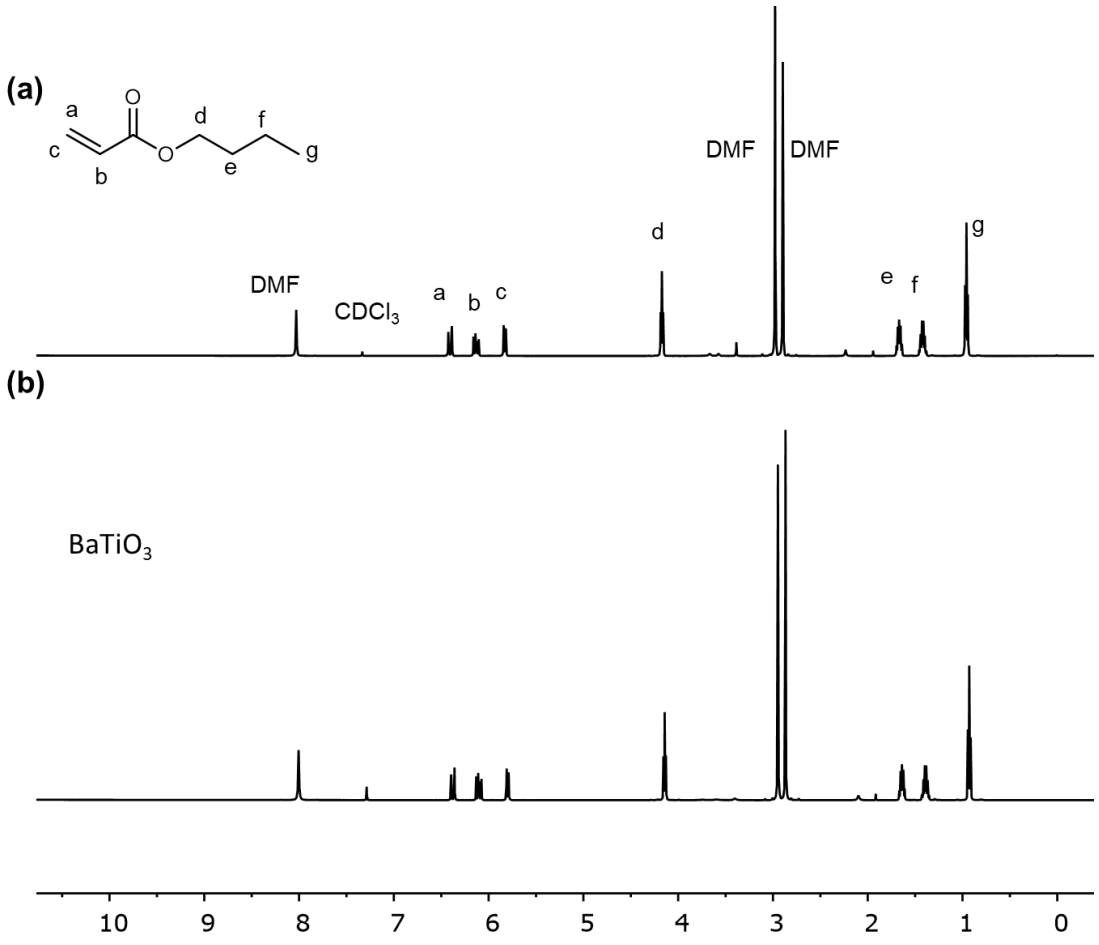
(a)
a
O
d
f
c
O
g
b
e
DMF
DMF
d
g
DMF
CDCl3
a
b
c
e
f
(b)
BaTiO3
10
9
8
7
6
5
4
3
2
1
0

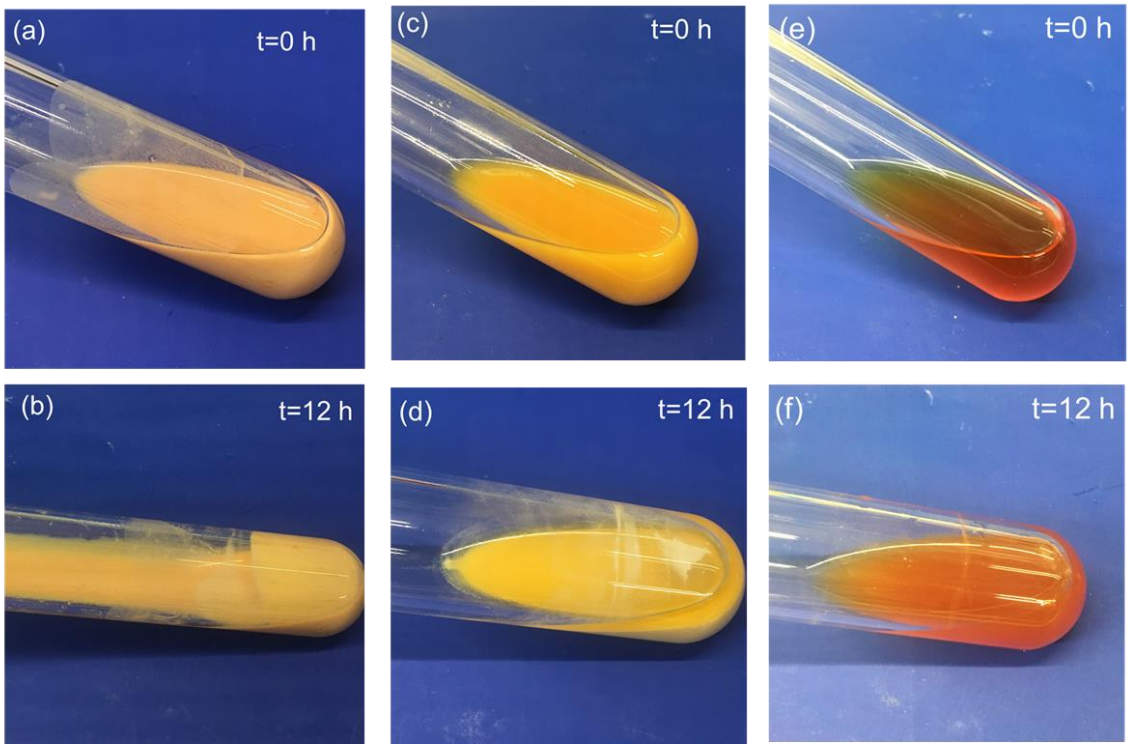

Figure B1. Photos of the reaction mixture at different reaction times and piezoelectric nanoparticles: (a) and (b) in the presence of ZnO; (c) and (d) in the presences of $BaTiO_3$, (e) and (f) without nanoparticle; under conditions [BA]: [EBiB]: [$FeCl_3{\cdot}6H_2O$]: [TDA-1] = 16: 0.16: 0.16: 0.32 mmol in 2 mL DMF; loading 9 wt% nanoparticle or without nanoparticle. Ultrasonic bath (20–30 °C, 40 kHz, 70 W).

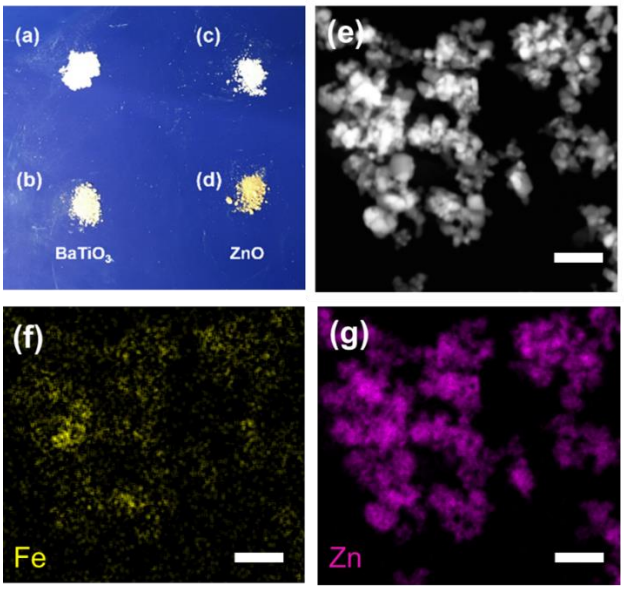

Figure B2. Optical image of piezoelectric nanoparticles before and after ultrasound agitation in the presence of $FeCl_3 \cdot 6H_2O$/TDA-1solution: (a) $BaTiO_3$ before ultrasonication (b) $BaTiO_3$ after ultrasonication (c) ZnO before ultrasonication (d) ZnO after ultrasonication; (e-g) HAADF-STEM image of ZnO and its corresponding element mapping recorded by EDS spectroscopy (e) HAADF-STEM image, (f) Fe element mapping analysis and (g) Zn element mapping analysis. Scale bar 200 nm.

Table B1. Polymerization kinetics for the various model polymerization of BA in DMF.

Entry[a]	Condition (all conc. in mmol)	Conversion[b]	M_n[c]	M_w/M_n
1	$[BA]_0$: $[FeCl_3 \cdot 6H_2O]_0$: $[TDA\text{-}1]_0$ = 16: 0.16: 0.32	22 %	323 500	1.19
2	$[BA]_0$: $[EBiB]_0$: $[TDA\text{-}1]_0$ = 16: 0.16: 0.32	11 %	247 100	1.34
3	$[BA]_0$: $[EBiB]_0$: $[FeCl_3 \cdot 6H_2O]_0$: = 16: 0.16: 0.16	14 %	394 300	1.45
4	$[BA]_0$: $[EBiB]_0$: = 16: 0.16	10 %	555 100	1.39

[a]Reaction conditions: $[BA]_0$: $[EBiB]_0$: $[FeCl_3 \cdot 6H_2O]_0$: $[TDA\text{-}1]_0$ = 16: 0–0.16: 0–0.16: 0–0.32 mmol in 2 mL DMF; add 9 wt% ZnO nanoparticles. Ultrasonic bath (20–30 °C, 40 kHz, 70 W). React for 6 hours.

[b]Conversion determined by ^{1}H NMR.

[c]Determined by GPC-MALS in THF.

Table B2. Results for mechano-radical polymerization of BA with different initiators.

Entry[a]	Initiator	Conversion[b]	Mn[c]	Mw/Mn
1	MBiB	46%	201300	1.36
2	MBP	52%	197 600	1.37
3	MBAc	18%	185 900	1.51
4*	mPEG bromoisobutyrate 5000	62%	197 800	1.18

[a]Reaction conditions: $[BA]_0$: $[Initiator]_0$: $[FeCl_3 \cdot 6H_2O]_0$: $[TDA\text{-}1]_0$= 16: 0.16: 0.16: 0.32 mmol in 2 mL solvent; loading certain amount of ZnO. Ultrasonic bath (20–30 °C, 40 kHz, 70 W). React for 21 hours. [b]Conversion determined by ^1H NMR.

[c]Determined by GPC-MALS in THF.

*Reaction conditions: $[BA]_0$: $[mPEG\text{-}Br]_0$: $[FeCl_3 \cdot 6H_2O]_0$: $[TDA\text{-}1]_0$ = 16: 0.04: 0.16: 0.32 mmol in 2 mL solvent; loading 9 wt% ZnO. Ultrasonic bath (20–30 °C, 40 kHz, 70 W). React for 21 hours.

Appendix C: Supporting information for Chapter 2.3: Mechanically-promoted thiol-ene polymerization

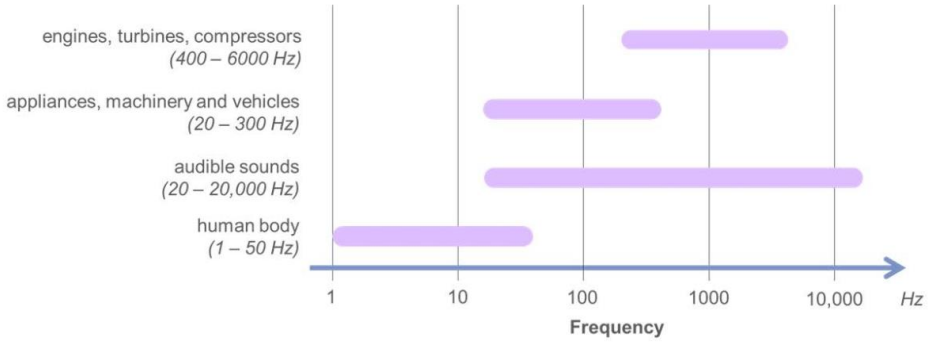

Figure C1. Frequency ranges of commonly encountered environmental vibrations.

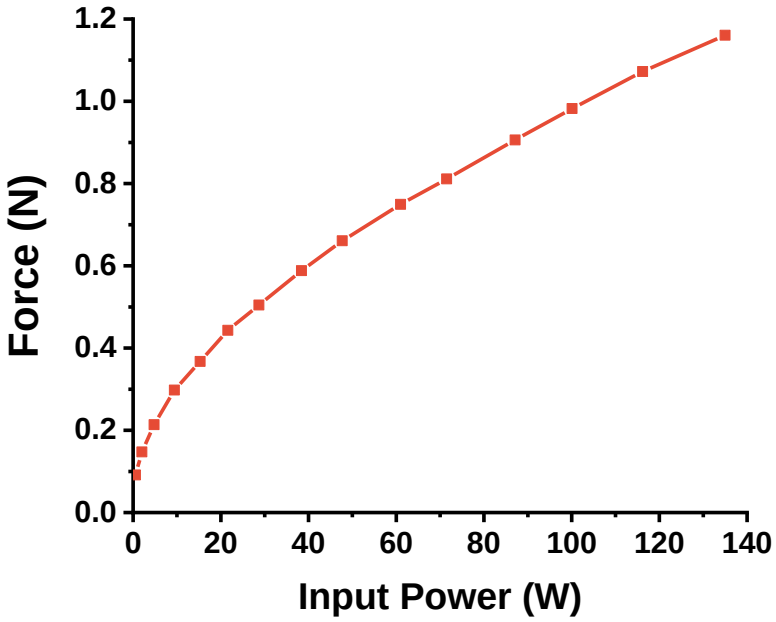

Figure C2. The output force as a function of input power. The electrodynamic shaker was set to vibrate at a frequency of 2000 Hz. Force was calculated based on the acceleration data obtained from the accelerometer.

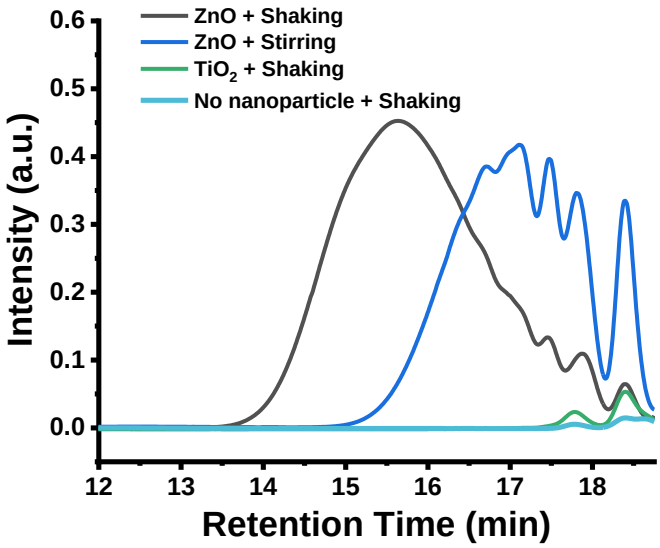

Figure C3. GPC traces of thiol-ene polymerization conducted under shaking (2000 Hz, 1.2 N) or stirring (400 rpm) for 4 hours.

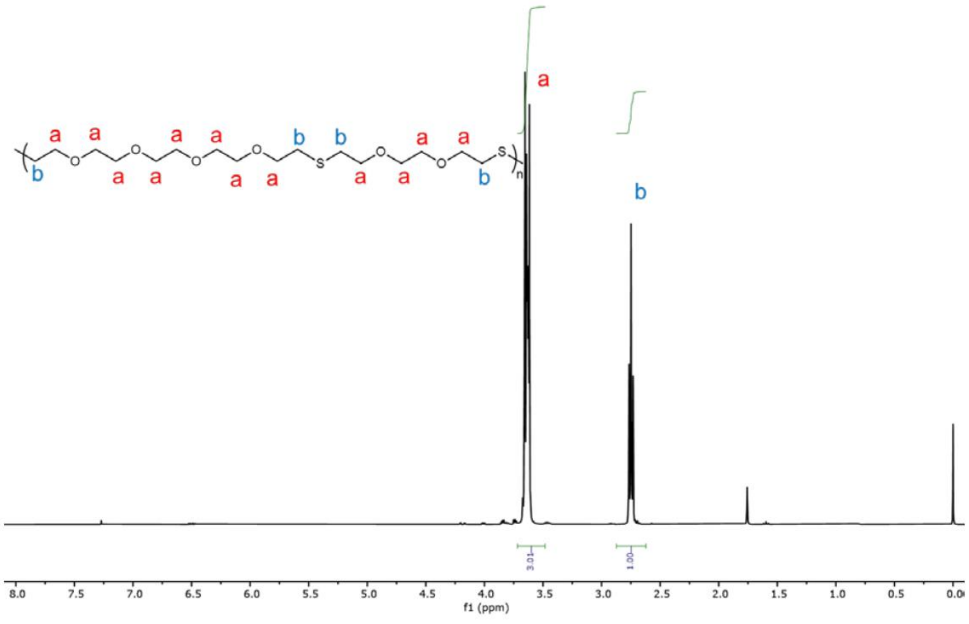

Figure C4. ^{1}H-NMR spectra of polythioether synthesized via mechano-thiol-ene polymerization.

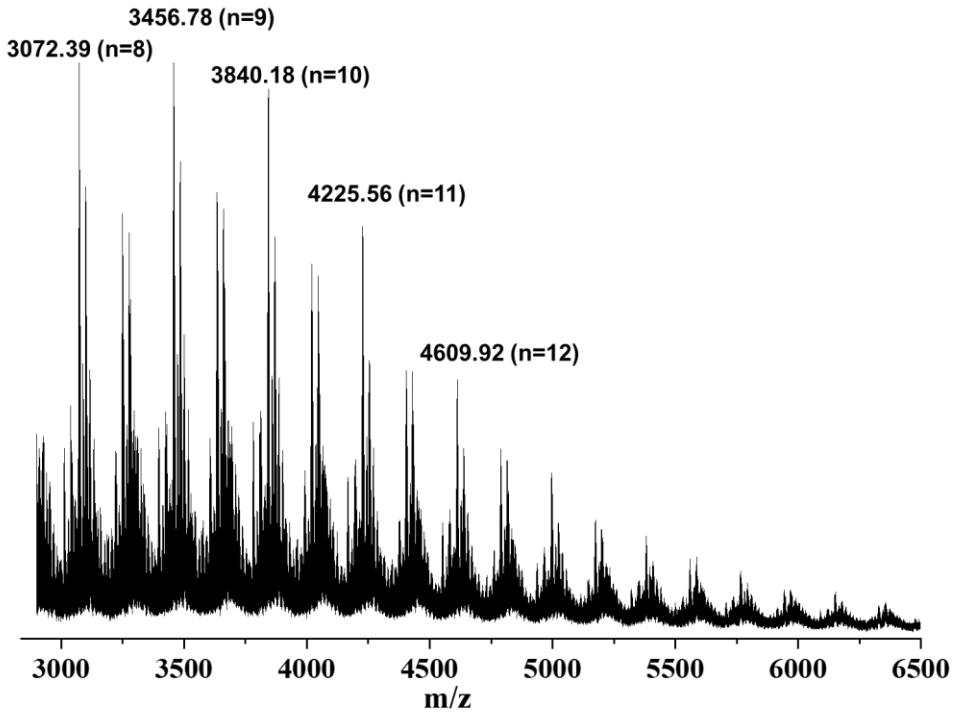

Figure C5. MALDI-TOF MS spectrum of polythioether.

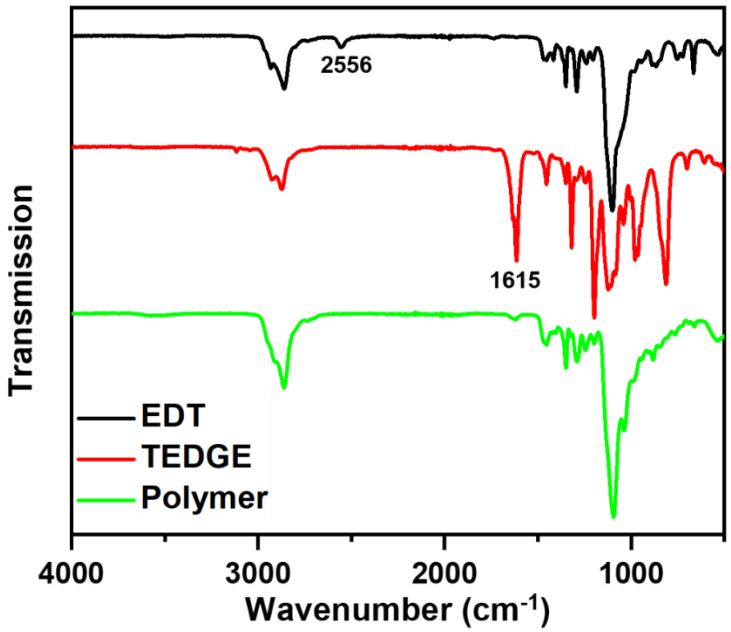

Figure C6. FT-IR spectra of EDT, TEGDE, and polythioether.

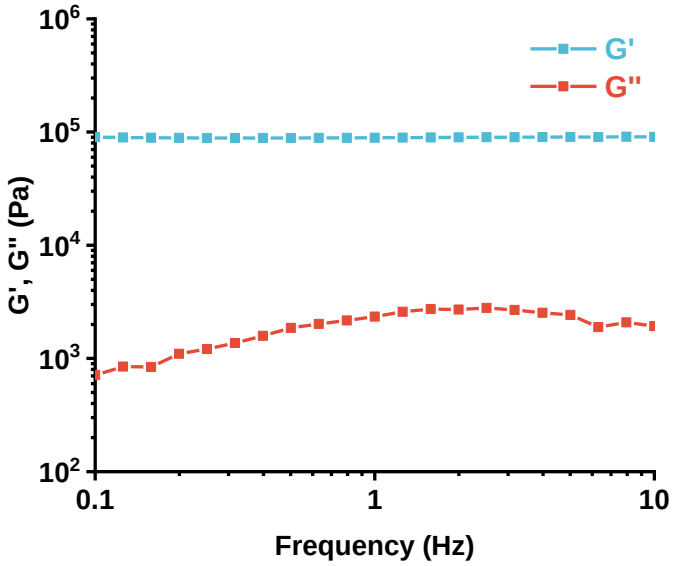

Figure C7. Storage (G') and loss (G") moduli as a function of frequency (Hz) of the mechano-thiol-ene gel. Measurements were carried out at a fixed shear strain amplitude of 1 %.

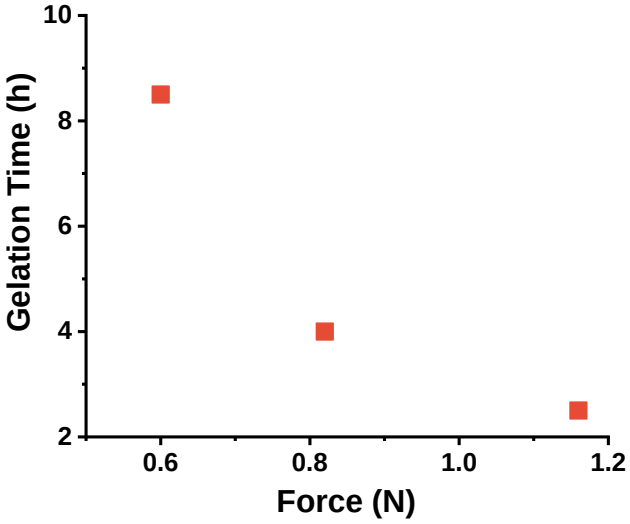

Figure C8. Gelation time as a function of force.

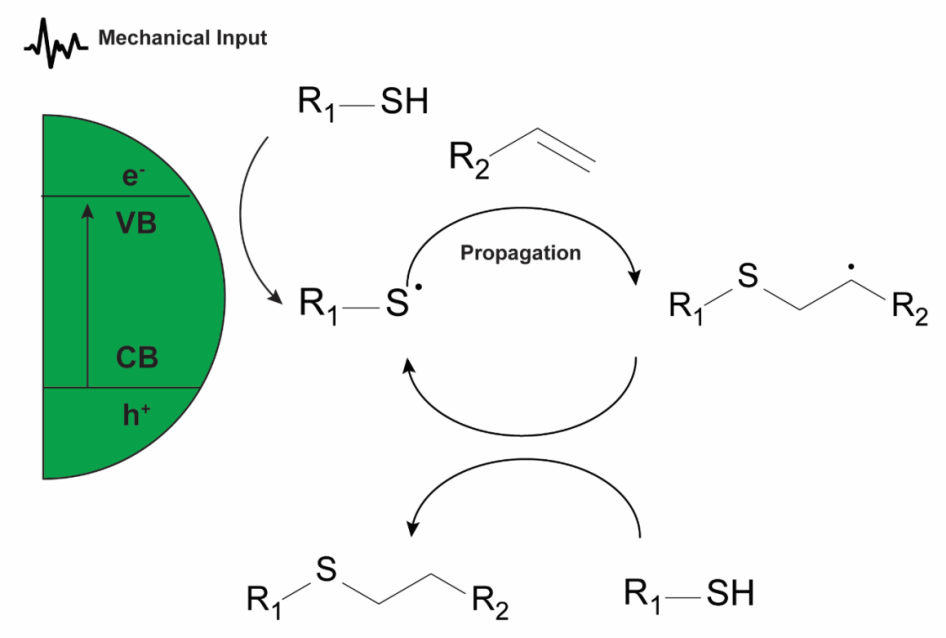

Figure C9. Plausible reaction mechanism for the mechano-thiol-ene polymerization.

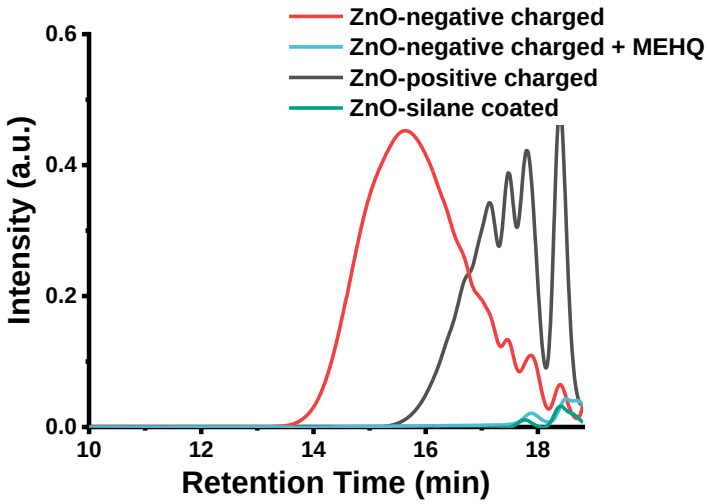

Figure C10. GPC traces of mechano-thiol-ene polymerization using different ZnO nanoparticles: positively charged, negatively charged, and silane-coated ZnO.

Table C1. Summary of reactions between different alkenes and EDT.

Alkene	ZnO	Vibration	Time (h)	Alkene conversion (%)[a]
Propyl vinyl ether	Yes	Yes	1.5	53
	Yes	No	1.5	23
	No	No	1.5	19
1-octene	Yes	Yes	3	44
	Yes	No	3	19
	No	No	3	11
Vinyl propionate	Yes	Yes	3	40
	Yes	No	3	23
	No	No	3	5
Allyl butyl ether	Yes	Yes	3	30
	Yes	No	3	20
	No	No	3	10

[a] The conversion was determined by ^{1}H-NMR spectroscopy.

Table C2. Zeta potential measurements of different ZnO nanoparticles.

Sample	Zeta potential (mV)
Positive charged ZnO	6.9
Negative charged ZnO	-24.0
Silane coated ZnO	-22.6

Appendix D: Supporting information for Chapter 3.2: Mechanically-promoted synthesis of reversible organogels via thiol-disulfide crosslinking

NMR spectra of mercapto-polymers

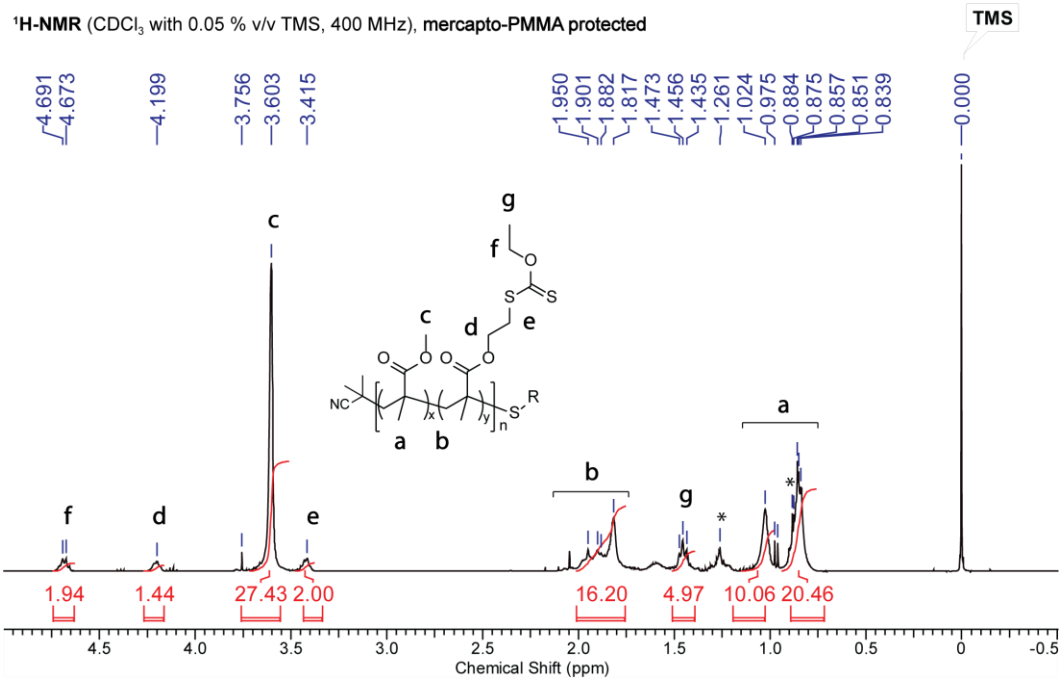

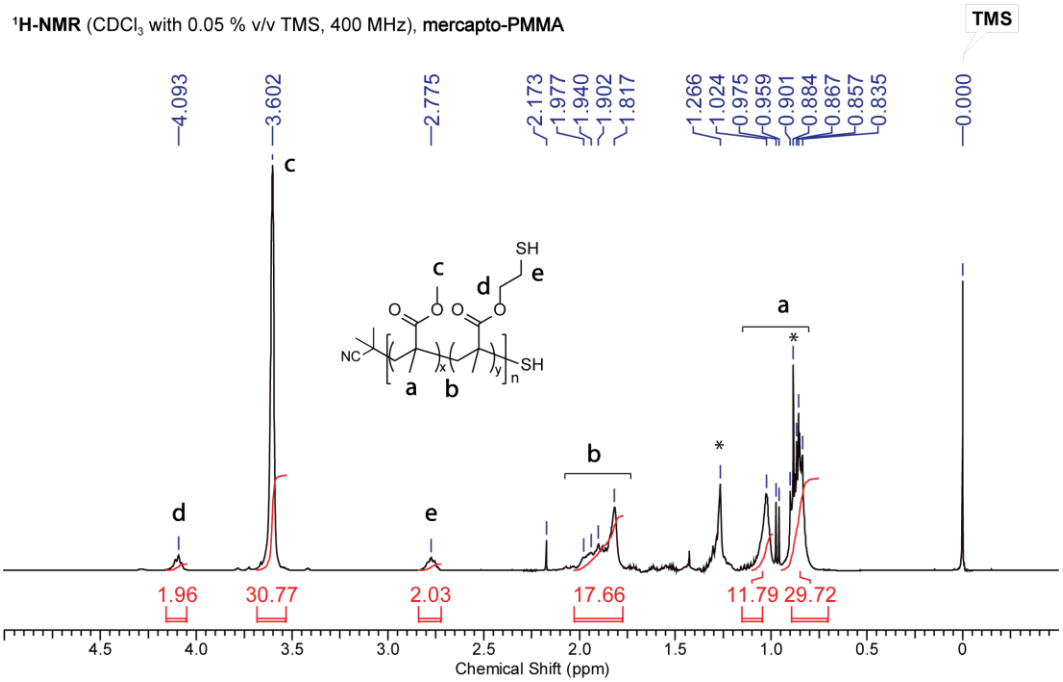

* Residual solvent: n-hexane.

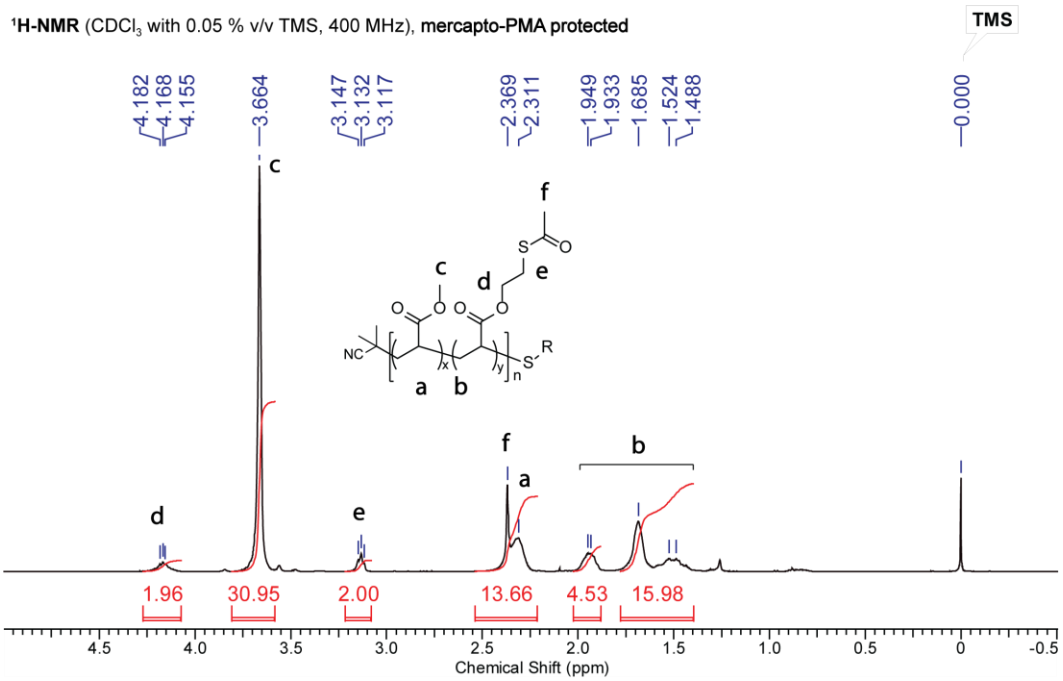
¹H-NMR (CDCl3 with 0.05 % v/v TMS, 400 MHz), mercapto-PMA protected
TMS
4.182
4.168
4.155
3.664
3.147
3.132
3.117
2.369
2.311
1.949
1.933
1.685
1.524
1.488
0.000
c
f
S
O
c
d
e
O
O
O
O
NC
x
y
S
R
n
a
b
f
a
b
d
e
1.96
30.95
2.00
13.66
4.53
15.98
4.5
4.0
3.5
3.0
2.5
2.0
1.5
1.0
0.5
0
-0.5
Chemical Shift (ppm)

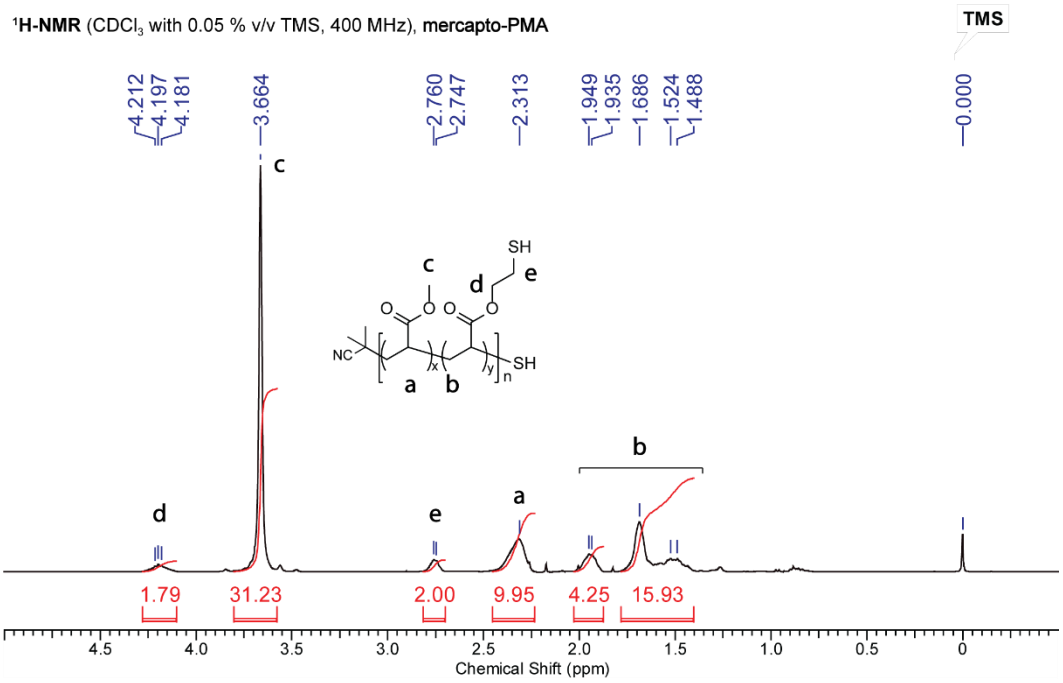
¹H-NMR (CDCl3 with 0.05 % v/v TMS, 400 MHz), mercapto-PMA
TMS
4.212
4.197
4.181
3.664
2.760
2.747
2.313
1.949
1.935
1.686
1.524
1.488
0.000
c
SH
c
d
e
O
O
O
O
NC
x
y
SH
n
a
b
b
d
e
a
1.79
31.23
2.00
9.95
4.25
15.93
4.5
4.0
3.5
3.0
2.5
2.0
1.5
1.0
0.5
0
Chemical Shift (ppm)

^{1}H-NMR ($CDCl_3$ with 0.05 % v/v TMS, 400 MHz), **mercapto-PS protected**

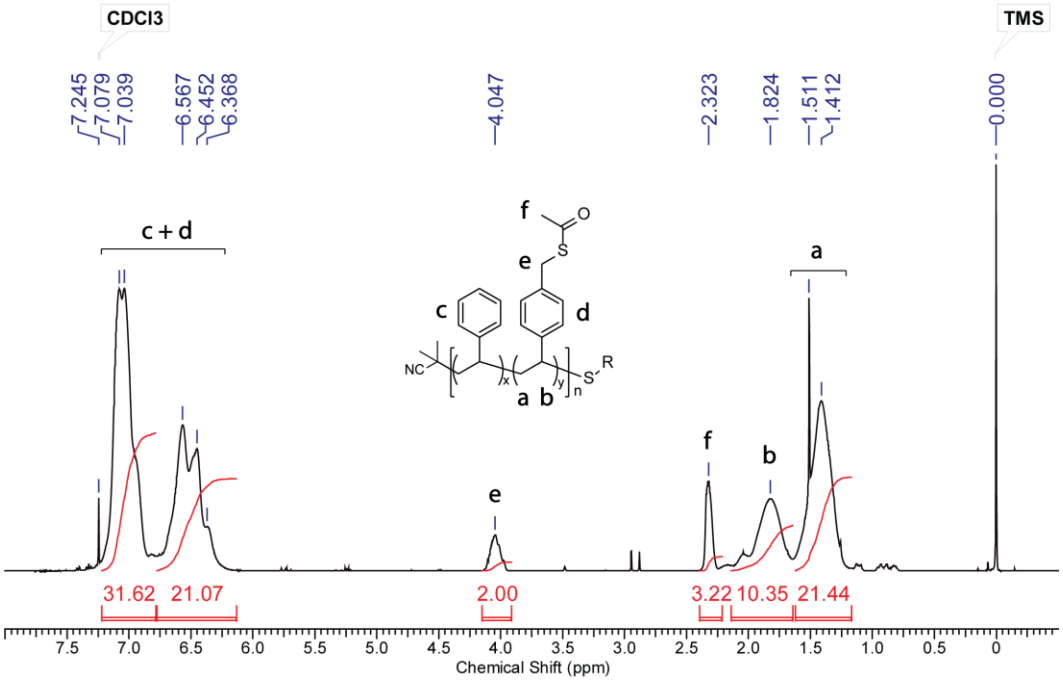

^{1}H-NMR ($CDCl_3$ with 0.05 % v/v TMS, 400 MHz), **mercapto-PS**

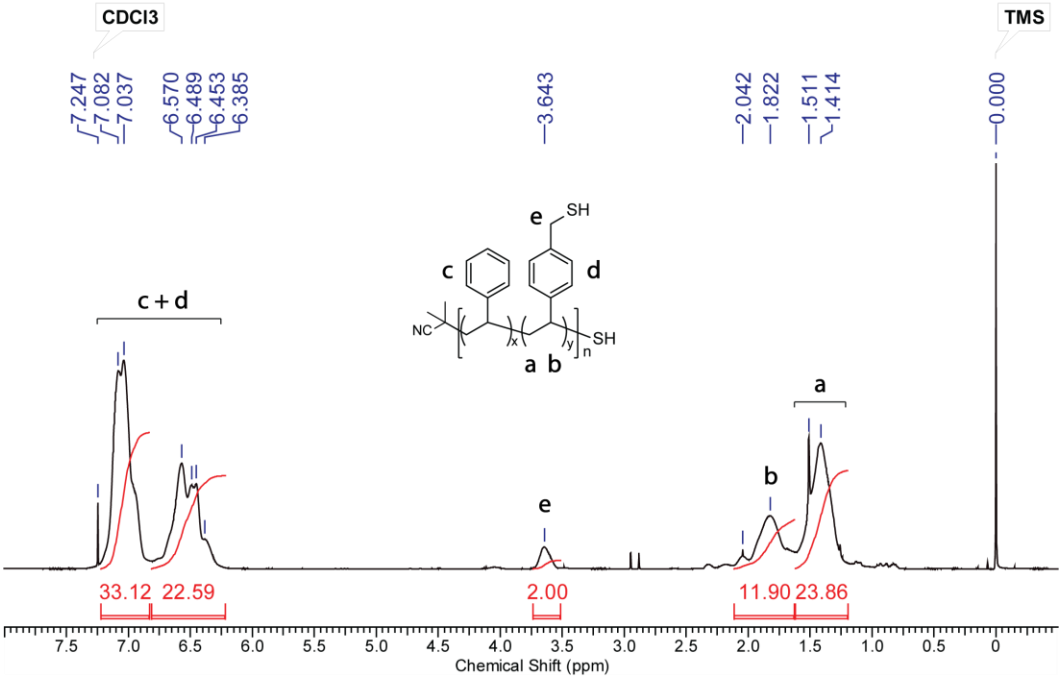

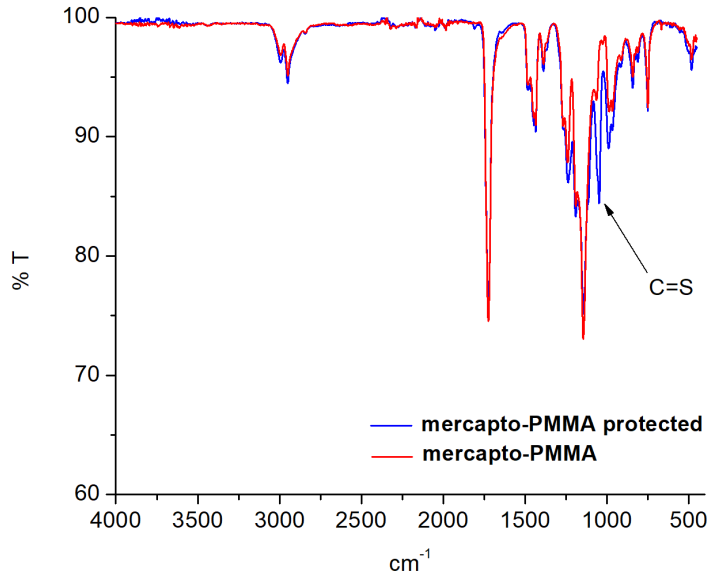

Figure D1. FTIR spectra of mercapto-PMMA. Disappearance of the C=S peak (1046 cm^{-1}) corresponding to the xanthate confirms deprotection of the thiol side groups.

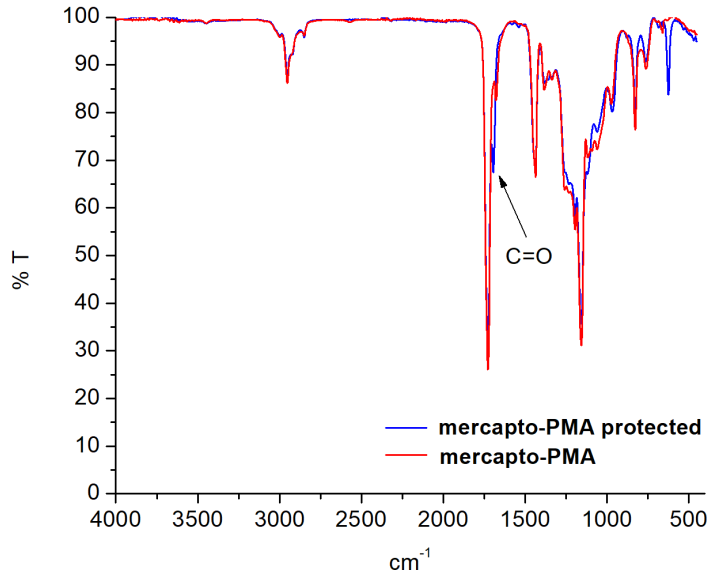

Figure D2. FTIR spectra of mercapto-PMA. Disappearance of the C=O peak (1691 cm^{-1}) corresponding to the thioacetate confirms the deprotection of the thiol side groups.

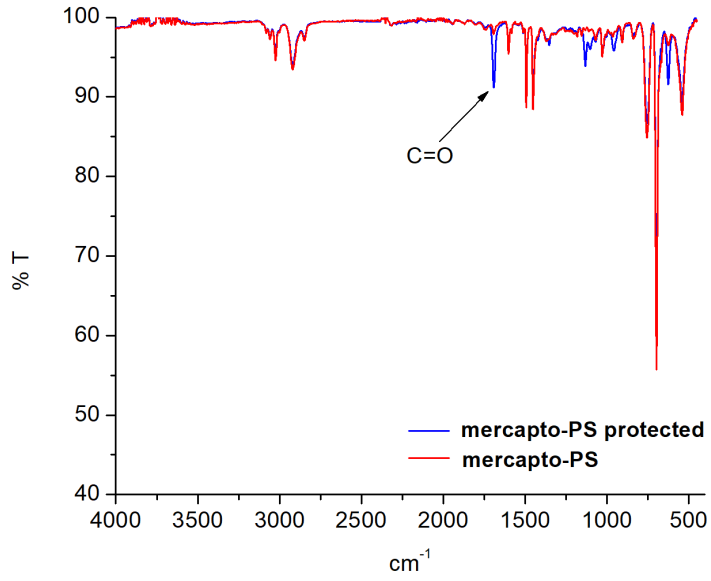

Figure D3. FTIR spectra of mercapto-PS. Disappearance of the C=O peak (1693 cm^{-1}) corresponding to the thioacetate confirms the deprotection of the thiol side groups.

Table D1. Molecular weight characterization of mercapto-polymers.

Polymer	**M_n (kDa)**[a]	**M_w (kDa)**[a]	**Đ (M_w/M_n)**[a]	**Thiol content (wt %)**[b]
mercapto-	11.7	15.1	1.3	12.6
mercapto-PMA	16.0	26.1	1.6	12.8
mercapto-PS	24.1	48.1	2.0	11.7

[a] Determined by GPC using standard calibration curves with PMMA or PS standards.

[b] Determined by ^{1}H-NMR.

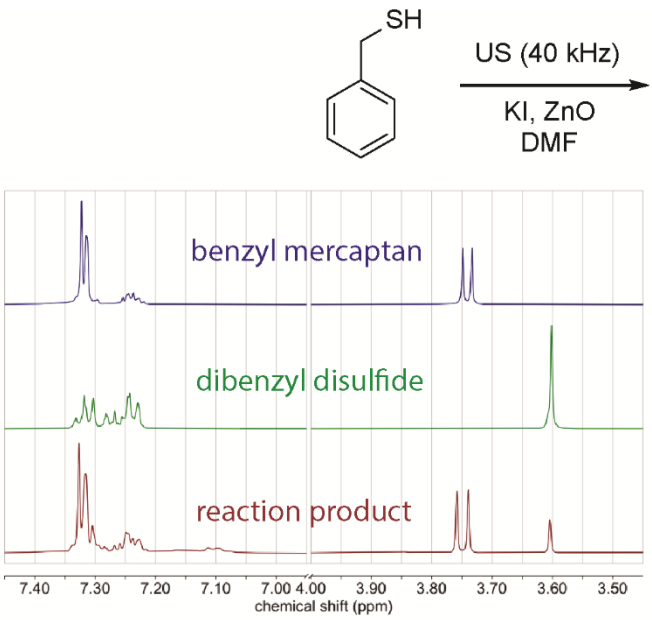

Experiment	% conversion*
All components	18.1
No ZnO	4.0
No US (stir)	5.5
No KI	11.1

*Average value of 2 measurements.

Figure D4. Mechanistic analysis of ultrasound-promoted disulfide bond formation. (a) Proton NMR study of model reaction with small molecule thiol. Benzyl mercaptan (59 μL, 0.50 mmol) and KI (42 mg, 0.25 mmol) were dissolved in DMF (400 μL) and mixed with ZnO nanoparticles 18 nm (15 mg, 2.5 wt %). The mixture was homogenized and sonicated for 12 h in an ultrasound bath (40 kHz). NMR graph showing the formation of dibenzyl disulfide under ultrasound conditions, as evidenced by the methylene singlet peak (CH_2) at 3.63 ppm. The table shows the percent conversion of thiol to disulfide as determined by qNMR for control reactions.

Spectra of samples for NMR study with benzyl mercaptan

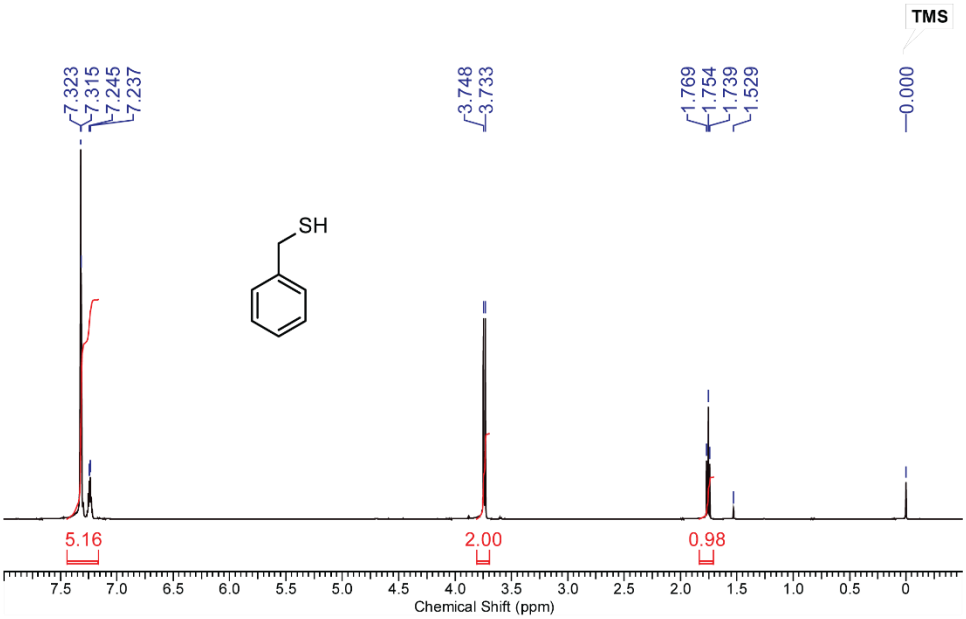

Benzyl mercaptan. **^{1}H-NMR** ($CDCl_3$ with 0.05% v/v TMS, 500 MHz): δ_H 7.32 (m, Ar-H, 4H), 7.24 (m, Ar-H, 1H), 3.74 (d, CH_2, 2H), 1.75 (t, SH, 1H).

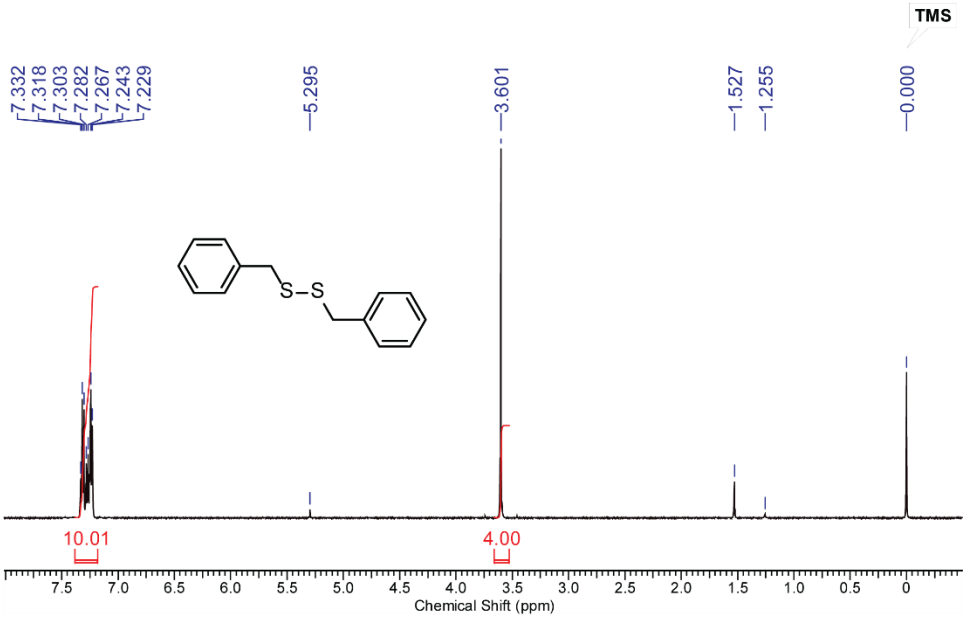

Dibenzyl disulfide. **^{1}H-NMR** ($CDCl_3$ with 0.05% v/v TMS, 500 MHz): δ_H 7.33-7.23 (m, Ar-H, 10H), 3.60 (s, CH_2, 4H).

All components

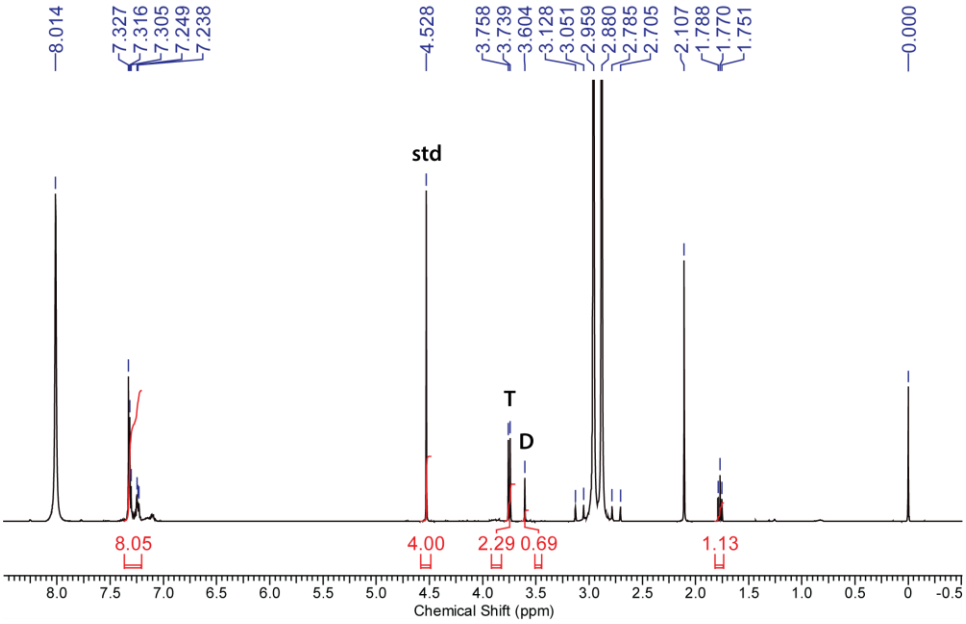

Control - no ZnO

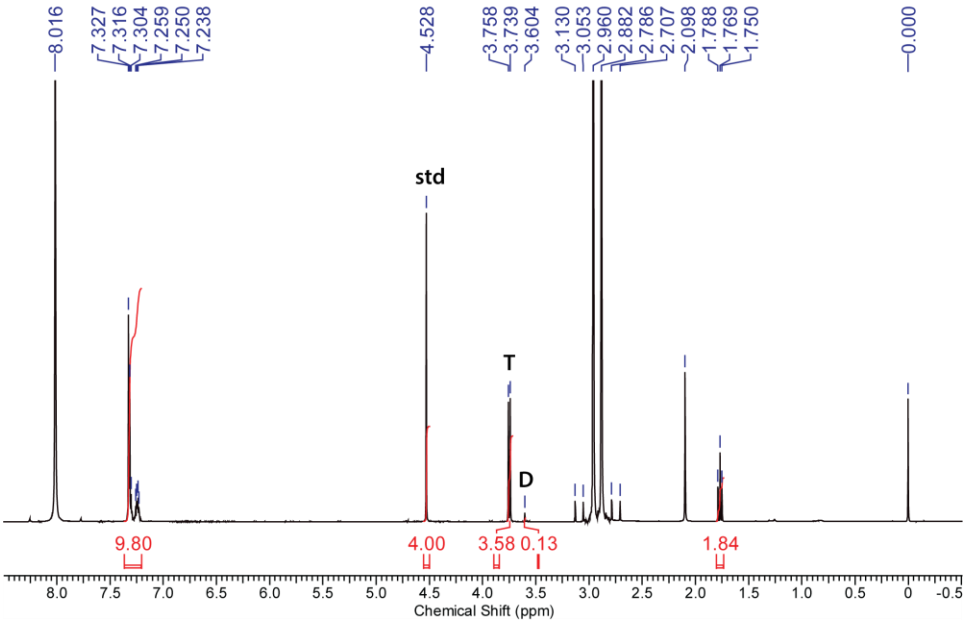

Control - no ultrasonication (stirred)

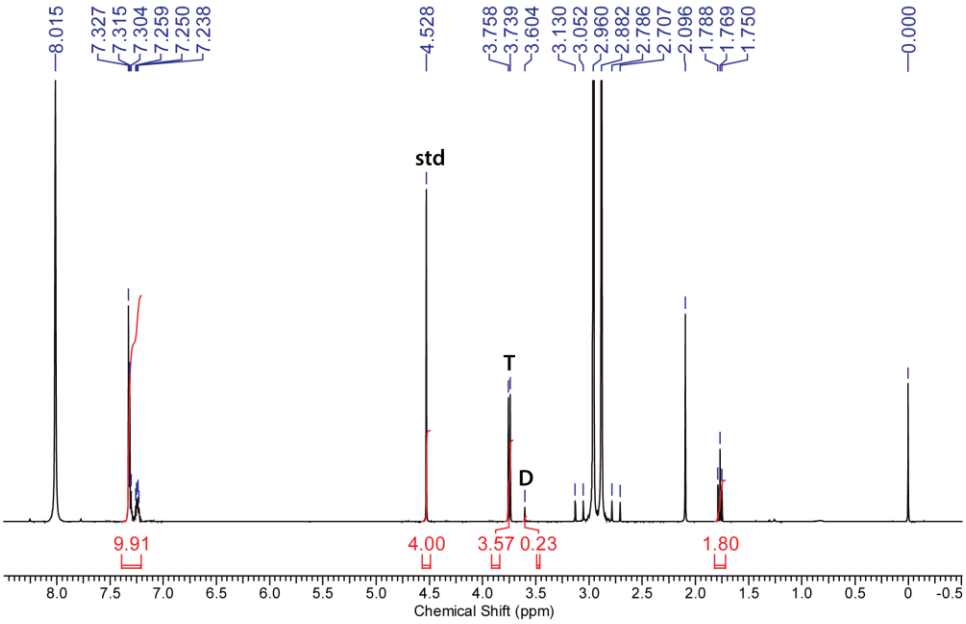

Control - no KI

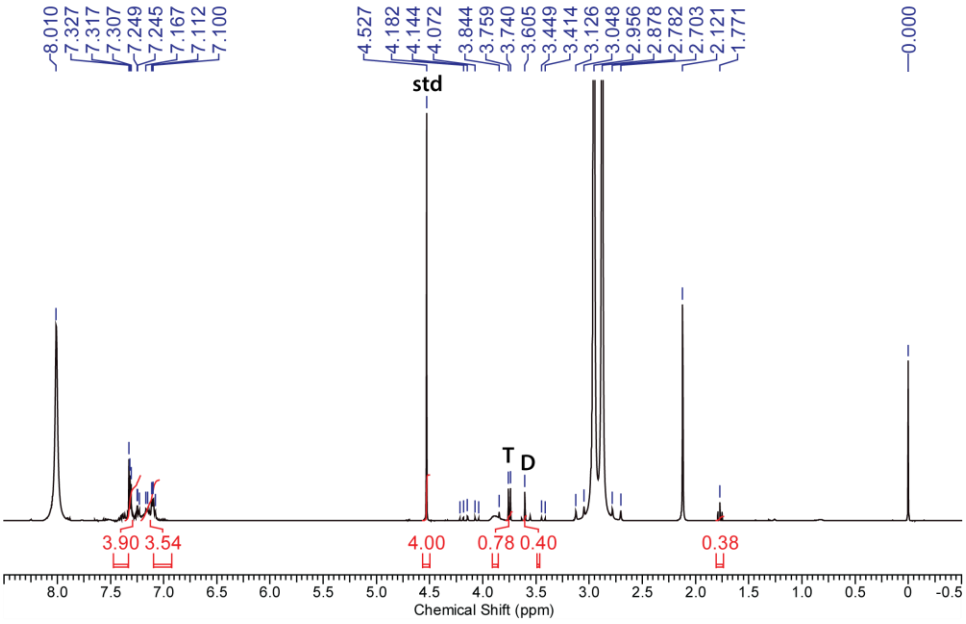

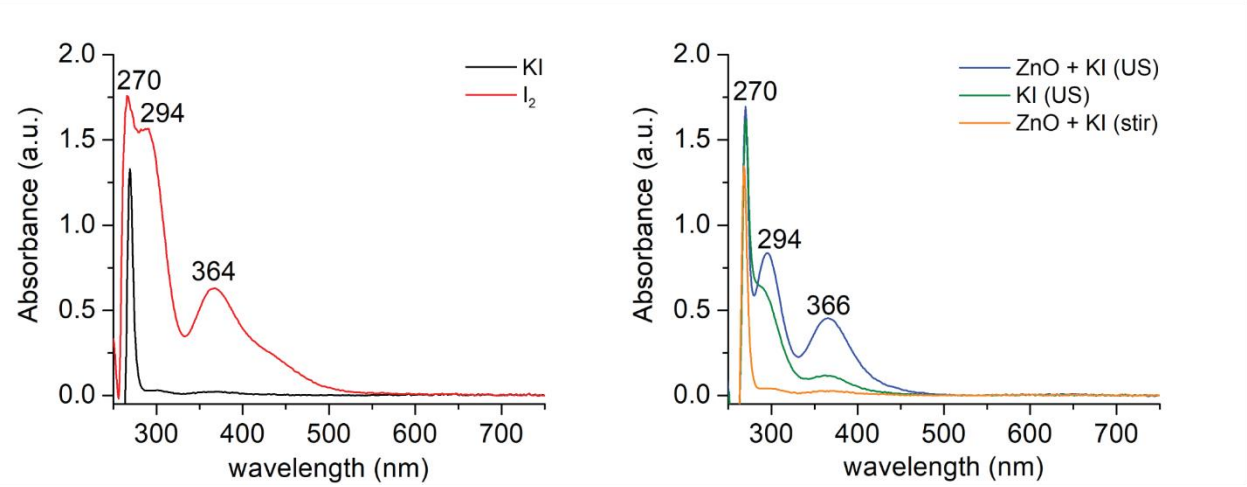

Figure D5. UV-vis study of I_2 formation via piezoelectrochemistry under ultrasound. UV-vis spectra of solutions of KI (28 mg/mL, 0.17 M) and I_2 (1 mM) in DMF (*left*), and control reactions (*right*).

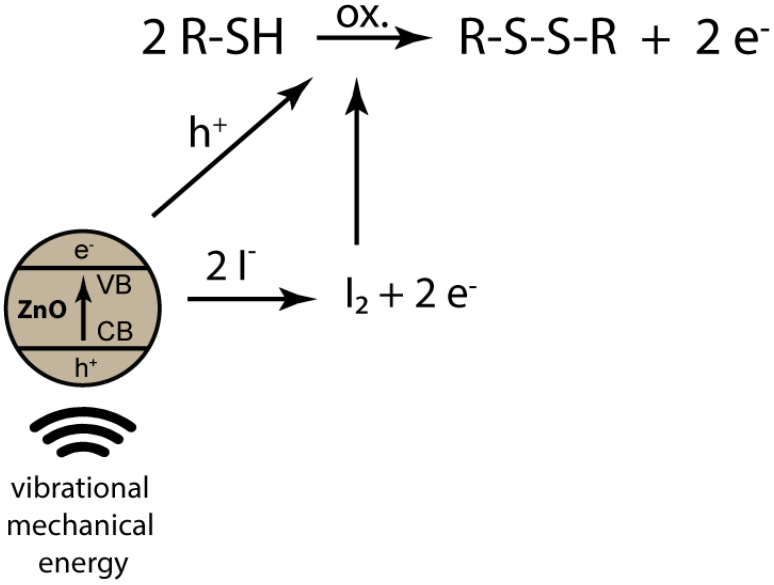

Figure D6. Possible mechanisms for piezo-oxidation of thiol to disulfide. Under mechanical agitation, ZnO nanoparticles could either directly oxidize the thiols through surface interactions with positive holes, or oxidize iodide anions to iodine, which can then subsequently oxidize the thiols in solution.

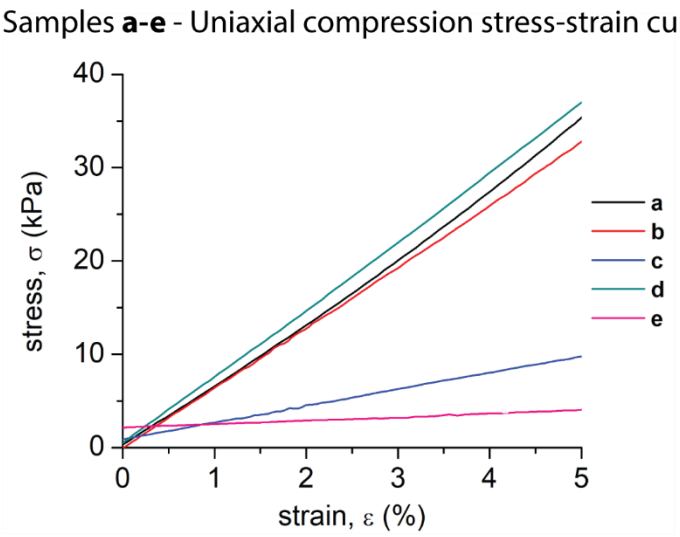

Figure D7. Stress-strain curves in the linear region of samples **a-e** (mercapto-PMMA).

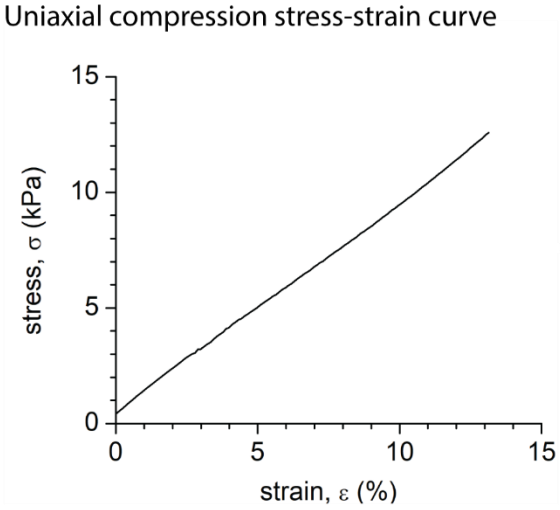

Figure D8. Stress strain curve in the linear region of sample **f**.

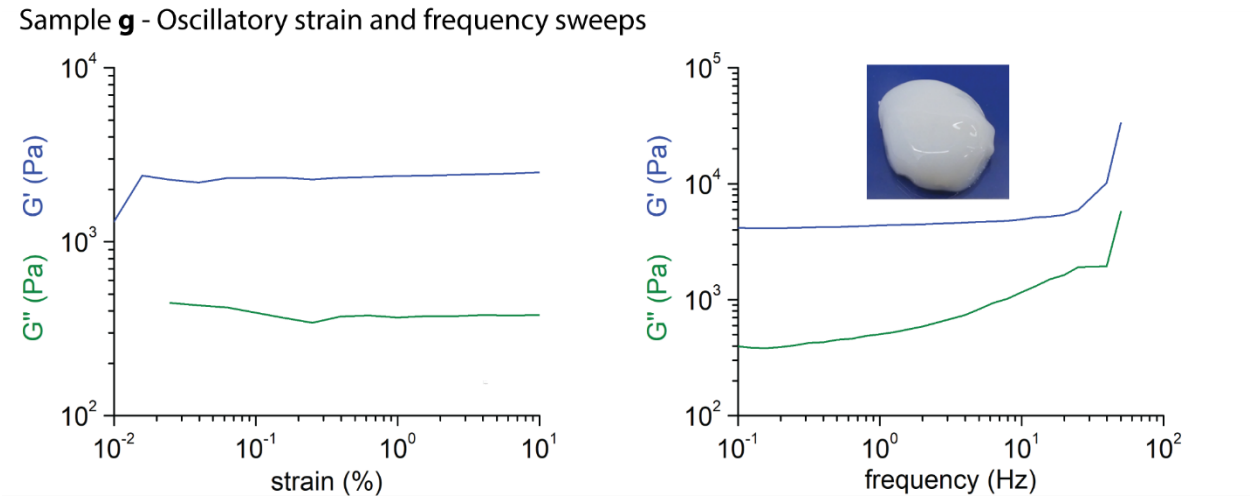

Figure D9. Rheological characterization of sample **g**.

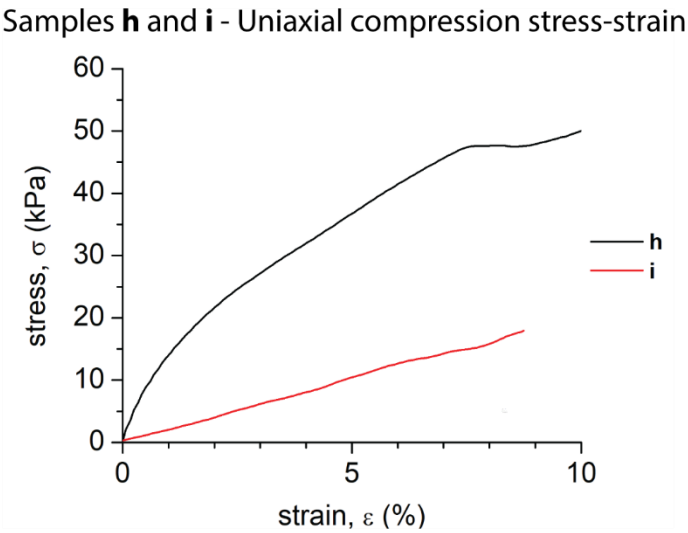

Figure D10. Stress strain curves in the linear region of samples **h** and **i** (mercapto-PS).

Gel fraction experiment: The mercapto-polymer gel was cut into small pieces (3 mm length) and dried under vacuum at 60 ºC for 48 h. The pieces were weighed, then placed in a vial and 4 mL of DMF were added. The vial was stirred at room temperature for 48 h. The gels were removed from the vial, dried under vacuum at 60 ºC for 48 h, and weighed. The gel fraction was calculated using the following formula:

$$Gel\ fraction\ (\%) = \left\{1 - \left[\frac{W_o - W_i}{W_o}\right]\right\} \times\ 100$$

where W_o is the initial weight of the dry gel and W_i is the weight of the extracted dry gel.

Equilibrium swelling experiment: The mercapto-polymer gel was dried at ambient conditions for 24 h and then at 60 °C under vacuum for 24 h. The composite was weighed and then placed into a vial, 5 mL of dry DMF were added and the vial was capped. The sample was allowed to sit still for 4 days in the dark. The gel was removed, the exterior of it dried with paper, and weighed. The degree of swelling was calculated using the following formula:

$$S\ (\%) = \frac{W_{swollen}}{W_{dry}} \times 100$$

where $W_{swollen}$ is the weight of the swollen gel and W_{dry} is the weight of the dry gel.

Table D2. Physical characterization of mercapto-polymer organogels.

Sample	Gel fraction (%)	Degree of swelling (%)
a (mercapto-PMMA)	93	183
f (mercapto-PMA)	80	497
h (mercapto-PS)	83	147

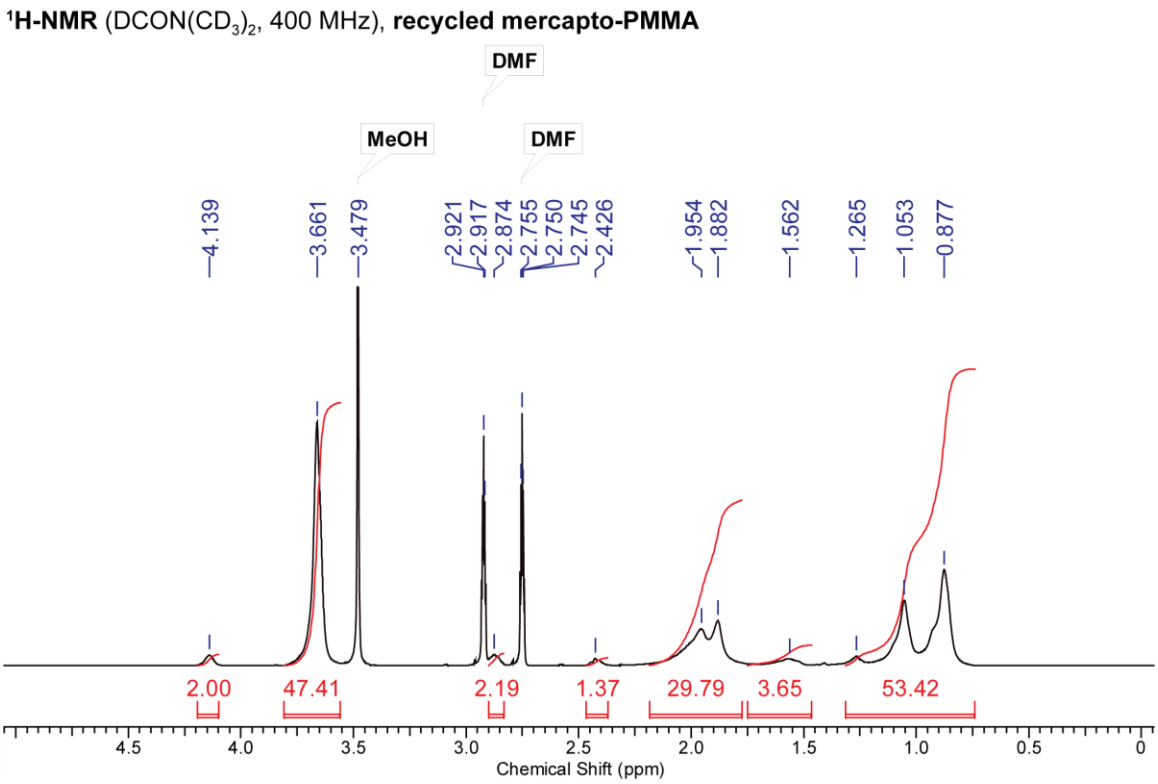

Figure D11. NMR spectrum of recycled mercapto-PMMA.

Table D3. Molecular weight characterization of mercapto-polymers in recycling experiments.

Sample	M_n , kDa (virgin polymer)[a]	M_n , kDa (recycled polymer, round 1)[a]	M_n , kDa (recycled polymer, round 2)[a]
a[b] (mercapto-PMMA)	18.3	249.8 68.4 22.3	196.0 42.6 14.6
e[c] (mercapto-PMMA)	18.3	24.1	-
f (mercapto-PMA)	19.3	22.6	23.4
h (mercapto-PS)	25.6	18.3	20.3

[a] Determined by GPC using standard calibration curves with PMMA or PS standards.
[b] Recycled polymer showed multimodal distribution (3 peaks), see GPC chromatogram below.
[c] Sample **e** is the mercapto-PMMA reference gel.

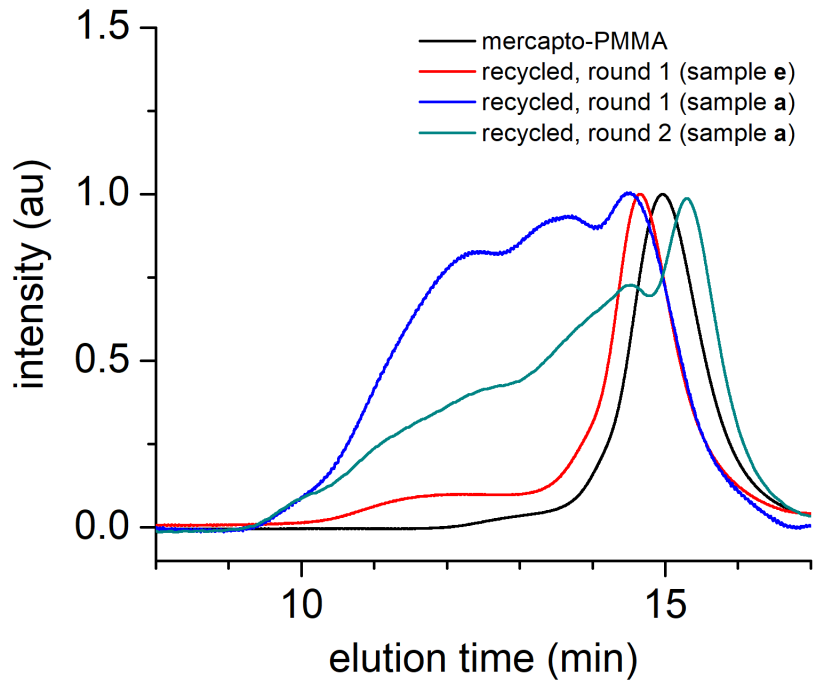

Figure D12. GPC trace curves of mercapto-PMMA gels (samples **a** and **e**) recycling experiments.

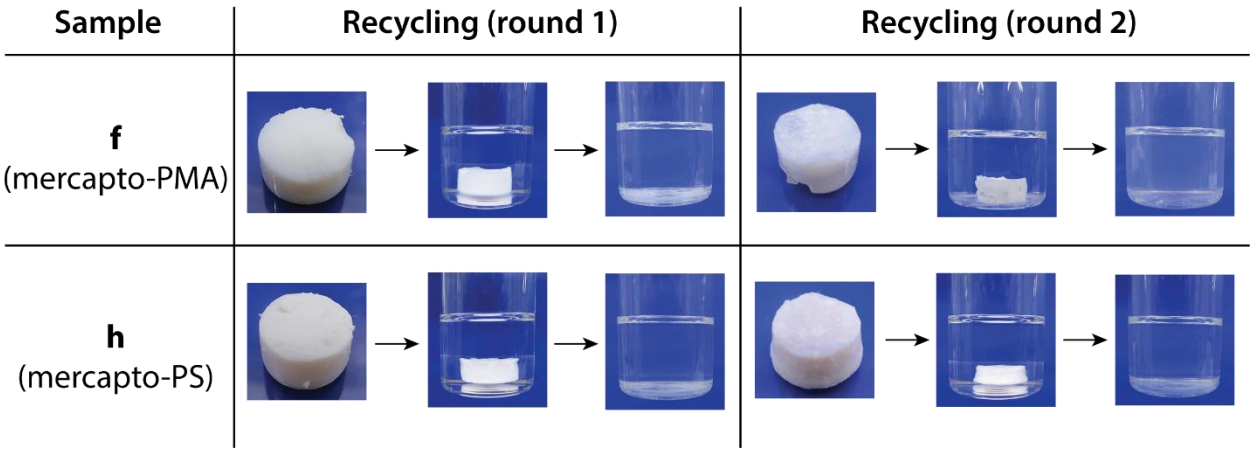

Figure D13. Pictures showing dissolution of samples **f** (mercapto-PMA gel) and **h** (mercapto-PS gel) from Table 3. The gels were dissolved by stirring in a TCEP hydrochloride solution in DMF (8 mL, 40 mg/mL, 0.16 M) at 50 ºC for 12 h. The solutions were centrifuged at 10k rpm to remove the ZnO nanoparticles and concentrated under vacuum. The polymers were recovered by precipitation in methanol (30 mL) and dried at 60 ºC under vacuum for 24 h. The recycled polymers were then reused to form a new gel via mechano-crosslinking. Briefly, recycled mercapto-polymer (75 mg) and virgin mercapto-polymer (75 mg) were dissolved in DMF (400 μL), mixed with ZnO nanoparticles (30 mg) and ultrasonicated (40 kHz) for 6 h. The newly formed gels could also be dissolved using the same procedure mentioned above.

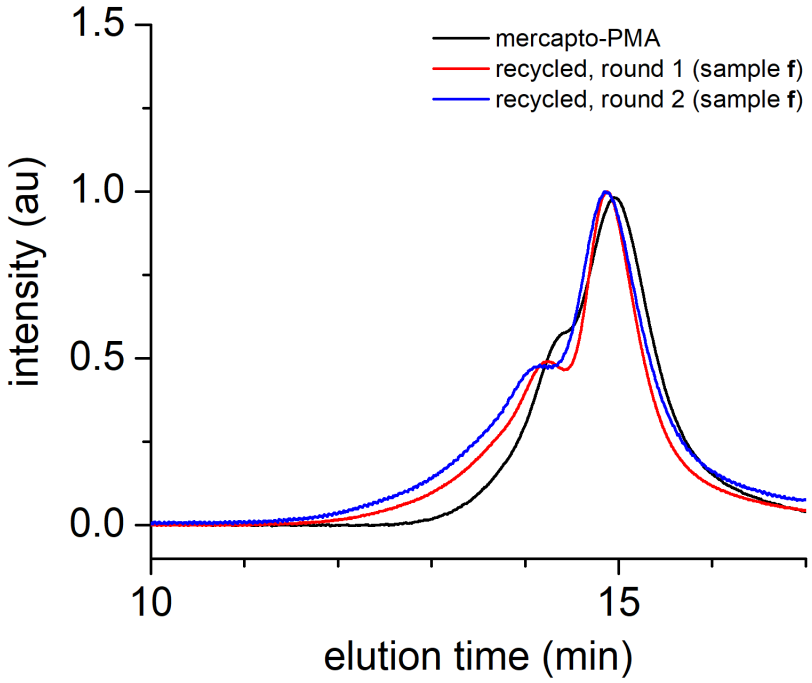

Figure D14. GPC trace curves of mercapto-PMA gel (sample **f**) recycling experiment.

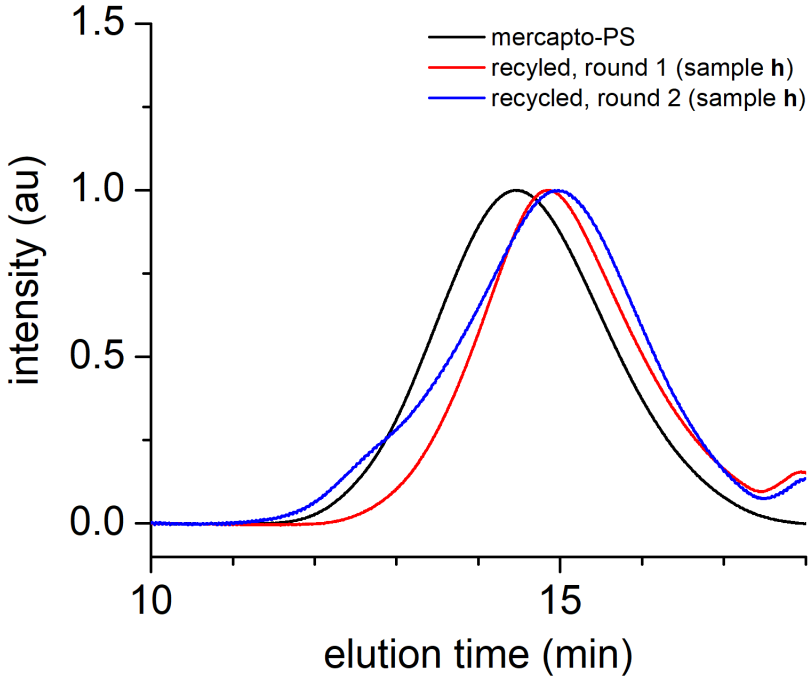

Figure D15. GPC trace curves of mercapto-PS gel recycling experiment (sample **h**).

Appendix E: Supporting information for Chapter 4: Mechanically-promoted mineralization of an organogel

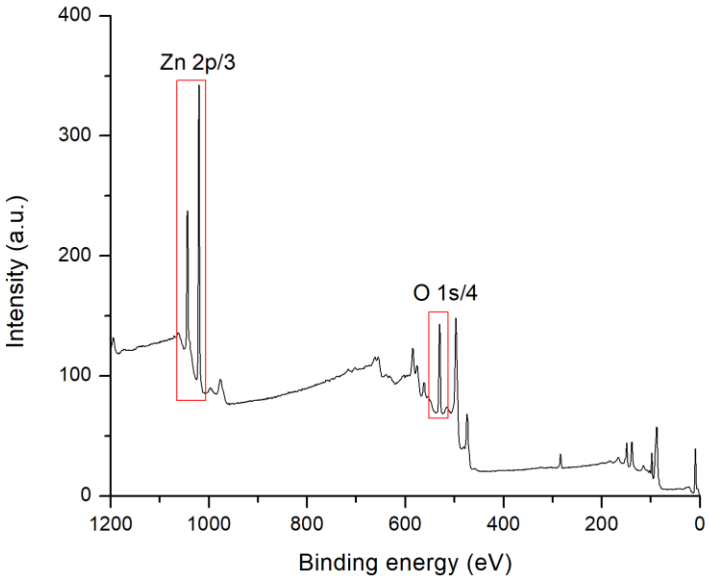

Figure E1. XPS spectrum of ZnO nanoparticles.

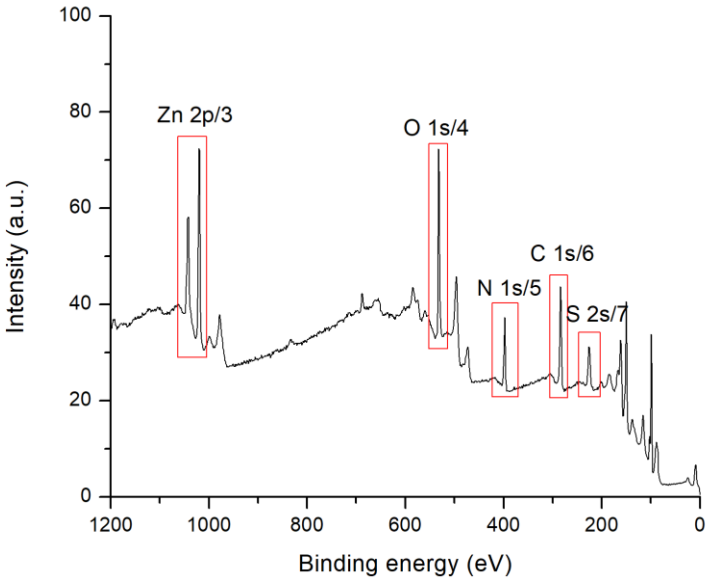

Figure E2. XPS spectrum of microrods.

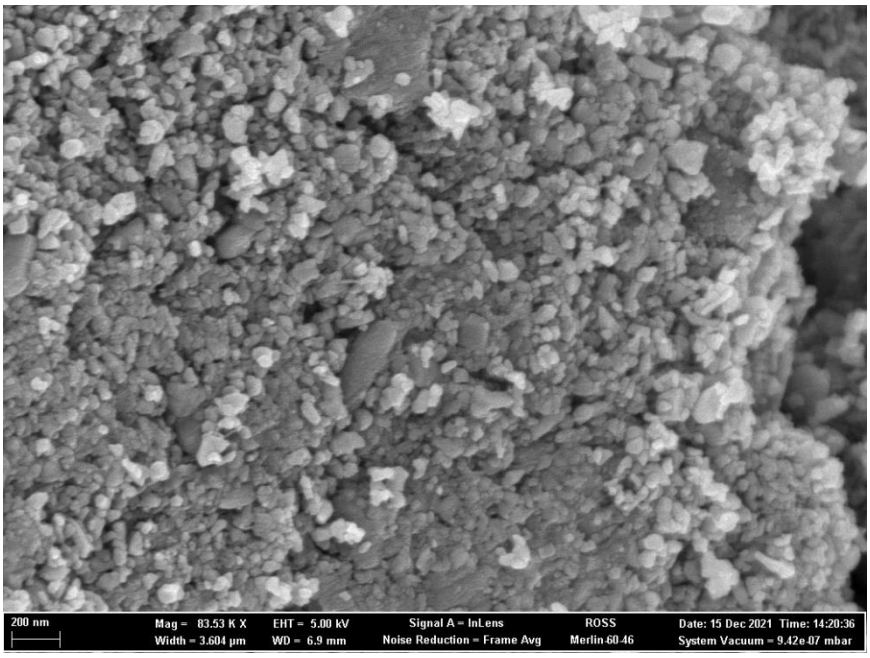

Figure E3. SEM image of particles at t = 0 h. Scale bar: 200 nm.

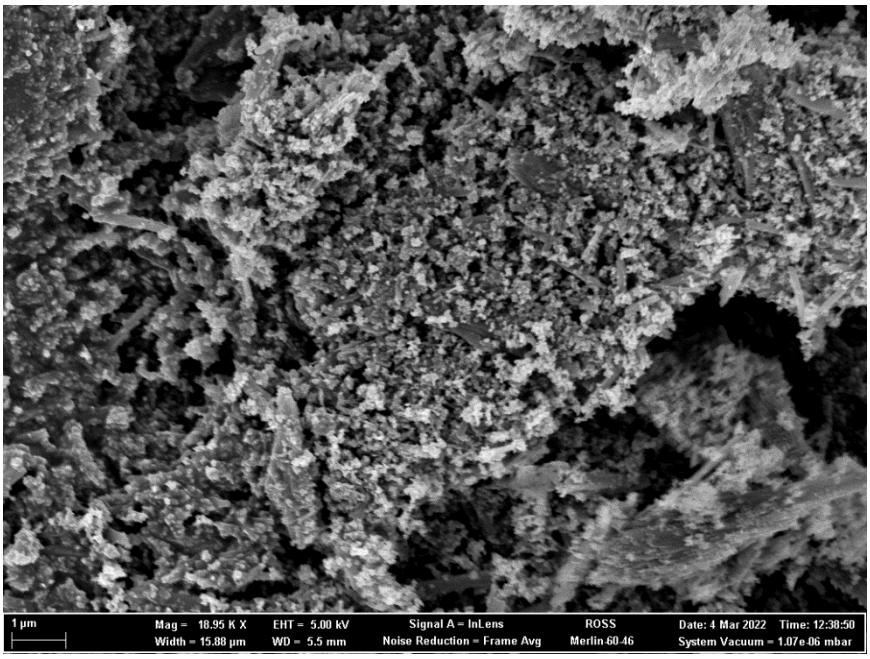

Figure E4. SEM image of particles at t = 1 h. Scale bar: 1 µm.

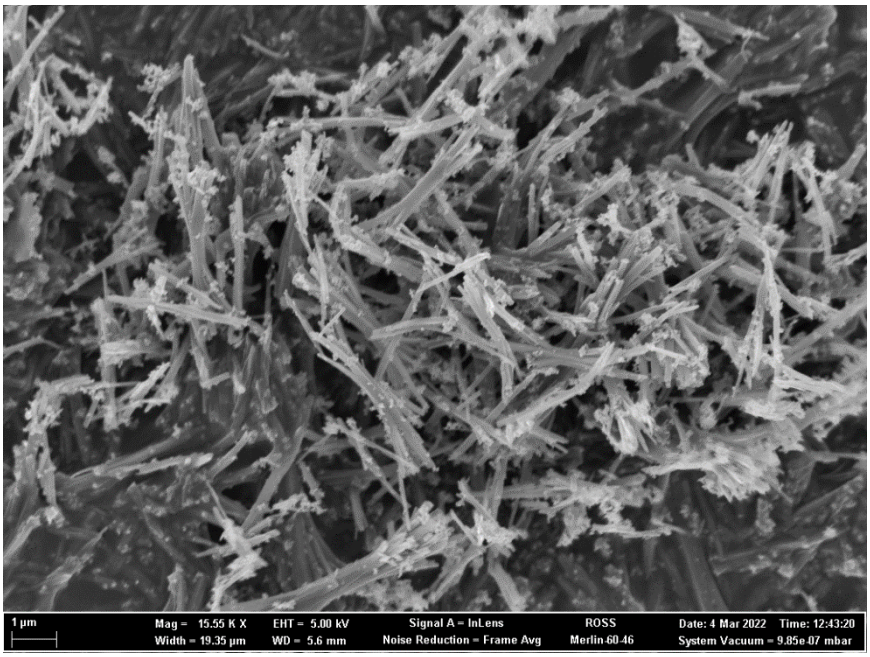

Figure E5. SEM image of particles at t = 2 h. Scale bar: 1 µm.

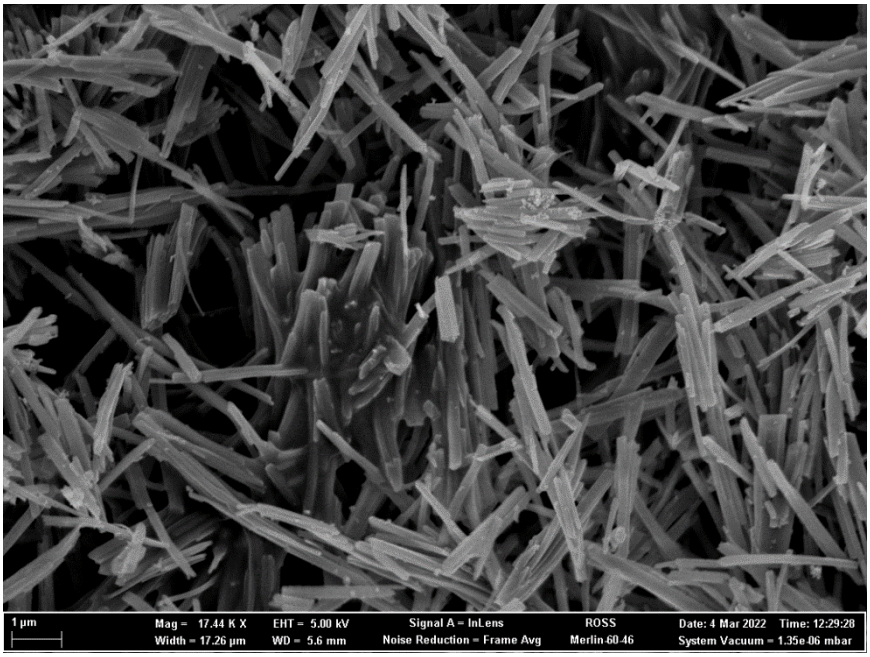

Figure E6. SEM image of particles at t = 4 h. Scale bar: 1 µm.

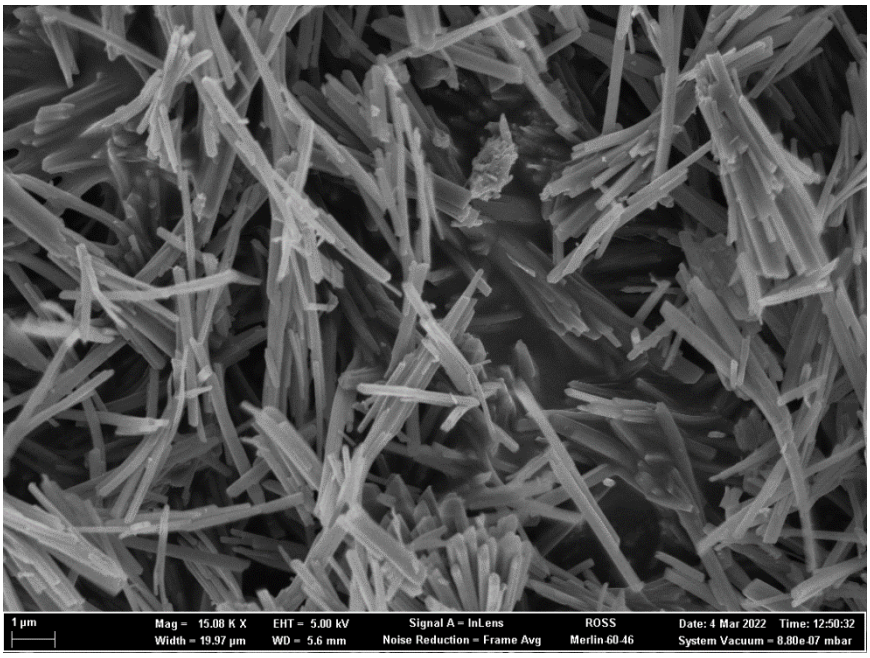

Figure E7. SEM image of particles at t = 6 h. Scale bar: 1 µm.

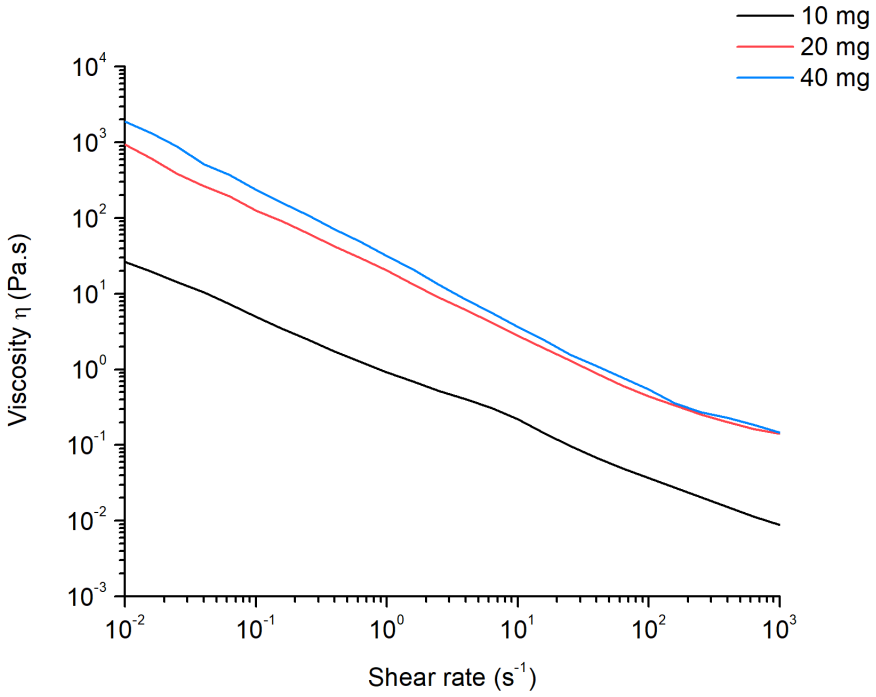

Figure E8. Shear rheology plots for experiments varying the concentration of ZnO nanoparticles with constant concentration of McMT (66 mg, 0.5 mmol).

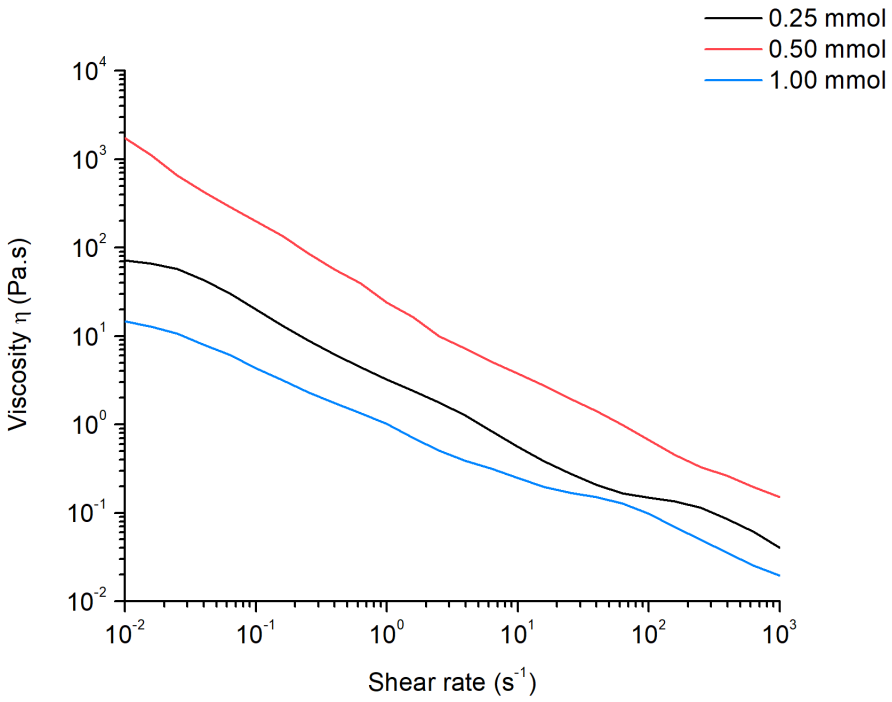

Figure E9. Shear rheology plots for the experiments varying the concentration of McMT with constant concentration of ZnO (20 mg, 0.25 mmol).

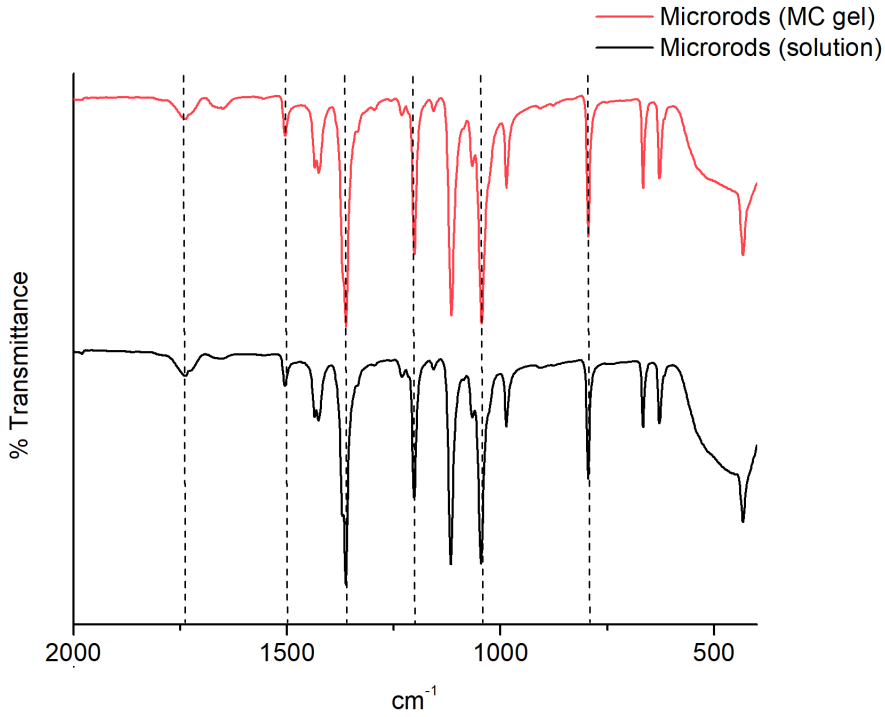

Figure E10. Comparison of FTIR spectra of the microrods prepared in solution vs microrods formed within the methyl cellulose organogel.

Additional data:

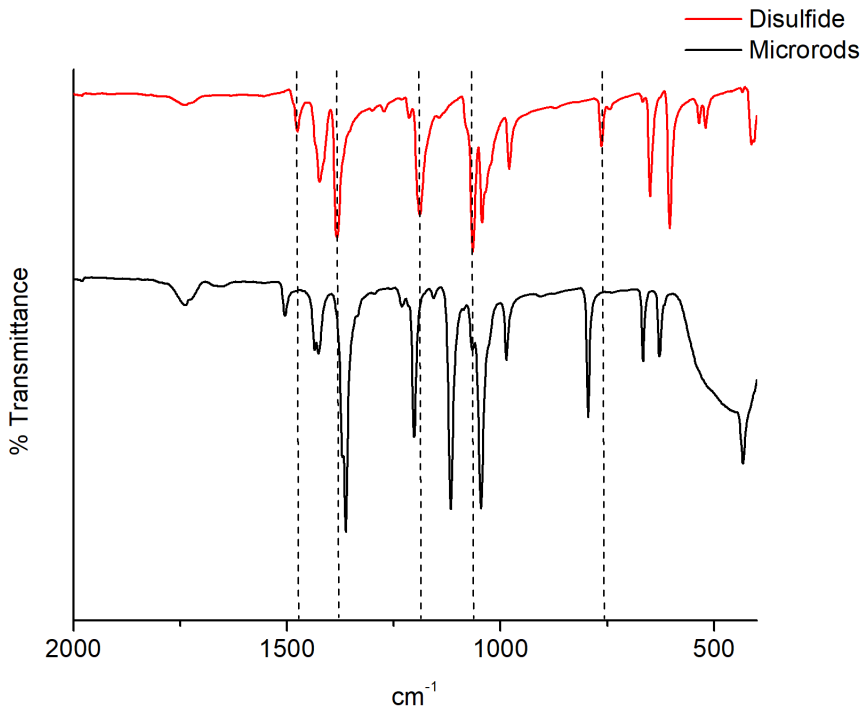

Figure E11. Comparison of FTIR spectra of the McMT disulfide and the microrods.

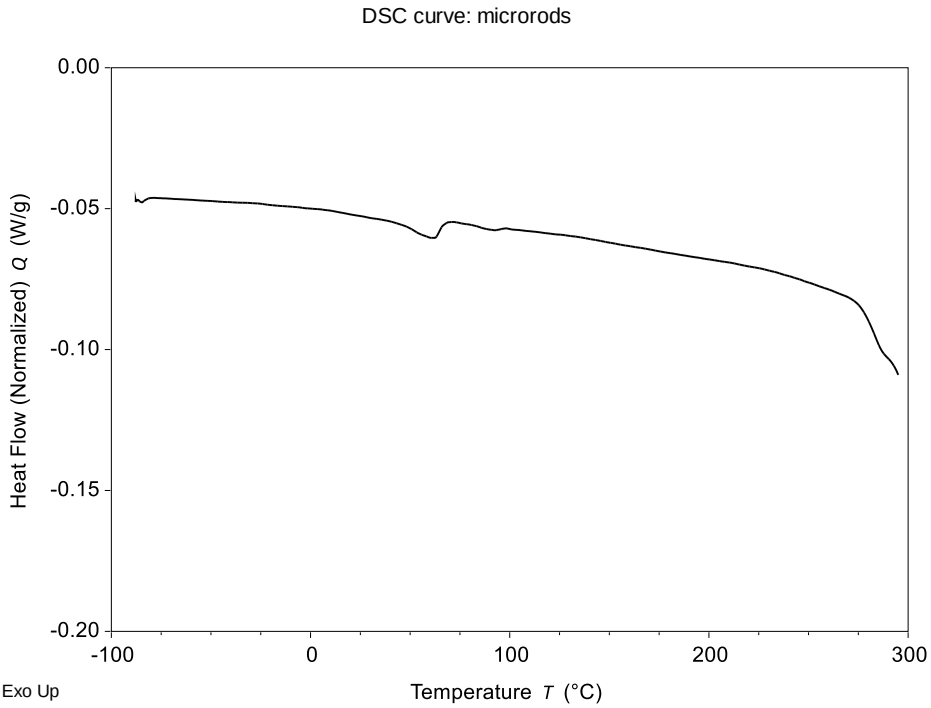

Figure E12. Modulated DSC curve of microrods.

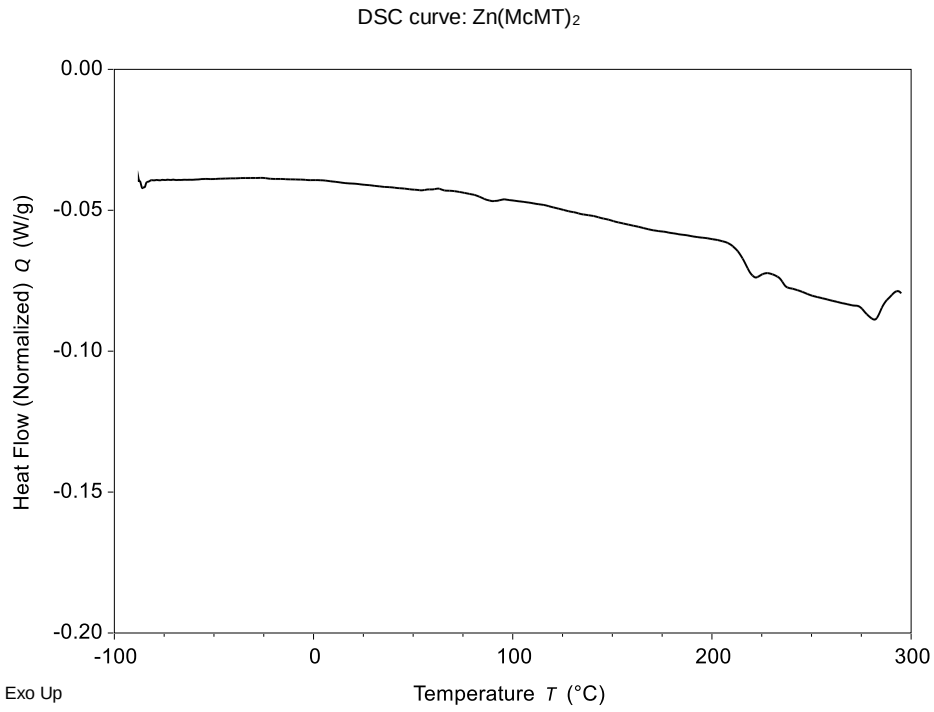

Figure E13. Modulated DSC curve of $Zn(McMT)_2$.

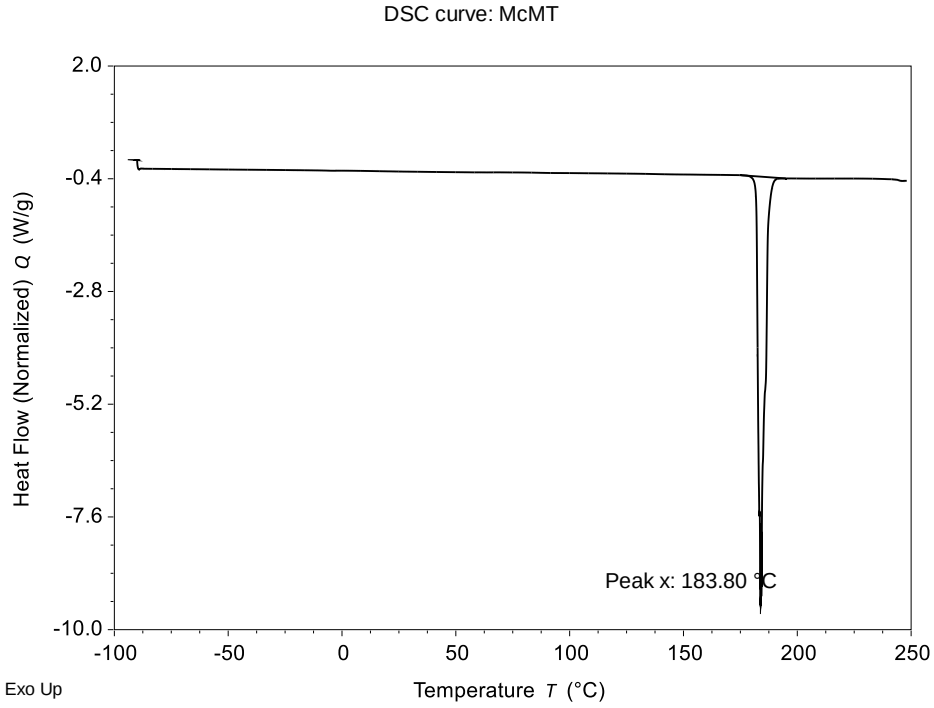

Figure E14. Modulated DSC curve of McMT.

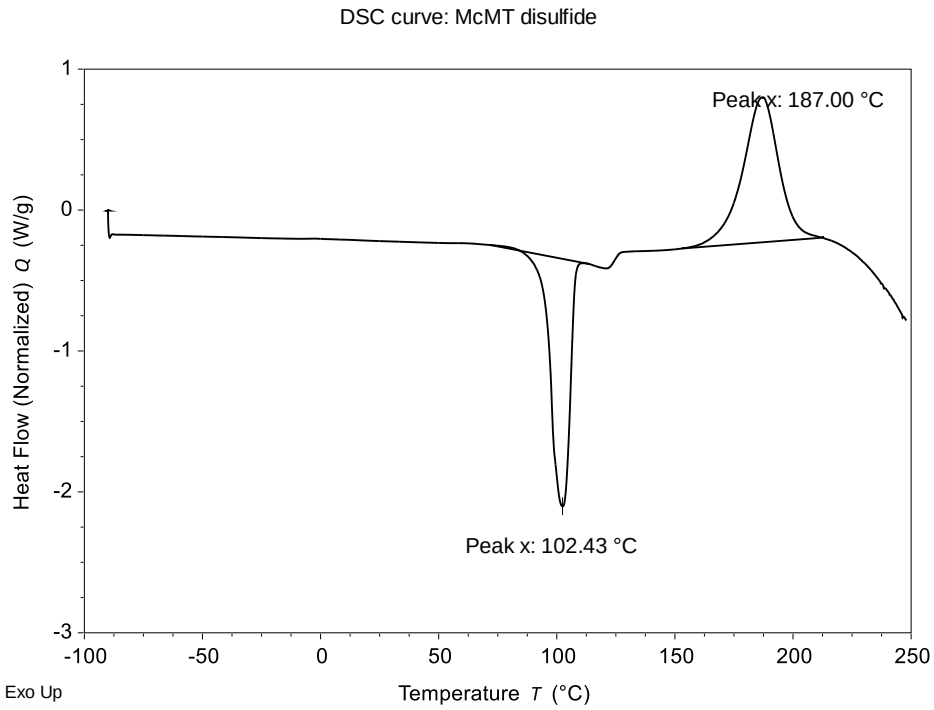

Figure E15. Modulated DSC curve of the McMT disulfide dimer.